Università degli Studi di Cagliari

DOTTORATO DI RICERCA

IN ARCHITETTURA

Ciclo XXVII

DYNAMIC BEHAVIOUR OF CURVED CABLE-STAYED BRIDGES

Settore/i scientifico disciplinare: ICAR-09

Tecnica delle costruzioni

Presentata da:	Fa Guanzhe
Coordinatore Dottorato	Prof.ssa Emanuela Abis
Tutor	Dr. Luigi Fenu

Esame finale anno accademico 2014 – 2015

SUMMARY

During the last decades, curved cable-stayed bridges have been regularly accepted due to their ability to cross long spans, for aesthetic reasons because of their enhanced geometric configurations and to the reduced costs involved in the bridge and roof construction. However, such structures are typically showed to several special geometric shapes, which lead to a different dynamic ability. Therefore, in order to verify the dynamic performance of the structure, it is necessary to investigate the effects on dynamic behaviour of such particular geometric shape and structure by considering both serviceability and ultimate working conditions. The enormous development in the field of the design of more splendid and ambitious civil structures like bridges, stadiums with irregular shapes as the landmark of the city. Regarding design, existing codes on curved and cable-stayed bridges, roofs etc. We discuss the different structure shapes and analysis the dynamic ability.

These require in-depth analysis concerning unlikely predictable behavior often necessary FE model's simplification. Thus arose the necessity for structural engineers to develop solid experimental tools able to identify dynamic and static structural properties in order to calibrate, update and validate the FE model used at the design phase. Fortunately, this was already accomplished by the necessity that rose early on in the field of Electronics and Mechanical Engineering, through years' efforts by both theory and practice circles to develop System Identification and Modal Analysis techniques. Still today the most widely used techniques in the field of experimentations provide the use of instrumentation like an impulse hammer, an electro-dynamic shaker, mass vibrator, capable of exciting the dynamic property of the structures in a controlled form. However, the price and as a consequence, the inadequate availability of input-output modal identification techniques, together with the difficulty to excite large civil structures, led the researcher to a more feasible method: Operational Modal Analysis (OMA).

This thesis provides the theoretical fundamentals of structure health monitoring especially focused on the FE model updating Optimization Process on curved cable-stayed bridge. A global view of techniques, tools, and physical assumptions made in the Vibration measurements phase and System Identification phase are provided in order to understand how to get the experimental data needed and how they should be treated to be easily compared with the numerical ones. Building a

finite element model, which accurately reflects the true structure's stiffness and mass distribution, can improve the precise of dynamic analysis results of curved cable-stayed bridges.

SOMMARIO

Durante gli ultimi decenni, le strutture sospese curve, capaci di attraversare lunghi percorsi, di presentare un alto livello estetico e una configurazione geometrica tale da ridurre i costi di costruzione di ponti e impalcati, sono state regolarmente accettate. Tuttavia, per tali strutture di diverse e particolari forme geometriche, inducono una diversa capacità dinamica. Pertanto, per verificare le prestazioni dinamiche della struttura, è necessario studiare gli effetti sul comportamento dinamico di tale particolare forma e struttura geometrica considerando sia la facilitá di manutenzione, sia le condizioni ultime di lavoro. Per quanto riguarda il progetto, nel rispetto delle normative esistenti in materia di strutture curve e sospese, ponti, viadotti, ecc si analizzeranno le diverse forme di struttura e si valuterá la capacità dinamica della struttura.

L'enorme sviluppo nel campo della progettazione di strutture sempre più imponenti e grandiose, quali ponti e stadi dalle forme irregolari, rappresentano un punto di forza delle città. Questi richiedono un'analisi approfondita sul comportamento di incerta previsione e spesso si necessita di una semplificazione con un modello FE. Così è nata la necessità, da parte di ingegneri strutturisti, di sviluppare strumenti sperimentali capaci di identificare le proprietà strutturali dinamiche e statiche, al fine di calibrare, aggiornare e validare un modello FE da utilizzare in fase di progettazione. Per fortuna lo sviluppo di tecniche di identificazione del sistema e dell' analisi modale, è stato già effettuato per l'esigenza che sorgeva nella fase iniziale nel campo dell'elettronica e Ingegneria Meccanica. Ancora oggi le tecniche più diffuse nel campo della sperimentazioni prevedono l'utilizzo di strumentazione come un martello ad impulso, un agitatore elettro-dinamico, vibratore di massa, che sono in grado di eccitare la proprietà dinamica delle strutture in maniera controllata. Tuttavia, il costo e di conseguenza, l'insufficiente disponibilità di tecniche di identificazione modale input-output, insieme alla difficoltà di eccitare grandi strutture civili, hanno portato la ricerca verso un metodo più fattibile: Operational Analisi modale (OMA).

Questa tesi fornisce i fondamenti teorici di un' analisi modale operativa (OMA) e in particolare si focalizza sulla realizzazione di un processo di ottimizzazione del modello FE. Per capire come ottenere i dati sperimentali necessari e come essi dovrebbero essere trattati per essere facilmente confrontati con quelli numerici, si

fornisce una visione globale di tecniche, strumenti, e ipotesi fisiche i quali sono stati considerati nella fase di misurazione delle vibrazione e nella fase di identificazione del sistema. La costruzione di un modello agli elementi finiti, che riflette accuratamente la rigidezza e la massa di distribuzione della struttura reale, può migliorare la precisione dei risultati di analisi dinamica delle strutture sospese curve.

DEDICATION

To my family

ACKNOWLEDGEMENTS

I would like to express my sincere gratitude to my advisor Prof. Luigi Fenu, Prof. Bruno Briseghella Prof. Minjuan He and Prof. Tobia Zodan for the opportunity of my Ph.D. study. Valuable learning opportunities inspires my enthusiasm on scholar. Their knowledge and expertise also have been a precious reference during these three years.

I would like to express my special appreciation and thanks to Prof. Leqia He Michele Iuliano and Munoz Miguel for their great kindest helps and advices on my studies. They have supported me throughout my thesis with their patience and knowledge, also create harmonious atmosphere and comfortable writing environment in Cagliari and Fuzhou during these three years.

Thanks go to Prof. Camelo Gentile in Politecnico di Milano, who gives me some advices to my studies. Thanks to SIBERC of Fuzhou University provides me with the help and their invaluable contribution to my thesis.

I want to thank the University of Cagliari for offering me the Ph.D. fellowship to commence this thesis.

I have also enjoyed a lot of support and sheared countless happiness in last three years. Thanks to all my dear friends I have meet in Italy.

Lastly, I want to give special thanks to my wife, my parents, who give me selfless love and strong support to my studies.

CONTENTS

LIST OF FIGURES

LIST OF TABLES

CHAPTER 1

1. INTRODUCTON

1.1. The Motivation of Research

During the last decades, curved cable-stayed bridges have been regularly accepted due to their ability to cross long spans. Cable stayed bridges, are being built in more particular styles for structural reasons and aesthetic reason. In addition to the many regular symmetric cable stayed bridges with spans exceed 1000 m, the asymmetric bridge or other designs becomes more and more usual. So the asymmetric bridges have interesting dynamic characteristics that need to be pay attention to investigate.

For aesthetic reasons because of their enhanced geometric configurations and to the reduced costs involved in the bridge and roof construction. Bridges and stadium roofs are the largest single structures in the city. Their appearances may have a positive emotional effect on the image of the city and the surrounding community. The primary reason and purpose of the curved structure designer is to unite the curved structure with its immediate environs or create the architectural style for future development of the city. They want to provide the future city designer a direction and guidance in the design process and helps assure that the aesthetic properties of the bridges are effective.

However, such structures are typically showed to several special geometric shapes, which lead to a different dynamic ability. Therefore, in order to verify the dynamic performance of the structure, it is necessary to investigate the effects on dynamic behaviour of such particular geometric shape and structure by considering both serviceability and ultimate working conditions. Regarding design, existing codes on curved and cable-stayed bridges, bridges and roofs etc. We discuss the different structure shapes and analysis the dynamic ability.

1.2. The Objectives and Methodologies

In order to investigate the dynamic behaviour of curved suspended structure, the primary objectives and methodologies of this research are:

1. Survey on the applications in worldwide, especially the current development of curved cable-stayed bridges bridges;

2. Conduct the literature review on operational modal testing and dynamic measuring method, to find the suitable methods in the design, and then propose and manual tune finite element models for curved suspended structure that could simulate the modal analysis, and so on.

3. To develop and improve an analytical solution algorithm for dynamic characteristics of curved cable-stayed bridges through evaluation and calibration of finite element models. Compared with the results with the symmetric shapes. Subsequently, the verification method according to two way of design are presented.

4. Perform parametric study on curved suspended structure based on FEM analysis, to further understand the dynamic performance of curved cable-stayed bridges and find the key components of the dynamic characteristics.

5. Based on operational model updating analysis of Magaz bridge, aim to verify the corresponding method for systemic structure. Compared the results and proposed method to develop modal updating of suspended curved structures.

6. Verify and investigate the dynamic performance of Marghera Bridge, which is a curved cable stayed bridge. Take it as case study, three period operational modal testing test are developed and create a FEM model and FE model updating are researched by different algorithms.

1.3. Structure of the Thesis

Besides this chapter, in the main body of the thesis, it consists of 6 chapters, from Ch.2 to Ch.6 that introduced as following:

Chapter 2, it states the current applications of structure health monitoring in practice. Previous experimental and analytical research studies and their main contributions are summarized and commented upon.

Chapter 3, it describes the vibration-based modal analysis of curved cable-stayed bridges in detail, a description of the theory, the instrumentation, the equipment setup, the input and output of experimental response are documented in this chapter.

Chapter 4, it presents a study on operational modal testing and FE model updating of an existing lightweight bridge with composite steel-concrete combination structure girder - Magaz Bridge. Based on different FEM updating analysis, the dynamic characteristics is investigated.

Chapter 5, taken Marghera Bridge as case study, dynamic tests of a curved cable-stayed bridge based on multi-year Monitoring was designed and performed. Both a direct method, known as the Douglas-Reid algorithm, and a sensitivity-based iterative method, namely the Trust-Region-Reflective algorithm, were applied for computational model updating of the bridge. The importance of a rational process that consists of vibration testing, identification and model updating is highlighted through the resulting FE model that reduces the uncertainties in modelling and reflects the changes in construction of the structure. Based on computational analyses, dynamic behavior of this structure was studied.

Chapter 6, Summary of the before three chapters' results, to explore the application of health monitoring technology on curved cable-stayed bridges. discussion of the updating results, base to different types of the bridges, finding the dynamic behaviors of curved cable-stayed bridges.

Chapter 7, the conclusions drawn from the research and recommendations for future investigation will be presented.

CHAPTER 2

2. STATE-OF-ART

A comprehensive literature survey helps not only to deepen the basic knowledge on the studied subject but also to emphasize advantages and disadvantages of previous experiences, so to give researchers space for further improvements. To provide a unitary framework, a detailed literature survey about the topic of model updating is presented.

Structural model updating methods have been proposed in the past to accord mathematical models, mostly discretized finite element models, with experimental data. The estimate of the optimal model from a parameterized class of models is sensitive to uncertainties that are due to limitations of the mathematical models used to represent the behavior of the real structure, the presence of measurement and processing error in the data, the number and type of measured modal or response time history data used in the reconciling process, as well as the norms used to measure the fit between measured and model predicted characteristics. The optimal structural models resulting from these methods can be applied for improving the model response and reliability predictions [Caetano E. et al. 2007], structural health monitoring applications (Avitabile P. 2001; Teughels A. 2003; Cunha A. et al. 2006; Chopra A.K. 2007) and structural control (Brincker R. 2007). Structural model parameter estimation problems based on measured data, such as modal characteristics (Avitabile P. 2001; Teughels A. 2003; Cunha A. et al. 2006; Chopra A.K. 2007) or response time history characteristics (Brincker R. et al. 1992), are often formulated as weighted least-squares problems in which metrics, measuring the residuals between measured and model predicted characteristics, are build up into a single weighted residuals metric formed as a weighted average of the multiple individual metrics using weighting factors. Standard optimization techniques are then used to find the optimal values of the structural parameters that minimize the single weighted residuals metric representing an overall measure of fit between measured and model predicted characteristics. Because of errors of the model and measurement noise, the results of the optimization are affected by the values assumed for the weighting factors. The model updating problem has also been formulated in a multi-objective context (Brincker R. et al. 2000) that allows the simultaneous minimization of the multiple metrics, eliminating the need for using arbitrary weighting factors for weighting the relative importance of each metric in the overall measure of fit. The multi-objective parameter estimation methodology

provides multiple Pareto optimal structural models consistent with the data and the residuals used in the sense that the fit each Pareto optimal model provides in a group of measured modal properties cannot be improved without deteriorating the fit in at least one other modal group. Theoretical and computational issues arising in multi-objective identification have been addressed and the correspondence between the multi-objective identification and the weighted residuals identification has been established (Reynders E. et al. 2006; Reynders E. et al. 2011). Emphasis was given in addressing issues ass ociated with solving the resulting multi-objective and single-objective optimization problems. For this, efficient methods were also proposed for estimating the gradients and the Hessians [Ibrahim S.R., Mikulcik E.C. 1977] of the objective functions using the Nelson's method (ANSYS Inc 2007) for finding the sensitivities of the modes and frequencies to model parameters. In this research work, the model of structure updating problems is to use modal residuals is formulated as single-optimization problems with the objective formed as a weighted average of the multiple objectives using weighting factors. Theoretical and computational issues are then reviewed and the model updating methodologies are applied to update two different finite element models for two different typologies of bridge: a concrete box girder bridge and a steel box girder curved cable-stayed bridge with cast in situ slab. Tests have been performed considering ambient vibration conditions.

2.1. Finite element method

FE overviews: The finite element method

The finite element method (FEM) is an extremely useful engineering tool for numerically approximating physical systems that are too complex for an analytical solution or are governed by behavior that is too complicated for classical analytical solution methods. Specifically, FEM is used in engineering to find an approximate solution to partial differential equations and integral equations. Finite element analysis (FEA) refers to numerical analysis of physical phenomena by dividing the region of interest into smaller pieces, finite elements. Over the finite elements, physical parameters are considered to be constant, vary linearly or vary according to a polynomial depending on the analysis method. Linear approximation is a common approximation and generates useful results for most applications. Complex physical problems governed by differential equations may be simplified using finite elements with linear elastic behavior modeled with gradients calculated by the finite difference method for the non-linear problem near the values of interest. Matrix algebra is then used to solve the linear approximation systematically.

Global equilibrium of the system with compatibility and constitutive relations for each element must be maintained in order to solve a given system. The value of each parameter of interest for a specific element is approximated and depends on the element size and approximation technique. Simple models with large elements are quickly computed, but overly approximated systems intrinsically contain numerical errors that render the FE model useless for physical interpretation of results. Complex models with fine resolution (small elements, fine mesh) can yield more realistic results at the cost of increased computational time.

An optimal model yields accurate, physically realistic results with minimal computational time. Each degree of freedom (such as x, y, or z translation or rotation of a node) added to the model increases the number of necessary computations, so models should be simplified whenever possible. Large, slender objects such as plates or beams may be approximated according to plane stress, plane strain or beam theory, thus reducing the total degrees of freedom in the model and thus the required computations. Convergence analysis can be implemented by evaluating a target response with an increasingly fine finite element mesh (decreasing element size) or by refining some other model parameter. If the results deviate instead of converge, an intrinsic problem with the finite element model likely exists and the results of the numerical analysis should not be trusted

FEM applications

FEM has been extensively utilized in structural and mechanical engineering and many FEA programs exist for the civil, aeronautical and automotive industries. Applications include structural, fluid flow, dynamic mechanical and electrostatic analysis. In structural analysis, the applications of FEM and FEA are virtually limitless and many analysis types and element types exist for solving special problems while new methodologies, programs and element types are constantly being developed.

Generally, FEA requires three steps: pre-processing, FE calculations and post processing. Many commercial FE software packages include graphical user interfaces for each of these steps and many are compatible at each step.

Pre-processing is the step where the FE model is built and the material properties, loads and boundary conditions are defined. This crucial step realizes the FE model and modeling parameters as to best represent the behavior of the object of interest. Many commercial FE programs utilize an inbuilt CAD-type (Computer Aided

Drafting) interface to build the model geometry in 1, 2 or 3 dimensions. Sometimes the model is imported from CAD files, IGES (Initial Graphics Exchange Specification) files, blueprints or text input files. Material properties for individual elements, as well as global environment parameters (e.g. gravity) are assigned to best represent reality. After the geometry is defined, element types are chosen and the model is transformed into a system of discrete elements by meshing. Commercial FE programs offer a choice between automatic meshing and user-defined meshing. The resulting discrete system is composed of finite elements. Boundary conditions must be carefully chosen as to provide constraints. Typical boundary conditions for structural analysis include constrained translation and rotation at foundations while typical internal constraints resist translation and rotation in connections between structural members. These constraints either allow no translation or rotation (fully-fixed DOF) or apply a load proportional to the node translation or rotation (linear-elastic spring at DOF). Finally, load cases are defined for the analysis; options include static, dynamic and frequency analysis.

The analysis step, which performs FE calculations, solves the equation system defined in the pre-processor. Model geometry, element types, material models, internal constraints and boundary conditions are all taken into consideration by the FE solver.

FE post-processing utilizes the results of the FE calculations for output, visualization and further analysis. At this point, FE results may be compared to measured values, hand calculations or other analyses for FE model verification. The verified model may then be used to predict behavior resulting from various loads and conditions. The FE model updating procedure compares the structural response and eigenvalues predicted by the FE model with field or laboratory measurements, and then updates uncertain FE modeling parameters to obtain a better correlation and to minimize modeling error.

(a) Modeling. In the FE pre-processing stage, the model is defined. Most structural FE models are use Cartesian coordinates (rectangular x, y, z coordinate system) in 2D or 3D modeling space. For a general node in 3D, there are six degrees of freedom (DOF): x, y, z translation (DOF: 1-3 in SAP2000) and x, y, z rotation (DOF: 4-6 in SAP2000).

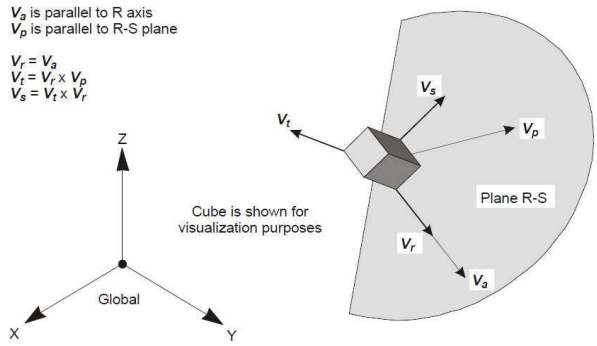

Fig.2. 1 SAP2000 degrees of freedom (DOF) in Cartesian coordinates

Global constraints (boundary conditions) typically constrain DOF of nodes of the entire assembled model. Boundary conditions are created by setting DOF of a particular node equal to zero or by making a resultant force linearly proportional to the displacement or rotation of the node.

(b) Structural analysis. Many FEA software programs exist to perform many types of analysis. Structural FEA, though only a subset of the available FEA, is a powerful tool for structural analysis. Typically, structural members are greatly simplified to evaluate the global response of the structure, but detailed analysis can be extremely useful when evaluating connections or specific structural details.

In most situations, static linear-elastic analysis is sufficient to determine structural behavior. Many options exist for such analysis and static analysis is frequently used in structural FEA. In the event that a system susceptible to second order effects is exposed to large magnitude time variant forces, dynamic analysis or equivalent static is necessary. Structural dynamic analysis evaluates the time variant behavior of a structure. Different time stepping routines may be used depending on required accuracy and available computational power. Dynamic analysis is quite common in the automotive and aerospace industries, but not as widely used in structural FEA since most structures are designed to resist time variant forces without experiencing significant motion or deformation. One exception is the dynamic response of slender bridges to wind and traffic. The structural integrity of all bridges must be verified when the structure is exposed to worst-case-scenario dynamic loading (though equivalent static loading may also be used). The characteristic natural frequencies (eigenfrequencies) are of interest because the eigenfrequencies and eigenmodes of a structure define the vibration behavior of the structure. Thus, frequency analysis is quite common, especially for large bridges. Frequency analysis should be carried out early in the design phase of second order structures.

Large amplitude vibrations can be avoided by changing the vibration characteristics of the structure by adding damping, increasing stiffness and decreasing mass.

(c) Elements. In order to model different physical phenomena, different FEM elements are used. In the simplest case, 1D linear elasticity, a 1 node spring and mass element with 1 DOF can be used. More complicated element types have more nodes with more DOF for each node and can represent increasingly complicated physical behavior. Elements with polynomial shape functions, known as higher order elements, can model bending more accurately than linear elements. Structural FEA typically utilizes small, simple elements for global analysis, larger elements with more DOF for complicated local structural behavior or a combination of simple and complicated elements to model both global and local structural behavior.

Efficient modeling of global structural behavior requires model simplification in order to reduce computational time and to permit calculation of eigenfrequencies and eigenmodes. The most common element types for modeling global behavior are truss, beam, membrane and shell elements. Truss elements have 2 nodes with 1 DOF for each node and can only model axial force and axial deformation. Cables and truss structures may be modeled using truss elements if one is certain that no moment is transferred from the cable or truss and that the structural member is sufficiently slender that the stress distribution is sufficiently uniform. Beam elements can transfer axial force, shear and bending. The cross-sectional properties of the beam may be defined using standard types (such as I-profiles and box beams) in commercial FE software, or generalized sections can be defined with user input data for area moment of inertia about the primary and secondary axis. Integration points span the cross-section and are used to discretize the inertial properties of the cross-section for numerical integration. Euler-Bernoulli beam theory assumes that plane sections remain plane, neglecting rotatory inertia, principal shear deformation and combined rotatory inertia and shear deformation. Euler-Bernoulli beam elements are valid for slender beams (aspect ratio, length divided by height, greater than 10) loaded primarily in bending such that bending deformation is much greater than shear deformation. Timoshenko beam theory includes rotatory inertia, principal shear deformation and combined rotatory inertia and shear deformation. Timoshenko beam elements can more accurately model deep beams (aspect ratio greater than 2), where shear deformation and rotatory inertia should not be neglected. Derivations of Euler-Bernoulli and Timoshenko beam theory from governing partial differential equations of motion are available in Craig et al. (2006). The Galerkin method can be used to derive the finite element matrix equation for

Euler-Bernoulli beam elements while the energy method can be used to derive the FE matrix equations for Timoshenko beam elements according to Kwon and Bang (2000).
Euler-Bernoulli beam theory,

$$\frac{\partial^2}{\partial x^2}\left(EI\frac{\partial^2 u}{\partial x^2}\right)-\left(p_y(x,t)-\rho A\frac{\partial^2 u}{\partial t^2}\right)=0 \tag{2.1}$$

Timoshenko beam theory,

$$\begin{aligned}&\frac{\partial^2}{\partial x^2}\left(EI\frac{\partial^2 u}{\partial x^2}\right)-\left(p_y(x,t)-\rho A\frac{\partial^2 u}{\partial t^2}\right)-\rho I\frac{\partial^4 u}{\partial u^2\partial t^2}+\\&\frac{EI}{\kappa GA}\frac{\partial^2}{\partial x^2}\left(p_y(x,t)-\rho A\frac{\partial^2 u}{\partial t^2}\right)-\frac{\rho I}{\kappa GA}\frac{\partial^2}{\partial t^2}\left(p_y(x,t)-\rho A\frac{\partial^2 u}{\partial t^2}\right)=0\end{aligned} \tag{2.2}$$

Surfaces may be modeled in FEM with membrane and shell elements. A quadrilateral membrane element has 4 nodes with 2 in-plane DOF for each node. Membrane elements are capable of modeling in-plane forces and bending. If out of plane bending for thin plates should be modeled, plate elements that utilize classical Kirchoff plate theory are often used. Classical plate theory assumes plane stress or plane strain and an undeformed neutral plane of the plate. Plate elements can be used to evaluate buckling risk for slender plate structures and to find deformation of plates loaded transversely to the plate plane. A derivation of the FE formulation for plate elements with classical Kirchoff plate theory is available in Ottosen and Petersson (1992). The Galerkin method is used to derive the FE matrix equation for a classical Kirchoff plate element in Kwon and Bang (2000). Shell elements have curvature along the surface and have 5 DOF for each node, three translational DOF and two rotational DOF. The curved surface of shell elements enables the modeling of curved structural members without requiring as fine of a mesh as is needed when discretizing using plate elements. Furthermore, solid continuum elements may be degenerated into shell elements, thus reducing total model DOF while retaining model accuracy. The effect of transverse shear deformation may be included using Mindlin-Reissner plate theory; a derivation of the FE matrix equation using internal energy is available in Kwon and Bang (2000).

Timoshenko beam theory,

$$\frac{\partial^4 u}{\partial x^4} + 2\frac{\partial^4 u}{\partial x^2 \partial y^2} + \frac{\partial^4 u}{\partial y^4} - \frac{12\left(1-\nu^2\right)}{Et^3} q(x,y) = 0 \qquad (2.3)$$

Once global behavior is obtained by simplified global analysis, local analysis can be used to assess structural details. Local analysis of structural details can be used to find the stresses in regions with non-uniform stress distribution, such as structural connections. Solid (continuum) elements are useful for such general modeling. Brick and tetrahedral elements with linear-elastic material properties are commonly used, especially for 3D SLS analysis, but higher order continuum elements with specialized constitutive material relations can be used for specialized purposes. A typical example of a specialized structural analysis is FEA of a continuous reinforced concrete beam loaded until failure. The stresses are redistributed across the beam cross-section after concrete cracking initiates and the concrete-reinforcement bond properties determine the cracking pattern. For accurate analysis, the constitutive equations must include non-linear crushing of the concrete, tensile softening of concrete, concrete reinforcement bond slip and elastic-perfectly-plastic reinforcement steel stress vs. strain. Special structural elements include springs, dashpots, point masses, point rotary inertias and rigid connections. These are especially useful for simplified global analysis, where a simplified model with beam elements does not adequately describe the dynamic behavior of the structure. Springs and rigid connections can provide internal constraints and boundary conditions to more realistically model structural geometry (e.g. rigid elements of the width of a beam with full interaction with the beam element can provide internal connections). Point mass, point rotary inertia and dashpots change the dynamic properties of the structure and can be used to tune the modal mass and modal damping matrices to better correspond to measurements. SLS behavior is of primary interest and accurate FE modeling was accomplished by simplified global analysis with beam elements and linear-elastic constitutive relations.

(d) Material properties. The stress-strain relationship is defined in the structural FEA according to the applicable material model. Isotropic material properties are used in this study and are the most common for FEA. Isotropic material properties are homogeneous and identical in all directions. Anisotropic materials are the most general and have material properties that depend on direction. Crystalline materials are anisotropic and material properties depend on crystalline plane and grain

boundary orientation. Orthotropy is a special case of isotropy and orthotropic materials have different material properties in orthogonal directions. These include glass and carbon fiber composites, wood and rolled steel. Hooke's Law of linear elasticity describes the relationship between stress and strain:

$$\sigma = E\varepsilon \tag{2.4}$$

Anisotropic stress vs. strain relation,

$$\begin{bmatrix} \sigma_{xx} \\ \sigma_{yy} \\ \sigma_{zz} \\ \sigma_{yz} \\ \sigma_{zx} \\ \sigma_{xy} \end{bmatrix} = \begin{bmatrix} E_{11} & E_{12} & E_{13} & E_{14} & E_{15} & E_{16} \\ E_{21} & E_{22} & E_{23} & E_{24} & E_{25} & E_{26} \\ E_{31} & E_{32} & E_{33} & E_{34} & E_{35} & E_{36} \\ E_{41} & E_{42} & E_{43} & E_{44} & E_{45} & E_{46} \\ E_{51} & E_{52} & E_{53} & E_{54} & E_{55} & E_{55} \\ E_{61} & E_{62} & E_{63} & E_{64} & E_{65} & E_{66} \end{bmatrix} \cdot \begin{bmatrix} \varepsilon_{xx} \\ \varepsilon_{yy} \\ \varepsilon_{zz} \\ \varepsilon_{yz} \\ \varepsilon_{zx} \\ \varepsilon_{xy} \end{bmatrix} \tag{2.5}$$

Isotropic stress vs. strain relation,

$$\begin{bmatrix} \sigma_{xx} \\ \sigma_{yy} \\ \sigma_{zz} \\ \sigma_{yz} \\ \sigma_{zx} \\ \sigma_{xy} \end{bmatrix} = \frac{E}{(1+\nu)(1-2\nu)} \begin{bmatrix} 1-\nu & \nu & \nu & 0 & 0 & 0 \\ \nu & 1-\nu & \nu & 0 & 0 & 0 \\ \nu & \nu & 1-\nu & 0 & 0 & 0 \\ 0 & 0 & 0 & 1-2\nu & 0 & 0 \\ 0 & 0 & 0 & 0 & 1-2\nu & E_{55} \\ 0 & 0 & 0 & 0 & 0 & 1-2\nu \end{bmatrix} \cdot \begin{bmatrix} \varepsilon_{xx} \\ \varepsilon_{yy} \\ \varepsilon_{zz} \\ \varepsilon_{yz} \\ \varepsilon_{zx} \\ \varepsilon_{xy} \end{bmatrix} \tag{2.6}$$

Structures analyzed in the serviceability limit state (SLS) utilize a linear-elastic stress strain relationship. This assumption allows for the calculation of deformations, natural frequencies, reaction forces, stresses and strains during the life of a structure. Linear elastic modeling is useful for determining the onset of yielding, but it cannot always predict the failure mechanism of a structure. Structures are normally designed in the ultimate limit state (ULS) to resist the rare load combination as designated in the structural design code. Perfect plasticity is a useful simplification assuming that the materials have sufficient ductility for ULS

load-bearing capacity. Modeling of reinforced concrete is especially difficult because the model must account for the softening plasticity of concrete while accounting for the plastic behavior of the reinforcing steel and the concrete-steel bond. Such complicated behavior requires a very specialized material model with a non-linear constitutive relation, thus simplifications are used whenever possible. Various non-linear analysis techniques exist for other cases, though linear-elastic analysis remains the most popular and most useful analysis type.

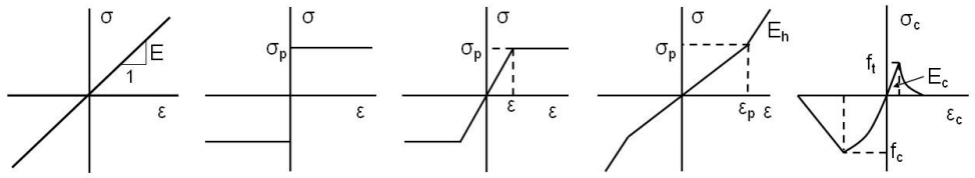

Fig.2. 2 Stress vs. strain relationship for: linear elasticity, perfect plasticity, elastic-perfectly plastic, hardening plasticity and concrete softening

(e) Meshing. In order to discretize a model for numerical analysis, the continuous body must first be meshed into discrete finite elements. During the meshing process, simplifications are made for the geometry of the continuous body. At curves along the surface of the body, the discretized model will have discontinuities in curvature if flat elements are used. An increased mesh density reduces the modeling error due to curvature discontinuities but a fine mesh has more elements and more DOF, thus requires more computational time. If the mesh density was infinite, the FE model geometry would be identical to the geometry of the continuous body, but such a system is not possible to model numerically. In reality, a balance exists between mesh density, desired model accuracy and computational time. As the element size is decreased, the FE response of a convergent FE model becomes increasingly accurate. During mesh refinement, an optimal mesh density is obtained when convergence is evident and the FE model is capable of modeling response to the desired accuracy.

FE general concept

(a) Equilibrium. In Force and moment equilibrium must be satisfied for each element. The static bending moment of a symmetric beam section normal to the x-axis and loaded about the x-z plane may be expressed as in terms of the stress components,

$$M = \int_A z\sigma_{xx} dA \tag{2.7}$$

Vertical shear force in a beam may be expressed as,

$$T = \int_A \sigma_{xz} dA \tag{2.8}$$

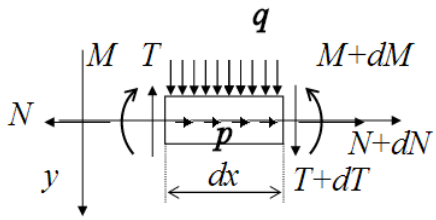

Fig.2. 3 Infinitesimal beam segment

Vertical force equilibrium of an infinitesimal beam segment,

$$\frac{dT}{dx} = q \tag{2.9}$$

Moment equilibrium of the infinitesimal beam segment,

$$\frac{dM}{dx} = T \tag{2.10}$$

Thus the differential equation for moment as a function of applied load is obtained,

$$\frac{d^2M}{dx^2} + q = 0 \tag{2.11}$$

Typical structural analysis employs matrix notation for the equation. For linear-elastic static analysis, the global force vector is the product of the global stiffness matrix and the nodal displacement.

$$\boldsymbol{f} = \boldsymbol{K}\boldsymbol{u} \tag{2.12}$$

In dynamic analysis, equilibrium equations account for body inertia, dissipative forces, internal loads carried by the structure and external loads (including reaction forces).

$$\boldsymbol{M}\ddot{\boldsymbol{u}}(\mathrm{t}) + \boldsymbol{C}\dot{\boldsymbol{u}}(\mathrm{t}) + \boldsymbol{K}\boldsymbol{u}(\mathrm{t}) = \boldsymbol{f}(\mathrm{t}) \tag{2.13}$$

The characteristic bending frequencies of a structure occur at equilibrium of inertial forces and internal forces caused by the structural deformation. Ignoring dissipative forces (e.g. damping) and assuming harmonic free-vibration, the eigenfrequencies (natural frequencies) and corresponding eigenmodes of the structure are obtained as follows,

$$\boldsymbol{M}\ddot{\boldsymbol{u}}(t) - \boldsymbol{K}\boldsymbol{u}(t) = 0 \tag{2.14}$$

Assuming harmonic free vibration,

$$\boldsymbol{u}(t) = \boldsymbol{U}\cos(\omega t + \alpha) \tag{2.15}$$

Taking the derivative with respect to time and substituting, the algebraic eigenvalue problem is obtained,

$$\left(\boldsymbol{K} - \omega^2 \boldsymbol{M}\right)\boldsymbol{U} = \boldsymbol{0} \tag{2.16}$$

The nontrivial solution to equation 2.16 is obtained from the characteristic equation,

$$\det\left(\boldsymbol{K}-\omega^2\boldsymbol{M}\right)=0 \tag{2.17}$$

For the eigenvalues, ω^2, obtained from equation 2.17, the modal matrix contains the corresponding mode shapes, Φ

$$\boldsymbol{\Phi}=\left[\Phi_1,\Phi_2\cdots\Phi_n\right] \tag{2.18}$$

The algebraic eigenvalue problem, equation 2.18, may be re-written for all n modes,

$$\boldsymbol{K\Phi}=\boldsymbol{M\Phi}\Lambda \tag{2.19}$$

With the corresponding eigenvalue matrix defined as, Λ,

$$\boldsymbol{\Lambda}=diag\left(\omega_1^2,\omega_2^2,\ldots,\omega_n^2\right) \tag{2.20}$$

(b) Kinematics. The kinematic relationship is assumed using theory. In the case of Euler-Bernoulli beam bending, the neutral axis is assumed to remain normal to beam cross sections during bending (thus neglecting shear deformation). Thus the longitudinal displacement, ux, is related to deflection due to bending, uz, for an infinitesimal beam segment as,

$$u_x=u_x^0-z\frac{du_z}{dx} \tag{2.21}$$

Considering the differential relationship between longitudinal displacement and longitudinal strain,

$$\varepsilon_{xx}=\frac{\partial u_x}{\partial x} \tag{2.22}$$

With beam curvature defined as,

$$\kappa = \frac{du_x}{dx^2} \tag{2.23}$$

Longitudinal strain (the only non-zero strain component) for an infinitesimal Euler-Bernoulli beam segment is related to deflection as,

$$\varepsilon_{xx} = \frac{du_x^0}{dx} - z\frac{d^2u_z}{dx^2} \tag{2.24}$$

$$\varepsilon_{yy} = \varepsilon_{zz} = \varepsilon_{xy} = \varepsilon_{yz} = \varepsilon_{xz} = 0 \tag{2.25}$$

(c) Constitutive relation. The relationship between stress and strain is defined by the constitutive relation. For Euler-Bernoulli beams, the linear elastic stress-strain relationship for isotropic materials described by Hooke's law is simplified due to kinematic assumptions, shear

$$\begin{bmatrix} \sigma_{xx} \\ \sigma_{yy} \\ \sigma_{zz} \\ \sigma_{yz} \\ \sigma_{zx} \\ \sigma_{xy} \end{bmatrix} = \frac{E}{(1+\nu)(1-2\nu)} \begin{bmatrix} 1-\nu & \nu & \nu & 0 & 0 & 0 \\ \nu & 1-\nu & \nu & 0 & 0 & 0 \\ \nu & \nu & 1-\nu & 0 & 0 & 0 \\ 0 & 0 & 0 & 1-2\nu & 0 & 0 \\ 0 & 0 & 0 & 0 & 1-2\nu & E_{55} \\ 0 & 0 & 0 & 0 & 0 & 1-2\nu \end{bmatrix} \cdot \begin{bmatrix} \varepsilon_{xx} \\ 0 \\ 0 \\ 0 \\ 0 \\ 0 \end{bmatrix} \tag{2.26}$$

Often the uniaxial stress state is the only stress state of interest and is simplified as,

$$\boldsymbol{\sigma} = \boldsymbol{E}\boldsymbol{\varepsilon}_{\boldsymbol{xx}} \tag{2.27}$$

There are preceding derivations as same as kinematic and constitutive derivations for plates are available in Ottosen and Petersson (1992).

(d) Discretization. The finite element chosen to discretize a structural member must satisfy the completeness and compatibility requirements. A shape function is assigned to a finite element and is chosen to represent the behaviour of interest.

For beam bending, completeness and compatibility are defined in Ottosen and Petersson (1992) as follows,

Completeness:

- The approximation for the deflection uz must be able to represent an arbitrary rigid-body motion.
- The approximation for the deflection uz must be able to represent an arbitrary curvature. Compatibility:
- The approximation for the deflection uz must vary continuously with continuous slopes over the element boundaries.

Shape functions describe the deflection of the beam element as a function of the longitudinal displacement. The “simplest possible beam element” capable of satisfying completeness and compatibility for Euler-Bernoulli beam theory is the cubic polynomial. Higher order polynomial terms are used for higher order elements.

(e) Boundary Conditions. Global force equilibrium requires equilibrium of all forces and moments. The global force vector of equation 2.12 is the sum of the boundary force vector, F_b, and the load vector, F_l

$$\boldsymbol{F} = \boldsymbol{F_b} + \boldsymbol{F_l} = \boldsymbol{Ku} \tag{2.28}$$

Static boundary conditions and kinematic boundary conditions constitute the global boundary conditions. For beam loading, the static boundary conditions are given by shear force T, and moment, M at the ends of the beam while the kinematic boundary conditions are described by the deflection, u_z, and slope, du_z/dx, at the ends of the beam.

Error analysis

Although the FEM technique estimates that was close to the exact analytical solution, there was a discrepancy, or error, because the numerical method involved an approximation (FRISWELL M.I. & MOTTERSHEAD J.E,1996). Actually, we can find optimization method that is available to solute to compute the error exactly. For

many engineering problems, we cannot obtain analytical solutions. Therefore, we cannot compute exactly the errors associated with our numerical methods. In these cases, we must settle for approximations or estimates of the errors.

2.1.4.1 Error definitions

Numerical errors arise from the use of approximations to represent exact mathematical operations and quantities (Chapra, Steven C., and Raymond P. Canale.1998). These include truncation errors, which result when approximations are used to represent exact mathematical procedures, and round-off errors, which result when numbers having limited significant figures are used to represent exact numbers (Link, M. 1998). For both types, the relationship between the exact, or true, result and the approximation can be formulated as

$$True\ value = approximation + error \tag{2.29}$$

By rearranging it, we find that the numerical error is equal to the discrepancy between the truth and the approximation, as in

$$E_t = true\ value\text{-}approximation \tag{2.30}$$

Where E_t is used to designate the exact value of the error. The subscript t is included to designate that this is the 'true' error. This is in contrast to other cases, as described shortly, where an 'approximate' estimate of the error must be employed.

A shortcoming of this definition is that it takes no account of the order of magnitude of the value under examination. There is one way to explain the magnitudes of the quantities is to normalize the error to the true value, as in

$$True\ fractional\ relative\ error = \frac{true\ error}{true\ value} \tag{2.28}$$

The relative error can also be multiplied by 100 percent to express it as

$$\varepsilon_t = \frac{true\ error}{true\ value} \times 100\% \tag{2.30}$$

Where ε_t designates the true percent relative error.

2.1.4.2 The error of Finite element method

Model updating is essentially a process of adjusting certain parameters of the finite element model. But should be aware of numerous sources of modelling error and make necessary adjustments paying particular attention to those aspects of the model that cannot be corrected by changing the values of selected model-updating parameters. Examples of such errors, listed in below, are related to the

mathematical structure of the model and generally referred to as model-structure errors. The errors listed under category (3) are typical of those that can be corrected by model updating（Mottershead, John E., Michael Link, and Michael I. Friswell.2011）.

(1) Idealization errors resulting from the assumptions made to characterize the mechanical behaviour of the physical structure. Such errors typically arise from:

- simplifications of the structure, for example, when a plate is treated like a beam, which might or might not be erroneous depending on the length to width ratio of the plate and the frequency range to be covered,
- inaccurate assignment of mass properties, for example, when distributed masses are modelled with too few lumped masses or when an existing eccentricity of a lumped mass is disregarded,
- when the finite element formulation neglects particular properties, for example, when the influence of transverse shear deformation or warping due to torsion in beam elements is neglected,
- errors in the connectivity of the mesh i.e. some elements are not connected or are connected to a wrong node,
- erroneous modelling of boundary conditions, for example, when an elastic foundation is assumed to be rigid,
- erroneous modelling of joints, for example, when an elastic connection is assumed to be rigid (clamped) or when an eccentricity of a beam or a plate connection is omitted from the model,
- erroneous assumptions for the external loads,
- erroneous geometrical shape assumptions,
- a non-linear structure assumed to behave linearly.

(2) Discretization errors introduced by numerical methods such as those inherent in the finite element method, for example:

- discretization errors when the finite element mesh is too coarse so that the modal data in the frequency of interest is not fully converged,
- truncation errors in order reduction methods such as static condensation,
- poor convergence and apparent stiffness increase due to element shape sensitivity.

(3) Erroneous assumptions for model parameters, for example:

- material parameters such as Young’s modulus or mass density,
- cross section properties of beams such as area moments of inertia,
- shell/plate thicknesses,

- spring stiffness or
- non-structural mass.

When the model includes idealization and discretization errors it may only be updated in the sense that the deviations between test and analysis are minimized. The same happens when the selected correction parameters are not consistent with the real source and the location of the error. The parameters in such cases may lose their physical meaning after updating. A typical result of updating such inconsistent models is that they may be capable of reproducing the test data but may not be useful to predict the system behaviour beyond the frequency range used in the updating. Similarly, they may not be able to predict the effects of structural modifications or to serve as a substructure model to be assembled as part of a model of the overall structure.

The purpose of all structural analyses to predict the structural response can be achieved if three kinds of modelling errors are minimized with respect to the given purpose of the structural analysis. Models which fulfil these requirements shall be called validated models. Model quality must therefore be assessed in three steps:
Step 1: Assessment of idealization and numerical method errors (model structure errors) prior to parameter updating.
Step 2: Correlation of analytical model predictions and test results and selection of correction parameters.
Step 3: Assessment of model quality after parameter updating. Since a unique solution cannot be expected, this requirement must be related to the intended purpose for which the model is used, for example:

•to predict the system behaviour to types of load or response other than those used in the test,
•to predict the system behaviour beyond the frequency range and/or at degrees of freedom other than those used for updating,
•to predict the effects of structural modifications,
•to check if the model, when used as a substructure within an assembled complete structure, will improve the response of the whole model.

2.2. Numerical optimization

Definition of problem

Numerical optimization is an important tool in the analysis of physical systems. A basic concept of optimization process is the so called objective (function), a quantitative measure of the performance of the system under study. This objective could be profit, time, potential energy, or any quantity or combination of quantities that can be represented by a single number. The objective depends on certain characteristics of the system, called variables or unknowns. Our goal is to find values of the variables that optimize the objective. Often the variables are restricted, or constrained, in some way. The process of identifying objective, variables, and constraints for a given problem is known as modelling. Construction of an appropriate model is the first step in the optimization process. If the model is too simplistic, it will not give useful insights into the practical problem. If it is too complex, it may be too difficult to solve. Once the model has been formulated, an optimization algorithm can be used to find its solution, usually with the help of a computer. There is no universal optimization algorithm but rather a collection of algorithms, each of which is tailored to a particular type of optimization problem. The responsibility of choosing the algorithm that is appropriate for a specific application often falls on the user. This choice is an important one, as it may determine whether the problem is solved rapidly or slowly and, indeed, whether the solution is found at all. After an optimization algorithm has been applied to the model, we must be able to recognize whether it has succeeded in its task of finding a solution. In many cases, there are elegant mathematical expressions known as optimality conditions for checking that the current set of variables is indeed the solution of the problem. If the optimality conditions are not satisfied, they may give useful information on how the current estimate of the solution can be improved. The model may be improved by applying techniques such as sensitivity analysis, which reveals the sensitivity of the solution to changes in the model and data. Interpretation of the solution in terms of the application may also suggest ways in which the model can be refined or improved (or corrected). If any changes are made to the model, the optimization problem is solved anew, and the process repeats.

Solution procedures

An optimization or a mathematical programming problem can be stated as follows:

$$\text{To find } \boldsymbol{x} = \begin{Bmatrix} x_1 \\ x_2 \\ \vdots \\ x_n \end{Bmatrix} \quad \text{Which minimize } \mathbf{f}(\boldsymbol{x}) \tag{2.31}$$

Subject to the constraints:

$$\begin{aligned} g_i(\boldsymbol{x}) &\le 0 \qquad i = 1,2,\ldots m \\ l_j(\boldsymbol{x}) &\le 0 \qquad j = 1,2,\ldots p \end{aligned} \tag{2.32}$$

where $\boldsymbol{x}$ is an n-dimensional vector called the design vector, $f(\boldsymbol{x})$ is called the objective function, and $g_i(\boldsymbol{x})$ and $l_j(\boldsymbol{x})$ are known as inequality and equality constraints, respectively. The number of variables n and the number of constraints m and/or p need not be related in any way. This type problem is called a constrained optimization problem. If the locus of all points satisfying $f(\boldsymbol{x})$ = a constant c, is considered, it can form a family of surfaces in the design space called the objective function surfaces. When drawn with the constraint surfaces as shown in Fig 2.4 we can identify the optimum point (maxima). This is possible graphically only when the number of design variables is two. When we have three or more design variables because of complexity in the objective function surface, we have to solve the problem as a mathematical problem and this visualization is not possible.

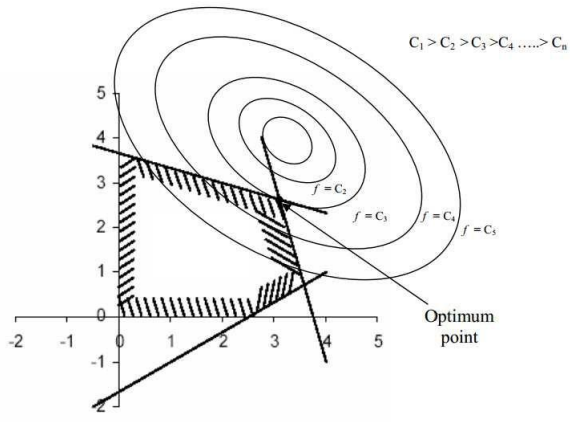

Fig.2. 4 Geometrical representation of the optimization problem

(a) Global and local minima. In the case of most deterministic optimization algorithms, local hill-climbing is used to find the location of a local minimum. Different algorithms utilize different strategies to maximize efficiency while traversing the objective space in search of the local minimum. One of the challenges of discrete optimization methods is to efficiently search for a local minimum in a region where the gradient of the objective function is near zero. Gradient based methods face ill-conditioning for the Jacobian and Hessian matrices and may encounter numerical difficulties at iteration steps. For such cases, conditioning should be monitored to ensure algorithm stability.

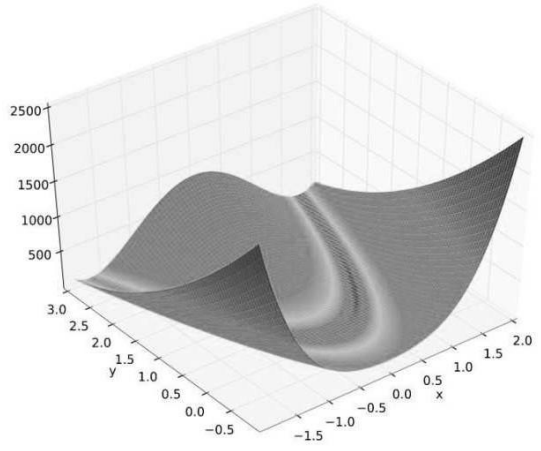

Fig.2. 5 Rosenbrock function

Non-linear functions of many variables can contain many local minima in addition to the global minimum. Most deterministic algorithms will converge to the local

minimum in the region of local convexity by local hill-climbing, but will fail to converge to the global minimum. When using a discrete function for which the analytical formulation is unknown, the shape of the objective function cannot be predicted and many local minima may exist. If the parameter space of the function is very large, finding a solution for global optimality is troublesome and can be computationally expensive. For such a problem, stochastic optimization methods are useful for determining the vicinity of a global optimum. The Nelder-Mead Simplex algorithm is capable of escaping local minima in some cases and can even handle discontinuities according to Coleman and Zhan（2007）. Hybrid algorithms that utilize a rough stochastic global optimality search in combination with local hill-climbing for refinement of the final optimal solution are ideal for practical problems.

(b) Least square problem. The Nonlinear Least-Square Problem is an iterative method which aim to the minimization of a nonlinear function. In the particular chase of the optimization problem it's called Objective function. It is generally presented in the following form:

$$\min_{\boldsymbol{x}} \quad \frac{1}{2}\sum_{j=1}^{n} \mathrm{r}_{\boldsymbol{i}}(\boldsymbol{x})^{2} = \frac{1}{2}\left\|\mathrm{r}_{\boldsymbol{i}}(\boldsymbol{x})\right\|^{2} \tag{2.33}$$

where r_i represent the objective function, a nonlinear function, of the n-vector of variables x. As shown in figure 2.6, due to its nonlinearity, the objective function may have multiple local minima, hence, finding the global minima can be very hard and requires an iterative procedure).

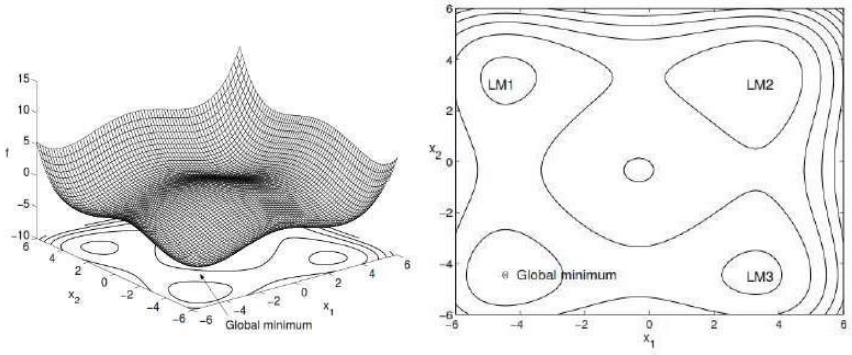

(a) *(b)*

Fig.2. 6 Objective function: (a) surface plot; (b) contour plot.

An engineering application of this algorithm occurs in the fitting of model function to experimental data. Suppose θ(x) represent the model function, depending on the x, parameter's vector, and b_j the corresponding experimental data, then each individual residual $r_j(x)$, defined as θ(x) - b_j, measure the discrepancies between the predicted and the observed outputs of the system (i.e. civil structure).

Defining the Jacobian of r as the matrix containing the first-order derivatives of the residual function $r_j(x)$ in the form:

$$J(x)_{ii} = \frac{\delta r_j(x)}{\delta x_j} \tag{2.34}$$

and the Hessian as the matrices containing the second-order derivatives of $r_j(x)$ in the form:

$$H_i(x)_{ik} = \frac{\delta^2 r_j(x)}{\delta x_i \delta x_k} \tag{2.35}$$

Therefore, the gradient and the laplacian of the objective function can be expressed as:

$$\nabla \boldsymbol{f}(\boldsymbol{x}) = \boldsymbol{J}(\boldsymbol{x})^T \boldsymbol{r}(\boldsymbol{x}) \tag{2.36}$$

$$\nabla^2 \boldsymbol{f}(\boldsymbol{x}) = \boldsymbol{J}(\boldsymbol{x})^T \boldsymbol{J}(\boldsymbol{x}) + \sum_{j=1}^{n} r_j(x) H_j(x) \tag{2.37}$$

From equation 2.37 the Hessian is shown as the combination of first-order and second-order derivatives of the objective function. Since it is usually assumed that the residual at the solution would be small, it is typical to consider the first-order derivatives dominating over the second-order ones. Therefore, instead of using a quadratic model formed in the Newton method, which as a faster convergence but involves the second-order derivatives, the Gauss-Newton method is here preferred and applied trough a specific Matlab code (see Appendix), since it has a lower computational weight.

2.3 Operational modal analysis

2.3.1 Vibration measurement

Proper execution of vibration measurements is the basis of a successful FE model update. In order to produce good results, a clear interpretation of the behavior of the structure, i.e. an appropriate identification of the main eigenmodes, is needed. In order to present a solid dissertation of the OMA, the following chapter details the precautions taken and the techniques used during the experimental campaign performed by the "University of Leuven" and the "Universidad Politecnica de Madrid"(Palacios J. G., et al. 2013) and the “Politecnico di Milano”. Several bridges have been tested. Among them is the and “Magaz Viaduct” and "Marghera bridge", on which this thesis has been developed.

2.3.1.1 Equipment setup

It is generally not feasible on an experimental campaign to have all measurement nodes to be measured in just one setup, as the number of the channels in the measuring system available is usually limited compared to the measurement nodes. Therefore, the measurement nodes shall be divided into several experimental setups. In order to combine the individual local experimental mode shape vectors from each setup into a global mode shape vector, some common nodes must be shared among all setups.

2.3.1.2 Measurements nodes

The measurement nodes are where the vibration responses (e.g. accelerations, velocities, displacements, strain) of the structure are measured. In the current document on the tested bridge (Chapter 4 and 5), only the accelerations in vertical direction were measured. The locations of the measurement nodes on the bridge are decided according to the vibration characteristics that are of interest. For modal-based damage identification methods, the structural damage is identified based on the changes of modal parameters (e.g. frequencies, mode shapes). Therefore, the measurement nodes shall be placed at (but not limited to) the location where the damage is likely to occur.

2.3.1.3 Reference node or Reference Sensor

Reference nodes are the measurement nodes that are common among the entire the experimental setup. These are used as the references for combining the local mode shape vectors of each setup. Accordingly, the sensors that will have the fixed locations at the reference nodes for the whole measurement duration are named reference sensors. When there is only one reference node, the local mode shapes from each individual experimental setup are scaled respectively according to this common reference node in order to be combined into the global experimental mode shape. When there is more than one reference node, a least square minimization between different setups for the modal displacements at the reference nodes is introduced in order to obtain a unique scaling factor for each individual setup (Reynders E. et al. 2011).

Due to their nature as 'references', these nodes shall not be placed at the nodes of the mode shapes where the modal displacement is zero. Neither shall they be placed at the nodes where the modal displacements are close to zero since the effect of the experimental errors, which are more significant at the nodes in vibrations with small amplitude, will be unavoidably magnified for the other nodes due to scaling. This will lead to unacceptable results of the combined global mode shapes. Therefore, a best choice is to place the reference nodes at the anti-nodes of a mode shape (i.e. where the amplitude of the modal displacement is a maximum). However, a compromise must be made when there are several modes of interest and the number of the reference sensors is limited.

2.3.1.4 Reference Channels

Reference channels of the reference-based stochastic subspace identification (SSI) methods are the chosen channels where data of all the other channels are projected (Peeters B., De Roeck G. 1999). The SSI method is based on the assumption that the excitation can be considered a white noise (a random signal or process with at power spectral density). As a result, the output covariance is in fact the impulse response of a deterministic linear time-invariant system which represents the same dynamic system as that of the original structure but with difference input and output quantities. The input is the impulse force at all the measurements channels and the output is the covariance calculated between the data of all measurement channels. Therefore, an analogy can be made between the input-output identification (such as in the EMA) and the output-only identification (such as in OMA) (Peeters B., De Roeck G 2001). By using the SSI method, the stochastic state-space model can be identified and the modal parameters (frequency, damping ratios, and mode shapes) can be extracted. In the reference-

based SSI method, the stochastic model is reconstructed which leads to the following modifications in the analogous deterministic system: the impulse input is applied at the reference channels instead of all the measurements channels, while the output is the covariance between the data of all the measurement channels and those of the reference ones. It is realized by projecting the data of all the channels into a limited number of the reference channels, which gives rise to the concept of the reference channels.

As mentioned in (Peeters B., De Roeck G. 1999), by using the reference-based SSI methods, not only the computational efficiency is improved but also more accurate results can be achieved since "the lower quality sensors are partially omitted" if "the 'best' sensors are selected as references". As the reference sensors are placed at the reference nodes where the mode shapes of interest are well present, they are a good choice of the reference channels considering the relative low signal-to-noise ratios at these channels.

2.2.1.4.5 Roving Sensor

Roving sensors have their locations changed from setup to setup. In each setup, their location shall generally be well distributed over the whole structure instead of being concentrated at a small part. The reason for this is that when the roving sensors focus on a small part of the structure, it will be difficult to identify some modes that happen to have almost zero modal displacements in certain setups at the locations of the roving sensors.

2.2.1.4.6 Measurements Duration

Measurement duration is the length of the data that is acquired for each setup. A rule of thumb for estimation of the measurement duration is 1000 times the fundamental period of the tested bridge. For a bridge with the fundamental frequency of 3Hz, it will be 333 seconds or around 5 mins. However, longer measurement duration reduces the uncertainty of the identification results, especially when data is very noisy (or the dynamic system is not stationary).

2.3.2 Techniques of modal identification

Modes are inherent properties of a structure that are determined by its material properties (mass, damping and stiffness) and boundary conditions. Each mode is defined by eigenfrequency, modal damping, and modal shape (Its modal

parameters). If either the material properties or the boundary conditions of a structure change, its modes will change. This happens for every kind of structure, whether it be a fishing pole, a car, or a suspension bridge. Since having the modal properties means having an accurate description of the structure, it is possible to understand what to change in the design of the particular object in order to obtain the best modal response in terms of safety, comfort, durability etc. Moreover, it is possible to explain the changing of modal data over time as a deterioration of the modal properties. This provides structural health monitoring of the structure over time. In the last 30 years, development in the field of personal computing and in the available acquisition tools, starting from the previous achievements in the fields of Mechanical and Electronic Engineering, even Civil Engineers have begun to feel the need to apply Vibration-Based Modal Analysis to civil structures as a Structural Health Monitoring (SHM) Technique.

2.3.2.1 Experimental Modal Analysis

Experimental modal analysis (EMA) is a process whereby the modal properties of a structure are extracted. EMA makes use of a forced input excitation as well as the measured dynamic response of the structure. The excitation is typically created with impact hammers, shakers, or drop weights while the output dynamic response is usually measured using traducers in order to get displacements, velocity, and acceleration. Therefore, EMA is based on the estimation of a set of Frequency Response Functions (FRFs) relating the applied force and the corresponding response at several pairs of points along the structure with enough high spatial and frequency resolution. The construction of FRFs requires the use of an instrumentation chain for structural excitation, vibration measurements, data acquisition and signal processing. Usually the FRFs evaluation is made through appropriate software for analysis and signal processing.

In case of medium size structures, the excitation can be induced by an impulse hammer that provides a wide-band input able to simulate different modes of vibration. As an alternative, a large variety of impulse devices have been built in order to provide a variety of input signals (e.g. random, sinusoidal, etc.) which allow a direct identification of the mode shapes. However, if the subjects of the SHM are Civil Structures, heavy excitation equipment is needed in order to gain a controlled excitation. The main drawback of this is a difficulty to measure the applied force and a considerable increase of costs.

Operational modal analysis (OMA) is a technique whereby the modal properties are extracted by analyzing its dynamic output response to its operational input excitation. In other words, OMA analyzes a structure's response based solely on ambient loads such as wind and traffic that it is exposed to.

The ambient excitation commonly has multiple input natures and wide band frequency content, stimulating a significant number of modes of vibration. For simplicity, output-only modal identification methods (i.e.OMA) assume the excitation input as a zero mean Gaussian white noise this means that the real excitation can be interpreted as the output of a suitable filter excited with that white noise input.
There are two main groups of output-only modal identification methods: non parametric methods developed in a frequency domain, and parametric methods developed in a time domain.

2.3.2.2 Frequency Domain

Frequency domains are based on the simple relation between the input and output Power Spectral Density (PSD) of a random process. The simplest technique in frequency domain is the Peak Picking (PP) technique (Garrett, D. S.et.al. 2011). in which the natural frequencies are directly obtained from the choice of peaks in the PSD graph. If the modes are well separated, this technique will lead to acceptable estimates (Ventura C.E., Horyna T. 1997). Despite the simplicity and the speed of this method, it presents some limitations. Among these are low accuracy for complex structures due to the dependency of the result to the resolution of PSD spectrum, low accuracy in calculation of the damping ratio, and no direct extraction of natural system mode shapes since only Operational Detection Shapes (ODS) are calculated. An improved frequency domain method was presented by Brincker et al. (2000) called Frequency Domain Decomposition (FDD). In this technique Singular Value Decomposition (SVD) of the output PSD in different frequencies is used as the Mode Indicator Function (MIF). In addition to identifying the modes, the noise and signal space gets separated. By using FDD, the natural frequencies and mode shapes can be obtained. Due to simplicity and applicability of FDD method in OMA, Brincker (2007) presented final evolution of this technique that proposed an automatic instruction for modal identification based on FDD. Nowadays, this instruction is implemented in commercial modal analysis software.

2.3.2.3 Time Domain

The time domain parametric methods involve the choice of an appropriate mathematical model to idealize the dynamic structural behavior and the identification of the values of the modal parameters. To that end the model fits, as much as possible, the experimental data following some appropriate criteria. These methods can be directly applied to discrete response times series evaluated using the Fast Fourier Transform (Brincker R. et al. 1992). The most applied method is the Ibrahim Time Domain (ITD) (Ibrahim S.R., Mikulcik E.C. 1977), the Covariance-Driven Stochastic Subspace Identification (SSI-COV) (Caetano E. et al. 2007) and an alternative method of the last one that allows direct application to the response time series, i.e. the Data-Driven Stochastic Subspace Identification (SSI-DATA) (Van Overschee, P., De Moor P.L. 1996).

As a summary of the presented chapter, figure 1.1 shows a schematic representation of output-only identification methods (Cunha A. et al. 2006).

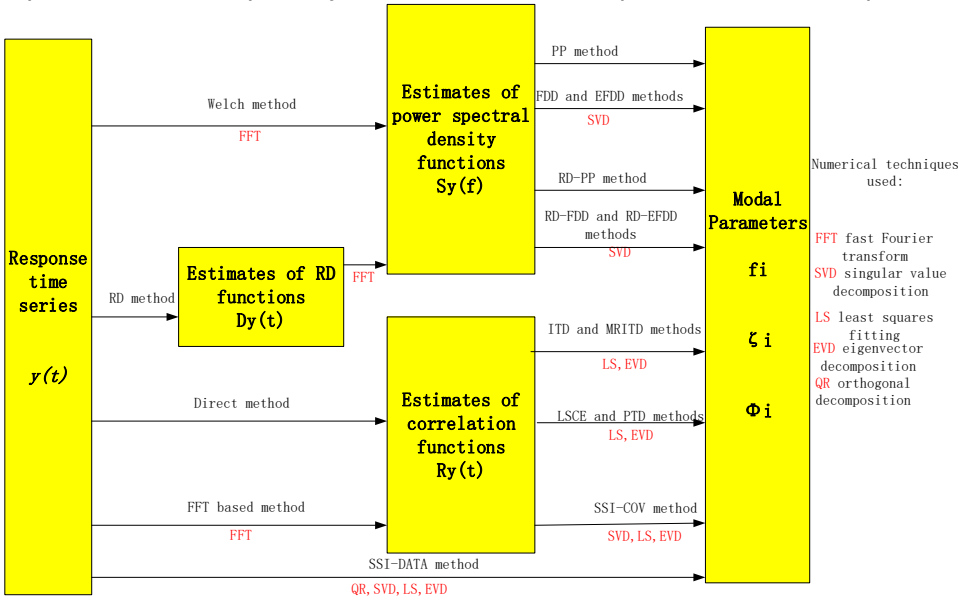

Fig.2. 7 A schematic representation of output-only identification methods

2.3. Finite Element Model Updating

Overview

Historically, FE model updating emerged in the 1990s as a tool for correcting invalid assumptions about a model using primarily vibration test data. FE model updating evaluates a FE model and compares the output target responses to experimental

data. Uncertain input parameters are then iterated until more accurate target responses are obtained. Many iterations may be required for convergence; thus models should be simplified as much as possible in order to reduce the computational time at each of the iterations. The improved FE model can then be used for assessment of the structure. Improved modelling is of great importance to the design, construction and maintenance of civil engineering structures.

Both direct and sensitivity based FE model updating techniques exist and have been used in the fields of civil engineering, mechanical engineering and aeronautics. Direct FE model updating techniques can directly update the global mass and stiffness matrices in one step so that the FE model will be capable of reproducing the measured eigenfrequencies and mode shapes, though the resulting FE model may not maintain structural connectivity according to Jaishi and Ren (2007). Due to lack of mode shape data and the requirement of a meaningful result, direct FE model updating techniques are beyond the scope of this study. The sensitivity-based parameter updating approach is useful for identifying structural parameters that can directly affect the response characteristics of the structure. Traditionally, only dynamic responses are used for FE model updating, two examples include Zhang et al. (2001) and Zivanovic et al. (2007). FE model updating has been expanded to include static load tests for the present study. Thus, both the dynamic response and the results of static load tests were used for FE model updating. Many modern major bridges are constructed with consideration of the entire service life and thus include sensors for monitoring strain, acceleration, temperature and wind data. The New Svinesund Bridge (Schlune, H.et.al.2009). includes many sensors capable of remote monitoring that provide measurements that can be used for FE model updating. Such monitoring can be used for routine structural assessment with an updated FE model.

Detailed information regarding FE model updating is available in Friswell and Mottershead (1995).

Model Updating as optimization problem

The following flow chart demonstrates the concept of FE model updating.

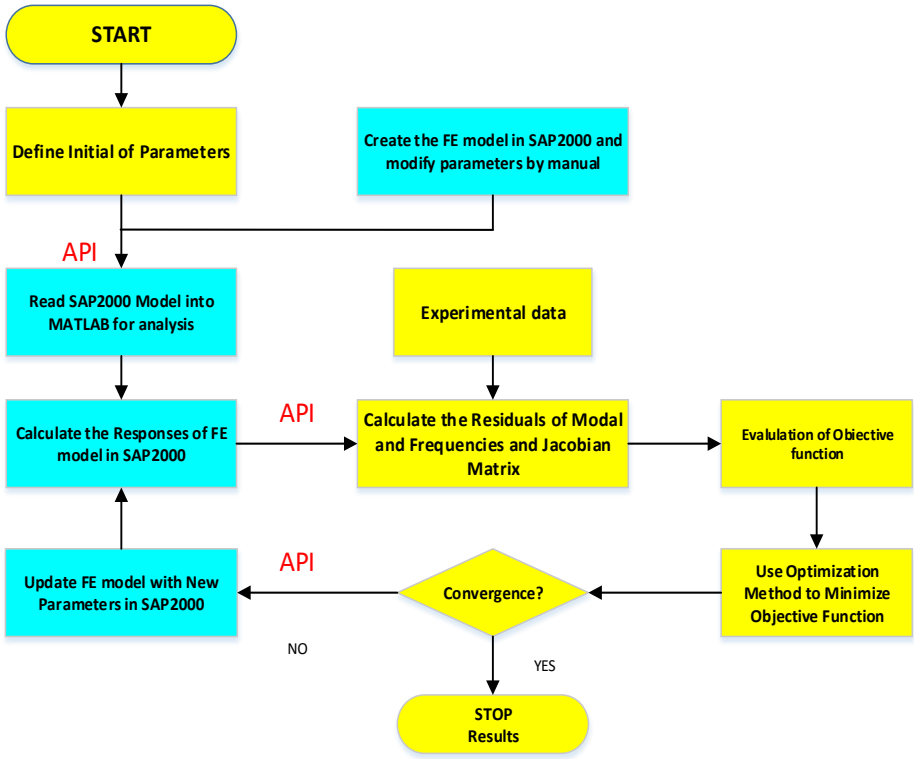

Fig.2. 8 Flow chart of the optimization problem

(a) Nonlinear least square problem. The objective function is represented by an ordinary least square problem is defined as a sum of squared difference:

$$f(\theta)=\frac{1}{2}\sum_{j=1}^{n}\left[z_j(\theta)-\tilde{z}_j\right]^2=\frac{1}{2}\sum_{j=1}^{n}\left[r_j(\theta)\right]^2 \tag{2.38}$$

where each $z_j(\theta)$ represent an analytical modal quantity which is a nonlinear function of the optimization problem. $\tilde{z}_j$ refers to the measured value of the quantity z. In order to obtain an unique solution, the number m of residuals $r_j(\theta) = z_j(\theta)-\tilde{z}_j$ should be greater than number n of unknowns θ.

Equation 2.38 represents the basic least squares function, but several variants exist and are tried out in literature. The specific process, needed to reach a good solution in the optimization problem, require a least square problem. In order to take into

account, the relative importance of the different types of residuals and their accuracy the residual vector has to be multiplied with a weighted matrix.

(b) Weighting. As stated before, the least squares problem formulation allows the residuals to be weighted separately. In particular, in the optimization process, different weight can be assigned to the residual vector of eigenfrequencies and mode shapes to be able to choose witch of them is better to prioritize in order to get a better matching between numerical and experimental modal data. Usually the experimental eigenfrequencies are the most accurate experimental data and due to their high sensitivity to the physical properties of the structure, they have a favorable effect on the problem condition. Experimental mode shapes on the other hand are usually much noisier, therefore an appropriate weighting is necessary. Furthermore, only the relative proportion of the weighting factors is important, not their absolute values. The weighting factor influence the results only in case of over-determined set of equation, i.e. when the number of residual is higher than the number of designed variables. The ability to weight the different data sets gives the method its power and versatility, but at the same time requires engineering insight to provide the correct weights. In a weighted least squares problem the following minimization problem is solved:

$$\min \frac{1}{2}\left[r_j(\theta)\right]^T W\left[r_j(\theta)\right] = \frac{1}{2}\left\| W^{\frac{1}{2}} r_j(\theta)\right\|^2 \tag{2.39}$$

with W the weighting matrix.

W is included to account the importance of each individual term in the residual vector and, even if it's difficult to estimate, it should include scaling in order to equalize the effect of amplitude (Palacios J. G., et al. 2013). Due to modeling and measurement errors, different results will be obtained for different weighting factors, hence no unique ideal solution exists. The most likely and realistic result should be selected based on engineering insight. Appropriate weights can be identified in an iterative way, for instance, if for the obtained results the eigenfrequencies correspond fully but the mode shapes show a considerable discrepancy, it can be assumed that too much weight is given to the eigenfrequency residuals. In the other hand, if a very non-smooth result is obtained, which refers to a too high influence from the mode shape measurements error, that correspond with eigenfrequencies which deviate much from experimental eigenfrequencies, the weight for the mode shapes should be decreased. However, other options can be found in literature

regarding the choice of the Weighting matrix. For instance, the weighting matrix can be chosen as the inverse of the covariance matrix of the experimental error (Unger J.F., et al. 2005).

(c) Residual vector. The discrepancies between the numerical modal data are contained in the residual vector r obtained from the least square problem:

$$\min \frac{1}{2} \left\| r_j(\theta) \right\|^2 \tag{2.40}$$

In general, two approaches exist, based on whether frequency domain or modal data are used for correlation. In both cases several types of residuals exist (Teughels A. 2003). However, in civil engineering, the use of modal data is most often applied since, for heavy civil structures like bridges, the frequency response functions are not available over a wide frequency domain (Cunha A. et al. 2006). Therefore, the residual vector contains the differences in the identified modal, such as eigenfrequencies and mode shapes. As stated before, those will be weighted in order to find a better solution of the objective function.

Whatever is the algorithm used to solve the nonlinear least square problem, it doesn't get any information about the correlation between numerical and experimental modal data. Therefore, in order to be compared, the modal data must be paired correctly such that they are related to the same modes. Arranging the eigenfrequencies in ascending order is not enough since, due to incorrect parameters estimates, the order of the modes, in both dynamic models (numerical and experimental), can differ. In particular, due to the iterative updating process, the order of the numerical modes can change; hence it has to be checked at each step. Furthermore, depending on the measurements setup used during the vibration tests, some modes may be incompletely measured, e.g. because there are not enough accelerometers or bad placed ones.

The most commonly and easy way used procedure to pair mode shapes vector correctly is based on the Modal Assurance Criterion (MAC):

$$\text{MAC}\ \left(\phi_i, \tilde{\phi}_j\right) = \frac{\left|\phi_i^T, \tilde{\phi}_j\right|^2}{\left(\phi_i^T, \tilde{\phi}_i\right)\left(\phi_j^T, \tilde{\phi}_j\right)} \tag{2.41}$$

with ϕ_i and $\tilde{\phi}_j$ a numerical and experimental mode shape vector, respectively. The MAC value is a correlation coefficient ranges from 0 to 1; a MAC value of 0 indicates that two mode shapes are completely uncorrelated, while a MAC value of 1 indicates perfect correlation between them. In general, a MAC value above 0.80-0.85 indicates a very good match while an if it is less than 0.4 is considered a poor match. Although, for many structure, the MAC value is unreliable in the correlation of local modes because they are described by only very few DOFs.

(d) Eigenfrequency. The residual of each eigenfrequency is formulated as:

$$r_f(\theta) = \frac{\lambda_j(\theta) - \tilde{\lambda}_j}{\tilde{\lambda}_j} \qquad j \in (1,2,\ldots m_f) \tag{2.42}$$

with eigenvalues $\lambda_j(\theta) = (2\pi\upsilon_j)^2$ and eigenfrequency λ_j, υ_j and $\tilde{\lambda}_j$ denote the numerical and corresponding experimental eigenvalues, respectively. M_f refers to the number of identified eigenfrequencies that are used in the updating process. Relative difference are taken in $r_f(\theta)$ in order to obtain a similar amplitudes for each eigenfrequency residual, since the higher the eigenfrequency, the higher the absolute difference between the analytical and experimental quantity will be. Therefore, in the first part of the residual vector are contained the differences between the numerical and experimental undamped eigenfrequency. The eigenfrequencies provide global information of the structure and they are very sensitive with respect to its stiffness properties. They usually are the most accurately measured and relatively easy to identified, hence, the eigenfrequencies are indispensable quantities to be used in the updating process.

(e) Mode shapes. The Although eigenfrequencies contain very valuable information they must be completed with spatial information about the dynamic behavior of the structure. In particular, these are required in order to identify local parameters in symmetrical structures. Therefore, the residual vector is extended with differences in mode shape displacement. Each mode shape residual is formulated as:

$$r_s(\theta) = \frac{\phi_j^l(\theta)}{\phi_j^r} - \frac{\tilde{\phi}_j^l}{\tilde{\phi}_j^r} \qquad j \in (1,2,\ldots m_s) \tag{2.43}$$

with $\phi_j(\theta)$ and $\tilde{\phi}_j$ the numerical and corresponding experimental mode shape vector, respectively. $\phi_j^l(\theta)$ and ϕ_j^r denote single components of the vector $\phi_j(\theta)$, the former refers to any component that is used in the updating process, the latter to a reference component. m_s denotes the number of identified mode shapes used in the updating process.

Civil engineering structure, due to their size, are most often measured in operational conditions such that the exciting forces come from unknown ambient sources like wind, traffic, etc. Due to this, the experimental mode shapes can only be measured for the translational degrees of freedom and cannot be absolutely scaled. Therefore, the experimental and the numerical mode shapes are normalized to 1 in a reference node, the one having the largest amplitude, chosen for each node separately. Due to the normalization, all modes contribute with a similar amplitude. Generally, if they are well measured, all the nodes are selected for the updating and, if necessary, the mode shapes could be smoothed in order to spread the measured noise all over the structure and obtain a smooth shape. Compared to the eigenfrequencies, the mode shapes are less sensitive to the stiffness parameters of the structure, also they need a large number of measurements location in order to be characterized and provide sufficient resolution for determining local parameters.

In conclusion, even if the mode shapes are more difficult to identify and more affected by noise then the eigenfrequencies, they are indispensable quantities in the updating process notwithstanding their unfavorable effect on the stability of the optimization problem.

Sensitivity matrix

The nonlinear least square problem (see Appendix) is solved with an iterative sensitivity based optimization method. Therefore, the Jacobian matrix needs to be calculated at each iteration. The Jacobian is the best approximation of a nonlinear function in a certain point, it contain the first-order derivatives of each residual r in the residual vector with respect to each chosen variables θ

$$[J_\theta] = \begin{bmatrix} & \vdots & \\ \cdots & \dfrac{\delta r_j}{\delta \theta_i} & \cdots \\ & \vdots & \end{bmatrix} \quad \text{with} \quad \begin{cases} j = 1,2,\ldots m \\ i = 1,2,\ldots n \end{cases} \tag{2.44}$$

with δr_j the first-order derivatives of the residual vector with respect to each designed variable θ_i. Regarding the optimization problem, the sensitivity of the eigenvalues λ and of the shape vector are needed. Therefore, it gives a "local" representation of the slope of the objective function, such that the quality of the iteration can be evaluated at each step until the tolerance, set on the variations of the designed variables, is satisfied, hence the solution is sufficiently converged. At last, as stated before by equation 2.34, if the residual vector r(θ) is additionally weighted, the sensitivity matrix should be multiplied with the corresponding weighting matrix:

Optimization algorithm

2.4.4.1 Iterative methods

The Optimization algorithm generally used in order to solve the nonlinear least squares problem (see Appendix) is the iterative sensitivity-based Gauss-Newton method. It is an approximation of second-order derivative, the Hessian, truncated after the first-order term, which is justified in the FE model updating since the residuals are expected to be small, at the minimum of the function, if an adequate model is used.

It is equivalent with solving the following linear least squares problem at each i-iteration:

$$\min_{\mathrm{d}} \ \frac{1}{2} \left\| \mathrm{r}(\theta_k) + \mathrm{J}_\theta(\theta_k) d \right\|^2 \tag{3.44}$$

that, if the residual is weighted become:

$$\frac{\min}{\mathrm{d}} \quad \frac{1}{2}\left\| \mathrm{W}^{\frac{1}{2}}\mathrm{r}(\theta_k) + \left[\mathrm{W}^{\frac{1}{2}}\mathrm{J}_{\theta}(\theta_k) d \right] \right\|^2 \tag{3.45}$$

Since multiple local minima are possible, due to nonlinearity of the problem, the solution found by the Gauss-Newton method is not guaranteed to be correct. The quality of the solution is strictly related to the FE model accuracy and to the choice of the physical parameters as design variables. It depends on the specific problem definition, the objective function contains, besides the global minimum, distinct local minima, hence, in order to apply the optimization algorithm, is needed to be found a variation of the design variables which induces a monotone variation in the modal data of the structures. Thus the optimization method, instead of using the line search version that characterize the pure Gauss-Newton method, is made more robust by using a trust region strategy by imposing bound constraints on the designed variables. Therefore, if the estimates parameters give an initial solution already placed in the region of a minimum, then the convergence will be faster and, most likely correct.

2.4.4.2 Direct Methods

The important feature of Direct Method is that it reproduces the measured data exactly. This is a strength that the updated model is able to reproduce the data. In another hand, the measured and analytical data are unlikely to be equal due to measurement error and model inadequacies. Updating is done in an attempt to optimize the parameters in the model but not with the intention of exactly reproducing the error. If the updated model exactly reproduces inaccurate measurements any subsequent analysis may be flawed. Thus, the direct method need an accurate modelling and high quality measurements with some means of eliminating results from faulty sensors. The natural frequencies of a structure can be measured accurately, but the quality of mode shape measurements cannot be considered completely accurate with current measurement technology.

The direct method reproduces the given set of measured data but can be introduce into the extra, spurious modes of the frequency range of interest. Actually, this is a problem although the updated finite element model should be check many times, both to ensure the measured modes are reproduced and no spurious modes are introduced.

Conclusions

The theoretical FE model update procedure is explained in this chapter. An initial FE model is tuned to the experimental modal data in order to find a better approximation of some unknown physical parameters, such as Young's modulus, density etc. The aim is to obtain a well corresponding between the numerical and the measured dynamic behavior. In order to do this, an optimization problem is solved as a nonlinear least square problem. A residual vector containing the discrepancies in eigenfrequencies and mode shapes is obtained through an iterative sensitivity-based method called Gauss-Newton, improved with a trust region approach. Depending on the quality of the initial FE model, of the estimated parameters, together with a skilled engineering insight, the local minima can be avoiding and the global minimum of the objective function can be found.

CHAPTER 3

3. ANALYSIS OF CURVED CABLE-STAYED BRIDGES

3.1. Suspension bridges

Suspension birdges are described in many excellent books (Gimsing, N.1998), (Scott, R.2001), (Troyano, L. F.2003). A suspension cable can be anchored into the soil (see Fig.3.1) and form a so called earth anchored system; or it can be anchored into the deck and create self-anchored systems (see Figs.3.2). The suspension cables can be situated above the deck, under the deck or above and under the deck.

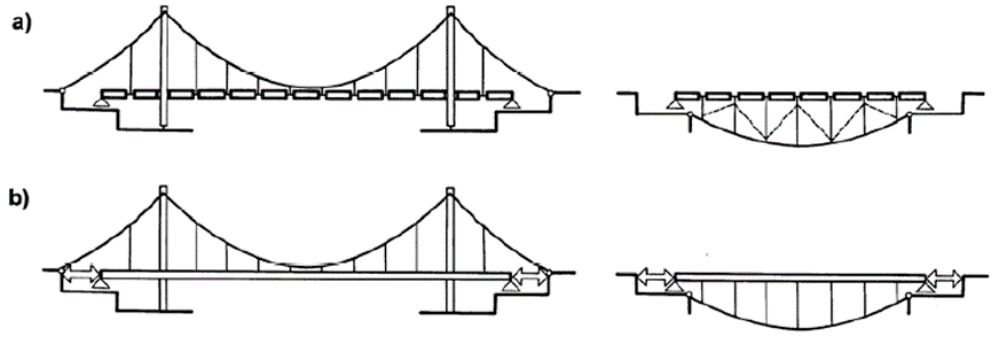

Fig.3. 1 Earth-anchored suspension structure: a) erection, b) service

The suspension cable has a funicular shape owing to the self-weight of the structure – it balances the effects of the self-weight and guarantees that the structural members are stressed by normal forces only. For service loads the suspension structure forms a complex system in which the deck distributes the load and all structural members contribute to the resistance of the structural system. The advantage of the earth anchored system is that the erection of the deck can be done independently on the terrain under the bridge. However, the suspension cables have to be erected at first and the anchor blocks have to transfer a large tension force into the soil.

On the other hand, the self-anchored suspension bridges do not require expensive anchor block and utilize the compression capacity of concrete deck. However, the erection of the deck has to be done at first; then the suspension cables can be

erected and tensioned. The fact that the erection of the deck requires a falsework and therefore it depends on the terrain under the bridge banned using this system in many cases.

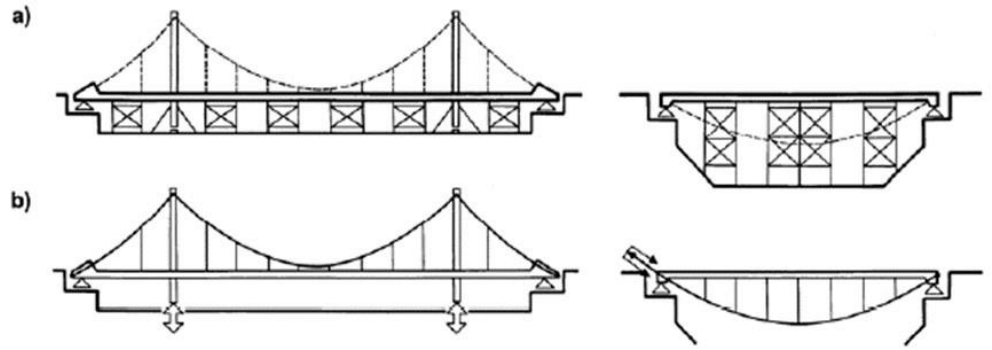

Fig.3. 2 self-anchored suspension structure: a) erection, b) service

In several new applications the erection of the structures is designed in such a way that anchor blocks are designed for erection loading only; when the erection is completed a portion or the whole tension force is transferred from the anchor blocks into the deck. In this way, a partial or total self-anchored system is created – see Fig.3.1b.

The earth suspension bridges are usually assembled of precast members (segments) that are suspended on suspension cables. Since the precast segments are mutually connected by pins, the suspension cables have automatically a funicular shape owing to the given load. The self-anchored structures are usually cast-in-place on the falsework. The self-weight is transferred into the suspension cables by their post-tensioning that can be done by jacking at their anchors or by lifting of the tower. This operation requires careful determining of the camber of the deck and non-tension length of the cables.

3.2. Cable-stayed bridges

In this part, cable-stayed bridges have been described in only additional information about structures formed by slender deck is presented.

Cable-stayed bridges are formed by a slender deck that is suspended on stay cables anchored in the tower and deck. It is possible to anchor back stays in the soil and create totally or partially earth cable stayed structure. From economic reasons

this solution makes sense only in special cases and/or for structures of long spans. The prevailing portion of the cable-stayed bridges is formed by self-anchored systems that stress the footings by vertical reactions only.

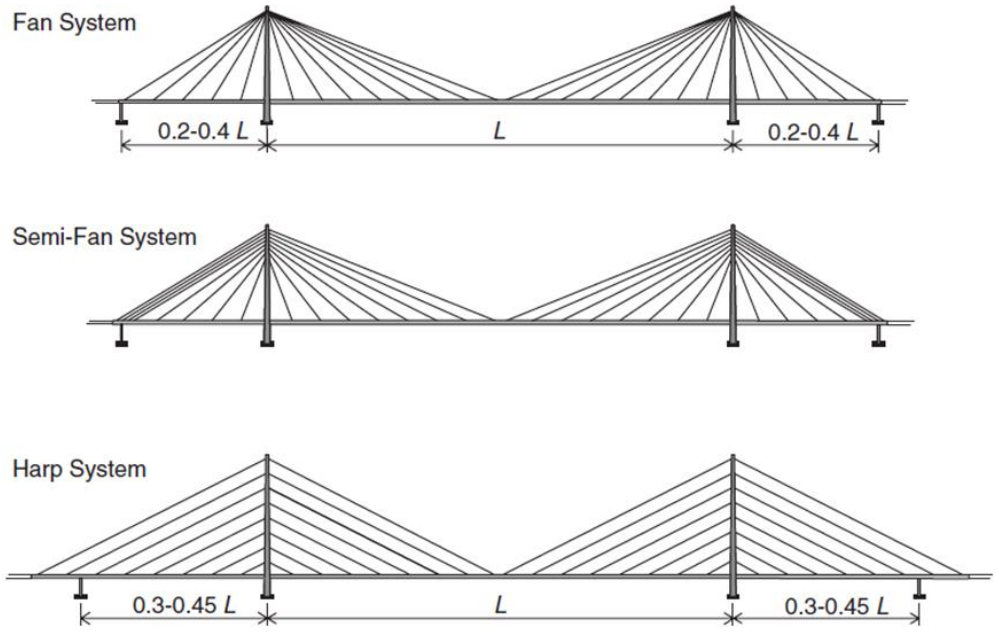

Fig.3. 3 Cable stayed bridge systems: (top) pure fan system; (centre) semi-fan system; (bottom) harp system

The cable-stayed system (Fig 3.3) contains straight cables connecting the deck to the pylons. In the fan system, all stay cables radiate from the pylon top, whereas parallel stay cables are used in the harp system.

Besides the two basic cable stayed systems (the fan system and the harp system), intermediate systems are often found. In the semi-fan system, the cable anchorages at the pylon top are spread sufficiently to separate each cable anchorage and thereby simplify the detailing. With cable anchorages positioned at minimum distances at the pylon top, the behaviour of the semi-fan system will be very close to that of the pure fan system.

The stay cable anchorages at the deck will generally be spaced equidistantly so in cases where the side spans are shorter than half of the main span, the number of stay cables leading to the main span will be greater than the number of stay cables leading to the side span. In that case the anchor cable from the pylon tops to the anchor piers will often consist of several closely spaced individual cables (as shown for the semi-fan system).

In the harp system, the number of cables leading to the main span will have to be the same as in the side spans. With the anchor pier positioned at the end of the side span harp, the length of the side span will be very close to half of the main span length. That might prove inconvenient in relation to the overall stiffness of the system. It can then be advantageous to position the anchor pier inside the side span harp as indicated in Fig 3.3. The position of the anchor pier closer to the pylon can also prove favourable in a fan system, if designed with fans of equal size in the main and side spans (Fig.3.4).

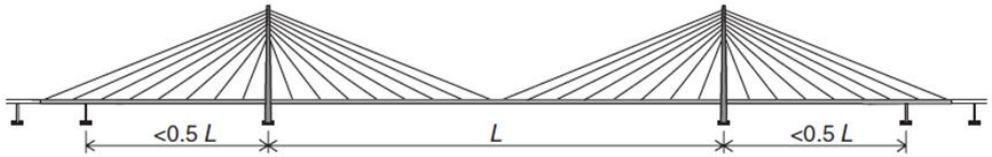

Fig.3. 4 Semi-fan system with side span pier inside the fan

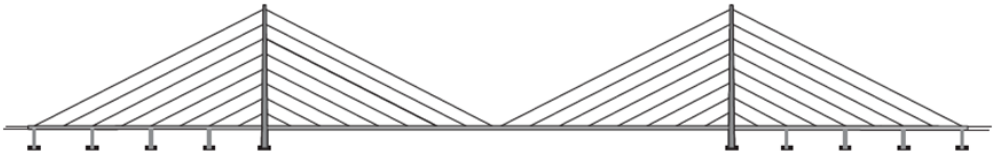

Fig.3. 5 Harp system with intermediate supports in the side spans

For the harp system the most efficient structural system will be achieved if a number of intermediate piers can be positioned under the side span harps (Fig.3.5). This will be the preferred solution if the side spans are on land or in shallow water.

The most common type of cable supported bridge is the three-span bridge with a large main span flanked by two smaller side spans. However, especially within cable stayed bridges, there are also examples of a symmetrical arrangement with two main spans of equal size or an asymmetrical two-span arrangement with a long main span and a somewhat shorter side span (Fig.3.6). If the two spans are of equal size, it will be necessary to stabilize the pylon top with two anchor cables whereas the asymmetrical arrangement often can be made with only an anchor cable in the shorter span.

The vast majority of cable supported bridges are built with three or two spans, but in a few cases this has not been sufficient. A straight forward solution that maintains the advantages of the three-span configuration is then to arrange two or more three-span bridges in sequence, as shown in Fig.3.7 (top). In appearance, the

bridge will have every second opening between pylons without a central pier and the other openings with a central anchor pier (or anchor block).

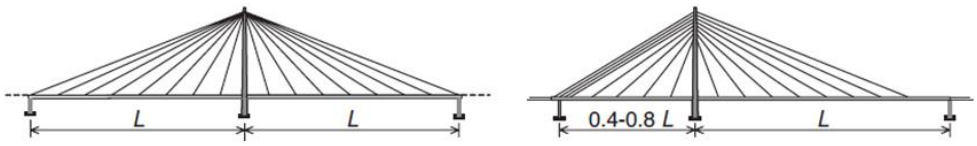

Fig.3. 6 Two-span cable stayed bridges

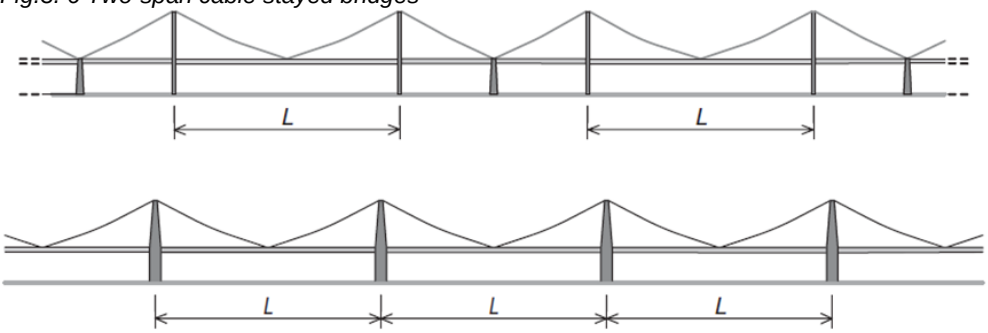

Fig.3. 7 Multi-span cable supported bridges

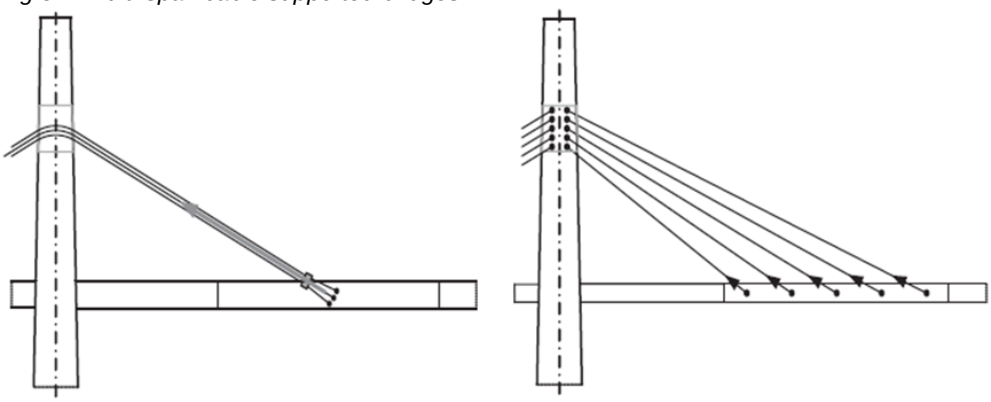

Fig.3. 8 Cable stayed system with few multi-strand cables (left) and a multi-cable system (right)

A true multi-span cable supported bridge will consist of a number of main spans back-to-back as shown in Fig.3.7 (bottom).

In many cases, a true multi-span cable stayed bridge (bottom) will be preferable to a series of three-span bridges (top) from the point of view of appearance and function. However, from a structural viewpoint, the true multi-span arrangement presents a number of problems.

Due to the lack of anchor cables leading from vertically fixed points at the deck level to the pylon tops, the pylon must possess a considerable flexural stiffness to be

able to withstand (with acceptable horizontal displacement at the top) a loading condition with traffic load in only one of the two spans adjacent to the pylon. In such a loading condition, the cable pull from the loaded span will be larger than from the unloaded span so the pylon must be able to withstand the difference between the horizontal force from the cable system in the loaded span and in the unloaded span. In the early cable stayed bridges built from the mid-1950.s to the mid-1970s, the distance between cable anchorages at deck level was generally chosen to be quite large and as a consequence each stay cable had to carry a considerable load. It was therefore necessary to compose each stay of several prefabricated strands joined together (Fig.3.8, left).

It was necessary to let the multi-strand cable pass over the pylon on a saddle as the space available did not allow the splitting and individual anchoring of each strand, and at the deck the anchoring of the multi-strand cable made it absolutely necessary to split it into individual strands.

In modern cable stayed bridges, the number of stay cables is generally chosen to be so high that each stay can be made as a mono-strand. This will ease installation, and particularly replacement, and it will render a more continuous support to the deck (Fig.3.8, right).

With the multi-cable system, it will be possible to replace the stays one by one if the deck is designed for it, which will often be required in the Design Specifications. The advantages gained in relation to erection, maintenance and replacement have to some extent been set against an increased tendency for the stays in a multi-cable system to suffer from wind-induced vibrations.

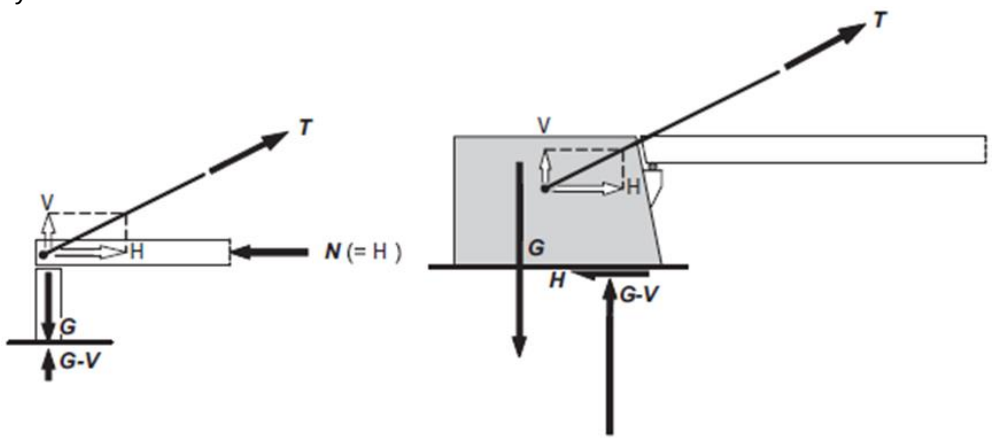

Fig.3. 9 Connection between the side span cable and the anchor pier/block in a self-anchored system (left), and in an earth-anchored system (right)

Besides the configuration of the cables, cable supported bridges can also be distinguished by the way the cable system is anchored at the end supports. In the self-anchored system, the horizontal component of the cable force in the anchor cable is transferred as compression in the deck, whereas the vertical component is taken by the anchor pier (Fig.3.9, left). In the earth anchored systems, both the vertical and the horizontal components of the cable force are transferred to the anchor block (Fig.3.9, right).

In principle, both earth anchoring and self-anchoring can be applied in suspension bridges as well as in cable stayed bridges. However, in actual practice, earth anchoring is primarily used for suspension bridges and self-anchoring for cable stayed bridges.

For the suspension bridges, self-anchoring is especially unfavourable in relation to structural efficiency and constructability. In modern practice, self-anchored suspension bridges are therefore only seen when the decision to use the system is taken by people without structural competence and who are not concerned about construction costs.

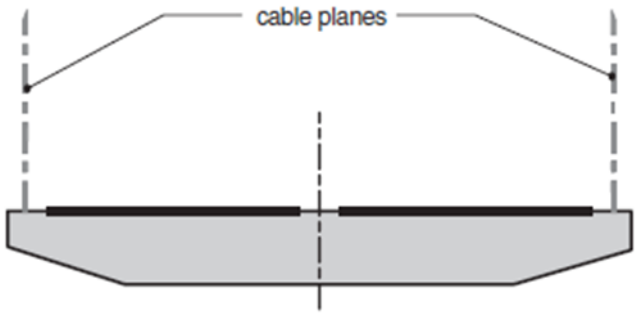

Fig.3. 10 System with two vertical cable planes attached along the edges of the bridge deck

In the transverse direction of the bridge, a number of different solutions for the arrangement of the cable systems can be found. The arrangement used traditionally in suspension bridges comprises two vertical cable planes supporting the deck along the edges of the bridge deck (Fig.3.10). In this arrangement (which is also seen in many cable stayed bridges), the cable systems support the deck by the both vertically and torsionally.

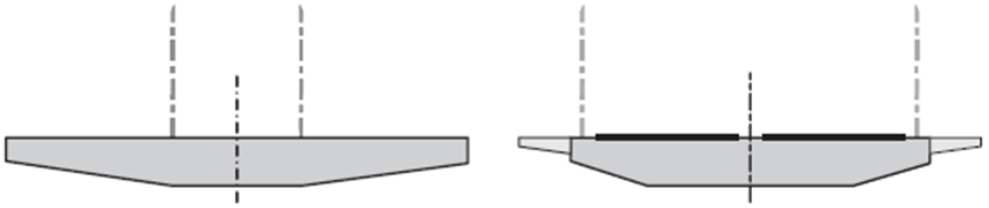

Fig.3. 11 Systems with two vertical cable planes positioned between three separate traffic lanes

In cases where the bridge deck is divided into three separate traffic areas, e.g. a central railway or tramway area flanked by roadway areas on either side, the two vertical cable planes might be positioned between the central area and the outer areas (Fig.3.11, left). This arrangement is especially attractive if the central area is subjected to heavy loads that would induce large sagging moments in the transverse girders if the cable planes were attached along the edges of the bridge deck. On the other hand, with the cable planes moved in from the edges towards the centre of the deck, the torsional support offered by the cable system will be drastically reduced. Amore moderate displacement of the cable planes from the edges of the deck is found in bridges with cantilevered lanes for pedestrians and bicycles (Fig.3.11, right).

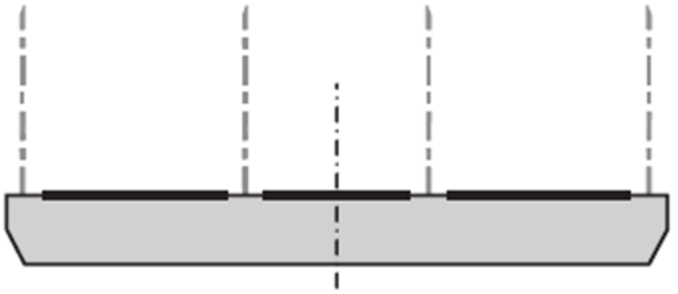

Fig.3. 12 System with four vertical cable planes positioned outside and between three separate traffic lanes

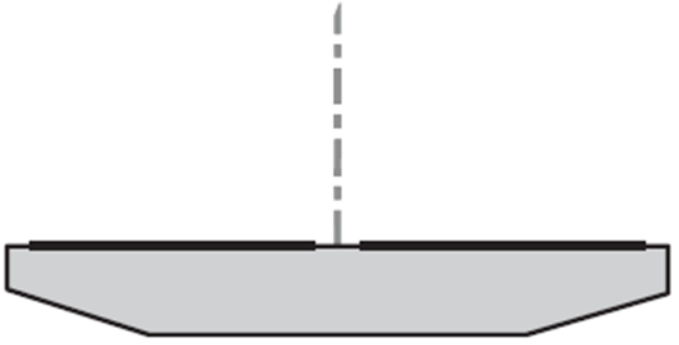

Fig.3. 13 System with one central cable plane

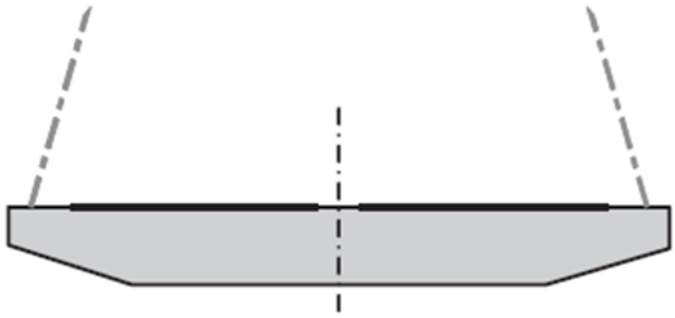

Fig.3. 14 System with two inclined cable planes

The application of more than two vertical cable planes (Fig.3.12) was seen in some of the large American suspension bridges from the end of the nineteenth century and the beginning of the twentieth century. In bridges with a wide bridge deck, more than two cable planes could still be considered, as the moments in the transverse girders will be significantly reduced. Only one vertical cable plane (Fig.3.13) has been widely used in cable stayed bridges. In this arrangement, the deck is only supported vertically by the cable system, and torsional moments must therefore be transmitted by the deck.

Consequently, the deck must be designed with a box-shaped cross-section. Inclined cable planes (Fig.3.14) attached at the edges of the bridge deck and converging at the top are found in cable stayed bridges with A-shaped pylons. In this arrangement the deck is supported both vertically and torsionally by the cable system.

Two inclined cable planes converging at the top can also be supported on a single vertical pylon penetrating the deck in the central reserve or in the gap between two individual box girders.

3.3. Curved suspension structures

Recently, several curved cable-supported structure have also been built successfully. They utilize a space arrangement of the cables and prestressing tendons to minimize the bending and shear stresses in the deck.

The curved deck can be suspended on both its edges, an outer edge or an inner edge. The arrangement depends on local conditions, the radius of the curvature and the required span length of the crossing (Str'ask'y, Jiř'I 2005)..

3.4.1 Suspension of the deck on both edges

If the deck can be suspended on both edges, it is possible to apply an arrangement that was developed in the design of the Ruck a Chunky Bridge, by T. Y. Lin International. Although this bridge has not been built, its design shows clearly how all internal forces could be balanced by external prestressing- by the arrangement of stay cables.

Fig.3. 15 Ruck a Chucky Bridge, CA, USA (Design by T. Y. Lin International)

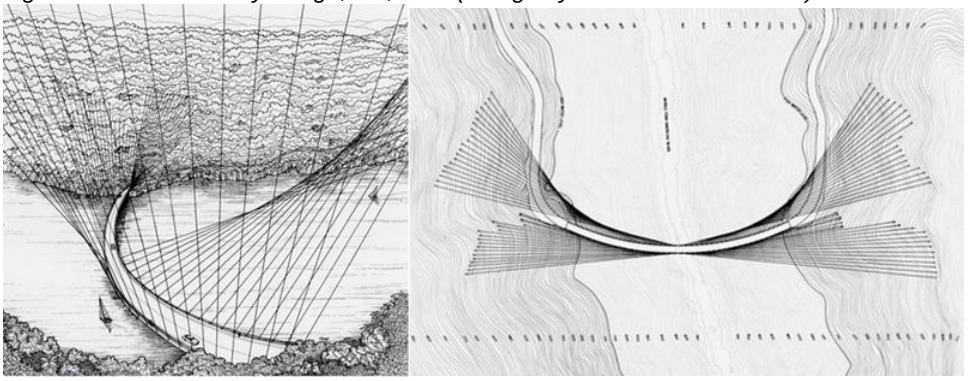

Fig.3. 16 Ruck a Chucky Bridge, CA, USA: Plan (Design by T. Y. Lin International)

The bridge with a span of 396.24 m crosses a reservoir on a plan curvature of 628m (see Figs 3.15 and 3.16). The deck is suspended on stay cables arranged in a hyperbolic paraboloid formation to create an array of tensile forces, which produce pure axial compression in the curved deck. The vertical-force components of the

cables balance the weight of the deck (see Fig.3.17 (a)). The resultants of the horizontal components act in the direction of the curved axis and are designed to reduce the horizontal bending moments at critical points to zero (see Fig.3.18 (b)). The design demonstrates how a pure engineering approach can create a structure of great beauty and elegance.

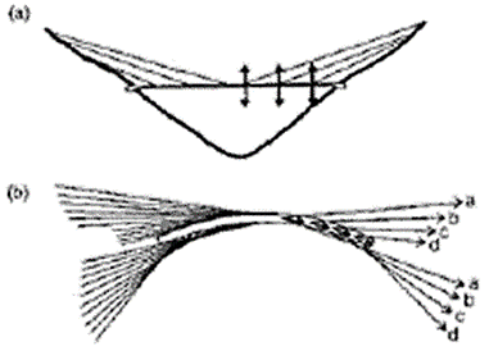

Fig.3. 17Ruck a Chucky Bridge, CA, USA: (a) balancing of the vertical forces, (b) balancing of the transverse forces

3.4.2 Suspension of the deck on an outer edge

If the radius of curvature is sufficiently large, the deck is usually suspended on V-shaped towers. However, the forces in the stays have to balance both the vertical and transverse effects of the dead load.

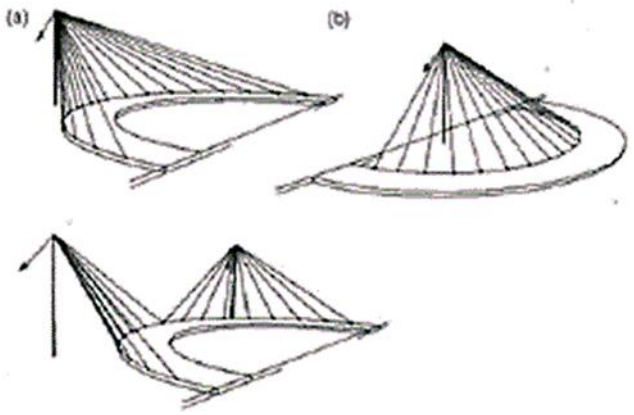

Fig.3. 18 Suspension of the curved deck: (a) outer edge, (b) inner edge

Fig.3. 19Tomoe-ryū Bridge, Japan

Fig.3. 20 Glorias Catalanas Bridge, Barcelona, Spain

Figure 3.18 shows a curved deck, which is suspended only on the (a) outer or (b) inner edge. From a first view, the suspension of the deck on the outer edge gives a feeling of safety (see Fig.3.19). Although the vertical components of the cable forces can reduce the torsional moment, the horizontal components of the cable forces create significant transverse moments in the deck. It is difficult to find an arrangement of the cables that balances the effects of dead load. This solution is suitable for suspending the two curved ramps that merge into one deck, such as is shown in Fig.3.20.

3.4.3 Suspension of the deck on an inner edge

Fig.3. 21 Kelheim Bridge, Germany: inclined hangers

Fig.3. 22 Malecon Bridge, Spain

on the other side, an arrangement of cables anchored in the inner deck edge that balances the effects of the dead load is relatively simply. The arrangement was developed by Professor Schlaich from Stuttgart for the Kelheim Bridge completed in 1987 in Germany (see Figs 3.21). The Malecon Bridge, designed by an engineering

office, Carlos Fernandez Casado, S.L. from Madrid, is also an excellent example (see Figs 3.22).

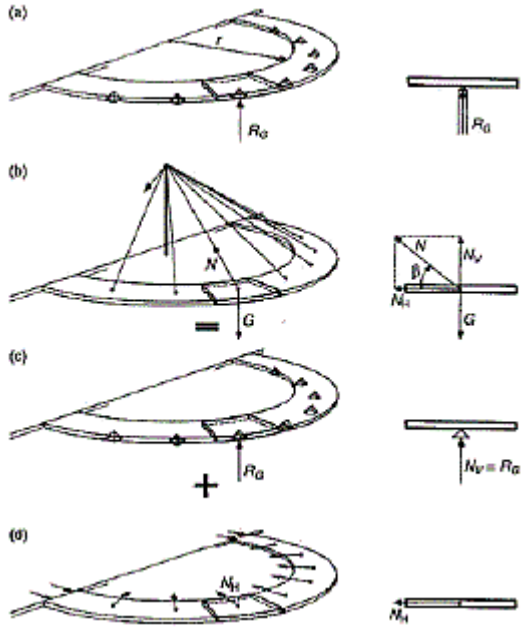

Fig.3. 23 Curved cable-stayed structure: (a) continuous beam, (b) cable-stayed structure, (c) effects of the stays' vertical components, (d) effects of the stays' horizontal components

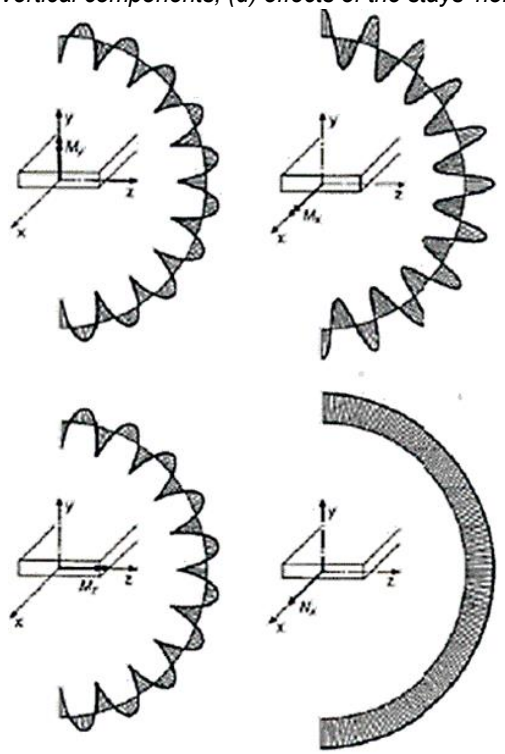

Fig.3. 24 Internal forces in the curved deck

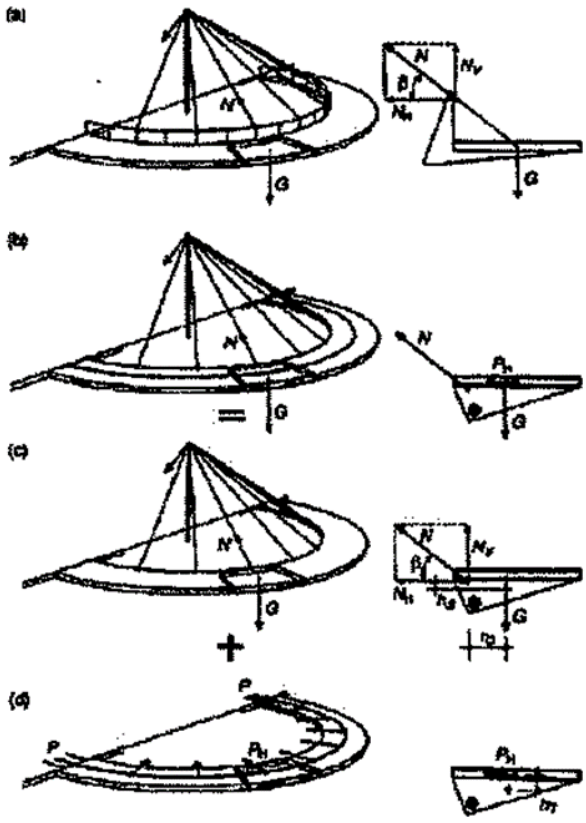

Fig.3. 25 Curved cable-stayed structure: (a) suspension above deck, (b) suspension at the deck, (c) effects of the stays, (d) effects of the post-tensioning

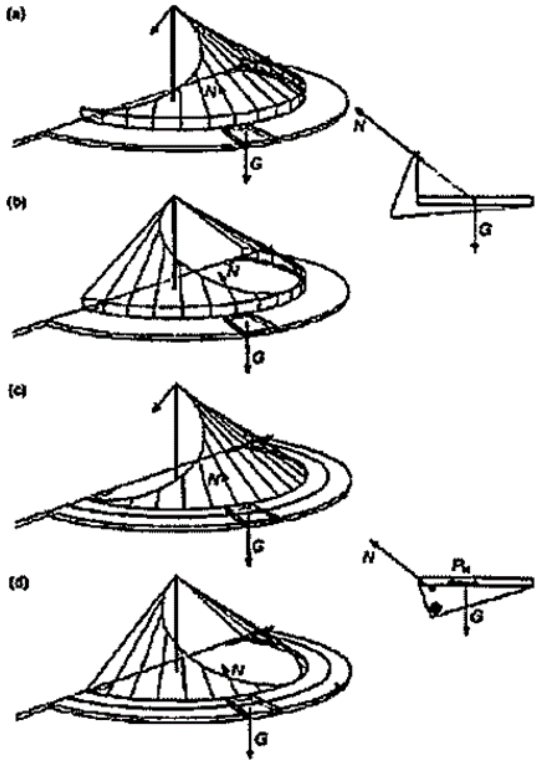

Fig.3. 26 Curved suspension structure: (a), (b) suspension above the deck; (c), (d) suspension at the deck

Development of the suspended system is showed from Figs 3.23 to 3.26. Figure 3.23(a) shows a circular deck that is supported by single columns situated on the bridge axis and that is fixed into abutments. Because of self-weight, the deck is stressed by bending moments My, Mx, and Mz. Their courses are shown in Fig.3.24.

Figure 3.22(b) shows the same deck that is on the bridge axis, suspended on radial cables anchored with a single mast. The cables are stressed by force N=G/sinß, where G corresponds to the vertical reaction that originates at single supports of the continuous structure shown in Fig. 3.23(a). It is evident that the vertical component of the cable force substitutes single supports (see Fig. 3.23(c)) and the horizontal component creates radical forces that stress the deck in the horizontal direction (see Fig 3.23(d)). Due to the deck is fixed at the abutments, it is stressed by uniform compression stresses.

Hence, the deck is stressed by the same bending moment My, Mx and Mz as the continuous beam, and by an additional normal force Nx (see Fig.3.24). When the distance between the stay cables is small (from 3 to 6m) the bending and torsional

stresses are also very little – this means that the stay cables balance the effects of the dead load and create compression in the deck.

Unfortunately, the stay cables anchored in the bridge axis prevent the use of one half of the bridge deck. Therefore, it is necessary to anchor the stay cables at the inner edge and find a solution that creates the same state of stresses. There are two possibilities:

(a) Anchoring the stay cables in a stiff member protruding above the deck. The anchor point of each cable is situated on the line that passes through the centre of gravity of the deck slab (see Fig. 3.25(a)).

(b) Anchoring the stay cable at the edge and adding prestressing tendons into the deck slab. The slender deck has to be supplemented by an additional member situated at a sufficient distance from the deck, or a deck of sufficient depth has to be created. In this case radical forces from the cable create a moment about the centre of gravity of the composite section, and the deck and additional member balance the forces.

In this circumstances a moment created by a couple of vertical forces $M_V = Gr_G = NVr_G = (N sin\beta) r_G$ is balanced by a moment that is created by a horizontal component of the stay force and by radical forces due to post-tensioning $M_H = N_H h_s + P_H h_T = N \cos\beta h_s + P_H h_T$.

It is quite evident that a similar arrangement can be developed for suspension structures in which a suspension cable supports inclined hangers (see Fig.3.21). Figure 3.26 shows two possibilities for the arrangement of the suspension cables: anchored at the stiff members protruding above the deck, or at the deck that is supplemented by prestressing tendons and an additional member. It is quite obvious that these basic arrangements can be combined, as was done in the design of the pedestrian bridge that was built inside a museum in Munich, Germany.

The arrangement of the cables and prestressing of the deck makes it possible to create an optimum state of stresses in the deck, which is primarily stressed by uniform compression stresses. However, depending on the stiffness of individual structural members, plan curvature and span length, the deck can be stressed by significant bending and torsional stresses caused by live and wind loads. Then the structure requires not only a sufficient moment arm between the deck slab and additional member, but also a torsionally stiff section.

3.4.4 Curved stress ribbon structure

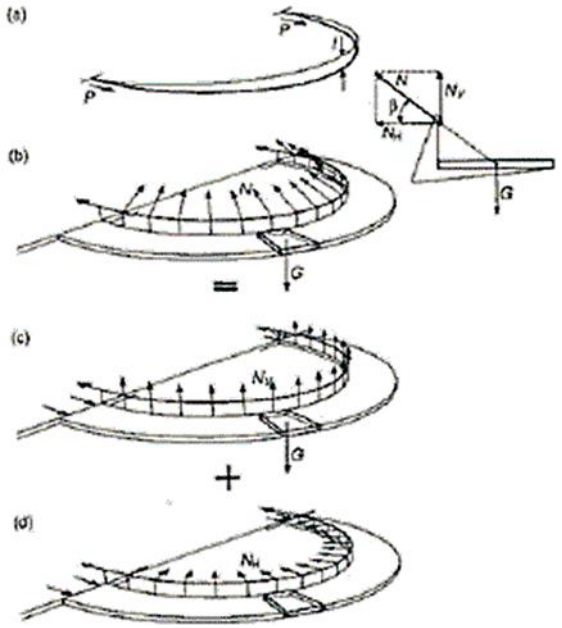

Fig.3. 27 Curved stress ribbon structure: (a) geometry, (b) effects of the bearing tendon, (c) effects of the tendon's vertical component, (d) effects of the tendon's horizontal component

Fig.3. 28 Curved stress ribbon structure

The idea of balancing the effects of the self-weight was also used in a study of curved stress ribbon structures carried out under the author's control (see Figs 3.28). A development of the solution is evident from Fig.3.27. The deck, which has a variable slope, is suspended on bearing tendons situated above the deck and is prestressed by a tendon situated at deck level. The forces in the bearing tendons are designed in such a way that their vertical component balances the self-weight of the ribbon, while the horizontal component balances the torsional moment caused by the self-weight. Nonetheless, the horizontal component also creates compression in the deck.

To resist the effects of live load a torsionally stiff, composite section is proposed. The section is formed by a slender, concrete deck slab and steel box that protrude above the deck. This steel box deviates the tendon and serves as a parapet.

CHAPTER 4

4. MAGAZ BRIDGE

4.1. Introduction

The bridge under investigation (fig. 4.3) is located in Spain, in the region ‘Castilla y Leon’ near the small village of Magaz de Pisuerga, 10 km from Palencia over the A62, named ‘Autovia de Castilla’, that goes from Palencia to Burgos.

Fig.4. 1 Global view of the bridge

Bridge Description

The deck is designed as a classical composite structure of steel and reinforced concrete, with a lower steel box girder of trapezoidal shape with internal reinforcing structures and stiffening braces (fig.4.4) and an upper slab of reinforced concrete connected by shear studs to the steel girder. The width of the slab is 11.6 m and the thickness is variable between 150 mm, in correspondence of its cantilever part and 300 mm, in its the central part. From a global static point of view, the bridge can be considered as a continuous beam. The end supports have vertical and lateral constrains, the 2 central supports, the piers, only restrain the vertical and torsional displacements. The central span is 42 m long and the two side spans are 25 m long (fig.4.2).

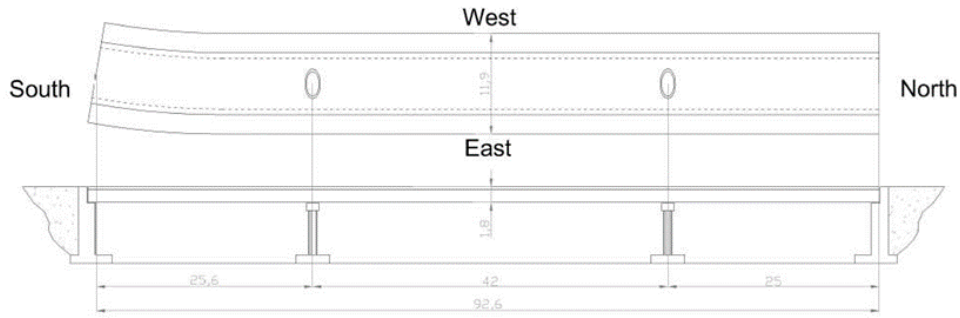

Fig.4. 2 Schematic view of the bridge and the main geometrical features

Fig.4. 3 Image extracted from the official blueprint (Concession of Gesturcal)

A couple of supporting points is clearly visible both on the two end supports, in correspondence of the abutments, and on the central piers (fig.4.6). These supporting points are constituted by 2 rectangular plates (60cm×70cm) with the interposition of some layers of neoprene to guarantee a homogeneous distribution of loads. The two piers are completely made up of reinforced concrete with a rounded section inscribed in a rectangular 220×120 cm and are founded on a big foundation slab with a rectangular shape (7.0× 6.5 m) and a thickness of 1.5 m. The height of the two piers is 6.1 m and 7.3 m.

The bridge is not completely straight, but it has a slightly curvature on the south lateral span (fig.4.2), which couples the bending and torsional dynamic behavior of the structure. The top surface of the slab is divided into three parts; the two lateral parts have a width of 2.3 m and are raised up respect to the central part of 20cm, whereas the central part, which is devoted to traffic passage, is characterized by a width of 7.0 m (Fig. 4.5)

Fig.4. 4 Internal view of the bridge

The steel box and the concrete deck are completely disconnected from the accessing ramps and, as can be seen from fig.4.6, also the steel railing has connection points only on the lateral part of the concrete deck. Moreover, the asphalt layer appears completely separated along the transition line between the slab and the accessing ramp; this fact confirms that the bridge is completely isolated from its environment.

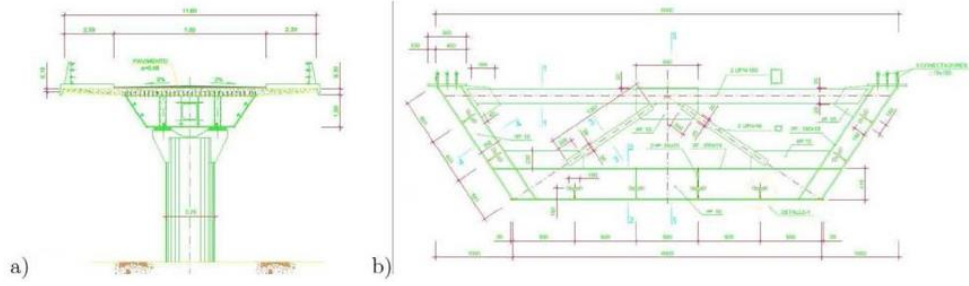

Fig.4. 5 (a) Global section of the bridge (b) Section of the steel box (Concession of Gesturcal)

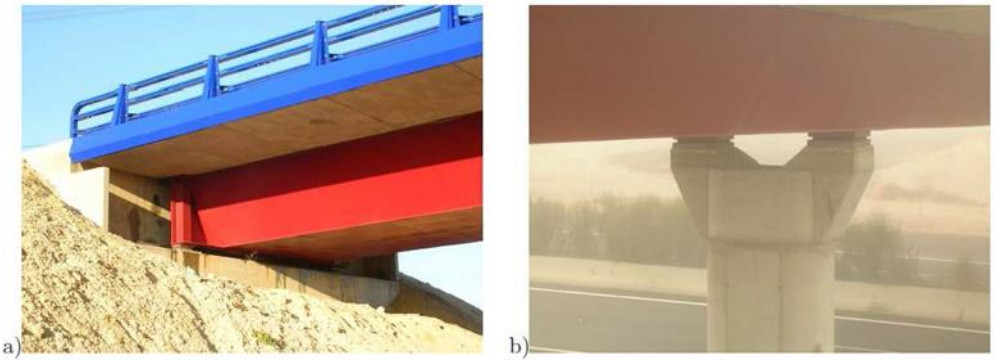

Fig.4. 6 Abutment (a); end support (b)

4.2. FE simulation

4.2.1 CAD modelling and FE model

In the CAD model, the geometry of the bridge was accurately defined accounting for the layout of the deck and its transverse slope, which was different in each bridge segment. In particular, the right end of the bridge is the curved. Furthermore, in the definition of the steel members of the deck (figure 4.4 and 4.5):

A detailed 3D FE model was developed to simulate a realistic response of the bridge. An isometric view of the FE model of the bridge is shown in Figure 4.3. The CAD model was subsequently transferred to the software SAP2000 to create the FE model of the bridge, that was formulated using the following assumptions:

1. The concrete slabs are simulated using eight-node solid elements. The elastic modulus of the concrete slab solid elements was initially computed based on the compressive strength of 28 Mpa, which is the listed value on the as-built drawings;
2. The steel girders are simulated using four-node shell elements. Properties of the steel grade S355 were used for plates and S275 for other structural components of the bridge as listed on the as-built drawings;
3. steel stringers, transverse cross-beams and bracing elements of the deck were modelled by two-nodes 3D beam elements. The modulus of elasticity and the weight per unit volume of the steel were assumed as 205 GPa and 785 kN/m3, respectively;

4. A second set of eight-nodes shell elements with negligible elastic modulus was added on top of the concrete slab shell elements to simulate the thickness of the asphalt overlay on the bridge deck. The density of asphalt layer is one of the main uncertainties for this problem, like its stiffness as well. For this reason, as better explained in the further paragraphs, this layer is considered combined with the concrete to form a single equivalent layer with specific characteristics;
5. All the cross-bracings are explicitly simulated in the model using beam elements;
6. The boundary conditions are used to simulate the fixed on top of the pier and on top of the abutments;
7. The structural mechanical details of the abutments and piers were included in the developed FE model;
8. Rigid links (without mass density) were used between the concrete slab and the pier;

The FE model, shown in Fig.4.7, has a total of 6961 nodes and 5627 elements (namely 202 beams, 4081 plate elements, and 1344 solid elements).

4.2.2 FE analysis and correlation with the experimental results

After the description of the procedure used for the identification, it is necessary to pass to the description of the model. A high-fidelity nonlinear three-dimensional (3D) FE model of the as-built bridge was developed using SAP2000 finite element software package version 16 （Computer & Structures, Inc. 2013, Berkeley, California, USA）. A detailed 3D FE model was developed to simulate a realistic response of the bridge. An isometric view of the FE model of the bridge is shown in Figure 3. The concrete slab and the steel girders are simulated using eight-node solid elements and four-node shell elements. The elastic modulus of the concrete slab solid elements was initially computed based on the compressive strength of 28 Mpa, which is the listed value on the as-built drawings. Properties of the steel grade S355 were used for plates and S275 for other structural components of the bridge as listed on the as-built drawings. A second set of eight-nodes shell elements with negligible elastic modulus was added on top of the concrete slab shell elements to simulate the thickness of the asphalt overlay on the bridge deck. The density of asphalt layer is one of the main uncertainties for this problem, like its stiffness as well. For this reason, as better explained in the further paragraphs, this layer is considered combined with the concrete to form a single equivalent layer with specific characteristics. Shear studs were used at the top of the steel girders to ensure that the slab was in composite action with the steel girders. The shear studs were explicitly simulated in the FE model by translational springs. These springs

were simulated at the exact location of the shear studs. The nodes at the two ends of these springs were connected to the nodes of the shell elements of the top flange of the steel girders and the concrete slab using translational constraint equations. Depending on the stiffness values used for the springs, full or partial composite action can be simulated between the steel girders and the concrete slab. All the cross-bracings are explicitly simulated in the model using beam elements. The boundary conditions are used to simulate the supports on top of the pier and on top of the abutments. These springs simulate the frictional resistance of the bearings and the stiffness have been evaluated considering the geometrical and mechanical properties of bearings themselves and of the piers. The structural mechanical details of the abutments and piers were not included in the developed FE model; however, half of the mass of the concrete at the abutment was distributed as nodal masses to the nodes of the steel girders and concrete slab. The added nodal mass to these nodes was assigned based on the tributary area of each node at the abutment end. Possible stiffness contributions of the abutments to the superstructure could be partly considered as springs. Also, the stiffness contribution of the piers to the superstructure can be partly considered as spring. Although the developed FE model has several nonlinear components, the linear portion of the stiffness matrix has been used for the modal analyses carried out in this study. In addition, all selected physical parameters (to be discussed in Section 4.4.3) for the purpose of model calibration are linear in nature.

Although the developed FE model has several nonlinear components, the linear portion of the stiffness matrix has been used for the modal analyses carried out in this study. In addition, all selected physical parameters for the purpose of model calibration are linear in nature.

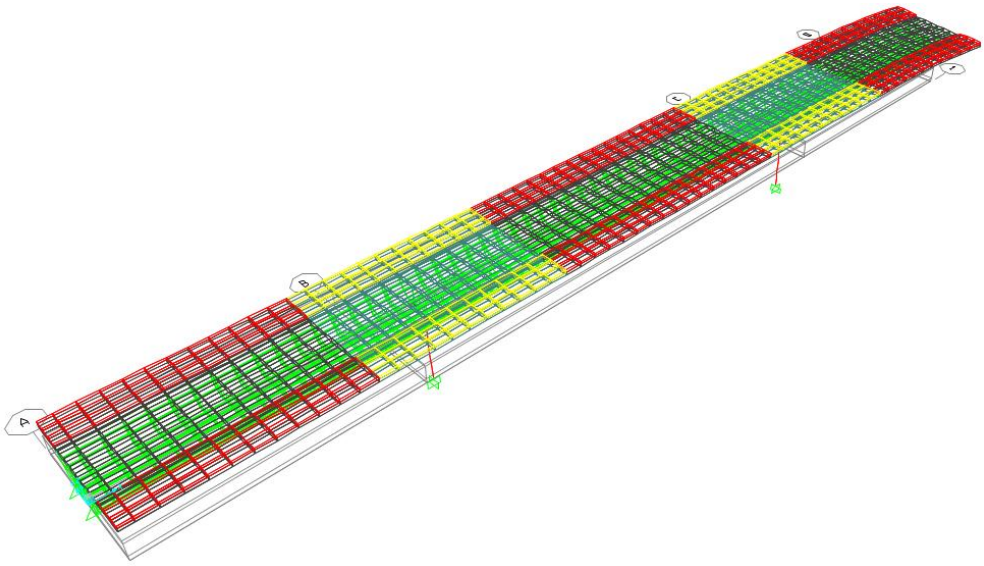

Fig.4. 7 3D finite element model of the bridge

Tab.4. 1 Comparison of the experimental and the Initial FE modes

Initials FEM results		Wireless results (35 min.)			
Mode	F_f [Hz]	Mode	F_{wl} [Hz]	Δf [%]	MAC
1	2.4634	1	2.4887	1.02	0.896
2	4.5685	2	4.8328	5.47	0.718
3	6.0997	3	5.417	-12.60	0.904
4	6.951	4	7.0886	1.94	0.824
5	7.2231	5	8.2895	12.86	0.687
6	9.4843	6	10.1299	6.37	0.885
7	11.3354	7	11.3124	-0.20	0.774
8	11.7299	8	12.1369	3.35	0.202
9	15.5602	9	15.3194	-1.57	0.44

It is worth to be noted that, as shown in Figure 4.18, even if both the MAC value and the difference in frequency have good results for the 1st mode, the identified modal displacement at node #34 is significantly larger than the FE calculated result. It suggests that the cross section in not well represented by the FE analysis, since the deformation is much smaller than the real structure. This is probably due to some of the simplification done in the FE modeling as the consideration of the side

barriers as a continuum, the transversal inclination of the deck or the damping ratio of the neoprene supports. In contrast, the on-site observation shown that the discontinuous concrete barriers were in fact connected to each other only by the handrails and the steel bars inside the troughs. And the steel bars were however disconnected in some joints. As a result, it becomes difficult to accurately simulate the effects of the side barriers to the local deformation of the slab. The effective location and the mechanics characteristic of the neoprene supports couldn't be verified before the vibration measurements. Indeed, the identified 3rd mode and 4th mode are very similar to each other. Both of them correspond to the 3rd FE mode with a very high MAC value. The difference between these two identified modes probably lies in the deformation of the slab under the shoulder and the side barriers, which were however not measured. Similar observations are on the identified 6th mode and 7th mode. Therefore, can be assume that the relatively large difference in natural frequencies between the FE and the experimental results for the identified 4th and 7th modes were probably due to the modeling inaccuracy of the side barriers, the boundary conditions and the cross section's angle. According the MAC values, the first seven order modes were selected to update.

4.3. Ambient Vibration Testing

4.3.1 Vibration Measurements in 2011

The testing setup is showed by Fig.4.8, the grid of 90 points where vertical accelerations were measured and according to the different colors of the setup planning. This solution was developed to take into account a number of wireless channels available equal to 16 and consists, totally, of 9 setups. The grid was developed according to results obtained from the finite element modal analysis. On the curved lateral side, the grid was refined a little. The idea was to measure all these grid points, using 6 reference positions (12, 26, 39, 50, 57 and 79), with the wireless system, and to measure only a reduced number of points with the wired National Instrument system, which had only 4 channels available. The test proceeded moving the two transversal rows of sensors, step by step, from the north side toward the South side. Sensors were fixed on steel plates manufactured for this purpose: these plates were positioned on the surface of the bridge and horizontally leveled. As already mentioned, three different types of accelerometers with three different characteristics were used during this measurement campaign.

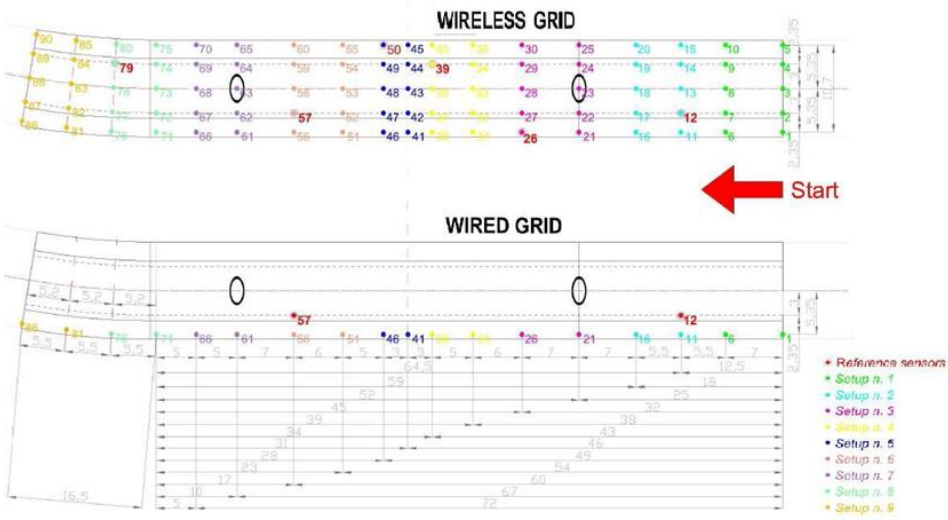

Fig.4. 8 Testing plan: Loctions of the measurement points pf the bridge

Operational modal analysis was performed on data 10 minutes long acquired from UPM boxes. These data were recorded at a sampling frequency of 3906.25Hz, which is a very high frequency for vibration of civil structures. Some preliminary preprocessing operation were performed on these data before using MACEC, the MATLAB toolbox for structural system identification, developed at the Structural Mechanical Department of KUL (Reynders E. et al. 2011). The first set of operations consists in: Signals, which are recorded in V, are converted to (m/s2) using conversion factors elated in tab.1; Signals were low pass filtered at a frequency of 25Hz with a zero-phase equi ripple digital filter, by processing the signals in both the forward and reverse directions (MATLAB command); S signals were re-sampled to a frequency of 50Hz; Each signal component was de-trended by removing its mean value in order to have zero-mean signals; Each signal was visually investigated and bad signals were removed before performing the system identification procedure;

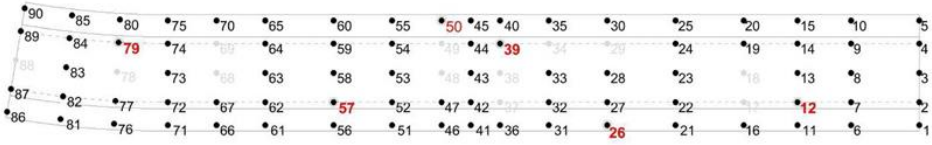

Fig.4. 9 Not corrupted signals for identification procedure (black and red) and corrupted signals (grey)

Fig.4.9 shows all the grid points which were measured and differentiates between available signal with color black (roving sensors) and red (reference sensors).

Corrupted signals with color grey. Likely reason for this malfunctioning can be the not so good connection of cable to BNC connectors and/or the battery of box N.4.

4.3.1.1 System Identification

System identification has been performed by using the covariance driven stochastic subspace identification algorithm (SSI-cov) (Peeters B., De Roeck G. 1999). From the observation of all the 9 stabilization diagram obtained from the different setups, 9 mode shapes and corresponding modal parameters were identified. These identified mode shapes were characterized by the presence in all setups and by a good stability respect to system order variation. Fig. 4.9 contains a couple of stabilization diagrams obtained from modal decomposition of identified state space matrices.

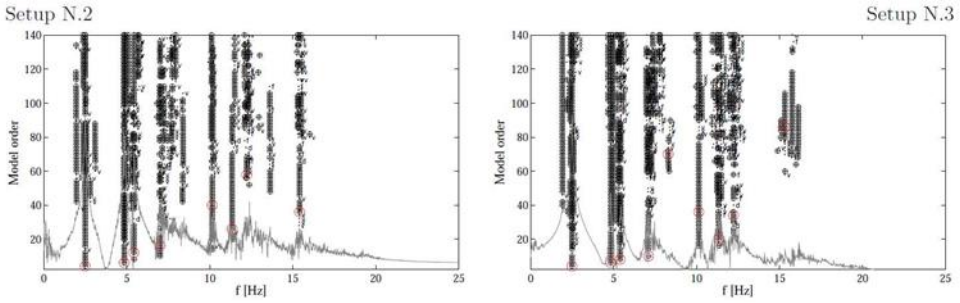

Fig.4. 10 A stabilization diagram: The stable poles with the power spectral density superimposed

Final results of operational modal analysis on the Magaz Bridge, compared with numerical results, are summarized in tab.4.1. Identified and numerical mode shapes are depicted from fig.4.11 to fig.4.20. The left side of these figures illustrates different views of mode shapes identified without considering corrupted channels; the right side of these figures represents an attempt to define modal displacements of positions with corrupted signals, using linear interpolation of modal displacements of surrounding positions with available channels. More information is given in tab.4.3.

Tab.4. 2 Master and slave nodes

Master	z	Slave	z	Master	z	Slave	z
12	1	17	0.2	50	1	49	0.3

22	1	17	0.2	44	1	49	0.3
19	1	17	0.1	54	1	49	0.2
16	1	17	0.3	53	1	58	0.2
19	1	18	0.3	63	1	58	0.2
16	1	18	0.1	60	1	58	0.1
13	1	18	0.2	57	1	58	0.3
23	1	18	0.2	60	1	59	0.3
30	1	29	0.2	57	1	59	0.1
28	1	29	0.2	54	1	59	0.2
24	1	29	0.3	64	1	59	0.2
39	1	29	0.1	70	1	69	0.3
39	1	34	0.3	67	1	69	0.1
24	1	34	0.1	64	1	69	0.2
33	1	34	0.2	74	1	69	0.2
35	1	34	0.2	74	1	69	0.2
32	1	37	0.2	73	1	68	0.2
42	1	37	0.3	63	1	68	0.2
36	1	37	0.3	67	1	68	0.3
39	1	37	0.1	70	1	68	0.1
39	1	38	0.3	70	1	68	0.1
36	1	38	0.1	79	1	78	0.2
33	1	38	0.2	77	1	78	0.2
43	1	38	0.3	73	1	78	0.2
43	1	48	0.3	83	1	78	0.2
53	1	48	0.2	89	1	88	0.3
47	1	48	0.3	83	1	88	0.3
50	1	48	0.1	87	1	88	0.3
47	1	49	0.1				

To compare mode shapes, coming from modal identification and from numerical modal analysis, some kind of normalization is necessary. In the present case components of mode shapes relative to not corrupted signals (fig.4.9) are normalized respect to their maximum absolute value, both for identified and numerical results.

Tab.4. 3 The experimental modes identified from the wireless data

Mode N.	fi [Hz]	ξ_i [%]	Mode
1	2.49	0.71	Vertical bending
2	4.83	0.81	Vertical bending

3	5.42	0.79	Vertical bending
4	7.09	1.23	Vertical bending
5	8.29	2.65	Torsional
6	10.13	1.06	Torsional
7	11.31	1.41	Vertical bending
8	12.14	1.35	Torsional
9	15.32	0.66	Torsional

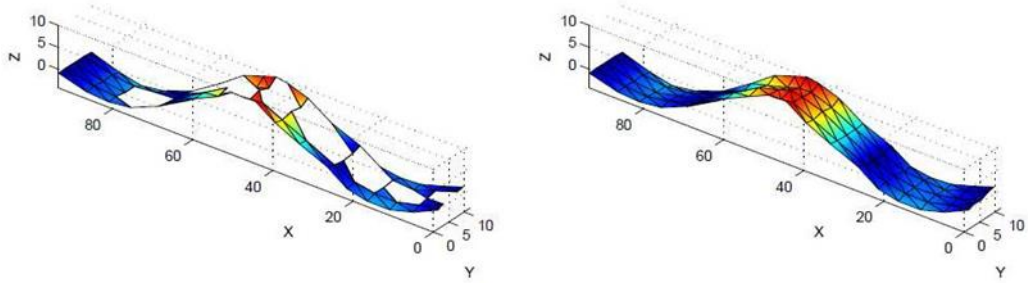

Fig.4. 11 First mode displayed both without and with slave points f = 2.49Hz

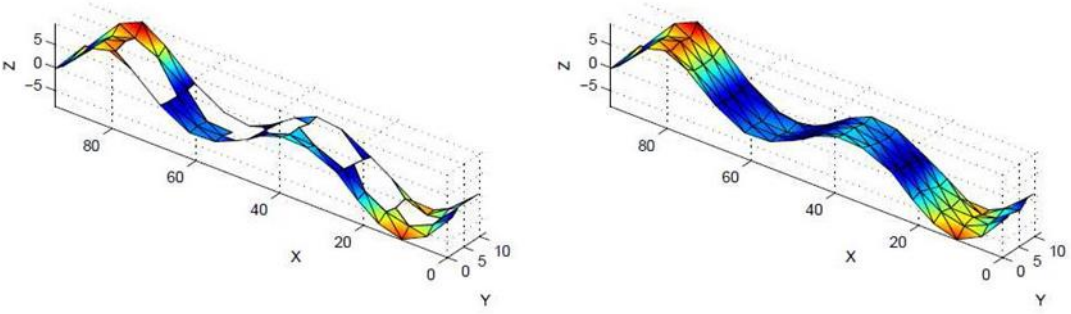

Fig.4. 12 Second mode displayed both without and with slave points f = 4.8Hz

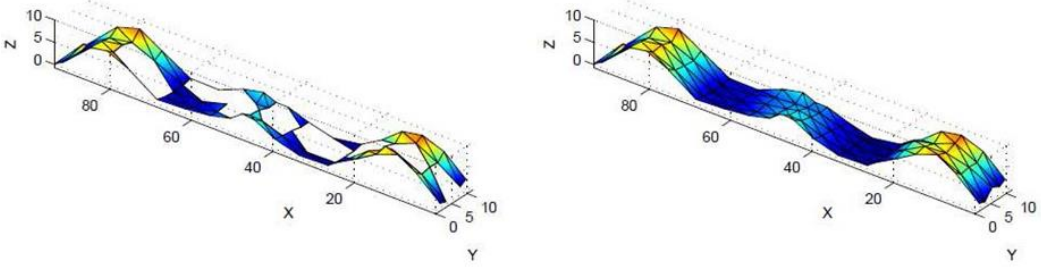

Fig.4. 13 Third mode displayed both without and with slave points f = 5.42Hz

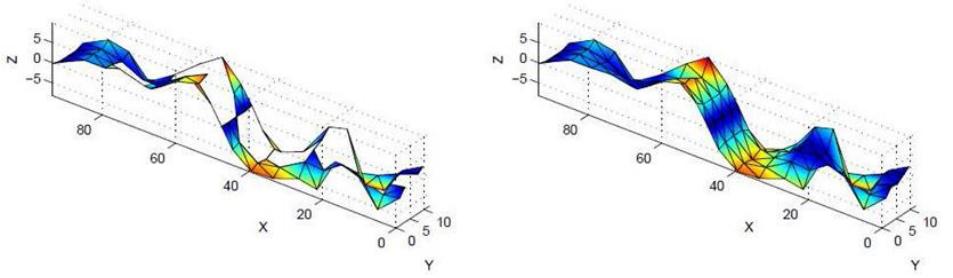

Fig.4. 14 Fourth mode displayed both without and with slave points f = 7.09Hz

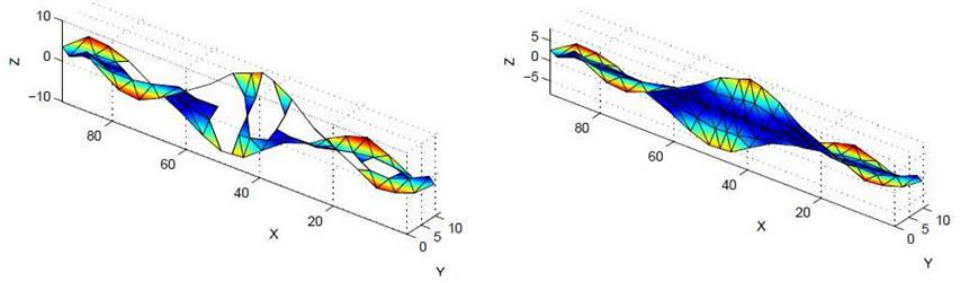

Fig.4. 15 Fifth mode displayed both without and with slave points f = 8.29Hz

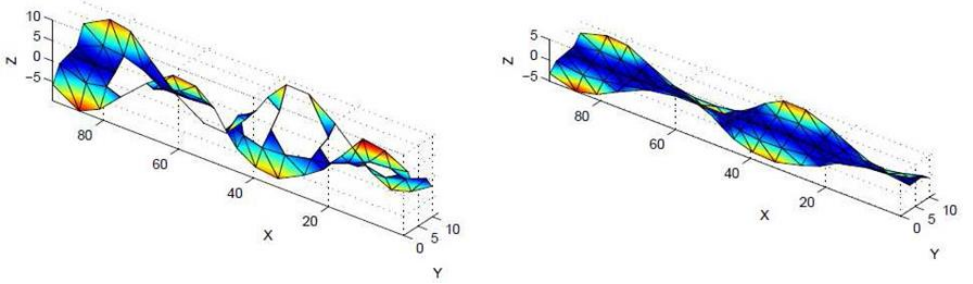

Fig.4. 16 Sixth mode displayed both without and with slave points f = 10.13Hz

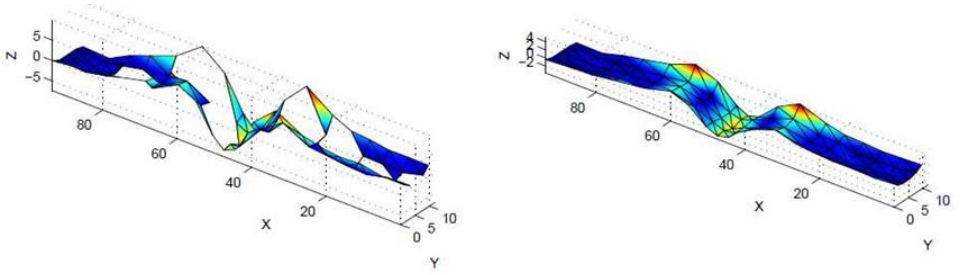

Fig.4. 17 Seventh mode displayed both without and with slave points f = 11.31Hz

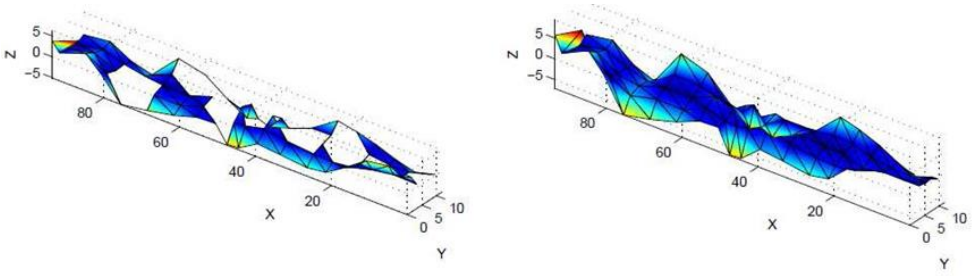

Fig.4. 18 Eighth mode displayed both without and with slave points f = 12.14Hz

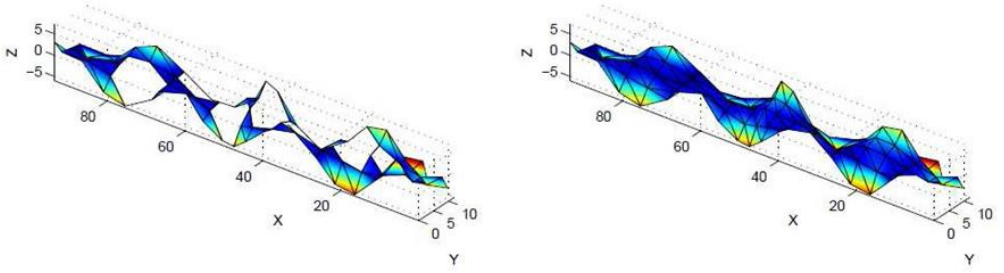

Fig.4. 19 Ninth mode displayed both without and with slave points f = 15.32Hz

4.4. FE tuning

4.4.1 The Douglas-Reid algorithm

In Douglas-Reid method（Douglas B. M., Reid, W. H., 1982）, the relationship between the *i-th* natural frequency of the model and the uncertain structural parameters X_k (k =1,2, …, N) of the model is approximated around the reference values of X_k, by the following:

$$f_i^* \left(X_i, X_2, \ldots, X_N\right) = \sum_{k=1}^{N}\left[A_{ik}X_k + B_{ik}X_k^2\right] + C_i \tag{4.1}$$

for i=1,2,...,N_f, where f_i^* represents the approximated *i-th* natural frequency of the FE model.

To satisfy the expression and solve the problem as stated in Eq. (4.1), (*2n +1*) constants (A_{ik} , B_{ik} , and C_i) must be determined beforehand to compare each f_i^* to its experimental counterpart. To calculate these constants, engineering judgment has to be made to estimate the reference values of the structural parameters X_k^0 and to decide the respective ranges where such structural

parameters may exist. Let's denote the lower and the upper limits of the uncertain parameters X_k as X_k^L, and X_k^U, respectively:

$$X_k^L \le X_k \le X_k^U \tag{4.2}$$

The 2*N* +1 constants A_{ik}, B_{ik} and C_i on the right-hand side of Eq. (4.1) are then determined by computing the *i-th* natural frequency f_i^{num} of the FE model under the 2*N* +1 combinations of the unknown parameters such as X_k^0, X_k^L and X_k^U (*k =1,2, …, N*). In details, the *2N + 1* conditions used to evaluate the constants in Eq. (4.1) are as follows:

$$\begin{cases} f_i^{num}\left(X_1^B, X_2^B, \cdots, X_N^B\right) = f_i^*\left(X_1^B, X_2^B, \cdots, X_N^B\right) \\ f_i^{num}\left(X_1^L, X_2^B, \cdots, X_N^B\right) = f_i^*\left(X_1^L, X_2^B, \cdots, X_N^B\right) \\ f_i^{num}\left(X_1^U, X_2^B, \cdots, X_N^B\right) = f_i^*\left(X_1^U, X_2^B, \cdots, X_N^B\right) \\ \vdots \\ f_i^{num}\left(X_1^B, X_2^B, \cdots, X_N^L\right) = f_i^*\left(X_1^B, X_2^B, \cdots, X_N^L\right) \\ f_i^{num}\left(X_1^B, X_2^B, \cdots, X_N^U\right) = f_i^*\left(X_1^B, X_2^B, \cdots, X_N^U\right) \end{cases} \tag{4.3}$$

The first line of the equation system (4.3) corresponds to X_k^0; then one of each structural parameter is varied, one at a time, from its reference value to the upper and the lower limits of X_k^L and X_k^U, respectively. Thus, the unknown constants A_{ik}, B_{ik}, and C_i can be uniquely determined by using Eq. (4.3). Once these constants are known, the approximation in Eq. (1) is defined. To update the uncertain parameters X_k, the following optimization problem can be introduced:

$$\mathbf{X}^* = \arg\min_{\boldsymbol{\theta}} J(\mathbf{X}) = \arg\min_{\boldsymbol{\theta}} \sum_i w_i (\varepsilon_i(\mathbf{X}))^2 \tag{4.4}$$

$$\text{With } \varepsilon_i(\mathbf{X}) = \tilde{f}_i - f_i^*\left(X_1, X_2, \cdots X_n\right)$$

and *i=1,2,...,N*$_f$, where $\tilde{f}_i$ and f_i^* represent the *i-th* experimentally identified and numerically calculated natural frequency (given by Eq.(4.1)), respectively. It aims at finding the best parameter set that minimizes the difference between the numerically predicted natural frequencies and their experimentally measured counterparts. A weighting constant w_i can be introduced to balance the contributions of each ε_i into the objective function. In the current study, a value $w_i = 1$ was used. Eq. (4.4) can readily be solved by using any optimization algorithm. Herein, the Rosenbrock search method (Rosenbrock, H. H., 1960) was

used, because it's particularly applicable to an optimization problem when the objective function is inexpensive to calculate such as in Eq. (4.4).

4.4.2 The sensitivity-based iterative algorithm

By using a sensitivity-based iterative algorithm, the FE model updating procedure is formulated into an optimization problem similar to that of the direct method. Whereas, no approximate relationship is needed to calculate the numerical modal data. Modal data of both the natural frequencies and the mode shapes are easily included into the objective function. In detail, the objective is to minimize over the optimization variable θ the following nonlinear least squares problem:

$$\boldsymbol{\theta}^* = \arg\min_{\boldsymbol{\theta}} J(\boldsymbol{\theta}) = \arg\min_{\boldsymbol{\theta}} \boldsymbol{\varepsilon}_z(\boldsymbol{\theta})^T \mathbf{W}_\varepsilon \boldsymbol{\varepsilon}_z(\boldsymbol{\theta}) = \arg\min_{\boldsymbol{\theta}} \sum_i w_{\varepsilon,i} \left(\varepsilon_{z,i}(\boldsymbol{\theta})\right)^2 \tag{4.5}$$

In the above equation, $\boldsymbol{\varepsilon}_z$ denotes the residuals between the numerical and experimental modal data z. For the undamped eigenvalue ($z = \lambda$), the residuals $\varepsilon_{\lambda,i}(\boldsymbol{\theta})$ are given by

$$\varepsilon_{\lambda,i}(\boldsymbol{\theta}) = \frac{\lambda_i(\boldsymbol{\theta}) - \tilde{\lambda}_i}{\tilde{\lambda}_i}, \text{ for } \lambda_i = \omega_i^2 = (2\pi f_i)^2 \text{ and } i \in \{1,\ 2,\ \ldots,\ n_\lambda\} \tag{4.6}$$

where the upper tilde denotes the experimental values and f (or ω) stands for the (angular) natural frequency. For the mode shape ($\mathbf{z} = \boldsymbol{\varphi}$), the residuals $\boldsymbol{\varepsilon}_{\phi,i}(\boldsymbol{\theta})$ are given by

$$\boldsymbol{\varepsilon}_{\phi,i}(\boldsymbol{\theta}) = \frac{\boldsymbol{\varphi}_i(\boldsymbol{\theta}) - \tilde{\boldsymbol{\varphi}}_i}{\left\|\tilde{\boldsymbol{\varphi}}_i\right\|_1}, \text{ for } i \in \{1, 2, \ldots, n_\phi\} \tag{4.7}$$

where both the numerical and experimental mode shape vectors ($\boldsymbol{\varphi}_i$ and $\tilde{\boldsymbol{\varphi}}_i$) are normalized to the maximum unity and only the real parts are considered in $\tilde{\boldsymbol{\varphi}}_i$. $\|\mathbf{x}\|_1 := \sum_j |x_j|$ is the sum of the absolute values of the vector x, according to the 1-norm. Each individual entities of the vector of the mode shape residuals $\boldsymbol{\varepsilon}_{\phi,i}(\boldsymbol{\theta})$ are considered as a residual item in Eq.(4.5), i.e., $\varepsilon_{\phi,j}(\boldsymbol{\theta})$, for $j \in \{1, 2, \ldots, n_\phi \times n_{DoF}\}$, being n_{DoF} the size of the mode shape vector. In Eq.(4.5), $\mathbf{W}_\varepsilon$ is the diagonal

weighting matrix, which provides a way to balance the contributions of each individual residual. Although the values of $w_{\varepsilon,i}$ can be estimated in different ways, herein we consider the requisite of an equal amplitude for the contributions of $\varepsilon_{\lambda,i}$ and $\boldsymbol{\varepsilon}_{\phi,i}$ by assuming:

$$w_{\varepsilon_\lambda,i}=1, \text{ for } i\in\{1,\ 2,\ \ldots,\ n_\lambda\} \text{ and } w_{\varepsilon_\phi,i}=1, \text{ for } i\in\{1,\ 2,\ \ldots,\ n_\phi\times n_{DoF}\}$$

In the current study, to update the uncertain structural parameters the optimization variable θ is chosen as θ =X= {X_1, X_2, …, X_N}. Eq.(4.5) is solved with an iterative sensitivity-based method, namely the Trust-Region-Reflective optimization algorithm implemented by MATLAB(REYNDERS E.et.al.2010). The upper and lower limits of the values of θ needs to be provided in order for the algorithm to find the solutions.

4.4.3 Choice of the uncertain structural parameters – multiple parameters

As the first step in the calibration process, a parametric study was performed to identify the most sensitive parameters affecting the FE model-computed modal frequencies and mode shapes. The changes in the selected parameters should potentially have a considerable effect on the global vibration response of the bridge rather than on local vibration responses. These parameters are those that contribute significantly to the mass or stiffness properties of the structure. Therefore, the material properties of the major structural components, size/thickness of those structural components, are just some of the potential parameters that can be selected for the FE model calibration. Also, parameters are selected among those whose exact values have high degrees of uncertainty. The uncertainty could be due to possible changes in the structure from the time of construction, differences between the as-built constructed structure and the engineering drawings, non-structural parameters that are not presented in the engineering drawings and, in general, any parameter where the required information cannot be found about their accurate values in the engineering drawings. After a careful consideration of the initial FE model and the available engineering drawings, 10 parameters were selected in the bridge FE model to perform sensitivity analyses. These parameters were related to either boundary conditions or the mass/stiffness properties of the FE model. The selected parameters along with the lower/upper bounds of their values are listed in Table 4.4.

Tab.4. 4 List of parameters used for the FE model updating process

Parameters	Mean	Min	Max
Equivalent mass of the sidewalk in the middle	25	12.5	37.5
Equivalent elastic modulus of the sidewalk in	36000000	28800000	43200000
Equivalent mass of the sidewalk on the	25	12.5	37.5
Equivalent elastic modulus of the sidewalk on	32400000	25920000	38880000
Equivalent mass of the slab in the middle	25	12.5	37.5
Equivalent elastic modulus of the slab in the	36000000	28800000	43200000
Equivalent mass of the slab on the supports	25	12.5	37.5
Equivalent elastic modulus of the slab	32400000	25920000	38880000
Vertical stiffness of the support for the pier 1	7883000	3941500	11824500

There were no data found in the engineering drawings about the thickness of the asphalt overlay on the bridge. This parameter was included in the model an equivalent material weighing the mechanical properties of the concrete with the mechanical properties of the asphalt. Similar procedure was developed for the elastic modulus and weight of the sidewalk, in practical a weighed value has been used in order to take into account the paving. A lower and upper range of +/- 20% was chosen as variation for the sensitivity parameters. Modal analyses were performed using the lower and upper bound values of the selected parameters listed in Table 4.4. The frequency values were obtained from a modal analysis of the FE model output. The sensitivity of the modal frequencies with respect to the selected value of any of the 10 parameters, pi, were computed using:

$$s_{ij} = \frac{p_i}{\Delta p_i} \cdot \frac{\Delta \omega_j}{\omega_j}$$

The calculated sensitivity values for the 10 selected parameters are shown in Figure 4.20. As can be seen in Figure 6, it was found that eight parameters, including all masses and elastic modulus of the material used. The parameters selected to simulate the boundary condition of the bridge did not show sensitivity as comparable to the parameters associated with the mass and stiffness properties of the bridge. As a result, these model parameters were not considered further during model updating.

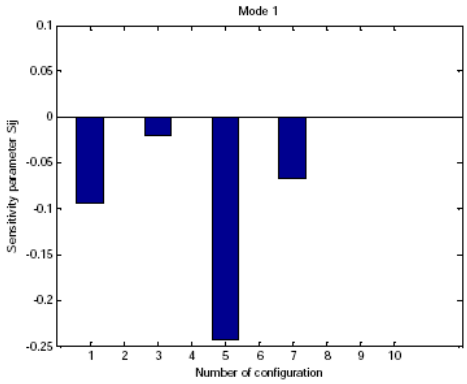
Mode 1
Sensitivity parameter Sij
Number of configuration

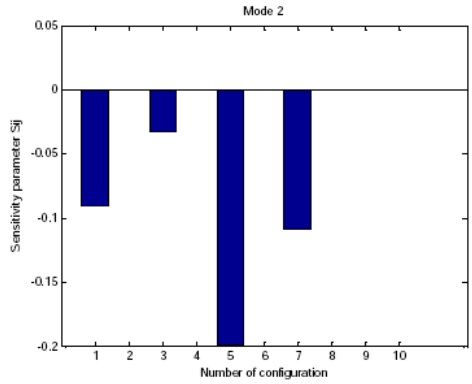
Mode 2
Sensitivity parameter Sij
Number of configuration

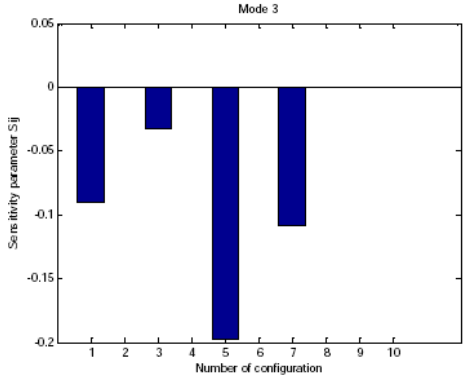
Mode 3
Sensitivity parameter Sij
Number of configuration

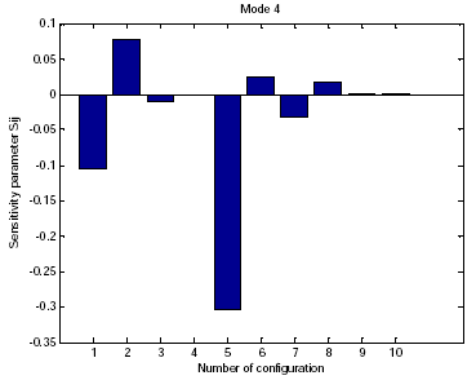
Mode 4
Sensitivity parameter Sij
Number of configuration

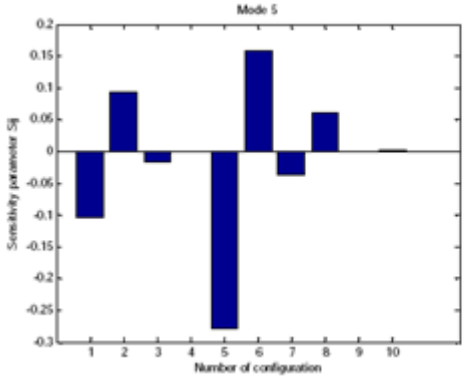
Mode 5
Sensitivity parameter Sij
Number of configuration

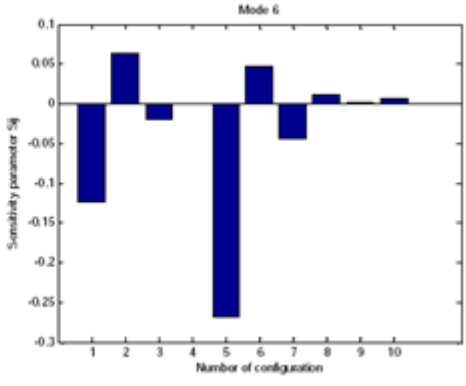
Mode 6
Sensitivity parameter Sij
Number of configuration

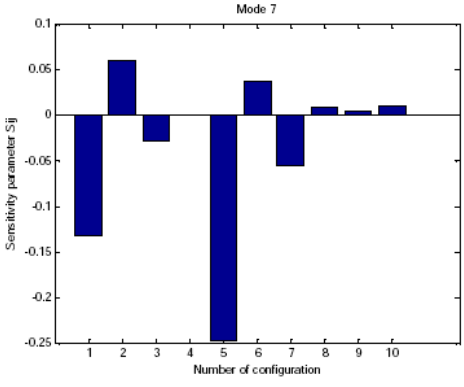
Mode 7
Sensitivity parameter Sij
Number of configuration

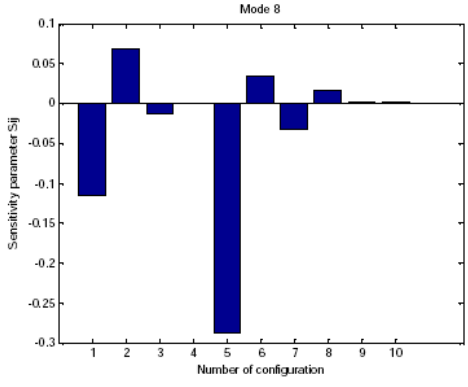
Mode 8
Sensitivity parameter Sij
Number of configuration

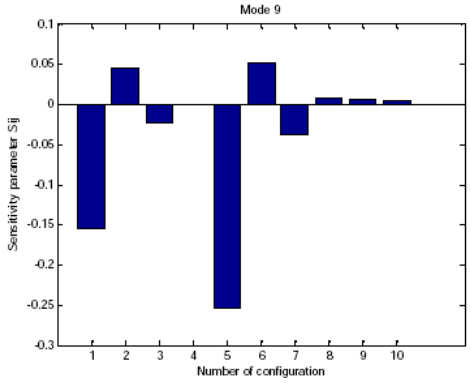
Mode 9
Sensitivity parameter Sij
Number of configuration

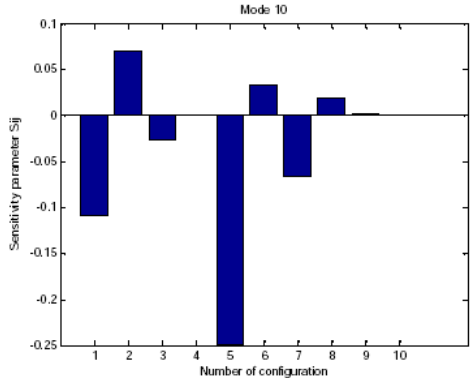
Mode 10
Sensitivity parameter Sij
Number of configuration

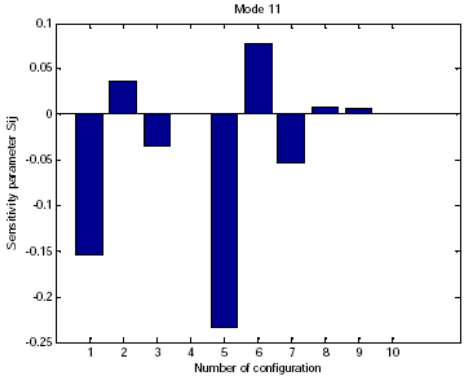
Mode 11
Sensitivity parameter Sij
Number of configuration

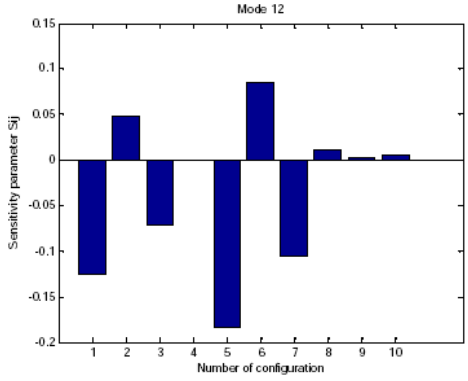
Mode 12
Sensitivity parameter Sij
Number of configuration

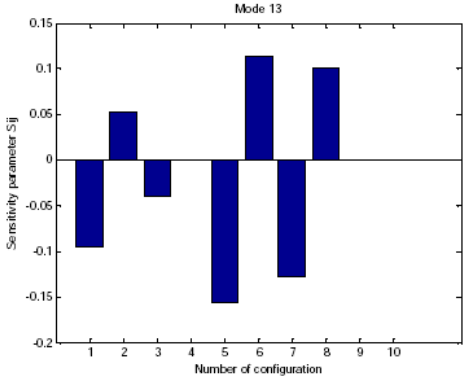
Mode 13
Sensitivity parameter Sij
Number of configuration

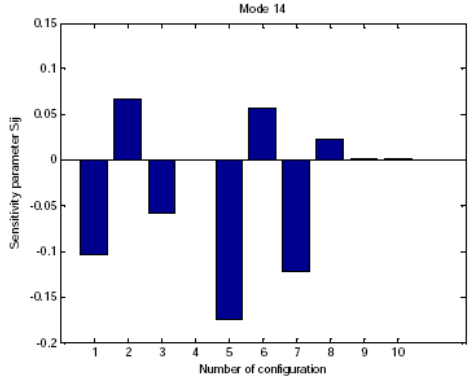
Mode 14
Sensitivity parameter Sij
Number of configuration

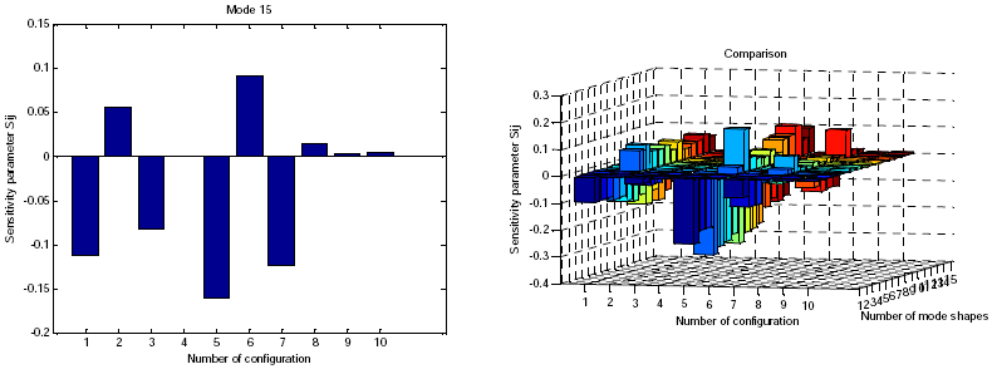

Fig.4. 20 The calculated sensitivity values for the 10 selected parameters

Five of them shown a satisfactory sensitivity, therefore they are designed as variables of the optimization process. The designed variables are here listed (ordered by sensitivity ratio):

- Equivalent elastic modulus of the slab on the supports;
- Equivalent elastic modulus of the slab in the middle spam;
- Equivalent elastic modulus of the sidewalk in the middle spam;
- Equivalent elastic modulus of the sidewalk on the supports;
- Equivalent elastic modulus of the pier;

4.4.4 Comparison of the two methods using simulated results—Muti-parameters

On the basis of the findings in the previous subsection, the experimental modal data were introduced as the target of FE updating in comparison of the two methods. The reference (or initial) values of E_S and E_C were chosen as E_{deck}^0=205GPa $E_{s\text{-}bracing}^0$=205GPa and E_{slab}^0=33GPa E_{pylon}^0=36GPa in both the direct method and the iterative method. The solutions of the direct method were found to be $_{deck}^0$=205GPa $E_{s\text{-}bracing}^0$=215GPa and E_{slab}^0=31.35GPa E_{pylon}^0=38GPa The solution of the iterative method were found to $_{deck}^0$=216GPa $E_{s\text{-}bracing}^0$=218GPa and E_{slab}^0=33.74GPa E_{pylon}^0=41.67GPa

Goodness of the model updating process depends on the values of the weighting factors, W_f and W_z, used to balance the importance of the modal frequency and mode shape parts of the objective function, respectively. One of the two weighting factors (W_f) was taken as 2 in all analyses since these factors define a relative importance between modal frequency and mode shape in the updating process. The value initially selected for Wz was 4. The reason for the large value of Wz with respect to W_f is that the errors between the measured and FE-computed mode

shapes are considered in the objective function in terms of the MAC values with MAC values always smaller than 1. Therefore, a larger Wz should be chosen to balance the importance of modal frequencies and mode shapes in the objective function. The final FE-updated modal frequencies are presented in Table 4.5. As seen in Table 4.5, the differences between the measured and initially calculated modal frequencies vary from 0.2% for the first mode to -12.86% for the fifth mode. In total, 7 modes between 2.463 Hz and 11.335 Hz are obtained by the FE modal analysis. The calculated natural frequencies and the mode types are listed. Both vertical bending modes along the longitudinal directions and vertical bending modes with deformation of the cross section are found in the modal analysis results. Local modes with deformation of the slab and the side barriers are also predicted by the FE analysis.

Table 4.5 provides a summary of the numerical modal results of the updated FE models in comparison to the experimental results. The numerical modal results of the reference/initial FE model (with $E_S = E_S^0$ and $E_C = E_C^0$) were also included. The subscripts ini, D and I denote the initial model, the updated model with the direct method and the updated model with the direct method, respectively. Whilst f_{2010} is the experimental natural frequencies. And the MAC values were calculated between the experimental and the numerical mode shapes.

Tab.4. 5 Numerical modal results of the updated FE models, in comparison to their experimental counterparts

Nr.	f_{2011}(Hz)	$f_{FE\text{-}ini}$(Hz)	$\Delta f_{FE\text{-}ini}$(%)	MAC	$f_{FE\text{-}D}$(Hz)	$\Delta f_{FE\text{-}D}$(%)	MAC_D	$f_{FE\text{-}I}$(Hz)	$\Delta f_{FE\text{-}I}$ (%)	MAC_I
1	2.489	2.463	-1.02	0.90	2.476	-0.51	0.91	2.492	0.13	0.92
2	4.833	4.569	-5.47	0.72	5.035	4.18	0.84	4.813	-0.41	0.88
3	5.417	6.100	12.60	0.90	5.743	6.02	0.91	5.633	3.99	0.94
4	7.089	6.951	-1.94	0.82	6.963	-1.77	0.86	6.949	-1.97	0.91
5	8.290	7.223	-12.86	0.69	7.834	-5.49	0.79	7.991	-3.60	0.84
6	10.130	9.484	-6.37	0.89	9.583	-5.40	0.88	9.774	-3.51	0.93
7	11.312	11.335	0.20	0.77	11.42	0.95	0.83	11.372	0.53	0.87

$\Delta f_{FE-ini} = (f_{FE-ini} - f_{2011})/f_{2011}$; $\Delta f_{FE-D} = (f_{FE-D} - f_{2011})/f_{2011}$;
$\Delta f_{FE-I} = (f_{FE-I} - f_{2011})/f_{2011}$

The relative differences of the natural frequencies between the experimental results and the initial and the updated models were calculated by introducing the following index $\Delta\bar{f} = \sqrt{\sum_{i=1}^{n} (\Delta f_i)^2}$ .It is found $\Delta\bar{f}_{ini} = 7.83\%$, $\Delta\bar{f}_D = 4.41\%$ and $\Delta\bar{f}_I = 2.65\%$. It is noted that the updated model obtained with the iterative method

is slightly improved with respect to the natural frequencies as compared to the initial model. Whereas the model that is obtained with the direct method is similar to the initial model with respect to the natural frequencies. It may be explained by the fact that assumed reference value of the updating parameter E_S and E_C are quite close to the "exact" solution. Since the initial model already match the experimental model results with a relatively high MAC values, no significant improvement is observed of the updated models for either the direct method or the iterative method with respect to the model shapes.

Conclusions

In summary of the findings of the two subsections, it can be concluded by using the iterative method the solutions of the updating parameters are generally more accurate as compared to the direct method. Nevertheless, both methods can lead to the models with satisfactory modal results as compared to the experimental data, if a good choice of the reference values is made. In addition, the relatively lower computational costs of the direct method shall also be noted.

CHAPTER 5

5. KEY STUDY-MARGHERA CABLE STAYED BRIDGE

5.1 Marghera cable stayed bridge

Cable-stayed bridges play an important part in transportation systems all round the world. Especially, in the last decade, cable-stayed bridges were built in unusual styles for the considerations of structure, aesthetics and so on. Examples include the investigated bridge in this paper – bridge of Porto Marghera (Figure 5.1).

Fig.5. 1 bridge of Porto Marghera

Fig.5. 2 bridge of Porto Marghera

Fig.5. 3 The curved cable-stayed bridge of Porto Marghera (Venice, Italy)

Fig.5. 4 The curved cable-stayed bridge of Porto Marghera (Venice, Italy)

The construction of the bridge was required to cross the West Industrial Canal in the Marghera basin and to complete the road link between the national highway and the port areas. The bridge is characterized by an inclined L-shape pre-stressed concrete pylon, a single set of cables with spatial arrangement and curved steel-concrete composite deck.

The unique structural styles of these bridges beautify the environment but also add to the difficulties in accurate structural analysis. The special geometric layout of the deck and of the inclined tower have motivated:

- extensive studies developed during the design and the construction phases aimed to adequately define static and dynamic behavior;
- the use of a permanent monitoring system, installed during construction in order to acquire control over the most significant construction phases.

For the realization of the monitoring system the use of a SOFO™ fiber optics sensor family (Inaudi et al. 1994) was chosen to assess both static and dynamic responses and extended to three times ambient vibration testing were done during period (LLORET et al., 2003). The system has been mainly designed for permanent static monitoring but linear deformation sensors and their locations have however been selected in order to allow the execution of periodic dynamic measurements and identification of the dynamic characteristics in terms of natural frequencies;

Before the opening of the bridge to traffic, a load test was carried out together with an ambient vibration dynamic tests with the objective of:

- fully understand the three-dimensional dynamic characteristics of the bridge, mainly determined by the deck curvature and by the inclined tower;
- provide a sound basis for the validation of a detailed finite element (F.E.) suitable for long term monitoring of the structure;
- provide a proper baseline for the future monitoring and a validation of the results of the monitoring system.

The results of operational (ambient vibration) modal testing and tuned FE model are presented on this paper.

Taking this FE model like the reference one, able to describe the actual state of the bridge, both from dynamic and static point of view, an analysis is conducted to investigate the real potentiality of the system to capture growing of specific critical damages for the bridge. Inclined pylon and cable have been identified like the critical elements for the bridge. The capacity of the SOFO™ monitoring system to capture alarming “signal” relative to bridge health is deeply discussed.

5.1.1 Bridge Description

The investigated bridge, roadway viaduct, linking the city of Mestre to the Commercial Harbor of Venice-Marghera, Italy (Figure 1), has a total length of 387 m on six spans (42 m + 105 m + 126 m + 30 m + 42 m + 42 m), with the first span on a straight alignment and the others curved with a radius of 175 m. Plan, elevation and typical cross-sections of the deck are shown in Figure 5.3. (Briseghella et. al. 2010). The two main spans of the bridge, crossing the West Industrial Canal, are arranged on a cable stayed layout with the stays, arranged on a single plane, connected to the center of the cross section to a box girder. The total width of the deck is 23.70 m for two traffic lanes and three pedestrian walkways (Figure 5.3).

The structural arrangement of the deck consists of a composite steel and concrete continuous girder, covering all the six spans. In such a frame, two main cross-sections can be identified: the first one, adopted at the end-spans, consists of four double-T steel girders while the second one, characterizing the central spans, consists of two outer double-T steel girders and one central girder of box section (Figure 2). The girders are stiffened by transverse cross-beams (namely double-T beams spaced every 5.25 m); steel girders and cross-beams have a height of 1.90

m and are connected to an overlaying cast-in place concrete slab, with a thickness of 25-27 cm (Figure 5.3). The cast-in-place pre-stressed concrete inclined tower is a visually memorable landmark and played a determining role in the conceptual and executive design of the bridge. The tower has a height of roughly 75 m and is characterized by a complex geometric layout, with the triangular cross section varying its dimensions along the inclined longitudinal axis. In the specific case, the base of the cross-section enlarges upward so to provide a more suitable anchorage zone for the stays.

It is worth mentioning that the tower was pre-stressed in order to reduce the eccentricity of the dead load due to the curved layout of the deck.

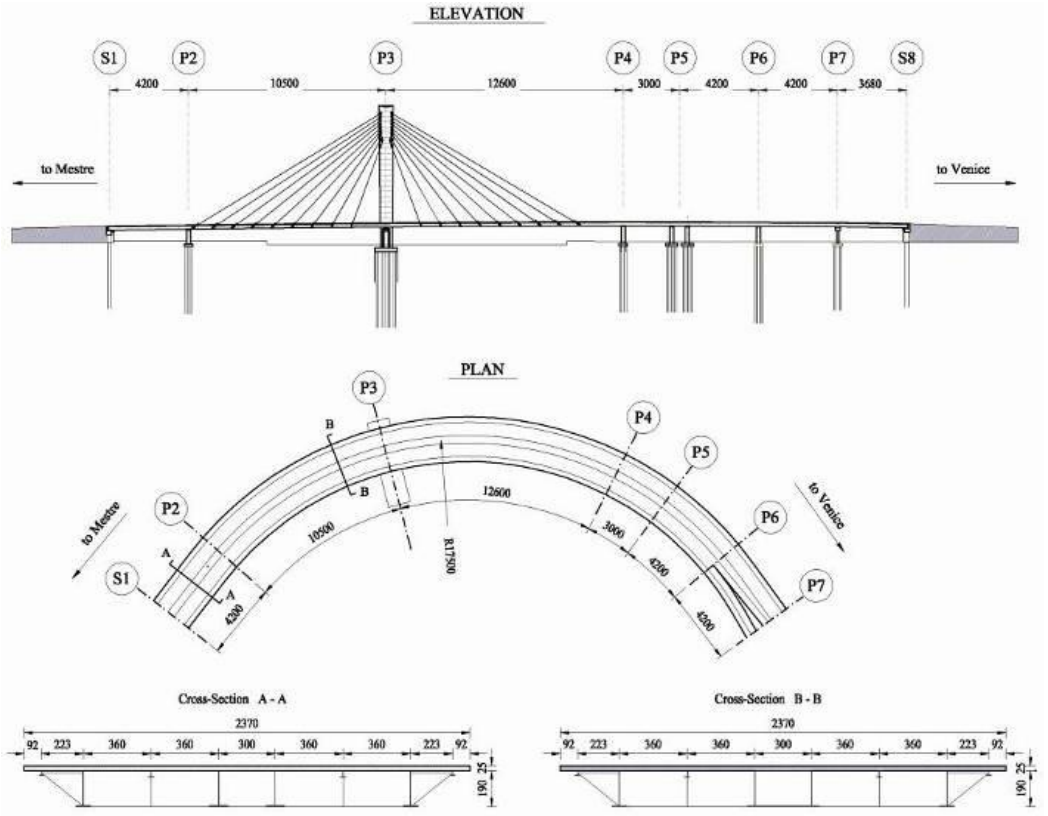

Fig.5. 5 Plan view, elevation and typical deck cross-section (dimensions in cm)

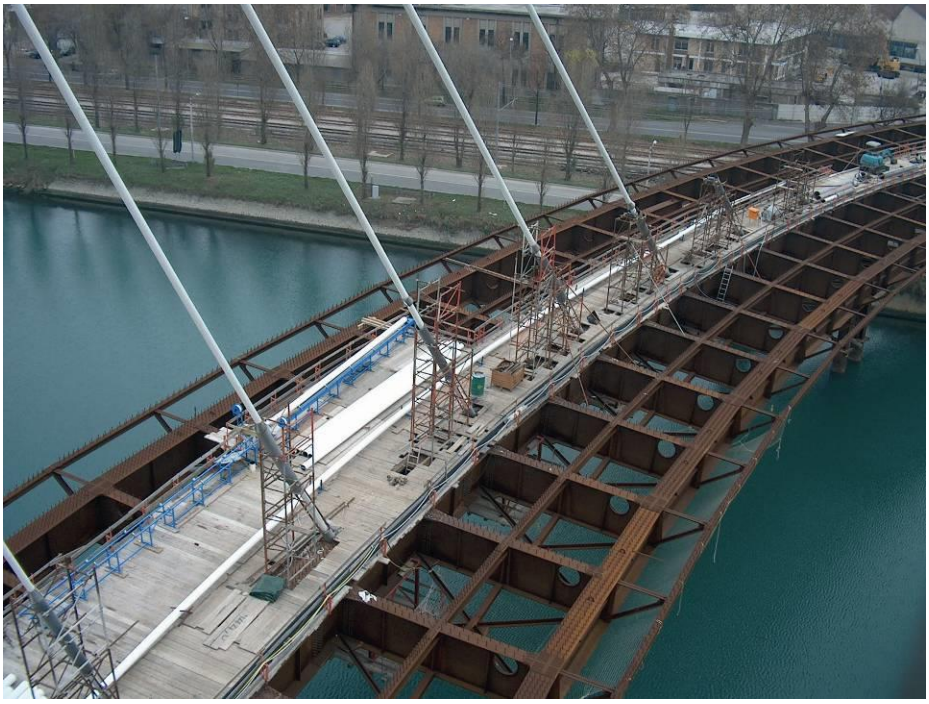

Fig.5. 6 View of the deck structural frame during construction

Fig.5. 7 View of the inclined tower

Fig.5. 8 View of the inclined tower

5.2 FE simulation

5.2.1 CAD modelling and FE model

In the CAD model, the geometry of the bridge was accurately defined accounting for the curved layout of the deck and its transverse slope, which was different in each bridge segment from S1 to S7 (figure 5.3). In particular, the transverse slope increases from S1 to S3, up to a maximum slope of 4.5%, and decreases from S3 to S7. Furthermore, in the definition of the steel members of the deck (figure 5.6): (a) the different types of beam cross-section were associated to different CAD layer; (b) all the beam elements were represented along the centroid axis; (c) vertical rigid offsets were drawn to connect the nodes of beam elements to the nodes of shell elements in order to model the steel-concrete composite action; (d) the mesh was already virtually defined manually. Finally, the tower and its basement were drawn in order to allow the later modelling by solid elements (figure 5.5 and 5.7).

The CAD model was subsequently transferred to the software SAP2000 to create the FE model of the bridge, that was formulated using the following assumptions:

1. Three- and four-nodes shell elements were used to model the concrete slab; Considering the influence of different elements of structure dynamic performance, we try to use six-nodes and eight-nodes to model the concrete slab and to comparison, the results were listed in the table 1.5 and 1.6.
2. the tower P3 and its basement were modelled by solid elements;
3. the concrete piers P1-P2 and P4-P8 were modelled by two-nodes 3D beam elements;
4. the weight per unit volume and the Poisson's ratio of the concrete were held constant and equal to 25,0 kN/m3 and 0,2, respectively;
5. an additional weight per unit surface of 1 kN/m2 was considered for the deck slab, to account for the effects of the asphalt pavement and walkways;
6. steel stringers, transverse cross-beams and bracing elements of the deck were modelled by two-nodes 3D beam elements. The modulus of elasticity and the weight per unit volume of the steel were assumed as 205 GPa and 785 kN/m^3, respectively;
7. rigid links (without mass density) were used: (a) between the concrete slab and the grid of steel stringers and transverse cross-beams; (b) to reproduce offsets between the structural members and (c) to account for the arrangement of strut-and-tie bracings of the deck;

8. the stays were modelled by 3D truss elements; In order to consider the effect of cable force on the dynamic performance, we compared adding the measured cable forces to without cable forces in the FE model.
9. The boundary conditions between piers P1-P9 and the foundation were assumed as fixed. The deck constraints were modelled by introducing translational beam end-releases between the transverse frame elements and the lower piles according to construction drawing.
10. The asphalt layers were added in the model, we consider the effect of the weight of the asphalt layers in the model, the results were listed in the table.

The FE model, shown in Fig.5.7, has a total of 8014 nodes and 6600 elements (namely 2946 beams, 18 trusses, and 3636 solid elements).

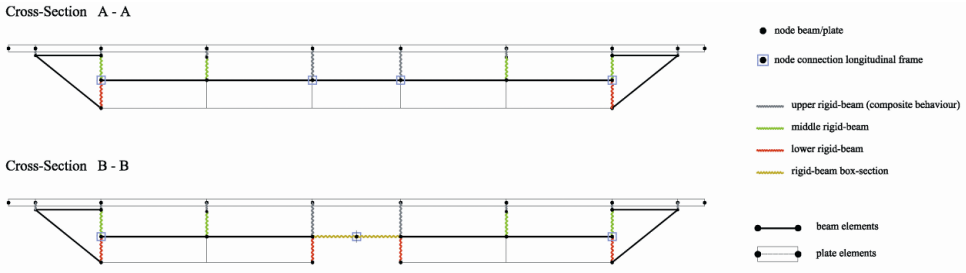

Fig.5. 9 Typical modelling of the deck cross-sections

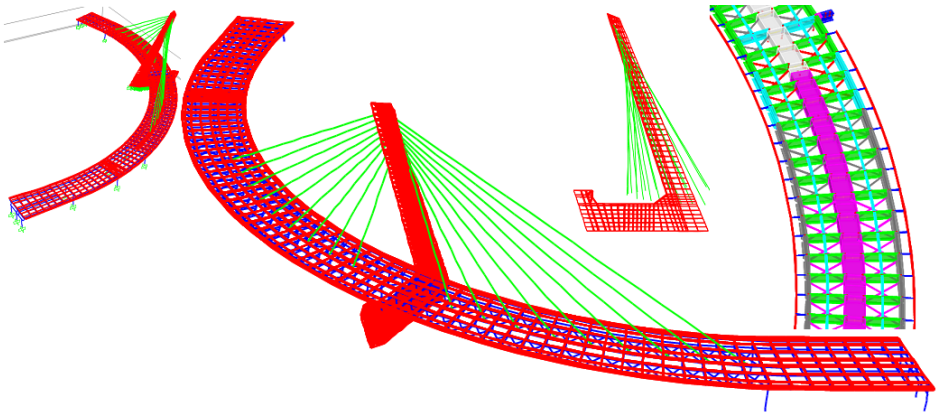

Fig.5. 10 General arrangement and details of the FE model

5.2.2 FE analysis and correlation with the experimental results

Since the FE model development accounted for the geometric and structural complexity of the viaduct with as much detail as possible, the main uncertainties are related to the actual behavior of the constraints and to the Young's modulus of the

concrete elements: deck (E_D), piers P1-P2-P4-P5-P6-P7 (E_P), tower and basement P3 (E_T). Hence, some preliminary dynamic analyses were performed to check the similarity between experimental and theoretical modal parameters. In these analyses, different values of E_D, E_T and E_P (ranging from 34 to 42GPa) were used; in each case, the correlation between theoretical and experimental modal behavior seems to provide a sufficient verification of the main assumptions adopted in the model, being a reasonable agreement between the mode shapes.

A first manual tuning (Gentile 2004, 2006)provided the following values of E_D, E_T and E_P:

$E_D = E_T = 40.0$ GPa $\qquad\qquad$ $E_P = 36.0$ Gpa

Selected mode shapes of this model are shown in figure 5.8. The modal characteristics of the model are compared with the experimental data in Table 5.1 and 5.2, through the through the frequency discrepancy $\Delta f_{FDD-FEM} = |(f_{FDD}-f_{FEM})/f_{FDD}|$. It can be observed that, although a couple of experimental modes are not correctly reproduced by the model, the relative error between natural frequencies is rather small (with the frequency discrepancy being generally less than 5% expect for modes T2, B7 and B8); in addition the measurement-based mode shapes and computed mode shapes exhibit a good match as well.

The above results clearly highlight that the model represents a fairly good approximation of the real structure and could surely be adopted either as baseline model for the long-term monitoring or suitable starting point" for more refined procedures of structural identification.

f_{FEM} = 0.674 Hz $\quad$ f_{FDD} = 0.645 Hz $\quad$ f_{FEM} = 0.965 Hz $\quad$ f_{FDD} = 0.996 Hz

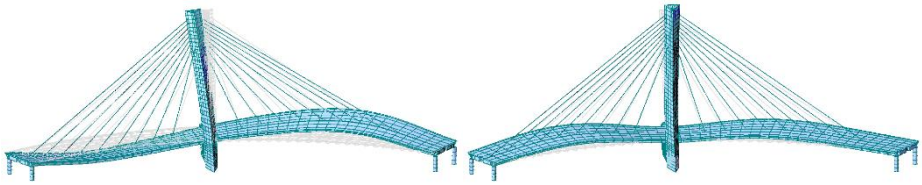

f_{FEM} = 1.198 Hz $\quad$ f_{FDD} = 1.191 Hz $\quad$ f_{FEM} = 1.400 Hz $\quad$ f_{FDD} = 1.445 Hz

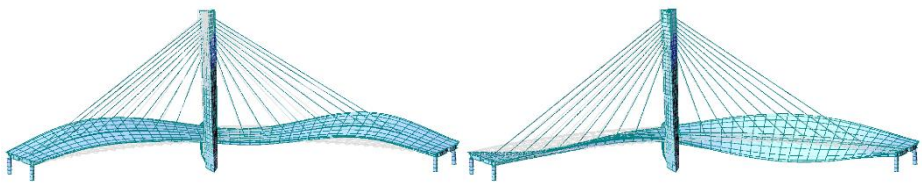

f_{FEM} = 1.647 Hz f_{FDD} = 1.582 Hz f_{FEM} = 1.594 Hz f_{FDD} = 1.699 Hz

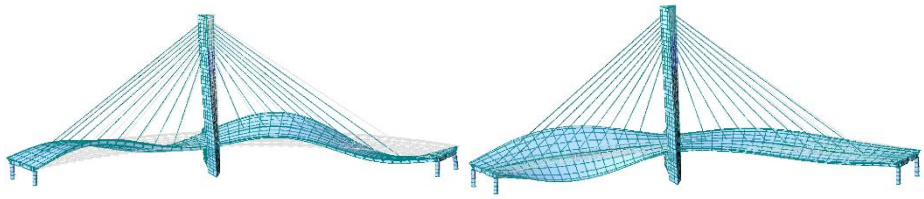

Figure 5.8 Selected vibration modes of the FE model (E_D = E_T = 40.0 GPa; E_P = 36.0 GPa)

5.2.3 The comparison of FEA and experiment data

Tab.5 1 The comparison of 2010 and FEA of mode shapes

6 **B=bending-dominate modes; T=torsion-dominate modes; M=mixed modes. O=original modes; +CF=modes of added cable forces; E=modes of changed the shell elements to solid elements;*

7 *+CE= modes of added cable forces and changed the shell elements to solid elements;*

8 *+C E A=modes of added cable forces and asphalt layer and changed the shell elements to solid elements;*

	f2010	O	Δf%	+ C F	Δf%	E	Δf%	+ C E	Δf%	+C E A	Δf%
B1	0.64	0.67	6.16	0.68	6.77	0.71	11.11	0.71	11.66	0.68	7.35
B2	1	0.96	-3.14	0.97	-2.39	0.97	-2.41	0.98	-1.72	0.97	-2.16
B3	1.14	1.2	4.85	1.2	5.02	1.25	9.44	1.25	9.52	1.19	4.68
T1	1.39	1.3	-6.21	1.3	-6.17	1.37	-1.31	1.37	-1.16	1.31	-5.79
M1	1.52	1.59	4.69	1.59	4.7	1.74	14.12	1.74	14.43	1.67	9.13
T2	1.6	1.65	2.78	1.65	2.82	1.79	11.69	1.79	11.73	1.74	6.05
B4	1.95	2.17	11.19	2.17	11.21	2.29	17.05	2.29	17.08	2.2	12.53
T3	2.64	2.68	1.71	2.68	1.72	2.99	13.35	2.99	13.35	2.9	7.57
T4	3.17	3.16	-0.48	3.16	-0.48	3.52	10.95	3.52	10.95	3.41	5.25
T5	4.05	3.78	-6.74	3.78	-6.74	4.13	1.87	4.13	1.87	3.96	-2.93
T6	4.93	4.58	-7.23	4.58	-7.22	5	1.4	5	1.4	4.8	-3.51
T7	-	5.33	-	5.34	-	5.76	-	5.76	-	5.54	-
T8	5.6	5.7	1.9	5.7	1.9	5.89	5.22	5.89	5.22	5.63	-0.01
T9		6.11	-	6.11	-	6.68	-	6.68	-	6.4	-
T10	6.83	6.73	-1.39	6.73	-1.39	7.1	4.05	7.1	4.03	6.81	-0.81

Tab.5 2 The comparison of 2011 and FEA of mode shapes

**B=bending-dominate modes; T=torsion-dominate modes; M=mixed modes. O=original modes; +CF=modes of added cable forces; E=modes of changed the shell elements to solid elements;*
+CE= modes of added cable forces and changed the shell elements to solid elements;
+C E A=modes of added cable forces and asphalt layer and changed the shell elements to solid elements;

	f_{2011}	O	Δf%	+ C F	Δf%	E	Δf%	+ C E	Δf%	+C E A	Δf%
B1	0.64	0.67	6.16	0.68	6.77	0.71	11.11	0.71	11.66	0.68	7.35
B2	1	0.96	-3.14	0.97	-2.39	0.97	-2.41	0.98	-1.72	0.97	-2.16
B3	1.14	1.2	4.85	1.2	5.02	1.25	9.44	1.25	9.52	1.19	4.68
T1	1.39	1.3	-6.21	1.3	-6.17	1.37	-1.31	1.37	-1.16	1.31	-5.79
M1	1.52	1.59	4.69	1.59	4.7	1.74	14.12	1.74	14.43	1.67	9.13
T2	1.6	1.65	2.78	1.65	2.82	1.79	11.69	1.79	11.73	1.74	6.05
B4	1.96	2.17	10.62	2.17	10.65	2.29	16.45	2.29	16.49	2.2	11.96
T3	2.65	2.68	1.37	2.68	1.38	2.99	12.97	2.99	12.97	2.9	7.21
T4		3.16	-	3.16	-	3.52	-	3.52	-	3.41	-
T5	4.07	3.78	-7.17	3.78	-7.17	4.13	1.39	4.13	1.4	3.96	-3.39
T6	4.95	4.58	-7.58	4.58	-7.58	5	1.01	5	1.01	4.8	-3.88
T7	5.33	5.34	0.15	5.34	0.15	5.76	8.11	5.76	8.12	5.54	2.98
T8	5.63	5.7	1.38	5.7	1.38	5.89	4.68	5.89	4.68	5.63	-0.52
T9	5.88	6.11	3.92	6.11	3.92	6.68	13.59	6.68	13.59	6.4	8.06
T10	6.84	6.73	-1.54	6.73	-1.53	7.1	3.89	7.1	3.88	6.81	-0.95

From the tables above, we can see the effects of cable forces on dynamic ability is smaller than using the different element types and adding asphalts layers.

5.3 Ambient Vibration Testing

The development of reliable analytical dynamic models is a crucial aspect of major importance in terms of the study of the dynamic response and of the health condition of both new and existing large span bridges under traffic, wind or seismic loads. Although sophisticated finite element codes are currently available for that

purpose, the success of their application is strongly dependent on the possibility of experimental verification of the results. An appropriate experimental calibration and validation of such analytical models, so that they can reflect correctly the structural properties and the boundary conditions, involves the experimental identification of the most significant modal parameters of the structure (natural frequencies, mode shapes and modal damping factors), and their correlation with the corresponding calculated values.

For bridges that cannot be taken out of service, traffic loading is the primary method for exciting the structure. Many times traffic excitation is coupled with other ambient excitation sources such as wind. With traffic excitation the assumption is often made that the ambient vibration source is a white noise random process. Turner and Pretlove (Turner, J. D. and A. J. Pretlove. 1988. "A Study of the Spectrum of Traffic-Induced Bridge Vibration," Journal of Sound and Vibration, 122, 31-42) state that this assumption is based on the random arrival times of individual vehicles; the random nature of the vehicles' suspension systems; and the randomly distributed road surface irregularities. Depending on the coupling between torsional and lateral modes, traffic excitation has the limitation that it may not sufficiently excite the lateral modes of a bridge and these modes are often of interest, particularly in seismic studies.

System Identification and Modal Analysis

After tests, the operational modal analysis (i.e. the identification of modal parameters from output-only time-histories data) will be carried out using the Frequency Domain Decomposition (*FDD*, Brincker et al. 2000) method, implemented in the ARTeMIS software. The *FDD* technique involves the following main steps:
1) evaluation of the spectral matrix **G**(*f*), i.e. the matrix where the diagonal terms are the autospectral densities (*ASD*) while the other terms are the cross-spectral densities (*CSD*). In the present application, the *ASD*s and the *CSD*s are estimated, after decimating the data.
2) singular value decomposition (*SVD*) of the matrix **G**(*f*) at each frequency, according to:

$$\mathbf{G}(f) = \mathbf{U}(f)\boldsymbol{\Sigma}\mathbf{U}^{H}(f) \tag{5.1}$$

where the diagonal matrix $\boldsymbol{\Sigma}$ collects the real positive singular values in descending order, **U** is a complex matrix containing the singular vectors as columns and the superscript H denotes complex conjugate matrix transpose;

3) Inspection of the curves representing the singular values to identify the resonant frequencies and estimate the corresponding mode shape using the information contained in the singular vectors of the *SVD*.

The principle in the *FDD* techniques is easily understood by recalling that any response can be written in modal co-ordinates and that the spectral matrix of a linear dynamic system subjected to a white-noise random excitation may be expressed as:

$$\mathbf{G}(f) = \phi \mathbf{G}_{qq} \phi^{H}(f) \tag{5.2}$$

where ϕ is the matrix of mode shapes and $\mathbf{G}_{qq}(f)$ is the spectral matrix of the modal co-ordinates. Since the modal co-ordinates are un-correlated, the matrix $\mathbf{G}_{qq}(f)$ is diagonal; hence, if the mode shapes are orthogonal, it is a SVD of the response spectral matrix. As a consequence, if only one mode is important at a given frequency f_r, as it has to be expected for well-separated modes, the spectral matrix can be approximated by a rank-one matrix:

$$\mathbf{G}(f_r) \approx \sigma_1(f_r) u_1(f_r) u_1^{H}(f_r) \tag{5.3}$$

and the first singular vector $u_1(f_r)$ is an estimate of the mode shape. On the other hand, the first singular value $\sigma_1(f)$ at each frequency represents the strength of the dominating vibration mode at that frequency so that the first singular function can be suitably used as a modal indication function (yielding the resonant frequencies as local maxima) whereas the successive singular values contain either noise or modes close to a strong dominating one.

Finite element (FE) modelling of bridges is now common in the normal design process of new structures or in the assessment of existing structures. With advances in numerical modelling, it is generally expected that FE models based on technical design data, as-built drawings and engineering judgement can reliably simulate both the static and dynamic structural behaviour. However, these FE models often cannot predict natural frequencies and mode shapes with the required level of accuracy, as a consequence of modelling uncertainties. A possible practice to fill the lack between the real structural performance and FE models is to employ some form of modal analysis on bridges in service. And then the results from test and FE analysis (FEA) can be compared through the absolute frequency discrepancy $D_F = |(f_{FDD} - f_{FEA})/f_{FDD}|$ and the Modal Assurance Criterion (*MAC*, Allemang ad Brown 1983). The MAC is probably the most commonly used procedure to correlate two sets of mode shape vectors and is defined as:

$$MAC(f_{A,k}, f_{B,j}) = \frac{(f_{A,k}^T f_{B,j})^2}{(f_{A,k}^T f_{A,k})(f_{B,j}^T f_{B,j})} \quad (5.4)$$

where $f_{A,k}$ is the *k*-th mode of data set A and $f_{B,j}$ the *j*-th mode of the data set B. coefficient analogous to the correlation coefficient in statistics and ranges from 0 to 1; a MAC value of 0 indicates that the two mode shapes are completely uncorrelated, while a MAC value of 1 indicates perfect correlation between them. In general, a MAC value greater than 0.80–0.85 is considered a very good match while a MAC value less than 0.40 is considered a poor match.

5.3.1 Vibration Measurements in 2006

The reception tests of the cable-stayed bridge included extensive measurements of ambient vibration responses induced by the environmental loads. Ambient vibration tests (AVT) were conducted using a 16-channel data acquisition system with 14 uniaxial piezoelectric accelerometers (WR model 731A). Each sensor (capable of measuring accelerations of up to ±0.50 g with a sensitivity of 10 V/g) was connected with a short cable (1 m) to a power unit/amplifier providing the constant current needed to power the accelerometer's internal amplifier, signal amplification and selective filtering. Two-conductor cables connected the power supplies to the data acquisition board, in turn controlled by a portable PC.

Since the AVTs were performed before the bridge was opened to traffic, two different series of ambient vibration data were recorded: in the first series, the excitation was provided only by micro-tremors and wind, while in the second series the excitation was provided by two-axle trucks, crossing the bridge with symmetric and eccentric passages, and velocities in the range of 10 to 50 km/h. In the following, these two different series of ambient vibration data will be referenced to as AV1 (micro-tremors and wind) and AV2 (simulated traffic condition).

In order to obtain a satisfactory spatial description of the bridge mode shapes, accelerations were measured in 34 selected points of the deck while only one cross-section of the tower (up-rising the deck of about 15 m) was instrumented by three sensors. Figure shows a schematic diagram of the sensor layout. The tests were performed in a total of 4 set-ups, as it is shown in figure 5.8: out of the 14 available sensors, 2 were considered as reference sensors and remained at the same points during all the set-ups, while the remaining sensors were placed in the other points, changing their position from set-up to set-up.

For each sensor layout and for each type of ambient excitation, time series of 3.000 s were collected. The data, originally sampled at 400 Hz, was decimated 20 times and high-pass filtered to remove any offset and drift. After decimation, the number of samples was 60.000 per record with a sampling interval of 0.05 s, corresponding to a Nyquist frequency of 10 Hz. Subsequently, data was processed in order to estimate the spectral matrix by using the modified periodogram method [9]; according to this approach, an average is made over each recorded signal, divided into *M* frames of *2n* samples, where windowing and overlapping is applied. In the present application, smoothing is performed by 1024-points Hanning-windowed periodograms that are transformed and averaged with 66.7% overlapping, so that a total number of 173 spectral averages was obtained. Since the re-sampled time interval is 0.05 s, the resulting frequency resolution is $1/(1024\times0.05) \approx 0.0195$ Hz.

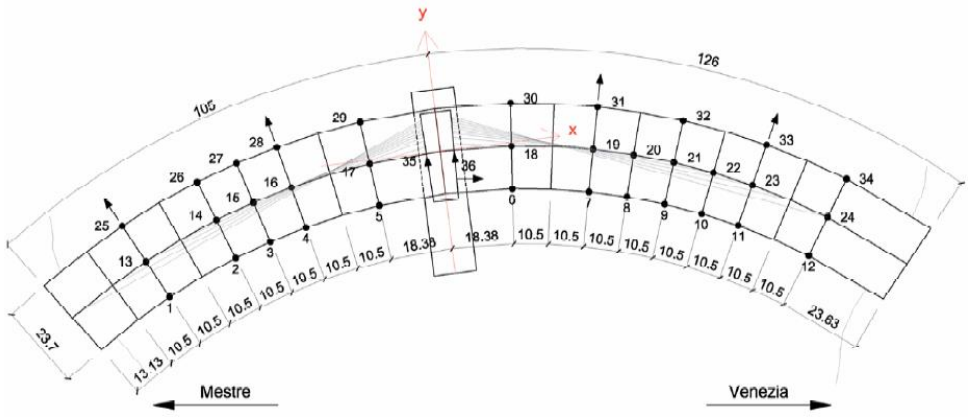

Fig.5. 11 The measurement nodes on top of the bridge deck: 26 and 28 are the common points

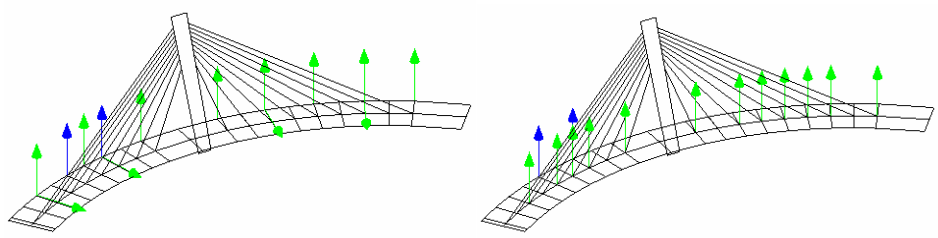

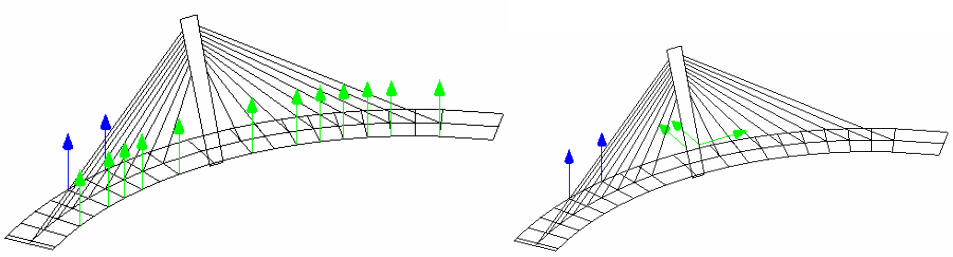

Fig.5. 12 Arrangement of the measuring points on deck and tower

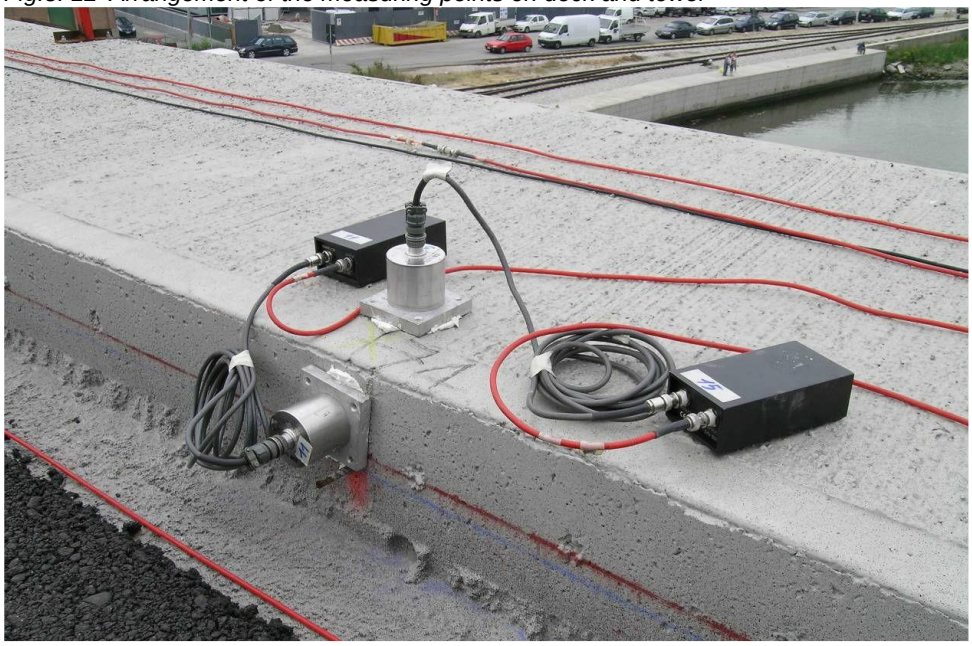

Figure 1. 1 The accelerometers on and stays ahead of the field testing

5.3.1.1 System Identification in 2006

Operational modal analysis and dynamic characteristics of the bridge
The identification of modal parameters from ambient vibration data was carried out by using two complementary output-only techniques: The *Frequency Domain Decomposition* (*FDD*) (BRINCKER et al, 2000) in the frequency domain and the data driven *Stochastic Subspace Identification* (*SSI*) (Van Overschee, P., De Moor P.L. 1996) in the time domain; these techniques are available in the commercial program ARTeMIS (SVS,2012).

The *FDD* technique involves the following main steps: (a) estimate of the spectral matrix in the frequency domain from the measured signals; (b) Singular Value Decomposition (*SVD*) of the spectral matrix at each frequency; (c) inspection of the curves representing the singular values to identify the resonant frequencies and estimate the corresponding mode shape from the singular vectors of the *SVD*.

Since the first (and largest) singular value at each frequency represents the strength of the dominating vibration mode at that frequency, the first singular value can be suitably used as a modal indication function (yielding the resonant frequencies as local maxima) whereas the successive singular values contain either noise or modes close to a strong dominating one.

The *SSI* method works in the time domain and is based on the discrete-time state-space form of the dynamics of a linear-time-invariant system under unknown excitation:

$$x_{k+1} = Ax_k + w_k \tag{5.5}$$

$$y_k = Cx_k + v_k \tag{5.6}$$

where $\boldsymbol{x}_k$ is the discrete-time state vector (containing displacements and velocities describing the state of the system at time instant $t_k = k\Delta t$), $\boldsymbol{w}_k$ is the process noise, $\boldsymbol{y}_k$ is the output vector, $\boldsymbol{v}_k$ is the measurement noise, $\boldsymbol{A}$ is the discrete state matrix (dependent on the mass, stiffness and damping properties of the structure) and $\boldsymbol{C}$ is the discrete output matrix (which maps the state vector into the measured output). Eq. (5.1) is generally called the state equation while Eq. (5.2) is called the observation/output equation.

It can be shown (PEETERS B,2000) that the modal parameters (natural frequencies, mode shapes and damping ratios) of a structure under white-noise excitation can be identified by relying only on the measured output responses $\boldsymbol{y}_k$. Once state space matrices are identified of different order *N*, *N*/2 modal parameters are extracted from a model of order *N*. If similar modal parameters are obtained with increasing model order, a physical eigenmode is identified. In the present application, stochastic state space models are identified of different order *N*, ranging from 2 to 200 in steps of 2.

The two sets of mode shapes resulting from the application of *FDD* and *SSI* techniques were then compared using the Modal Assurance Criterion (*MAC*) (MAC, Allemang and Brown 1983). The *MAC* is a coefficient analogous to the correlation coefficient in statistics and ranges from 0 to 1. In general, a *MAC* value greater than 0.80 is considered a good match while a *MAC* value less than 0.40 is considered a poor match.

As it has to be expected, several vibration modes were identified in the investigated frequency range from both the AV1 and AV2 data series. The results of ambient vibration tests in terms of natural frequencies can be summarised through the spectral plots of figures 5.10 and 5.11, which show the average of normalized Singular Values of the spectral matrices of all data sets obtained from data series AV1 and AV2, respectively. Inspection of figure 5.10 shows that 23 modes are reasonably well represented in the AV1 data series, while few peaks in the first Singular Value are lost in the AV2 data series (figure 5.11). Furthermore, the

inspection of figures 5.10 and 5.11 clearly highlights the correspondence of the natural frequencies between AV1 and AV2 data series, with the corresponding resonant peaks being placed practically at the same frequencies in the two plots.

Owing to the curvature of the bridge girder and to tower geometry, all mode shapes are in principle three-dimensional. The degree of coupling between vertical and transverse motion of the deck at each mode was investigated simply by computing the ratio *mcr* (DANIELL W.E.et al,2007), (GENTILE, C.et al,2004) between the maximum absolute modal displacements of structural component in one direction divided by the maximum vertical modal displacement of the deck. This analysis highlighted that the *mcr* is less than 0.20 for all vibration modes; hence, although slight coupling in the longitudinal and transverse direction is always present, the vertical components strongly dominate the identified modal behaviour.

Figure 5.12 shows a selected number of mode shapes identified by applying the *FDD* algorithm to AV1 data series. Table 5.3 summarizes the modal parameters identified from the same AV1 series by the *FDD* and *SSI* methods and the mode classification; furthermore, Table 1 compares the corresponding mode shapes and scaled modal vectors obtained from the two different identification procedures through the absolute frequency discrepancy $\Delta f_{FDD-SSI} = |(f_{FDD} - f_{SSI}) / f_{FDD}$ and the *MAC*. The observed modes can be basically arranged as follows:

1. Bending-dominate modes (B). These modes are dominated by the vertical bending of the bridge deck, with anti-symmetric deck modes generally involving a greater longitudinal participation of the tower than the symmetric ones. Due to the curved layout of the deck and to the transverse slope, these modes are characterised by different displacements of the internal and the external borders of the girder;
2. Torsion-dominate modes (T). These modes are dominated by the torsion behaviour of the deck and are usually coupled with transverse displacement of the deck;
3. Mixed modes (M), where bending and torsion behaviour of the deck are simultaneously present. These modes generally involve a significant transverse deformation of the cross-section (see e.g. the mode at 2.77 Hz in figure 1.15).

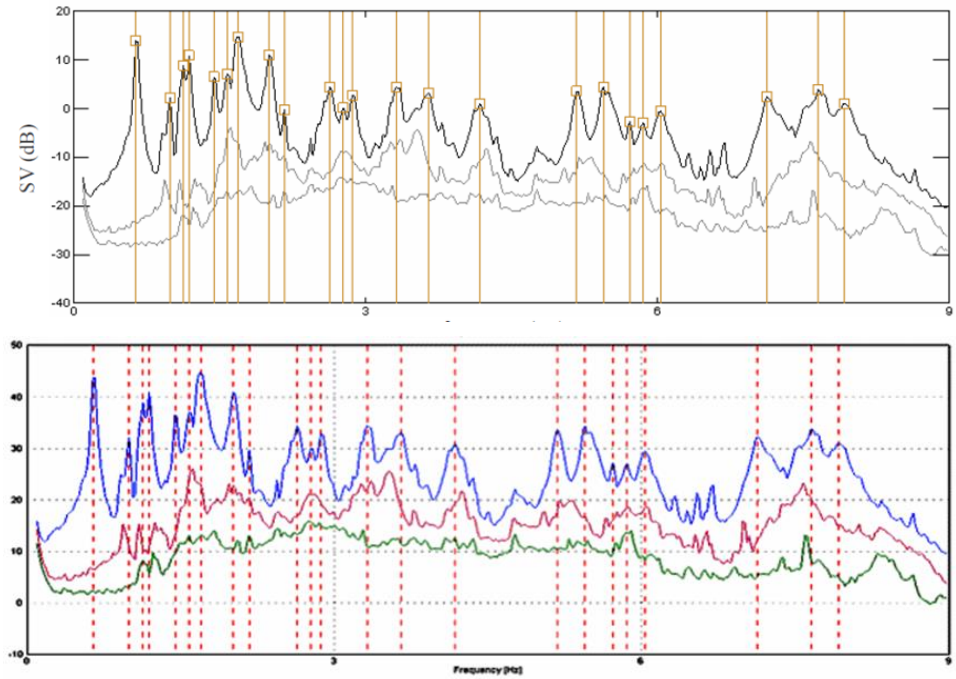

Fig.5. 13 AV1 (micro-tremors and wind): Singular Value (SV) and identification of natural frequencies

Fig.5. 14 AV1 (micro-tremors and wind): Singular Value (SV) and identification of natural frequencies

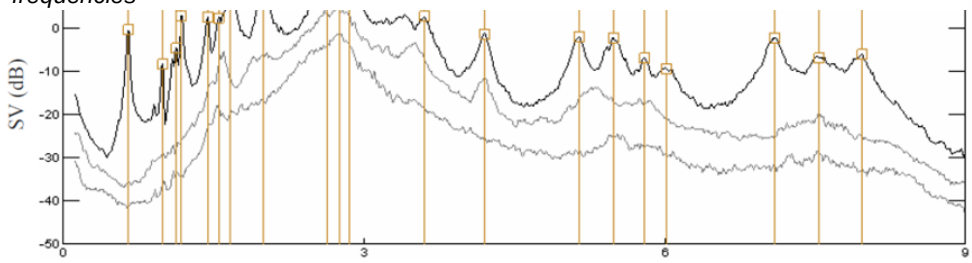

Fig.5. 15 AV2 (simulated traffic condition):Singular Value (SV) and identification of natural frequencies

Fig.5. 16 AV2 (simulated traffic condition):Singular Value (SV) and identification of natural frequencies

Mode	Frequency (Hz)		Mode	Frequency (Hz)	
	AV1	AV2		AV1	AV2
1	0.645	0.654	13	3.320	–
2	0.996	0.996	14	3.652	3.604
3	1.133	1.133	15	4.180	4.209

4	1.191	1.191	16	5.176	5.146
5	1.445	1.445	17	5.449	5.488
6	1.582	1.553	18	5.723	–
7	1.699	1.680	19	5.859	5.801
8	2.012	2.002	20	6.035	6.006
9	2.168	–	21	7.129	7.100
10	2.637	2.637	22	7.656	7.539
11	2.773	2.754	23	7.930	7.969
12	2.871	2.861			

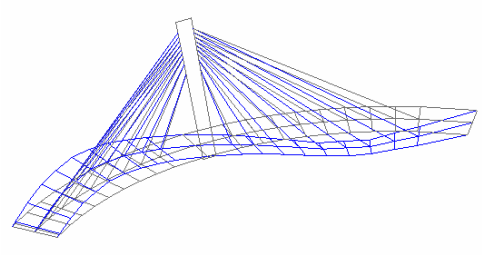

f=0.645 Hz

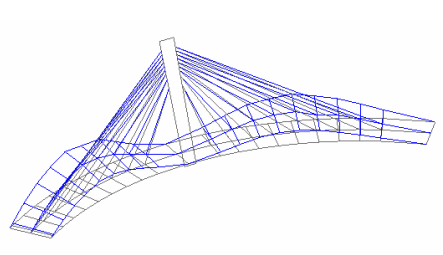

f=0.996 Hz

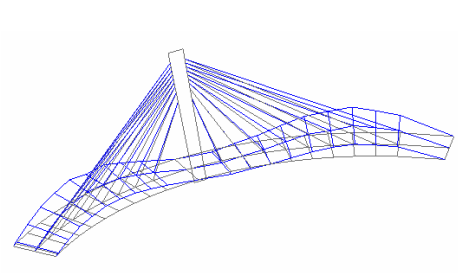

f=1.133 Hz

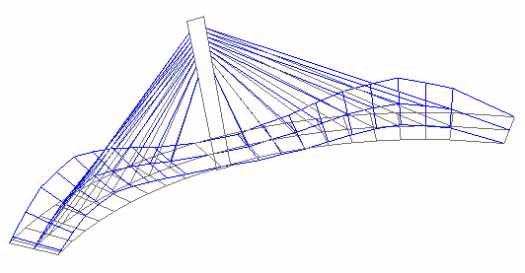

f=1.191 Hz

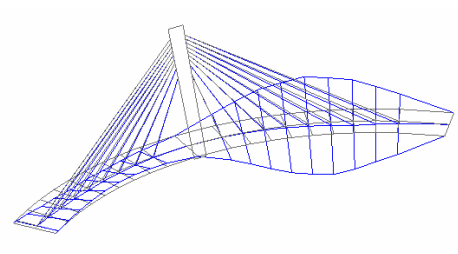

f=1.445 Hz

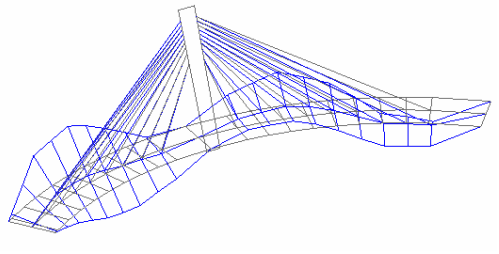

f=1.582 Hz

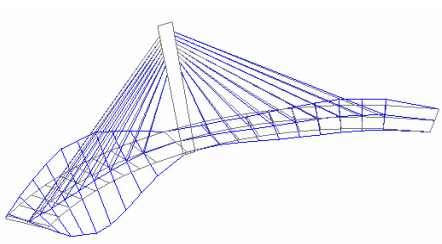

f=1.699 Hz

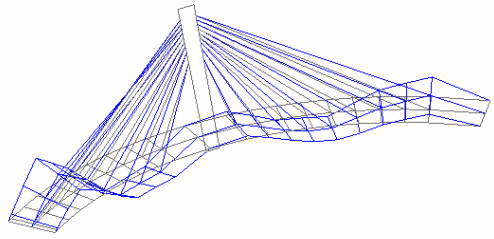

f=2.012 Hz

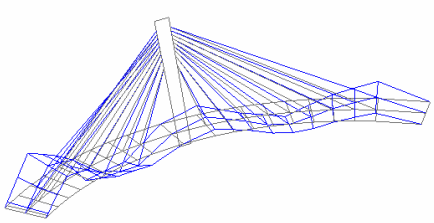

f=2.168 Hz

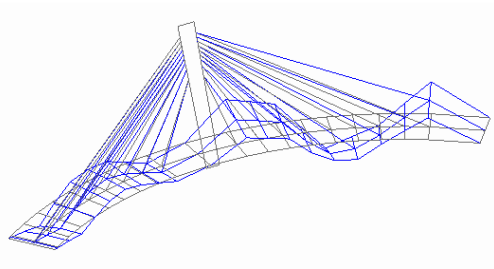

f=2.637 Hz

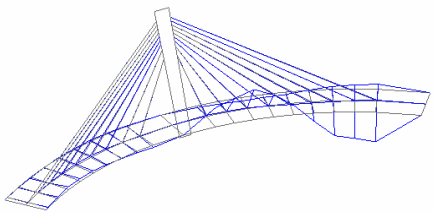

f=2.773 Hz

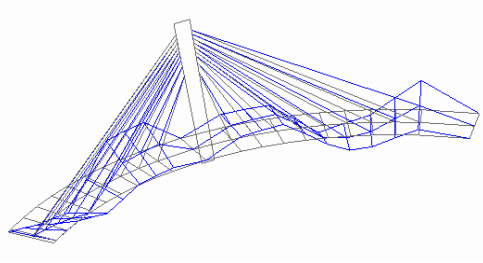

f=2.871 Hz

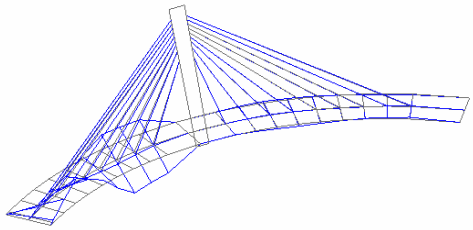

f=3.320 Hz

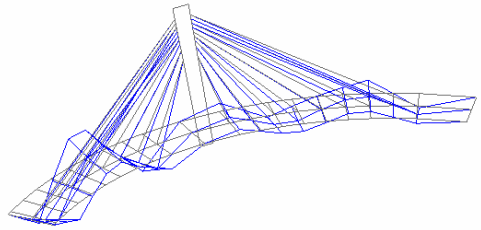

f=3.652 Hz

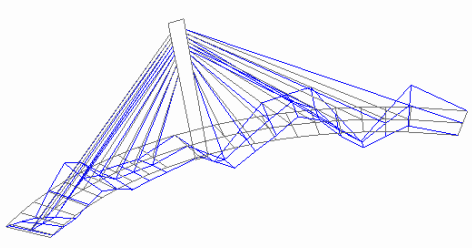

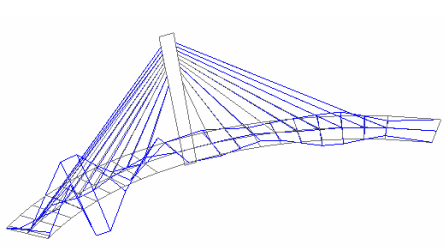

f=4.180 Hz

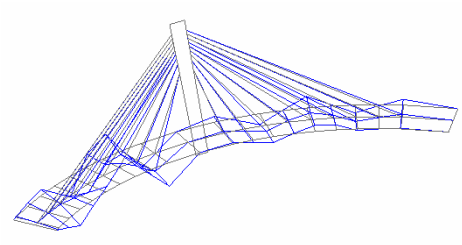

f=5.176 Hz

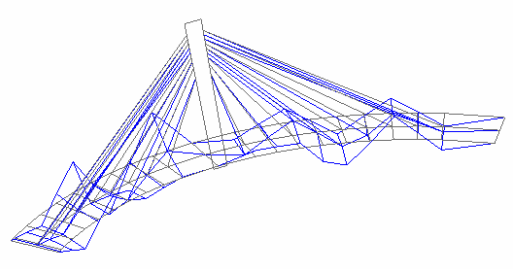

f=5.449 Hz

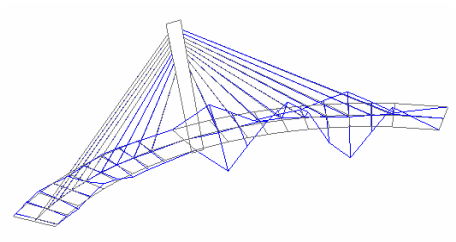

f=5.723 Hz

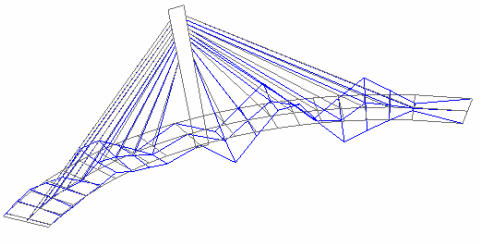

f=5.859 Hz

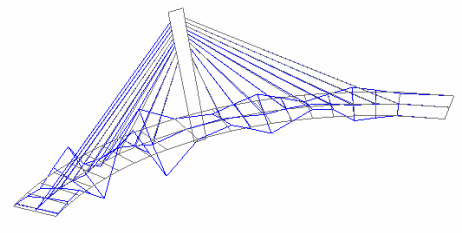

f=6.035 Hz

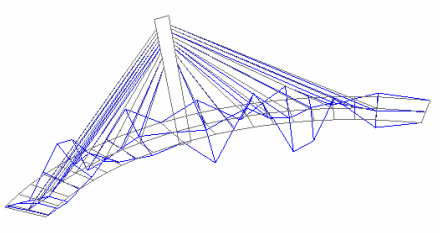

f=7.129 Hz

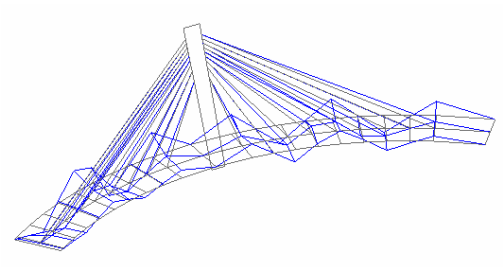

f=7.656 Hz

f=7.930 Hz

Fig.5. 17 the selected modes of SV1

As expected, several vibration modes were identified in the investigated frequency range from both the AV1 and AV2 data series. For example, figure 5.10 shows the average of normalized Singular Values of the spectral matrices of all data sets

obtained from data series AV1. Inspection of figure 5.11 shows that 23 modes are reasonably well represented in the AV1 data series (while few peaks in the first Singular Value are lost or less clearly detected in the AV2 data series).

Bending-dominate modes (DV+). These modes are dominated by the vertical bending of the bridge deck, with anti-symmetric deck modes generally involving a greater longitudinal participation of the tower than the symmetric ones. The first bending mode is an anti-symmetric half sine wave of the deck with a frequency of 0.65 Hz. Due to the curved layout of the deck and to the transverse slope, DV+ modes are characterised by different displacements of the internal and the external borders of the girder;

Torsion-dominate modes (DV−). These modes are dominated by the torsion behaviour of the deck and are usually coupled with transverse displacement of the deck;

Mixed modes (DV±), where bending and torsion behaviour of the deck are simultaneously present. These modes generally involve a significant transverse deformation of the cross-section.

Tab.5 4 Experimental (AV1 data series) and theoretical modal behaviour

Mode Type	f_{FDD} *(Hz)*	*Deck* m_{CR}		*Tower* m_{CR}		f_{SSI} *(Hz)*	ζ_{SSI} *(%)*	D_F *(%)*	*MAC*
		X	*Y*	*X*	*Y*				
B1	0.645	0.025	0.07	0.118	0.009	0.657	0.51	1.86	1
B2	0.996	0.026	0.114	0.203	0.376	-	-	-	-
B3	1.133	0.016	0.072	0.019	0.084	1.129	0.65	0.35	0.990
B4	1.191	0.014	0.06	0.013	0.058	1.197	1.08	0.5	0.997
T1	1.445	0.018	0.035	0.006	0.001	1.466	0.64	1.45	0.991
M1	1.582	0.059	0.114	0.065	0.016	1.584	0.92	0.13	0.987
T2	1.699	0.025	0.078	0.08	0.009	1.715	1.31	0.94	0.907
B5	2.012	0.031	0.115	0.031	0.019	2.019	0.87	0.35	0.998
B6	2.168	0.104	0.201	0.025	0.017	-	-	-	-
B7	2.637	0.036	0.07	0.028	0.026	2.638	1.25	0.04	0.993

M2	2.773	0.015	0.029	0.005	0.006	-	-	-	-
M3	2.871	0.037	0.122	0.044	0.05	2.875	0.79	0.14	0.987
T3	3.32	0.024	0.104	0.003	0.007	3.326	0.97	0.18	0.992
B8	3.652	0.031	0.06	0.057	0.005	3.641	1.7	0.30	0.984
B9	4.18	0.013	0.026	0.065	0.023	4.168	1.00	0.29	0.977
T4	5.176	0.023	0.045	0.013	0.006	5.186	0.71	0.19	0.992
B10	5.449	0.028	0.122	0.017	0.013	5.49	1.03	0.75	0.965
B11	5.723	0.03	0.124	0.008	0.013	-	-	-	-
T5	5.859	0.007	0.029	0.005	0.006	5.851	0.55	0.14	0.967
B12	6.035	0.022	0.044	0.062	0.059	6.045	0.67	0.17	0.959
T6	7.129	0.026	0.114	0.009	0.005	7.149	0.82	0.28	0.992
T7	7.656	0.025	0.111	0.025	0.011	7.692	0.92	0.47	0.814
B13	7.93	0.022	0.096	0.006	0.01	7.957	1.25	0.34	0.948

Inspection of Table 5.4 clearly highlights that for the deck the ratio m_{CR} is again less than 0.20 for all vibration modes meaning that, although slight coupling in the longitudinal and transverse direction is always present, the vertical components dominate the identified modal behaviour. Hence, the observed modes can be basically arranged as follows: (a) bending-dominate modes (B); (b) torsion-dominate modes (T); (c) mixed modes (M), where bending and torsion behaviour of the deck are simultaneously present and a significant transverse deformation of the cross-section is often detected (see e.g. the mode placed at 2.77 Hz in Fig.5.12). The correlation values listed in Table 5.3 show a very good agreement between the *FDD* and the *SSI* techniques in terms of natural frequencies, with the frequency discrepancy being usually less than 1%. A similar correspondence is detected also for the estimates obtained from AV2 data series.

Stay-Cables behavior

By numbering the stay-cables of the Mestre side in descending order (i.e. the longer cable is referred to as —Stay-cable n. 1“while the shorter is referred to as —Stay-cable n. 9“), the following fundamental frequencies of the stays were identified from both AV1 and AV2 data series (BERGAMINI,2001):

Tab.5 5 The fundamental frequencies of cables

Stay-cable n.	Fundamental frequency(Hz)	Stay-cable n.	Fundamental frequency(Hz)
1	0.957	6	1.484
2	1.094	7	1.582
3	1.23	8	1.133
4	1.27	9	1.23
5	1.348		

Beyond the traditional use of the above values for estimating the tension *T* in the stay-cables, it should be noticed that the lower global modes of the bridge (i.e. 0.996 Hz, 1.133 Hz, 1.191 Hz, 1.445 Hz and 1.582 Hz) occur at stay cable frequencies or very close to stay-cable frequencies.

Experimental investigation of a two different curved cable-stayed bridges has been presented and discussed. The following main conclusions can be drawn:

1. Within the frequency range 0−10 Hz, the *FDD* and the *SSI* techniques provided the identification more than 20 vibration modes (Venice bridge), respectively.
2. Notwithstanding the curved layout of the bridge superstructures, slight coupling between vertical and transverse vibration of the deck was observed at the low level of vibration that existed during the tests. For each vertical mode, either bending or torsion, the vertical component exceeds the transverse one by at least a factor of 5;
3. Few mixed bending+torsion modes were identified for the Porto Marghera bridge and such modes generally involve a significant transverse deformation of the deck cross-section;
4. some global modes of the Porto Marghera bridge were found to occur at (or very close to) the fundamental frequencies of the stay-cables.

5.3.2 Vibration Measurements in 2010

The reception tests of the cable-stayed bridge included extensive measurements of ambient vibration responses induced by the environmental loads. Ambient vibration tests (AVT) were conducted using a 16-channel data acquisition system with 14 uniaxial piezoelectric accelerometers (WR model 731A). Each sensor (capable of measuring accelerations of up to ±0.50 g with a sensitivity of 10 V/g) was connected with a short cable (1 m) to a power unit/amplifier providing the constant current needed to power the accelerometer's internal amplifier, signal amplification and

selective filtering. Two-conductor cables connected the power supplies to the data acquisition board, in turn controlled by a portable PC.

Since the AVTs were performed after the bridge was opened to traffic, the ambient vibration data were recorded and provided only by micro-tremors and wind, In the following, the ambient vibration data will be referenced to as AV (micro-tremors and wind).

In order to obtain a satisfactory spatial description of the bridge mode shapes, accelerations were measured in 51 selected points of the deck while only one cross-section of the tower (up-rising the deck of about 15 m) was instrumented by three sensors. Figure 5.13 shows a schematic diagram of the sensor layout. The tests were performed in a total of 3 set-ups, as it is shown in figure 5.14: in the first set-up, 15 sensors were placed at the inner border of the deck, 3 were considered as reference sensors and remained at the same points during all the set-ups; In the second set-up, 17 sensors were placed at the middle of the deck and only one cross-section of the tower (up-rising the deck of about 13.5 m) was instrumented by three sensors; In the third set-up, 16 sensors were placed at the outer border of the deck.

For each sensor layout and for each type of ambient excitation, time series of 3.000 s were collected. The data, originally sampled at 400 Hz, was decimated 20 times and high-pass filtered to remove any offset and drift. After decimation, the number of samples was 60.000 per record with a sampling interval of 0.005 s, corresponding to a Nyquist frequency of 10 Hz. Subsequently, data was processed in order to estimate the spectral matrixby using the modified periodogram method [9]; according to this approach, an average is made over each recorded signal, divided into *M* frames of *2n* samples, where windowing and overlapping is applied. In the present application, smoothing is performed by 1024-points Hanning-windowed periodograms that are transformed and averaged with 66.7% overlapping, so that a total number of 173 spectral averages was obtained. Since the re-sampled time interval is 0.005 s, the resulting frequency resolution is $1/(1024 \times 0.005) \approx 0.195$ Hz.

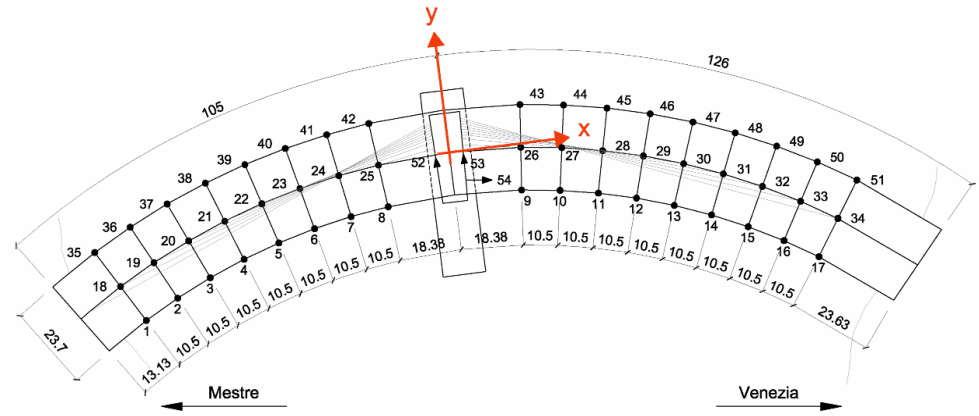

Fig.5. 18 The measurement nodes on top of the bridge deck: 6, 11 and 45 are the common points

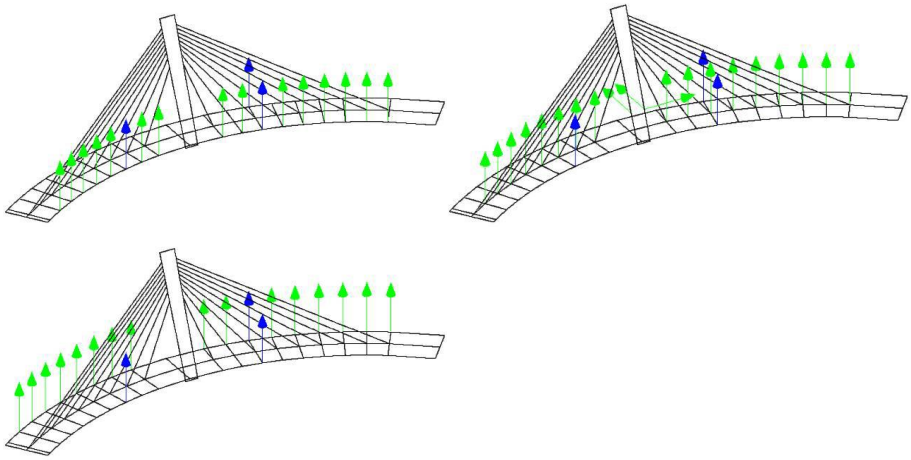

Fig.5. 19 The set-ups of vibration Measurements in 2010

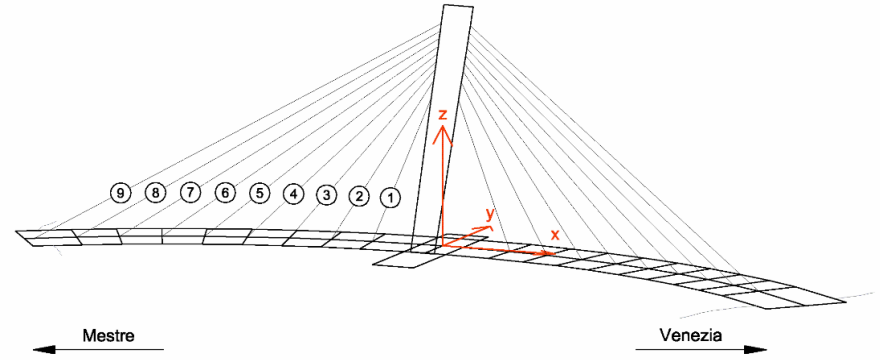

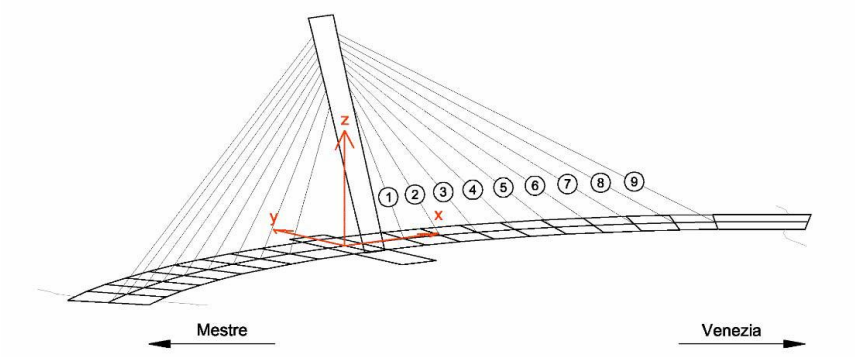

Fig.5. 20 Arrangement of measurement points on stayed cables: (a) side of Mestre; (b) side of Venice

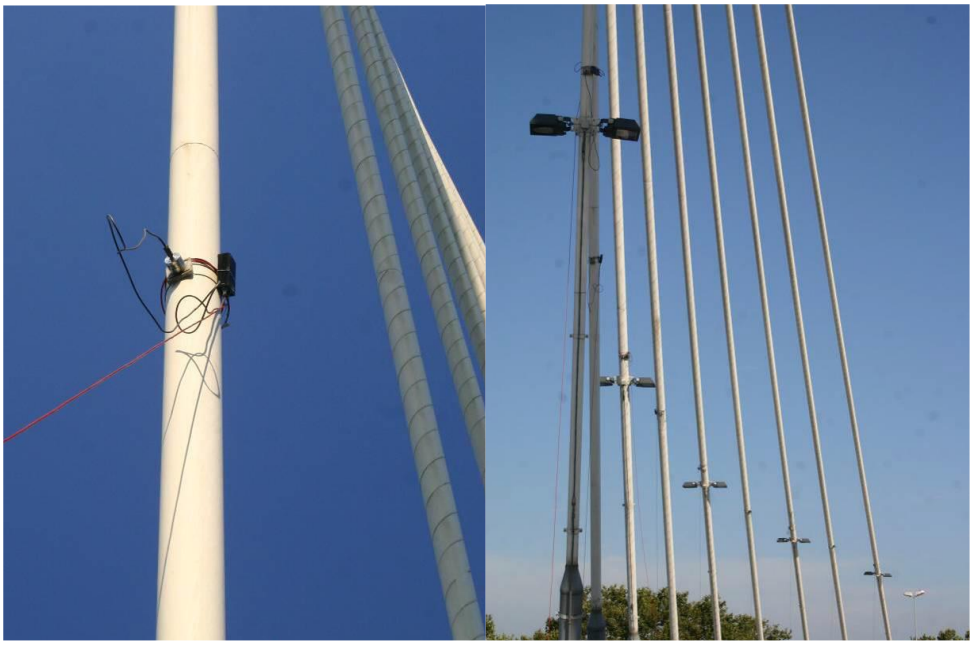

Fig.5. 21 the accelerometers on and stays ahead of the field testing

5.3.2.1 System Identification in 2010

Operational modal analysis and dynamic characteristics of the bridge

The identification of modal parameters from ambient vibration data was carried out by using output-only techniques: The *Frequency Domain Decomposition* (*FDD*) in the frequency domain, the technique is available in the commercial program ARTeMIS.

The *FDD* technique involves the following main steps: (a) estimate of the spectral matrix in the frequency domain from the measured signals; (b) Singular Value Decomposition (*SVD*) of the spectral matrix at each frequency; (c) inspection of the curves representing the singular values to identify the resonant frequencies and estimate the corresponding mode shape from the singular vectors of the *SVD*.

Since the first (and largest) singular value at each frequency represents the strength of the dominating vibration mode at that frequency, the first singular value can be suitably used as a modal indication function (yielding the resonant frequencies as local maxima) whereas the successive singular values contain either noise or modes close to a strong dominating one.

The two sets of mode shapes (Gentile C,2006,2010) resulting from the application of *FDD* techniques were then compared using the Modal Assurance Criterion (*MAC*) (Figure 5.6). The *MAC* is a coefficient analogous to the correlation coefficient in statistics and ranges from 0 to 1. In general, a *MAC* value greater than 0.80 is considered a good match while a *MAC* value less than 0.40 is considered a poor match.

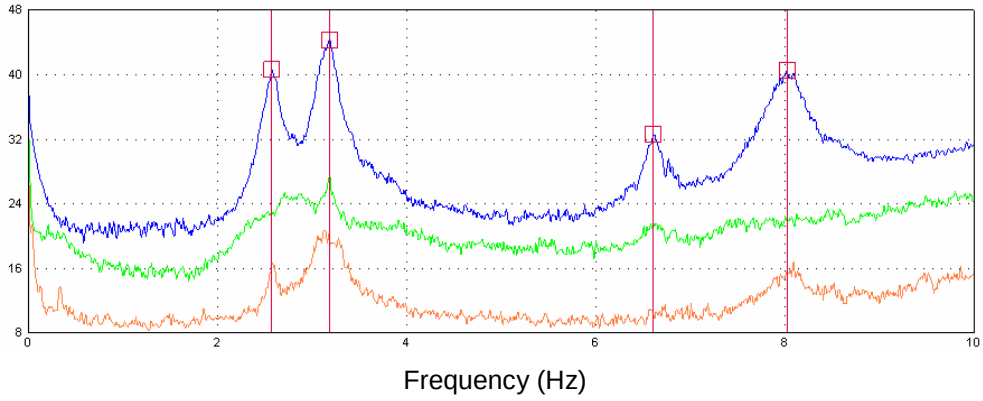

Fig.5. 22 Typical pattern of the first singular value of the matrix spectral

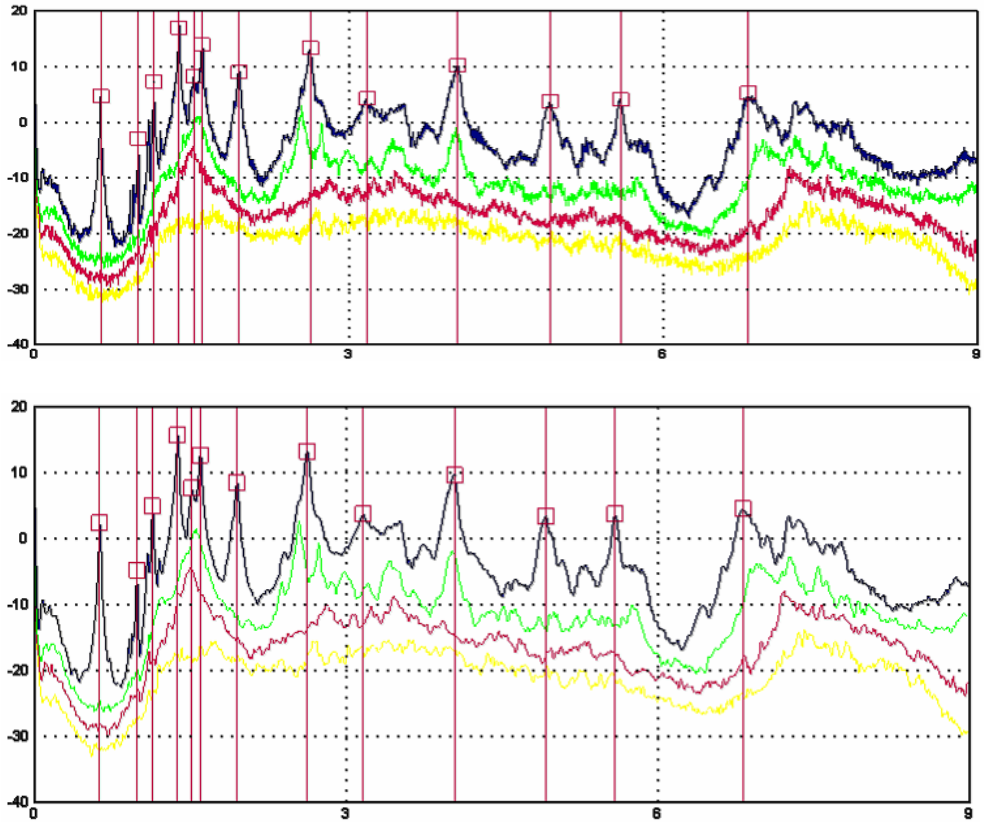

Fig.5. 23 Singular Value (SV) and identification of natural frequencies

The analysis of acceleration signals recorded on the bridge deck and antenna led to the identification of 13 key frequencies to vibrate to the frequency 0-9 Hz. The results of experimental modal in terms of natural frequencies can be summarized through the diagrams shown in Figure 5.17. These diagrams represent the trend of the first singular values of the matrices spectral, evaluated with two different frequency resolutions according to the signals recorded in excitation conditions environmental. As mentioned above, the singular value decomposition of the spectral matrix allows identification of natural frequencies through the peak values of the first singular value where the corresponding singular vectors represent an estimate of the associated mode shapes. Figure 5.18 allows for clear identification of 13 spectral peaks.

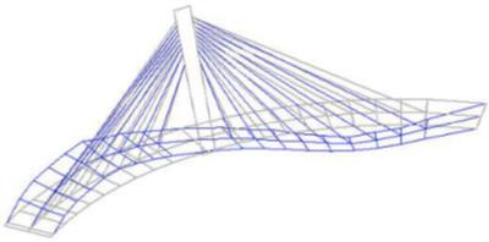

Mode 1. f = 0.635 Hz

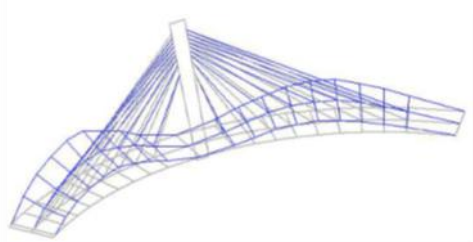

Mode 2. f = 0.996 Hz

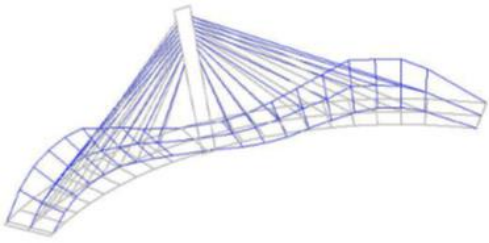

Mode 3. f = 1.143 Hz

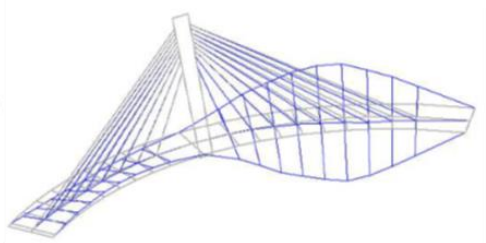

Mode 4. f = 1.387 Hz

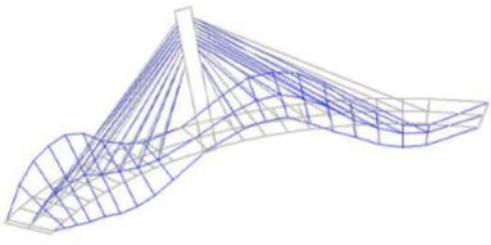

Mode 5. f = 1.523 Hz

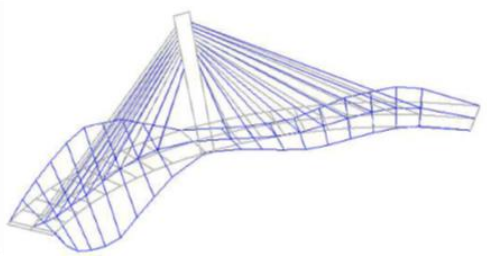

Mode 6. f = 1.602 Hz

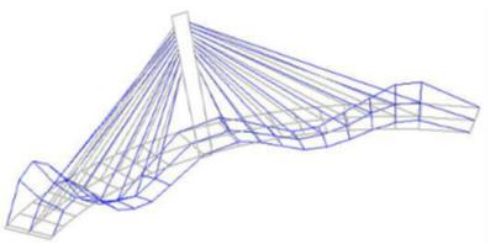

Mode 7. f = 1.953 Hz

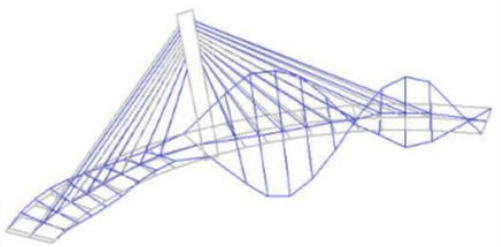

Mode 8. f = 2.637 Hz

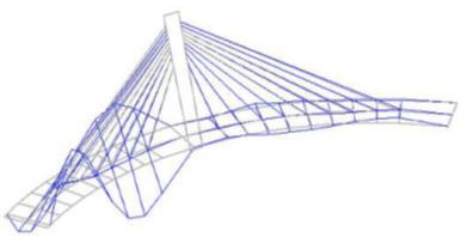

Mode 9. f = 3.174 Hz

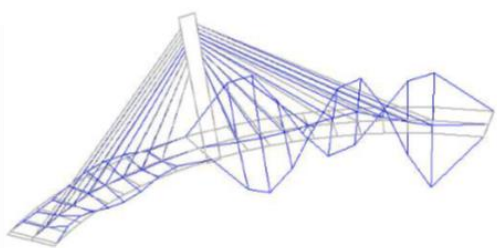

Mode 10. f = 4.053 Hz

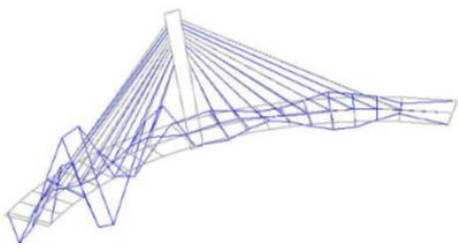

Mode 11. f = 4.932 Hz

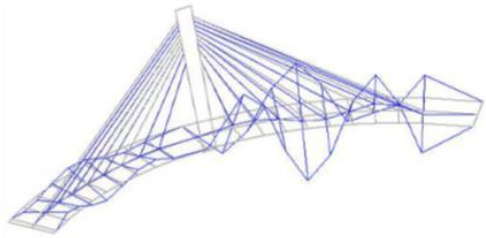

Mode 12. f = 5.596 Hz

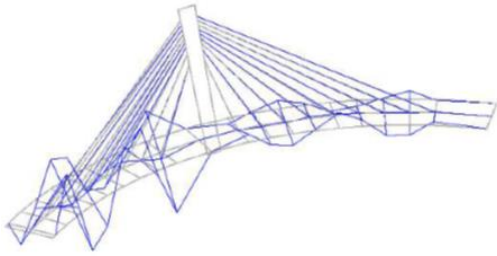

Mode 13. f = 6.826 Hz

Fig.5. 24 the selected mode shape identified from field testing

Fig.5. 25 the selected mode shape identified from field testing

Tab.5 6 Summary of the experimental mode types

Mode	Type	f(Hz)	Mode	Type	f(Hz)
1	Vertical bending	0.635	8	Torsion	2.637
2	Vertical bending	0.996	9	Torsion	3.174
3	Vertical bending	1.143	10	Torsion	4.053
4	Torsion	1.387	11	Torsion	4.932
5	Bending-Torsion	1.523	12	Torsion	5.596
6	Bending-Torsion	1.602	13	Torsion	6.826
7	Vertical bending	1.953	—	—	—

Tab.5 7 The comparison of frequency and MAC of 2006 and 2010

Mode N	f2006(Hz)	f2010(Hz)	△f (%)	MAC
1	0.645	0.635	−1.55	0.994
2	0.996	0.996	−	0.996
3	1.191	1.143	−4.03	0.988
4	1.445	1.387	−4.01	0.996
5	1.582	1.523	−3.73	0.963
6	1.699	1.602	−5.71	0.959
7	2.012	1.953	−2.93	0.974

8	2.773	2.637	−4.90	0.895
9	3.32	3.174	−4.40	0.975
10	−	4.053	−	−
11	5.176	4.932	−4.71	0.945
12	5.859	5.596	−4.49	0.905
13	7.129	6.826	−4.25	0.829

Stay-Cables behavior

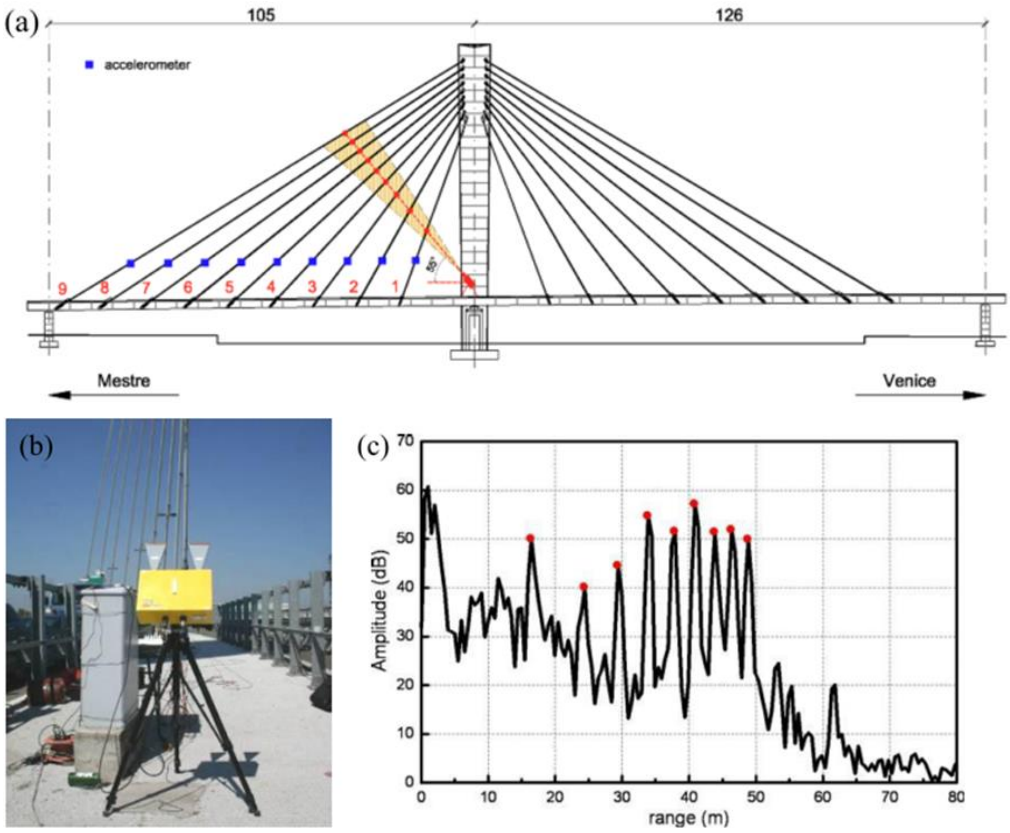

Fig.5. 26 Dynamic survey of the array of stay cables on Mestre side: (a) accelerometers and radar position; (b) view of the radar vibrometer on site; (c) range profile of the test scenario

Fig.5. 27 Dynamic survey of the array of stay cables on Mestre side: (a) accelerometers and radar position; (b) view of the radar vibrometer on site; (c) range profile of the test

Fig. 5.20a shows the accelerometers and radar position in the test of the stay cables on Mestre side. The radar was placed at the cross-section of the deck that is vertically supported by the basement of the tower and inclined 55° upward (Fig. 5.20b); a similar set-up was adopted in testing the array of stay cables of the opposite (Venice) side of the bridge. In both tests, time series of 3000 s were simultaneously collected by the accelerometers and the radar sensor, at rate of 200 Hz.

Fig.5.20a also shows the angle of transmission covered by the main lobe of the antenna in the vertical plane, with all the points inside the shadowed area of Fig.5.20a being observable from the sensor. It is worth underlining that the sensor transmits electromagnetic waves also in the horizontal plane and that different transmission angles in the vertical and horizontal plane could be obtained by using different antennas. Due to the cone-shaped emission of the sensor, notwithstanding the slightly spatial arrangement of the cables of each array, all the cables are clearly detected and identified in the range profiles. Fig.5.20c shows the range profile of the scenario on the Mestre side and is characterized by the presence of nine well defined peaks clearly identifying the position of the stay cables in the array.

Fig.5.21 shows the auto-spectral densities (ASD) of the ambient responses acquired, by using the two measurement systems, on the longer cable of the Mestre-side array. Although the ASDs of Fig.5.21 are associated to different mechanical quantities measured (displacement and acceleration) and to different points of the stay cable, the spectral plots clearly highlight that:

a) a large number of local resonant frequencies of the cables are identified from radar data and these natural frequencies are in excellent agreement with the ones obtained from accelerometer;
b) the number of frequencies identified from radar data is large enough to establish if the cables behave as a taut string or deviate from a taut string. Hence, accurate estimate of the cable tensions can be retrieved from the identified natural frequencies as well.

It is worth underlining that similar results, in terms of number and agreement of natural frequencies, have been obtained for all the stay cables of the two arrays, with the exception of the two shorter ones (cables 1-2 in Fig.5.20a). For the shorter stays, the radar technique detected the lower 3-4 local natural frequencies only, whereas the accelerometers (probably as a consequence of their position) provided a larger number of cable frequencies.

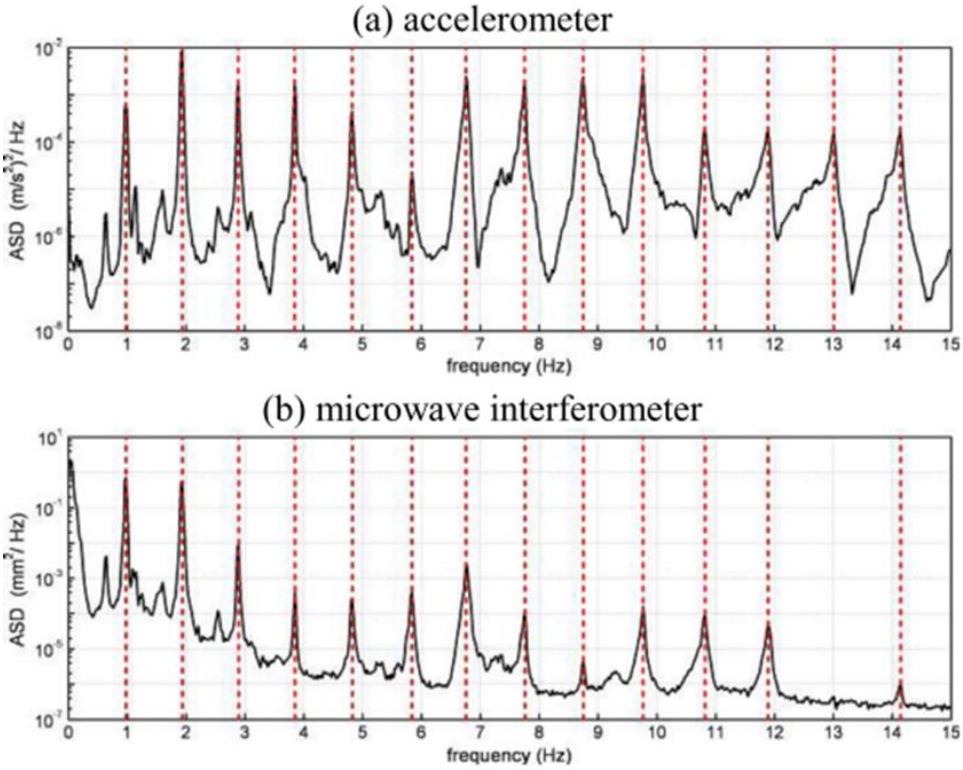

Fig.5. 28 Stay cable 9 on Mestre side: (a) Auto-spectrum of the acceleration data measured by the conventional sensor; (b) Auto-spectrum of the displacement data measured by the radar

Fig.5. 29 Stay cable 9 on Mestre side: (a) Auto-spectrum of the acceleration data measured by the conventional sensor; (b) Auto-spectrum of the displacement data measured by the radar

ıer
ble

n. 9“), the following fundamental frequencies of the stays were identified from both AV and radar data series:

Tab.5 8 The frequencies of the cables were identified by AVT and radar in 2006 and 2010

Mestre side		Venice side		
Cable N.	f_{2006} (Hz)	f_{2010} (Hz)	Cable N.	f_{2010}(Hz)
1	1.23	1.25	1	1.445

2	1.133	1.211	2	1.309
3	1.582	1.621	3	1.641
4	1.484	1.543	4	1.563
5	1.348	1.387	5	1.426
6	1.27	1.289	6	1.328
7	1.23	1.25	7	1.23
8	1.094	1.113	8	1.094
9	0.957	0.977	9	0.938

Beyond the traditional use of the above values for estimating the tension *T* in the stay-cables, it should be noticed that the lower global modes of the bridge (i.e. 0.996 Hz, 1.133 Hz, 1.191 Hz,1.445 Hz and 1.582 Hz) occur at stay cable frequencies or very close to stay-cable frequencies.

5.3.3 Vibration Measurements in 2011

The reception tests of the cable-stayed bridge included extensive measurements of ambient vibration responses induced by the environmental loads. Ambient vibration tests (AVT) were conducted using a 16-channel data acquisition system with 14 uniaxial piezoelectric accelerometers (WR model 731A). Each sensor (capable of measuring accelerations of up to ±0.50 g with a sensitivity of 10 V/g) was connected with a short cable (1 m) to a power unit/amplifier providing the constant current needed to power the accelerometer's internal amplifier, signal amplification and selective filtering. Two-conductor cables connected the power supplies to the data acquisition board, in turn controlled by a portable PC.

Since the AVTs were performed after the bridge was opened to traffic, the ambient vibration data were recorded and provided only by micro-tremors and wind, In the following, the ambient vibration data will be referenced to as AV (micro-tremors and wind).

In order to obtain a satisfactory spatial description of the bridge mode shapes, accelerations were measured in 51 selected points of the deck while only one cross-section of the tower (up-rising the deck of about 15 m) was instrumented by three sensors (selected the same points as 2010). Figure 5.22 shows a schematic diagram of the sensor layout. The tests were performed in a total of 3 set-ups, as it

is shown in figure 5.23: in the first set-up, 17 sensors were placed in the middle of the deck, 4 were considered as reference sensors and remained at the same points during all the set-ups; In the second set-up, 15 sensors were placed in the inner border of the deck and only one cross-section of the tower (up-rising the deck of about 13.5 m) was instrumented by three sensors; In the third set-up, 15 sensors were placed at the outer border of the deck.

For each sensor layout and for each type of ambient excitation, time series of 3.000 s were collected. The data, originally sampled at 400 Hz, was decimated 20 times and high-pass filtered to remove any offset and drift. After decimation, the number of samples was 60.000 per record with a sampling interval of 0.005 s, corresponding to a Nyquist frequency of 10 Hz. Subsequently, data was processed in order to estimate the spectral matrix (i.e. the matrix of auto- and cross-spectral densities, see e.g. [8]) by using the modified periodogram method [9]; according to this approach, an average is made over each recorded signal, divided into *M* frames of *2n* samples, where windowing and overlapping is applied. In the present application, smoothing is performed by 1024-points Hanning-windowed periodograms that are transformed and averaged with 66.7% overlapping, so that a total number of 173 spectral averages was obtained. Since the re-sampled time interval is 0.005 s, the resulting frequency resolution is $1/(1024\times0.005) \approx 0.195$ Hz.

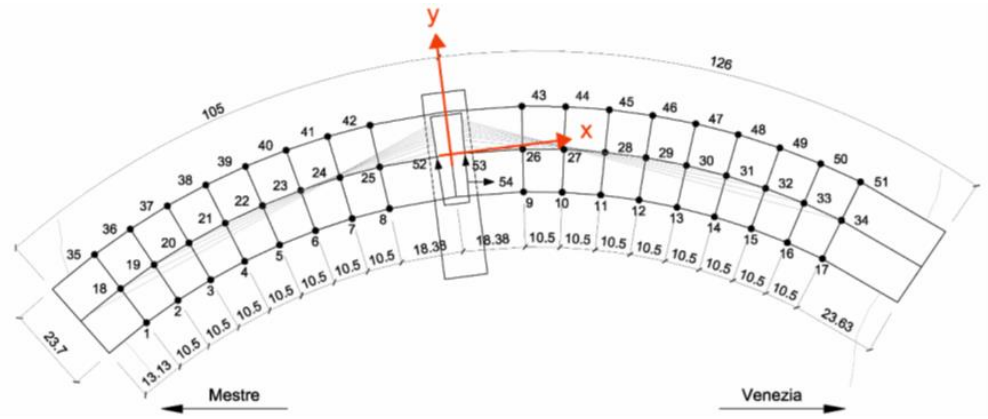

Fig.5. 30 The measurement nodes on top of the bridge deck: 6, 11 and 40,45 are the common points

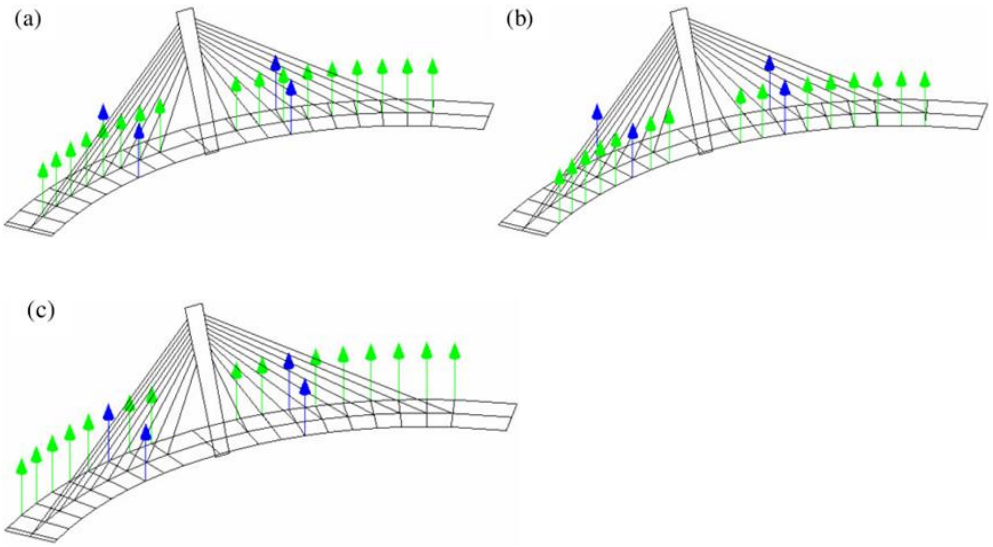

Fig.5. 31 The set-ups of testing in 2011

Fig.5. 32 The set-ups of testing in 2011

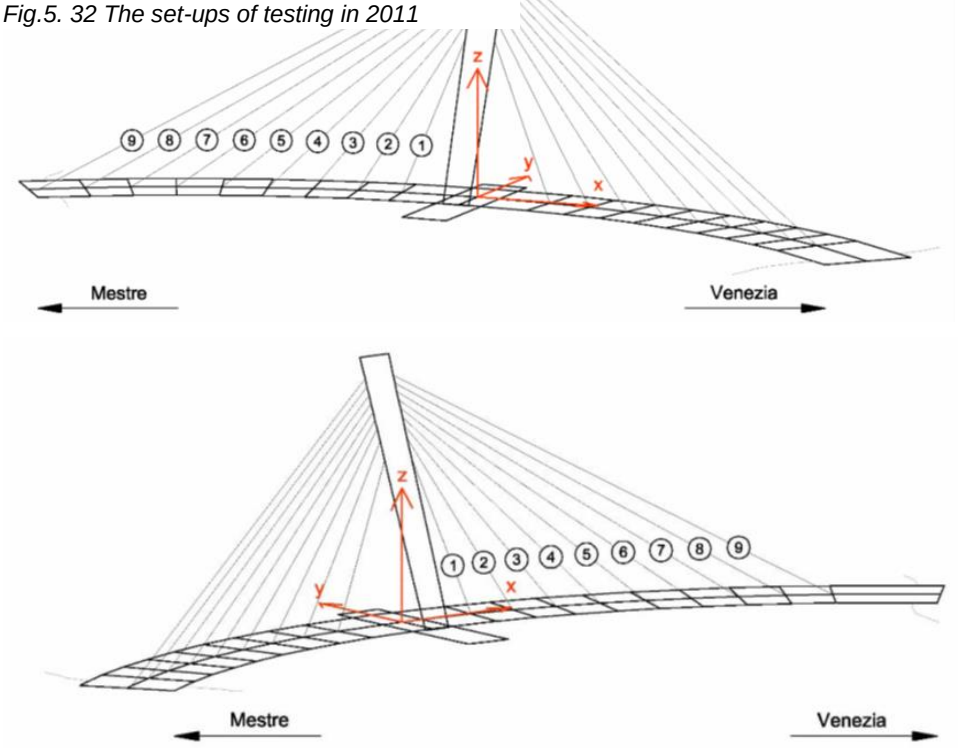

Fig.5. 33 Arrangement of measurement points on stayed cables: (a) side of Mestre; (b) side of Venice

Fig.5. 34 Arrangement of measurement points on stayed cables: (a) side of Mestre; (b) side of Venice

Fig.5. 35 The accelerometers on and stays ahead of the field testing

5 *Fig.5. 36 The accelerometers on and stays ahead of the field testing*

Operational modal analysis and dynamic characteristics of the bridge
The identification of modal parameters from ambient vibration data was carried out by using output-only techniques: The *Frequency Domain Decomposition* (*FDD*) in the frequency domain, the technique is available in the commercial program ARTeMIS .

The *FDD* technique involves the following main steps: (a) estimate of the spectral matrix in the frequency domain from the measured signals; (b) Singular Value Decomposition (*SVD*) of the spectral matrix at each frequency; (c) inspection of the curves representing the singular values to identify the resonant frequencies and estimate the corresponding mode shape from the singular vectors of the *SVD*.

Since the first (and largest) singular value at each frequency represents the strength of the dominating vibration mode at that frequency, the first singular value can be suitably used as a modal indication function (yielding the resonant frequencies as local maxima) whereas the successive singular values contain either noise or modes close to a strong dominating one.

The two sets of mode shapes (Gentile C,2010 and 2011) resulting from the application of *FDD* techniques were then compared using the Modal Assurance Criterion (*MAC*) . The *MAC* is a coefficient analogous to the correlation coefficient in

statistics and ranges from 0 to 1. In general, a *MAC* value greater than 0.80 is considered a good match while a *MAC* value less than 0.40 is considered a poor match.

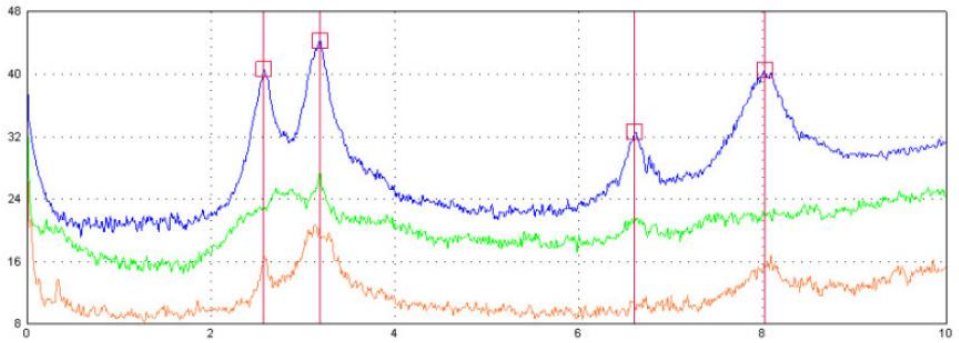

Fig.5. 37 typical pattern of the first singular value of the matrix spectral

Fig.5. 38 typical pattern of the first singular value of the matrix spectral

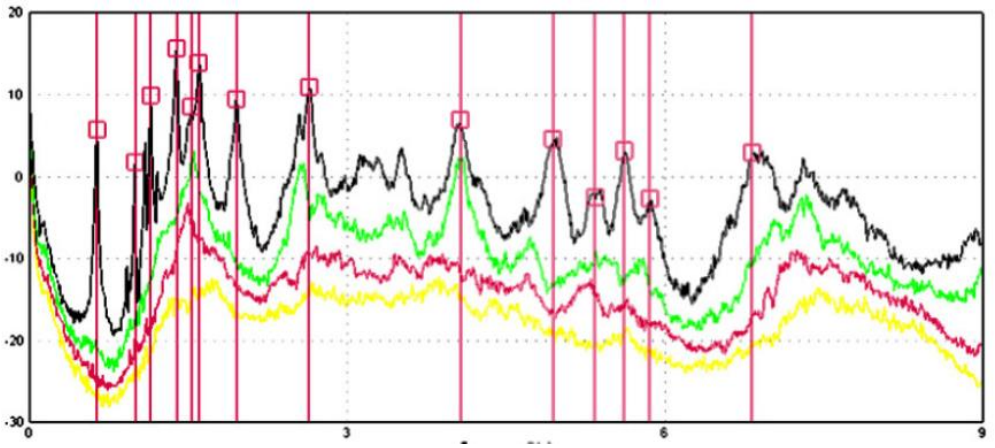

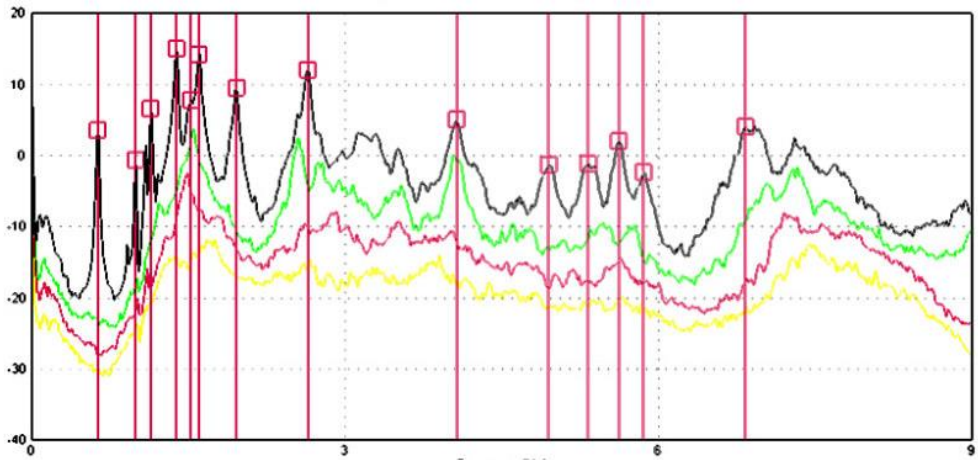

Frequency (Hz)

Fig.5. 39 Singular Value (SV) and identification of natural frequencies

The analysis of acceleration signals recorded on the bridge deck and antenna led to the identification of 13 key frequencies to vibrate to the frequency 0-9 Hz. The results of experimental modal in terms of natural frequencies can be summarized through the diagrams shown in Figure 5.27. These diagrams represent the trend of the first singular values of the matrices spectral, evaluated with two different frequency resolutions according to the signals recorded in excitation conditions environmental. As mentioned above, the singular value decomposition of the spectral matrix allows identification of natural frequencies through the peak values of the first singular value where the corresponding singular vectors represent an estimate of the associated mode shapes. Figure 5.27 allows for clear identification of 14 spectral peaks.

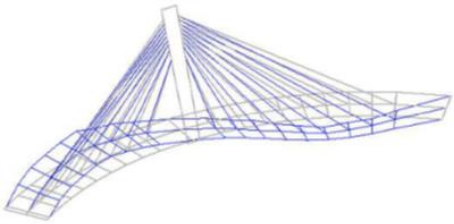

Mode 1. f = 0.635 Hz

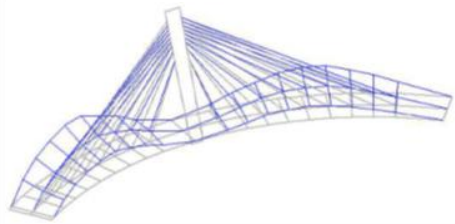

Mode 2. f = 0.996 Hz

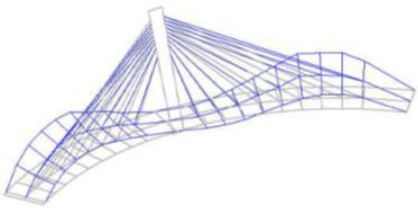

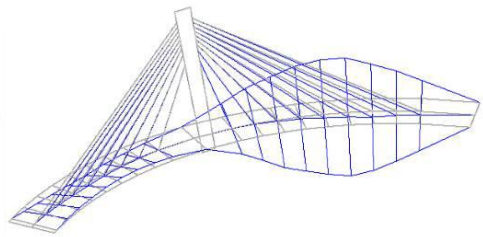

Mode 3. f = 1.143 Hz

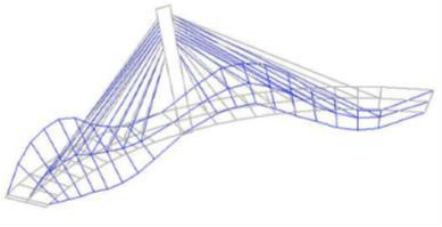

Mode 4. f = 1.387 Hz

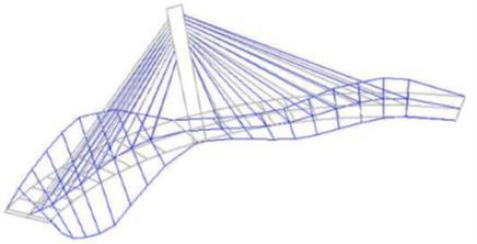

Mode 5. f = 1.523 Hz

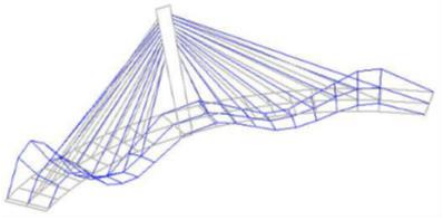

Mode 6. f = 1.602 Hz

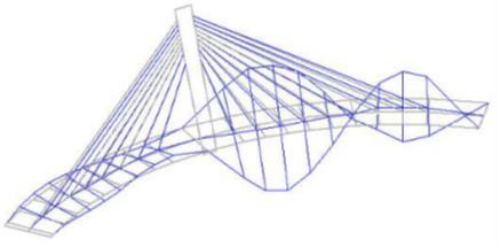

Mode 7. f = 1.953 Hz

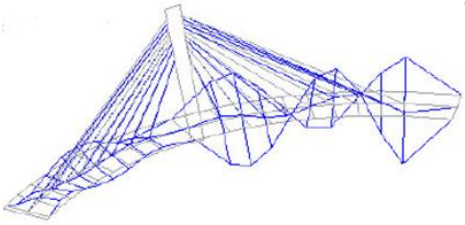

Mode 8. f = 2.646 Hz

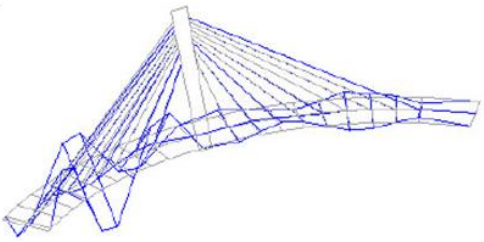

Mode 9. f = 4.072Hz

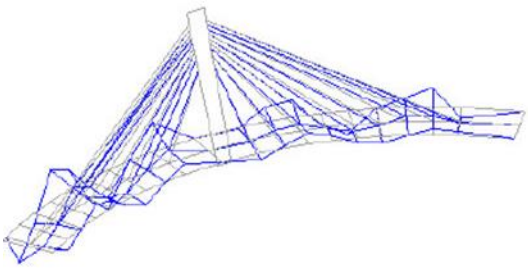

Mode 10. f = 4.951 Hz

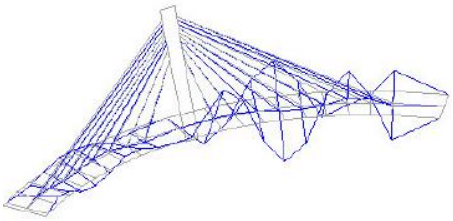

Mode 11. f = 5.332 Hz

Mode 12. f = 5.625 Hz

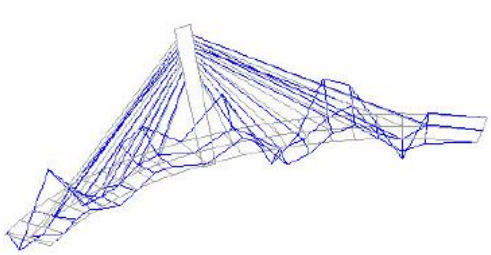

Mode 13. f = 5.859 Hz

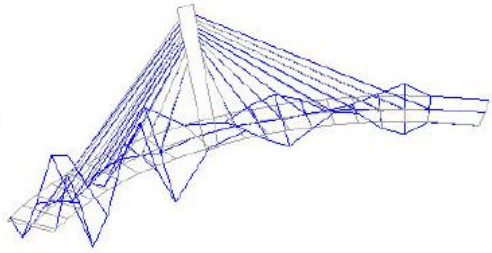

Mode 14. f = 6.836 Hz

Fig.5. 40 the selected mode shape identified from testing

Tab.5 9 Summary of the experimental mode types.

Mode	Type	f (Hz)	Mode	Type	f (Hz)
1	Vertical bending	0.635	8	Torsion	2.646
2	Vertical bending	0.996	9	Torsion	4.072
3	Vertical bending	1.143	10	Torsion	4.951
4	Torsion	1.387	11	Torsion	5.332
5	Bending-Torsion	1.523	12	Torsion	5.625
6	Bending-Torsion	1.602	13	Bending-Torsion	6.826
7	Vertical bending	1.953	14	Torsion	6.836

Tab.5 10 The comparison of frequency and MAC of 2010 and 2011

f_{2010}(Hz)	f_{2011}(Hz)	Δf (%)	MAC
0.635	0.635	-	0.988
0.996	0.996	-	0.980
1.143	1.143	-	0.958
1.387	1.387	-	0.998
1.523	1.523	-	0.982
1.602	1.602	-	0.990
1.953	1.963	0.510	0.988
2.637	2.646	0.340	0.983
3.174	-	-	-
4.053	4.072	0.470	0.954
4.932	4.951	0.390	0.836
-	5.332	-	-

5.596	5.625	0.520	0.835
-	5.859	-	-
6.826	6.836	0.150	0.968

The quantitative comparison between the modal parameters of 2010 and 2011, summarized in Table5.10. clearly shows:

1. the substantial invariance in time of the frequencies of all modes corresponding with percentage differences of entities detected significantly less than 1% (from 0.15% to 0.52%);
2. the similar invariance of modal deformed between the two experimental observations (MAC values for the corresponding modes have very high values, generally exceeding 0.95).

Stay-Cables behavior

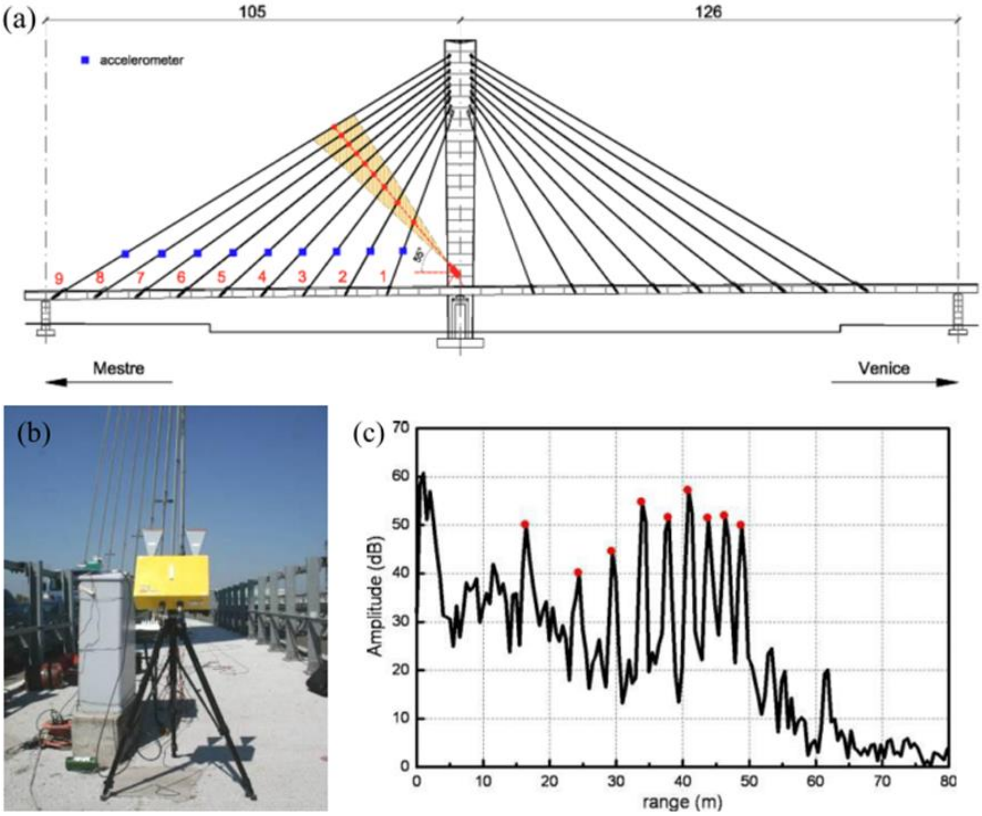

Fig.5. 41 Dynamic survey of the array of stay cables on Mestre side: (a) accelerometers and radar position; (b) view of the radar vibrometer on site; (c) range profile of the test scenario

Fig.5. 42 Dynamic survey of the array of stay cables on Mestre side: (a) accelerometers and radar position; (b) view of the radar vibrometer on site; (c) range profile of the test scenario

Fig.5.29a shows the accelerometers and radar position in the test of the stay cables on Mestre side. The radar was placed at the cross-section of the deck that is vertically supported by the basement of the tower and inclined 55° upward (Fig. 5.29b); a similar set-up was adopted in testing the array of stay cables of the opposite (Venice) side of the bridge. In both tests, time series of 3000 s were simultaneously collected by the accelerometers and the radar sensor, at rate of 200 Hz.

Fig.5.29a also shows the angle of transmission covered by the main lobe of the antenna in the vertical plane, with all the points inside the shadowed area of Fig.5.29a being observable from the sensor. It is worth underlining that the sensor transmits electromagnetic waves also in the horizontal plane and that different transmission angles in the vertical and horizontal plane could be obtained by using different antennas. Due to the cone-shaped emission of the sensor, notwithstanding the slightly spatial arrangement of the cables of each array, all the cables are clearly detected and identified in the range profiles. Fig. 5.29c shows the range profile of the scenario on the Mestre side and is characterized by the presence of nine well defined peaks clearly identifying the position of the stay cables in the array.

Fig.5.29c shows the auto-spectral densities (ASD) of the ambient responses acquired, by using the two measurement systems, on the longer cable of the Mestre-side array. Although the ASDs of Fig.5.29c are associated to different mechanical quantities measured (displacement and acceleration) and to different points of the stay cable, the spectral plots clearly highlight that:

a) a large number of local resonant frequencies of the cables are identified from radar data and these natural frequencies are in excellent agreement with the ones obtained from accelerometer;

b) the number of frequencies identified from radar data is large enough to establish if the cables behave as a taut string or deviate from a taut string. Hence, accurate estimate of the cable tensions can be retrieved from the identified natural frequencies as well.

It is worth underlining that similar results, in terms of number and agreement of natural frequencies, have been obtained for all the stay cables of the two arrays, with the exception of the two shorter ones (cables 1-2 in Fig.5.29a). For the shorter stays, the radar technique detected the lower 3-4 local natural frequencies only, whereas the accelerometers (probably as a consequence of their position) provided a larger number of cable frequencies.

Tab.5 11 The comparison of frequency of cables in 2010 and 2011

Cable N.	Vinece side		Vinece side	
	f2010 (Hz)	f2011 (Hz)	f2010(Hz)	f2011(Hz)
1	1.25	1.23	1.445	1.406
2	1.211	1.211	1.309	1.289
3	1.621	1.621	1.641	1.641
4	1.543	1.543	1.563	1.563
5	1.387	1.387	1.426	1.406
6	1.289	1.289	1.328	1.328
7	1.25	1.25	1.23	1.23
8	1.113	1.094	1.094	1.113
9	0.977	0.977	0.9375	0.9375

5.4 FE Tuning

5.4.1 Choice of the uncertain structural parameters --- double parameters

The modulus of elasticity of steel and concrete in the initial FE model, denoted as E_S and E_C, respectively, were chosen as the updating parameters. A sensitivity analysis was performed for the thirteen modal frequencies with respect to E_S and E_C for each type of structural elements, e.g., the stringers, cross-beams, bracings, tower, slab and pedestrian overlay. It was found that the natural frequencies were more sensitive to the changes of the modulus of elasticity in the stringers, cross-beams, tower, slab and the pedestrian overlay. Hence, only these parts of the model were updated. Moreover, it was found that the influence of the boundary conditions and the modelling uncertainness that is related to the cross-section type 1 (See Fig.5.3) might be of significance to the numerical modal results, especially regarding the mode shapes of higher modes. Nevertheless, further investigation goes beyond the range of the current study, which focuses on the comparison of different updating methods.

5.4.1.1 Comparison of the two methods using simulated results

The two different updating methods are first compared to each other using the simulated modal data as the target. Both the direct method and the iterative method are used using different reference (or initial) values. The lower and upper limits of E_S and E_C were assumed as $[0.9x\ E_S^0,\ 1.1x\ E_S^0]$ and $[0.9x\ E_C^0,\ 1.1x\ E_C^0]$ of both the direct method and the iterative method, respectively. The choice of the reference (or initial) values and the respective updating results of both methods are

summarized in Table 5.12. The relative error is defined as the difference between the result and the target values divided by the target one.

Tab.5 12 Target value and original value and updated value, in comparison to different methods

		Direct method – round 1			*Direct method – round 2*		
	Target (GPa)	*Ref. (GPa)*	*Results (GPa)*	*Relative error(%)*	*Ref. (GPa)*	*Results (GPa)*	*Relative error(%)*
E_c	*33*	*31*	*32.22*	*-2.38*	*34.65*	*36.3*	*10*
E_s	*205*	*210*	*225.5*	*10*	*215.3*	*196.8*	*-4*
		Iterative method – round 1			*Iterative method – round 2*		
	Target (GPa)	*Ref. (GPa)*	*Results (GPa)*	*Relative error(%)*	*Ref. (GPa)*	*Results (GPa)*	*Relative error(%)*
E_c	*33*	*31*	*32.19*	*-2.44*	*34.65*	*32.67*	*-1.00*
E_s	*205*	*210*	*196.20*	*-4.29*	*215.3*	*202.7*	*-1.12*

It is observed that the results of the iterative method are less vulnerable to the influences of the different reference (initial) values as compared to the direct method. Moreover, using the iterative method normally leads to more accurate results of the identified parameters (SMITH, SUZANNE WEAVER BEATTIE,1991).

5.4.1.2 Comparison of the two methods using experimental results

On the basis of the findings in the previous subsection, the experimental modal data were introduced as the target of FE updating in comparison of the two methods. The reference (or initial) values of E_S and E_C were chosen as E_S^0=205GPa and E_C^0=33GPa in both the direct method and the iterative method. The solutions of the direct method were found to be E_S=206GPa and E_C=31.35GPa. The solution of the iterative method was found to E_S=202.7GPa and E_C=32.67GPa.

Table 5.13 provides a summary of the numerical modal results of the updated FE models in comparison to the experimental results. The numerical modal results of the reference/initial FE model (with $E_S = E_S^0$ and $E_C = E_C^0$) were also included. The subscripts ini, D and I denote the initial model, the updated model with the direct method and the updated model with the direct method, respectively. Whilst f_{2010} is the experimental natural frequencies. And the MAC values were calculated between the experimental and the numerical mode shapes.

Tab.5 13 Numerical modal results of the updated FE models, in comparison to their experimental counterparts

Nr.	Mode	f_{2010}(Hz)	$f_{FE\text{-}ini}$(Hz)	$\Delta f_{FE\text{-}ini(\%)}$	MAC	$f_{FE\text{-}D}$(Hz)	$\Delta f_{FE\text{-}D}$(%)	MAC_D	$f_{FE\text{-}I}$(Hz)	$\Delta f_{FE\text{-}I}$ (%)	MAC_I
1	B1	0.635	0.619	-2.5	0.957	0.616	-2.9	0.957	0.642	1.1	0.957
2	B2	0.996	0.905	-9.2	0.960	0.888	-10.8	0.962	0.96	-3.6	0.960
3	B3	1.143	1.095	-4.2	0.983	1.092	-4.5	0.984	1.133	-0.9	0.983
4	T1	1.387	1.376	-0.8	0.891	1.375	-0.9	0.908	1.433	3.3	0.921
5	M1	1.523	1.441	-5.4	0.963	1.442	-5.3	0.963	1.517	-0.4	0.962
6	T2	1.602	1.498	-6.5	0.880	1.498	-6.5	0.877	1.6	-0.1	0.878
7	B4	1.953	1.952	0.0	0.973	1.953	0.0	0.973	2.076	6.3	0.973
8	T3	2.637	2.525	-4.3	0.843	2.527	-4.2	0.865	2.704	2.5	0.820
9	T4	3.174	2.833	-10.7	0.934	2.833	-10.7	0.932	3.171	-0.1	0.936
10	T5	4.053	3.949	-2.6	0.946	3.941	-2.8	0.941	4.182	3.2	0.946
11	T6	4.932	4.772	-3.2	0.910	4.777	-3.2	0.911	5.034	2.1	0.908
12	T7	5.596	5.464	-2.4	0.946	5.469	-2.3	0.945	5.759	2.9	0.945
13	T8	6.826	6.668	-2.3	0.891	6.664	-2.4	0.901	7.006	2.6	0.921

$\Delta f_{FE-ini} = (f_{FE-ini} - f_{2010})/f_{2010}$; $\Delta f_{FE-D} = (f_{FE-D} - f_{2010})/f_{2010}$;

$\Delta f_{FE-I} = (f_{FE-I} - f_{2010})/f_{2010}$

The relative differences of the natural frequencies between the experimental results and the initial and the updated models were calculated by introducing the following index $\Delta\overline{f} = \sqrt{\sum_{i=1}^{13} (\Delta f_i)^2}$. It is found $\Delta\overline{f}_{ini} = 18.48\%$, $\Delta\overline{f}_D = 19.43\%$ and $\Delta\overline{f}_I = 10.09\%$. It is noted that the updated model obtained with the iterative method is slightly improved with respect to the natural frequencies as compared to the initial model. Whereas the model that is obtained with the direct method is similar to the initial model with respect to the natural frequencies. It may be explained by the fact that assumed reference value of the updating parameter E_S and E_C are quite close to the "exact" solution. Since the initial model already match the experimental model results with a relatively high MAC values, no significant improvement is observed of the updated models for either the direct method or the iterative method with respect to the model shapes.

In summary of the findings of the two subsections, it can be concluded by using the iterative method the solutions of the updating parameters are generally more

accurate as compared to the direct method. Nevertheless, both methods can lead to the models with satisfactory modal results as compared to the experimental data, if a good choice of the reference values is made. In addition, the relatively lower computational costs of the direct method shall also be noted.

5.4.2 Choice of the uncertain structural parameters -- multiple parameters

As the first step in the calibration process, one parametric analysis was performed to identify the most sensitive parameters affecting the FE model-computed modal frequencies and mode shapes. The changes in the selected parameters should potentially have a considerable effect on the global vibration response of the bridge rather than on local vibration responses. These parameters are those that contribute significantly to the mass or stiffness properties of the structure. Therefore, the material properties of the major structural components, size/thickness of those structural components, are just some of the potential parameters that can be selected for the FE model calibration. Also, parameters are selected among those whose exact values have high degrees of uncertainty. The uncertainty could be due to possible changes in the structure from the time of construction, differences between the as-built constructed structure and the engineering drawings, non-structural parameters that are not presented in the engineering drawings and, in general, any parameter where the required information cannot be found about their accurate values in the engineering drawings. After a careful consideration of the initial FE model and the available engineering drawings, 10 parameters were selected in the bridge FE model to perform sensitivity analyses. These parameters were related to either boundary conditions or the mass/stiffness properties of the FE model. The selected parameters along with the lower/upper bounds of their values are listed in Table5.14.

Tab.5 14 The limits of the selected parameters

Parameters	*Mean(GPa)*	*Min(GPa)*	*Max(GPa)*
Equivalent elastic of the pier	*33*	*29.7*	*36.3*
Equivalent elastic modulus of the pier cap	*33*	*29.7*	*36.3*
Equivalent elastic modulus of the base	*33*	*29.7*	*36.3*
Equivalent elastic modulus of the slab	*33*	*29.7*	*36.3*
Equivalent elastic modulus of the surface	*33*	*29.7*	*36.3*
Equivalent elastic modulus of the pylon 1	*28.2*	*29.7*	*43.2*
Equivalent elastic modulus of the pylon 2	*28.2*	*29.7*	*43.2*

Equivalent elastic modulus of the pylon 3	*28.2*	*29.7*	*43.2*
Equivalent elastic modulus of the pylon 4	*28.2*	*29.7*	*43.2*
Equivalent elastic modulus of the steel	*210*	*297*	*363*
Equivalent elastic modulus of the steel	*210*	*297*	*363*

There were no data found in the engineering drawings about the thickness of the asphalt overlay on the bridge. This parameter was included in the model an equivalent material weighing the mechanical properties of the concrete with the mechanical properties of the asphalt. Similar procedure was developed for the elastic modulus and weight of the sidewalk, in practical a weighed value has been used in order to take into account the paving. A lower and upper range of +/- 1% was chosen as variation for the sensitivity parameters. Modal analyses were performed using the lower and upper bound values of the selected parameters listed in Table 5.14. The frequency values were obtained from a modal analysis of the FE model output. The sensitivity of the modal frequencies with respect to the selected value of any of the 10 parameters, pi, were computed using:

$$s_{ij} = \frac{p_i}{\Delta p_i} \cdot \frac{\Delta \omega_j}{\omega_j}$$

The calculated sensitivity values for the 11 selected parameters are shown in Figure 5.30. As can be seen in Figure 5.30, it was found that 11 parameters, including all elastic modulus of the material used. The parameters mass of the bridge easy to determine as comparable to the parameters associated with the stiffness properties of the bridge. As a result, these model parameters were not considered further during model updating.

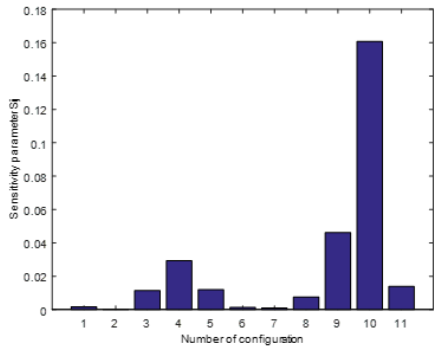

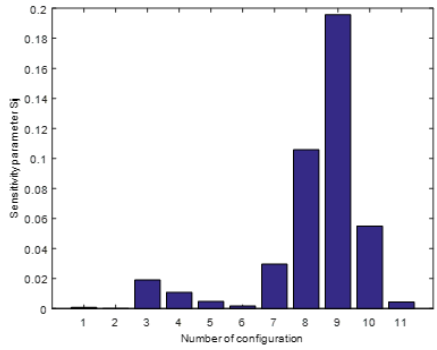

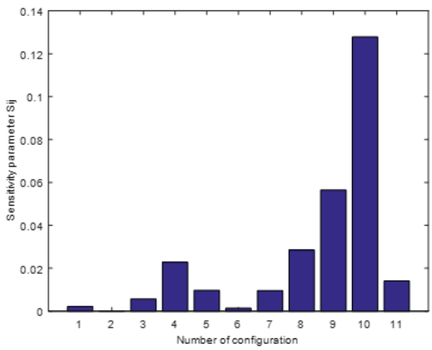
Sensitivity parameter Sij
0.14
0.12
0.1
0.08
0.06
0.04
0.02
0
1 2 3 4 5 6 7 8 9 10 11
Number of configuration

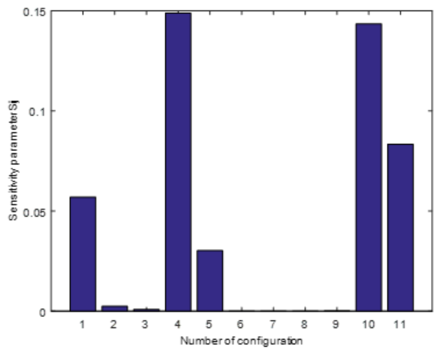
Sensitivity parameter Sij
0.15
0.1
0.05
0
1 2 3 4 5 6 7 8 9 10 11
Number of configuration

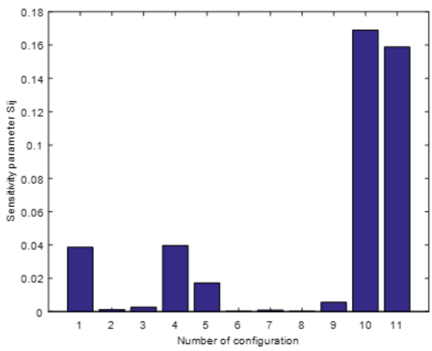
Sensitivity parameter Sij
0.18
0.16
0.14
0.12
0.1
0.08
0.06
0.04
0.02
0
1 2 3 4 5 6 7 8 9 10 11
Number of configuration

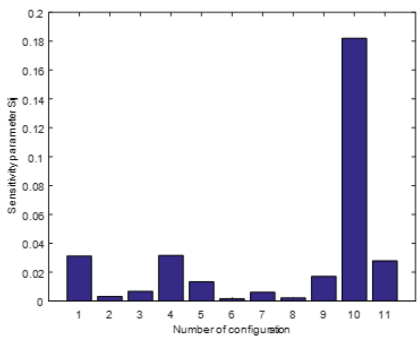
Sensitivity parameter Sij
0.2
0.18
0.16
0.14
0.12
0.1
0.08
0.06
0.04
0.02
0
1 2 3 4 5 6 7 8 9 10 11
Number of configuration

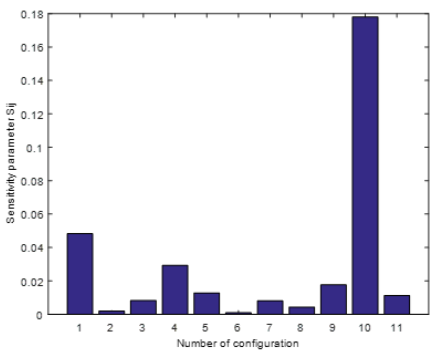
Sensitivity parameter Sij
0.18
0.16
0.14
0.12
0.1
0.08
0.06
0.04
0.02
0
1 2 3 4 5 6 7 8 9 10 11
Number of configuration

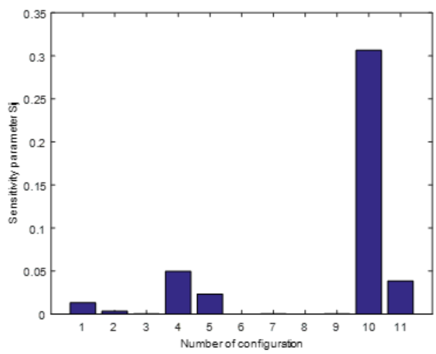
Sensitivity parameter Sij
0.35
0.3
0.25
0.2
0.15
0.1
0.05
0
1 2 3 4 5 6 7 8 9 10 11
Number of configuration

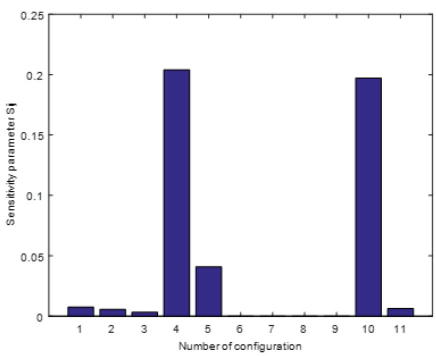
Sensitivity parameter Sij
0.25
0.2
0.15
0.1
0.05
0
1 2 3 4 5 6 7 8 9 10 11
Number of configuration

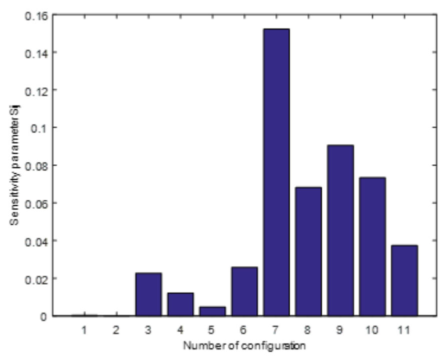
Sensitivity parameter Sij
0.16
0.14
0.12
0.1
0.08
0.06
0.04
0.02
0
1 2 3 4 5 6 7 8 9 10 11
Number of configuration

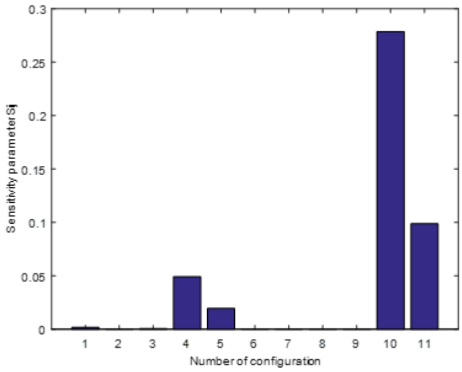
Sensitivity parameter Sj
Number of configuration

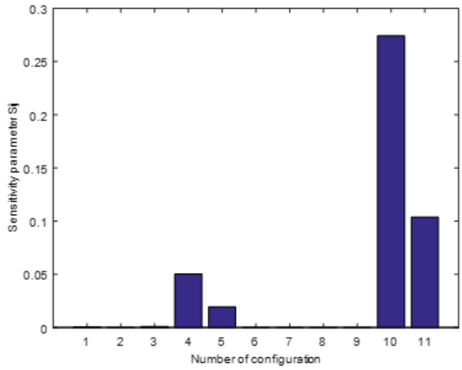
Sensitivity parameter Sj
Number of configuration

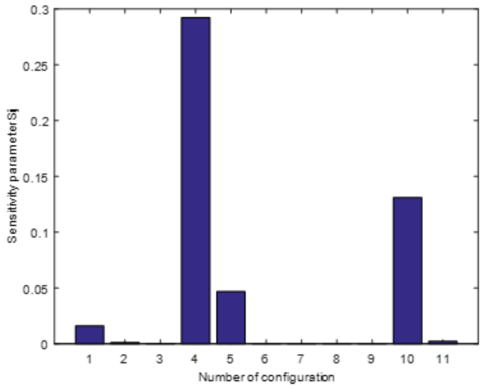
Sensitivity parameter Sj
Number of configuration

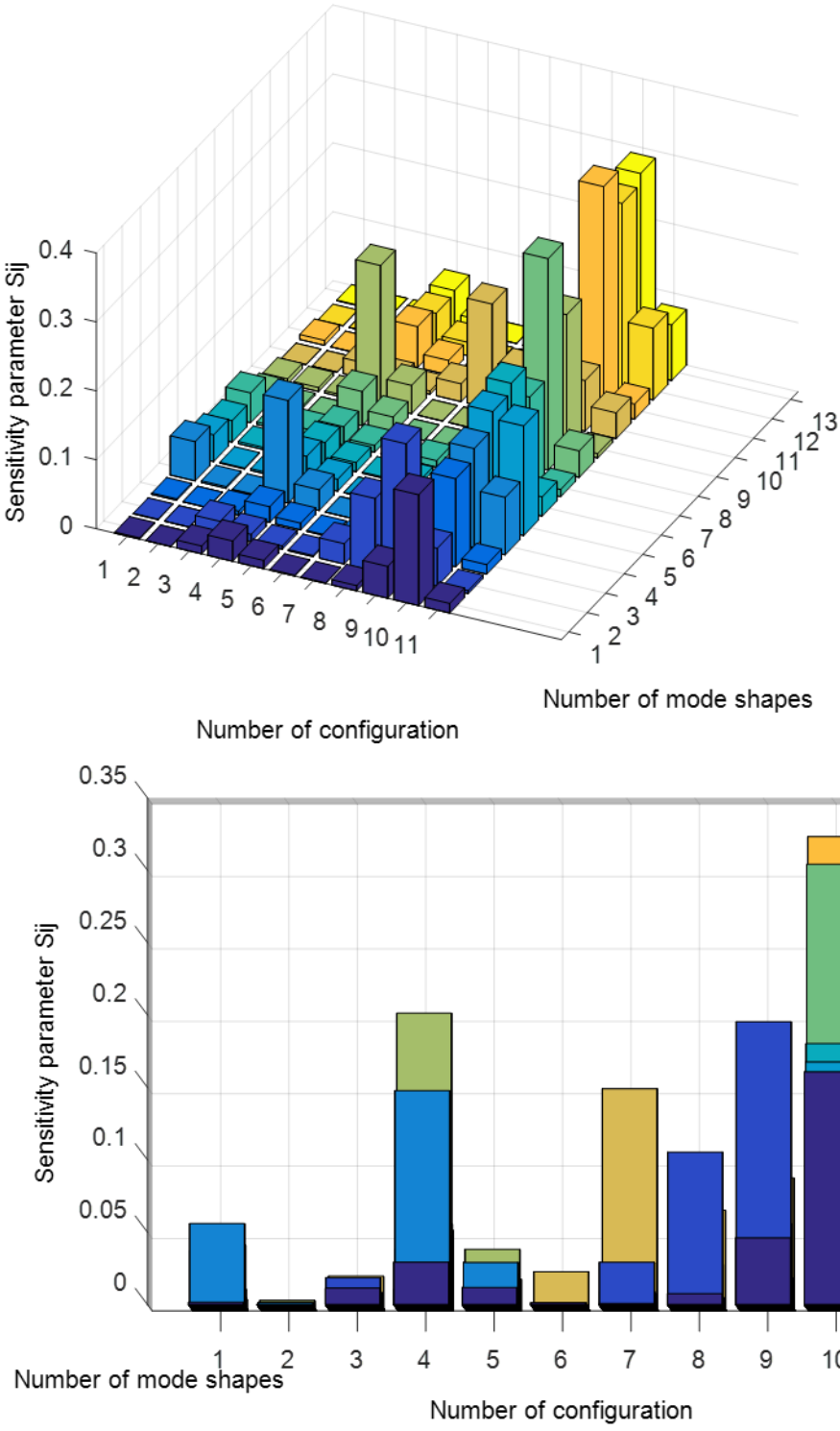

Fig.5. 43 The sensitivity analysis of the selected parameters

After the most sensitive FE model parameters were identified, a brief study was done to investigate how variations in any of the 11 identified parameters impact the FE-computed mode shapes. To do this, the upper limit values, lower limit values and average values for each of the four parameters were used to obtain FE-computed mode shapes. The mode shapes for the upper and lower bounds were compared to those extracted from the model using average values of the parameters. For comparison purposes, the MAC value is assessed between the mode shapes generated by varying one model parameter to one of its bounds (i.e. upper of lower) to the mode shapes associated with the model parameters set to their average values. The MAC values derived from this analysis are tabulated in Figure 5.30 for each model parameter and for each of the modes that matched by experimental modes. The more the MAC value of a parameter deviates from unity, the more sensitive the mode shape is to that parameter.

5.4.2.1 Comparison of the two methods using simulated results— Muti-parameters

On the basis of the findings in the previous subsection, the experimental modal data were introduced as the target of FE updating in comparison of the two methods. The reference (or initial) values of E_S and E_C were chosen as E_{deck}^0=205GPa $E_{s\text{-}bracing}^0$=205GPa and E_{slab}^0=33GPa E_{pylon}^0=36GPa in both the direct method and the iterative method. The solutions of the direct method were found to be $_{deck}^0$=205GPa $E_{s\text{-}bracing}^0$=215GPa and E_{slab}^0=31.35GPa E_{pylon}^0=38GPa The solution of the iterative method were found to $_{deck}^0$=216GPa $E_{s\text{-}bracing}^0$=218GPa and E_{slab}^0=33.74GPa E_{pylon}^0=41.67GPa

Goodness of the model updating process depends on the values of the weighting factors, W_f and W_z, used to balance the importance of the modal frequency and mode shape parts of the objective function, respectively. One of the two weighting factors (W_f) was taken as 2 in all analyses since these factors define a relative importance between modal frequency and mode shape in the updating process. The value initially selected for Wz was 4. The reason for the large value of Wz with respect to W_f is that the errors between the measured and FE-computed mode shapes are considered in the objective function in terms of the MAC values with MAC values always smaller than 1. Therefore, a larger Wz should be chosen to balance the importance of modal frequencies and mode shapes in the objective function. The final FE-updated modal frequencies are presented in Table 5.15. As seen in Table 5.15, the differences between the measured and initially calculated modal frequencies vary from 0% for the first mode to -10.7% for the fifth mode. In total, 13 modes between 0.62 Hz and 6.67 Hz are obtained by the FE modal

analysis. The first, second and third are purely translational and they are neglected. The calculated natural frequencies and the mode types are listed. Both vertical bending modes along the longitudinal directions and vertical bending modes with deformation of the cross section are found in the modal analysis results. Local modes with deformation of the slab and the side barriers are also predicted by the FE analysis.

Table 5.15 provides a summary of the numerical modal results of the updated FE models in comparison to the experimental results. The numerical modal results of the reference/initial FE model (with $E_S = E_S^0$ and $E_C = E_C^0$) were also included. The subscripts ini, D and I denote the initial model, the updated model with the direct method and the updated model with the direct method, respectively. Whilst f_{2010} is the experimental natural frequencies. And the MAC values were calculated between the experimental and the numerical mode shapes.

Tab.5 15 Numerical modal results of the updated FE models, in comparison to their experimental counterparts

Nr.	Mode	f_{2010}(Hz)	$f_{FE\text{-}ini}$(Hz)	$\Delta f_{FE\text{-}ini}$(%)	MAC	$f_{FE\text{-}D}$(Hz)	$\Delta f_{FE\text{-}D}$(%)	MAC_D	$f_{FE\text{-}I}$(Hz)	$\Delta f_{FE\text{-}I}$(%)	MAC_I
1	B1	0.635	0.62	-2.5	0.96	0.62	-1.76	0.96	0.64	0.78	0.96
2	B2	0.996	0.91	-9.2	0.96	0.93	-6.41	0.95	0.97	-2.98	0.95
3	B3	1.143	1.10	-4.2	0.98	1.10	-3.62	0.98	1.13	-1.24	0.98
4	T1	1.387	1.38	-0.8	0.89	1.33	-3.86	0.98	1.39	0.11	0.98
5	M1	1.523	1.44	-5.4	0.96	1.44	-5.39	0.97	1.49	-2.22	0.97
6	T2	1.602	1.50	-6.5	0.88	1.50	-6.62	0.90	1.54	-3.81	0.85
7	B4	1.953	1.95	0	0.97	1.95	-0.20	0.97	2.00	2.64	0.87
8	T3	2.637	2.53	-4.3	0.84	2.53	-4.21	0.97	2.63	-0.37	0.94
9	T4	3.174	2.83	-10.7	0.93	2.86	-9.93	0.93	2.98	-6.18	0.93
10	T5	4.053	3.95	-2.6	0.95	3.94	-2.80	0.94	4.10	1.19	0.94
11	T6	4.932	4.77	-3.2	0.91	4.77	-3.26	0.93	4.97	0.74	0.92
12	T7	5.596	5.46	-2.4	0.95	5.46	-2.39	0.95	5.69	1.65	0.95
13	T8	6.826	6.67	-2.3	0.89	6.62	-3.00	0.92	6.90	1.05	0.92

$\Delta f_{FE-ini} = (f_{FE-ini} - f_{2010})/f_{2010}$; $\Delta f_{FE-D} = (f_{FE-D} - f_{2010})/f_{2010}$;
$\Delta f_{FE-I} = (f_{FE-I} - f_{2010})/f_{2010}$

The relative differences of the natural frequencies between the experimental results and the initial and the updated models were calculated by introducing the following

index $\Delta\bar{f} = \sqrt{\sum_{i=1}^{13}(\Delta f_i)^2}$. It is found $\Delta\bar{f}_{ini} = 18.48\%$, $\Delta\bar{f}_D = 2.95\%$ and $\Delta\bar{f}_I = 0.82\%$. It is noted that the updated model obtained with the iterative method is slightly improved with respect to the natural frequencies as compared to the initial model. Whereas the model that is obtained with the direct method is similar to the initial model with respect to the natural frequencies. It may be explained by the fact that assumed reference value of the updating parameter E_S and E_C are quite close to the "exact" solution. Since the initial model already match the experimental model results with a relatively high MAC values, no significant improvement is observed of the updated models for either the direct method or the iterative method with respect to the model shapes.

In summary of the findings of the two subsections, it can be concluded by using the iterative method the solutions of the updating parameters are generally more accurate as compared to the direct method. Nevertheless, both methods can lead to the models with satisfactory modal results as compared to the experimental data, if a good choice of the reference values is made. In addition, the relatively lower computational costs of the direct method shall also be noted.

5.5 Conclusions

Two different numerical methods are used to the FE model updating of a curved cable-stay bridge. The unique design of the bridge structure provides an interesting case study. Both methods can lead to satisfactory results as compared to the experimental modal data when proper choices are made in the updating procedure.

CHAPTER 6

6. DISSCUSION OF THE UPADATING RESULTS

Recent decades, due to their pleasant aesthetics, and economical and efficient construction techniques, cable-stayed bridges have increased in prevalence all over the world. With the development of high strength materials and construction technologies, cable-stayed bridges with aesthetically appealing geometries such as curvature in the deck and different shapes of pylon cannot be ruled out in the right circumstances.

Cable-stayed bridges with a single pylon and multi-spans have not yet been studied in depth, although considerable numbers of such bridges have already been constructed. Curvature in the deck in a cable-stayed bridge makes it more aesthetically pleasing, also many construction sites require curvature in the deck of cable-stayed bridges, but such bridges have not been paid much attention in reported research. Cable-stayed bridges with shorter spans are more influenced by dynamic vibrations than aerodynamic vibrations, however curved cable-stayed bridges do have span limitation due to stability issues. So a detailed response of curved cable-stayed bridges needs to be studied. For the reason of Marghera bridge (chapter 5) is the key study of thesis, so the following curved structures are simplified by Marghera bridge.

The dynamic response of the structures has to be carefully checked for vibration induced by people and wind. Also response to earthquake loading has to be verified. Typically, the first step is to determine the natural modes and frequencies followed by a check of the dynamic response due to the moving load. For preliminary calculations the vertical natural modes can be determined using the formulas for vibration of a simple cable. The dynamic test has proved their validity. For final design the dynamic analysis should be done with a calculation model that includes modal analysis. It is important to realize that the dynamic analysis is usually linear.

A typical one span structure is characterised by natural modes that are presented in Fig.6.1. The vertical modes are denoted as A and B; the first swing mode is denoted as C; and the first torsional mode is denoted as D. Due to the vertical curvature of the prestressed band, a horizontal movement is always combined with torsion and it is therefore difficult to find a pure torsional mode. Since the vibration following the first vertical mode (A) requires an elongation of the cable, the

corresponding frequency is in some cases higher than the frequency of the second vertical mode (B).

When analyzing multi-span structures, it is noted that the bridge behaves as a continuous structure only when there is horizontal displacement of the supports. For a small load, as caused by a group of pedestrians, the change of stresses is very small and the individual spans behave as isolated cables. Therefore, when the structure is checked for motions that can cause unpleasant feeling, the dynamic analysis should be done for the individual spans in addition to the overall structure.

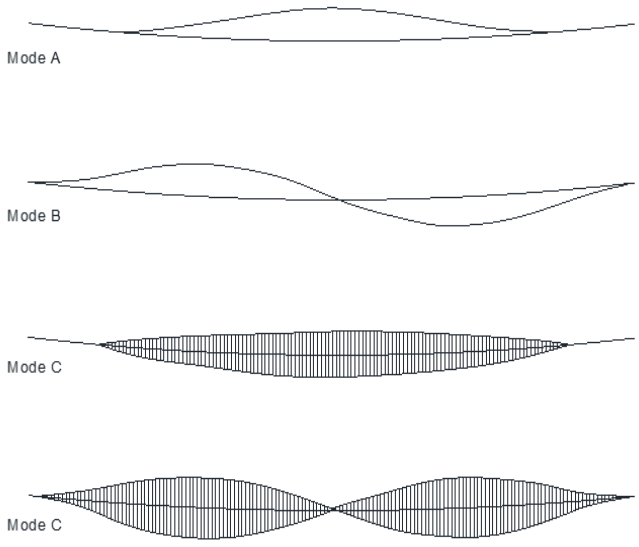

Fig.6. 1 Natural modes

6.1 Dynamic analysis of straight and curved structure

6.1.1 Dynamic analysis of straight continuous girder bridge and curved continuous girder bridge

Cable-stayed bridges are investigated using FEM software SAP2000 V16 by developing 3D models. For optimization of time and accuracy of results, the deck and pylon using 3D BEAM element. FEM models of straight and curved continuous girder bridges in SAP2000 are shown in Figure 6.2. The following assumptions are made in the study: (a) material is homogeneous, isotropic and linearly elastic; (b) only geometric nonlinearities are taken into consideration; (c) cables are perfectly

flexible and have only tension stiffness; (d) cable–deck, cable–pylon and deck–pylon deck-pier connections are assumed to be fixed.

To study the behaviour of cable-stayed bridge with change in its geometry, in-plane curvature is introduced to the deck. The total length of 387 m on six spans (42 m + 105 m + 126 m + 30 m + 42 m + 42 m) which is kept constant. The radius of curvature is 175 m (Sasmal S.et al 2007).

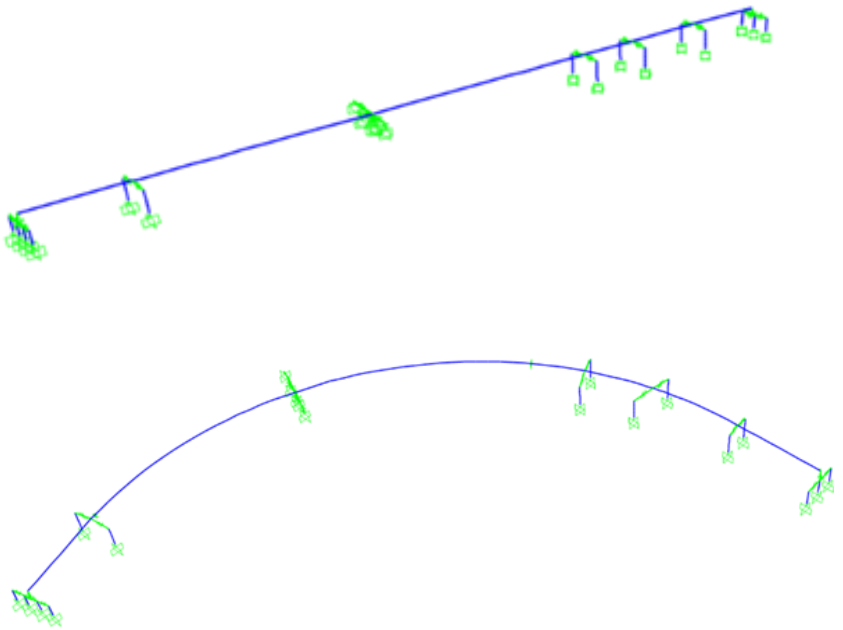

Fig.6. 2 FEM model of straight (top) and curved (below) continuous girder bridges

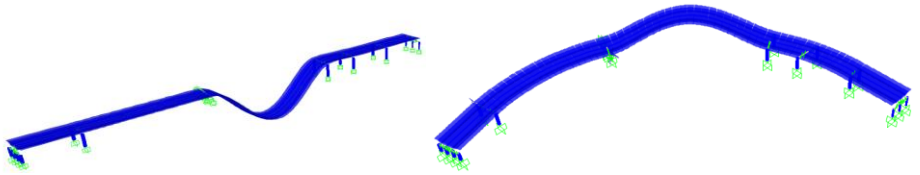

Fig.6. 4 1st vertical bending mode for staight (L) and curved continuous girder bridges (R)

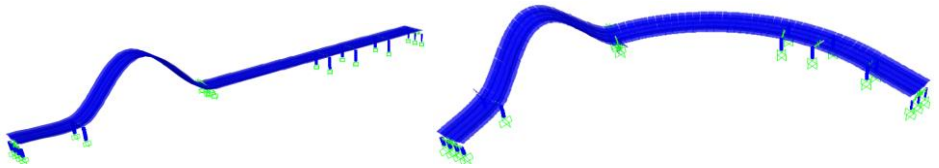

Fig.6. 5 2nd vertical bending mode for staight (L) and curved continuous girder bridges (R))

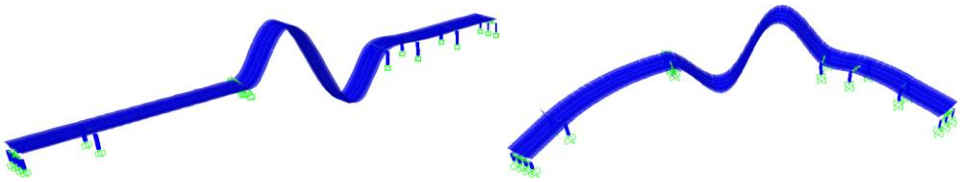

Fig.6. 6 3rd vertical bending mode for staight (L) and curved continuous girder bridges (R)

Fig.6. 7 4th vertical bending mode for staight (L) and curved continuous girder bridges (R)

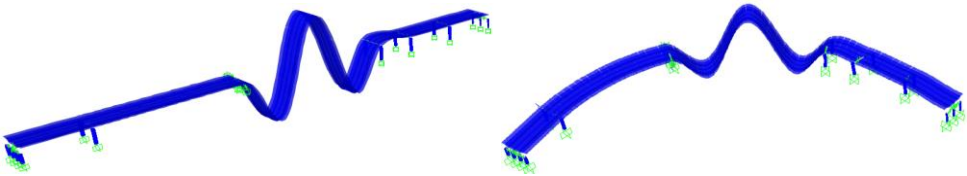

Fig.6. 8 5th vertical bending mode for staight (L) and curved continuous girder bridges (R)

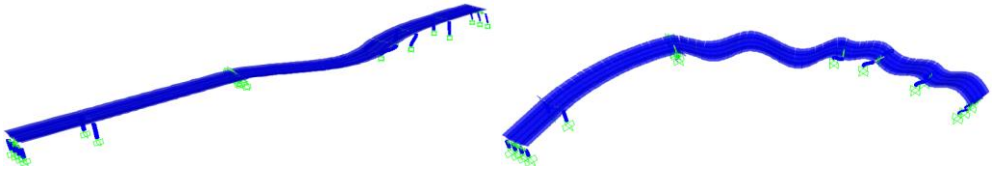

Fig.6. 9 1th torsion mode for staight (L) and curved continuous girder bridges (R)

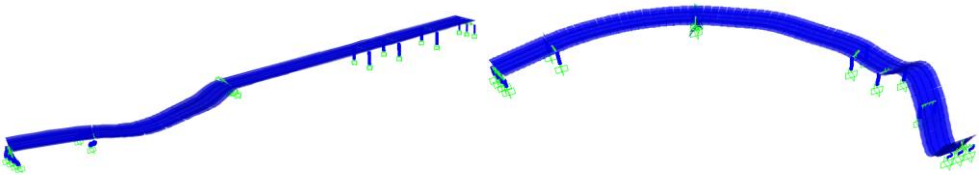

Fig.6. 10 2nd torsion mode for staight (L) and curved continuous girder bridges (R)

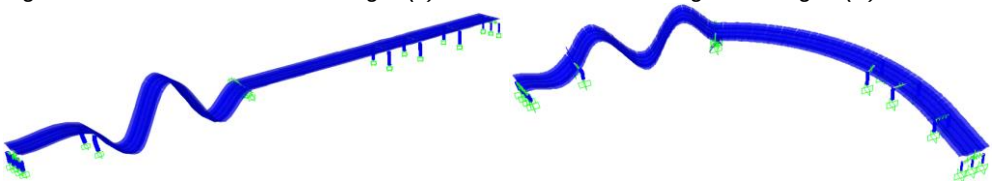

Fig.6. 11 6th vertical bending mode for staight (L) and curved continuous girder bridges (R)

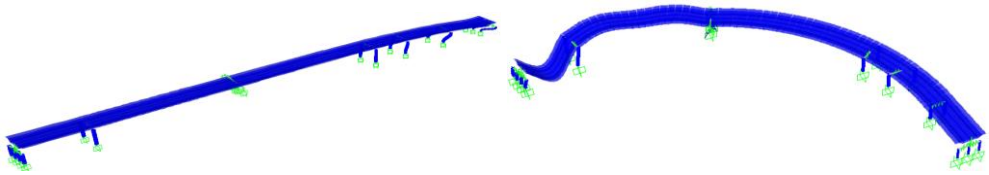

Fig.6. 12 3rd torsion mode for staight (L) and curved continuous girder bridges (R)

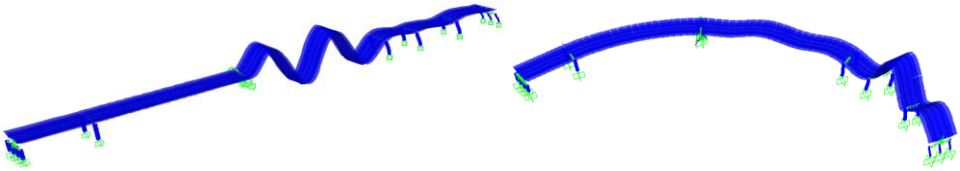

Fig.6. 13 7th vertical bending mode for staight (L) and curved continuous girder bridges (R)

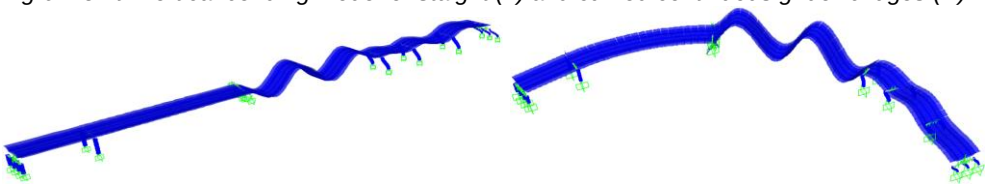

Fig.6. 14 8th vertical bending mode for staight (L) and curved continuous girder bridges (R)

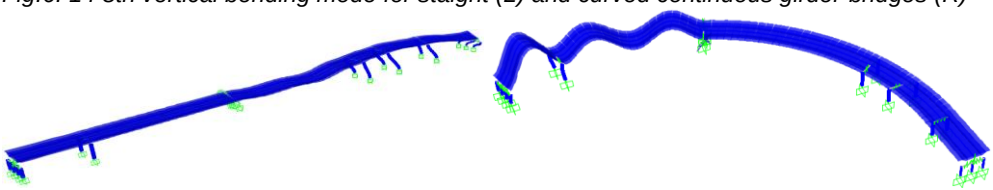

Fig.6. 15 4th torsion bending mode for staight (L) and curved continuous girder bridges (R)

Tab.6. 1 Modal characteristics and frequencies (Hz) for straight and curved cintinuous girder bridges

	Straight Structure		Curved Structure	
No.	frequency (Hz)	Mode type	frequency (Hz)	Mode type
1	0.611	V	0.511	V
2	0.755	V	0.744	V
3	1.621	V	1.402	V
4	2.018	V	2.005	V
5	3.127	V	2.718	V
6	3.443	T	3.186	T
7	4.009	T	3.357	M
8	4.064	V	3.813	V
9	4.634	T	3.963	M
10	5.264	V	4.088	V
11	5.465	V	4.438	T
12	5.623	T	4.451	V

T: torsional mode V: vertical mode M: the mixed of torsional and vertical modes

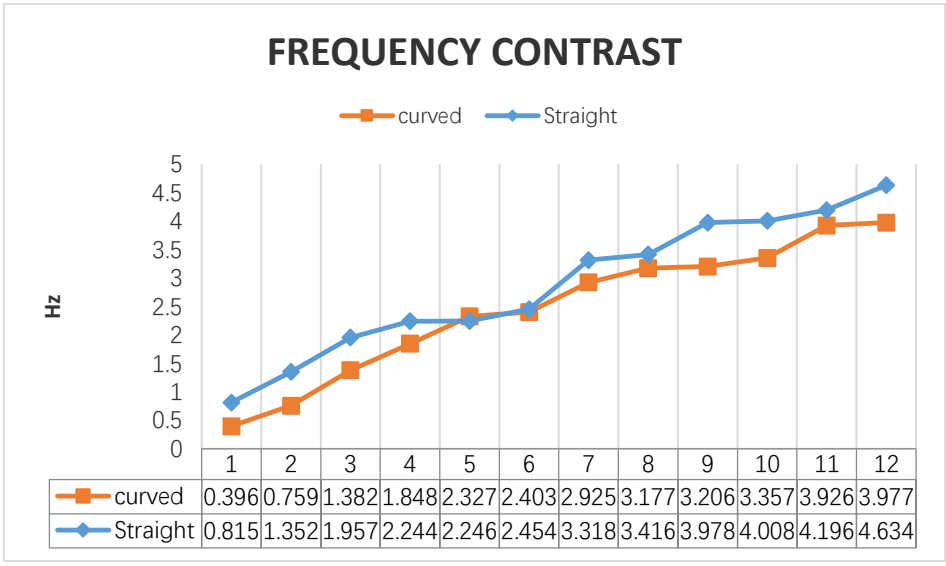

	1	2	3	4	5	6	7	8	9	10	11	12
curved	0.396	0.759	1.382	1.848	2.327	2.403	2.925	3.177	3.206	3.357	3.926	3.977
Straight	0.815	1.352	1.957	2.244	2.246	2.454	3.318	3.416	3.978	4.008	4.196	4.634

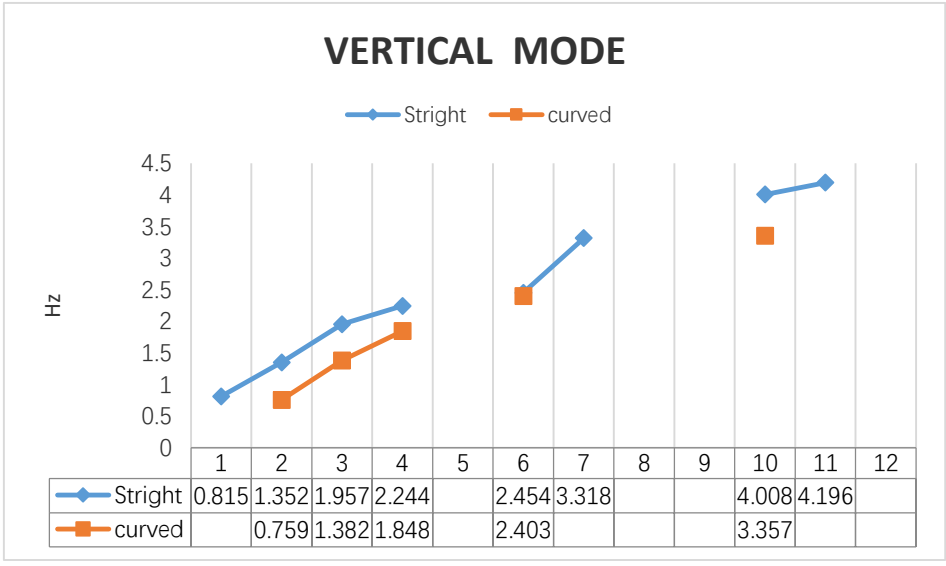

	1	2	3	4	5	6	7	8	9	10	11	12
Stright	0.815	1.352	1.957	2.244		2.454	3.318			4.008	4.196	
curved		0.759	1.382	1.848		2.403				3.357		

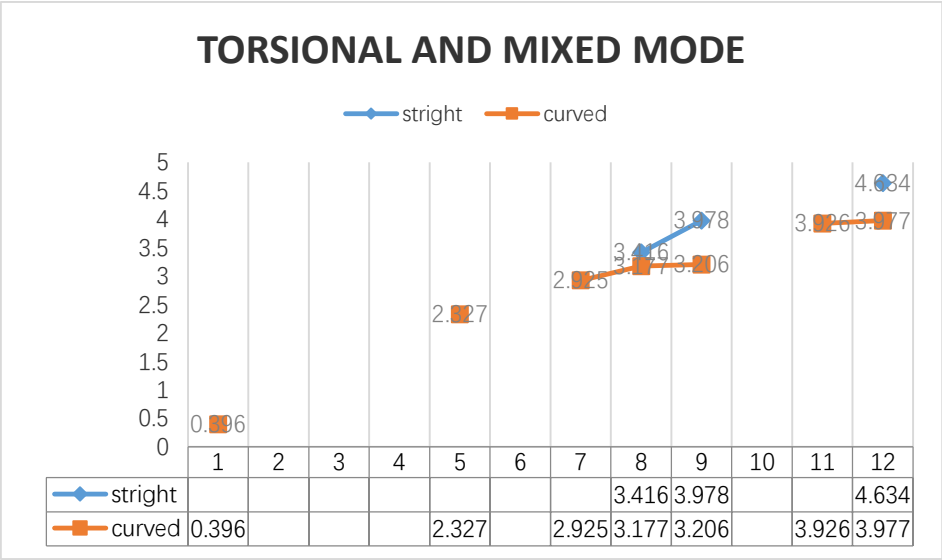

Fig.6. 16 The frequency contrast of stright and curved continuous girder bridge

Modal analysis of straight and curved continuous girders bridges is carried out to understand frequencies and mode shapes. Figures 6.4-6.15 are representative, showing similar mode shapes obtained from the free vibrational analysis of straight and curved continuous girder bridge.

Figures 6.4 to 6.9 and 6.11 show the first, second, third fourth, fifth sixth vertical bending mode shape, Figure 6.9 and 6.10 shows torsion mode and Figure 6.10 and 6.12 shows torsional mode of the deck of a straight bridge and 1st and 2nd mixed of torsional and vertical modes of a curved bridge. and Figure 6.14 shows vertical mode of the deck of a straight bridge and 2nd torsional mode of a curved bridge. It is observed that deck torsion is observed almost in all modes, which is obvious due to a shift in the center of gravity away from the mid width of the deck. Therefore, curvature in the deck introduces mixing of torsion in the deck almost in all the modes, which is not desirable for any regular conventional design. So, special care has to be taken for designing against developed forces and detailing of reinforcements of the curved cable-stayed bridges.

Frequencies of the first twelve modes of straight and curved continuous girder bridges are compared in detail. For better representation and qualitative evaluation, mode numbers and their corresponding frequencies and their shape description are

given in Tables 6.1. From the results presented in these tables, with the introduction of curvature in deck of bridge, frequency of similar modes decreases but the difference is notable. Torsional modes occur earlier in curved bridges. Even in first vertical bending mode some torsion in deck is observed. From Figure 6.9 it is clear that as curvature is introduced in the deck, the difference in vertical displacement of the deck of the cable-stayed bridge goes on increasing, which in turn introduces torsion in deck.

6.1.2 Dynamic analysis of straight single plane cable-stayed structure and curved single plane cable-stayed structure

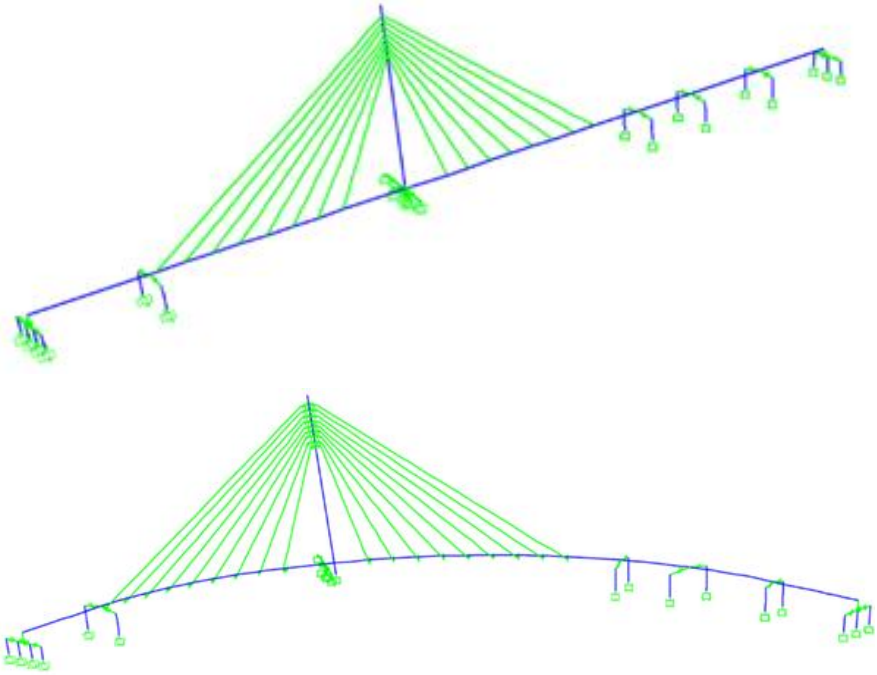

Fig.6. 17 FEM model of straight (top) and curved (below) cable-stayed bridges

Tab.6. 2 Modal characteristics and frequencies (Hz) for straight and curved single plane cabl-stayed bridges

	Straight Structure		Curved Structure	
No.	frequency (Hz)	Mode type	frequency (Hz)	Mode type
1	0.815	V	0.396	TP
2	1.352	V	0.759	V
3	1.957	V	1.382	V
4	2.244	V	1.848	V
5	2.246	TP	2.327	M

6	2.454	V	2.403	V
7	3.318	V	2.925	M
8	3.416	T	3.177	T
9	3.978	T	3.206	M
10	4.008	V	3.357	V
11	4.196	V	3.926	T
12	4.634	T	3.977	M

T: torsional mode V: vertical mode M: the mixed of torsional and vertical modes

TP: transverse bending of pylon

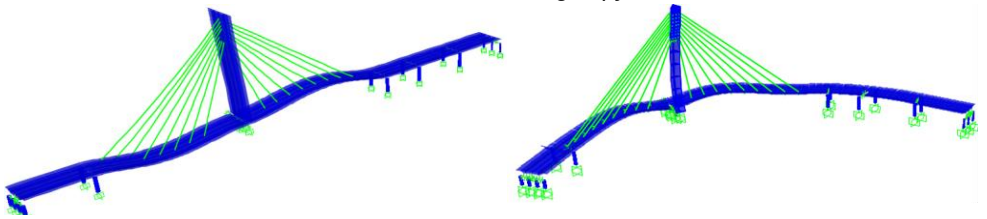

Fig.6. 18 1st mode for staight (L) and single plane curved cable-stayed bridges (R)

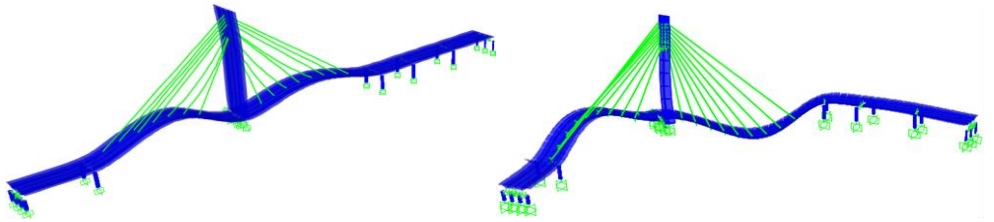

Fig.6. 19 2nd mode for staight (L) and single plane curved cable-stayed bridges (R)

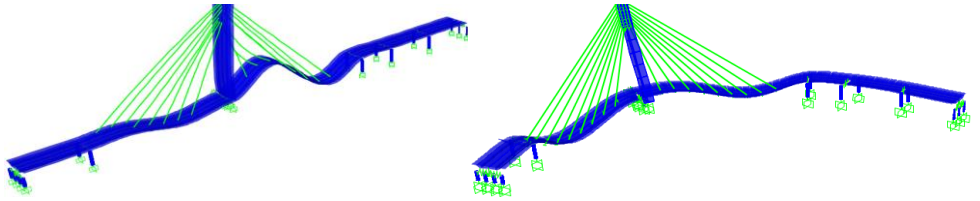

Fig.6. 20 3rd mode for staight (L) and single plane curved cable-stayed bridges (R)

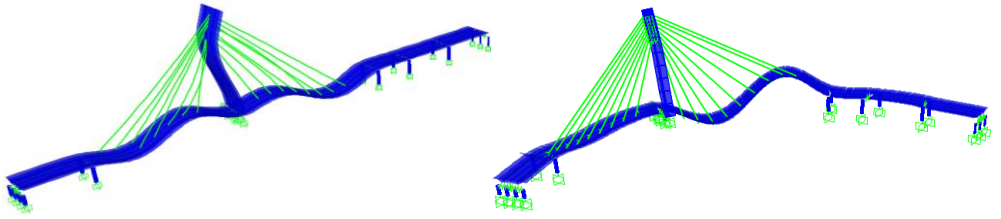

Fig.6. 21 4th mode for staight (L) and single plane curved cable-stayed bridges (R)

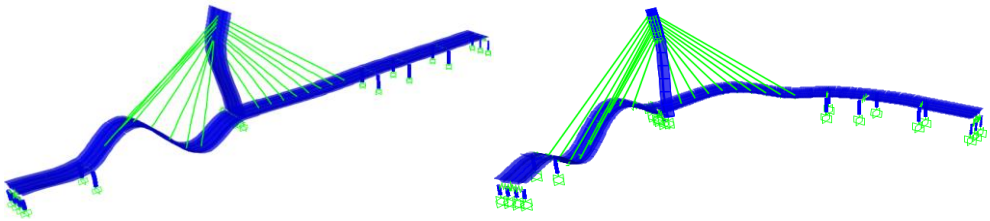

Fig.6. 22 5th mode for staight (L) and single plane curved cable-stayed bridges (R)

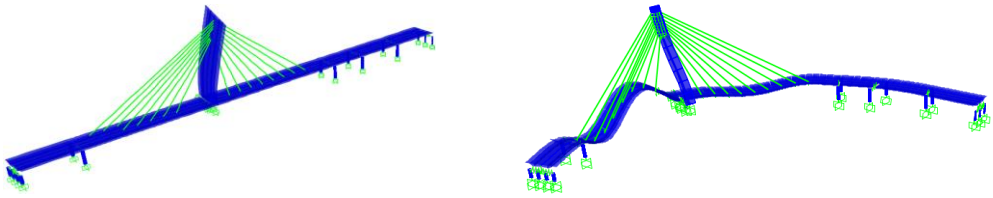

Fig.6. 23 6th mode for staight (L) and single plane curved cable-stayed bridges (R)

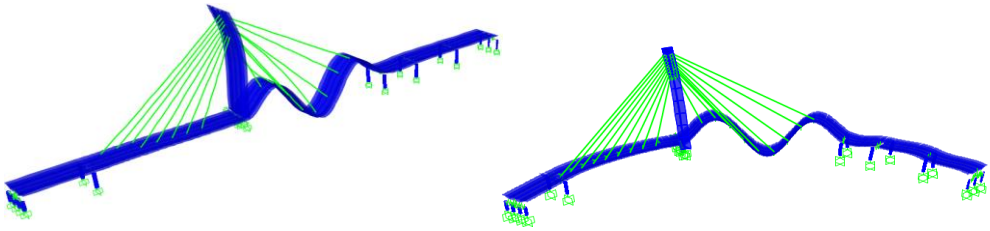

Fig.6. 24 7th mode for staight (L) and single plane curved cable-stayed bridges (R)

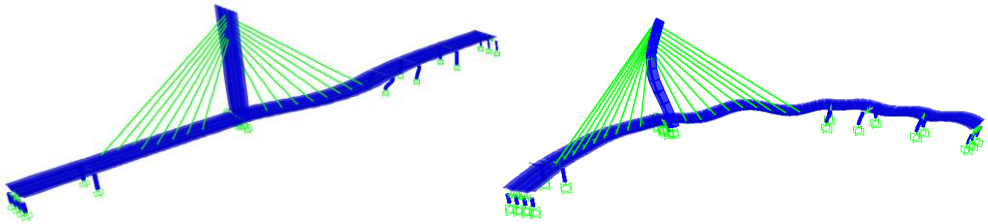

Fig.6. 25 8th mode for staight (L) and single plane curved cable-stayed bridges (R)

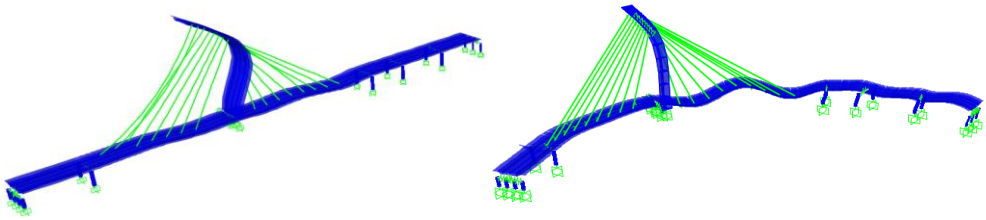

Fig.6. 26 9th mode for staight (L) and single plane curved cable-stayed bridges (R)

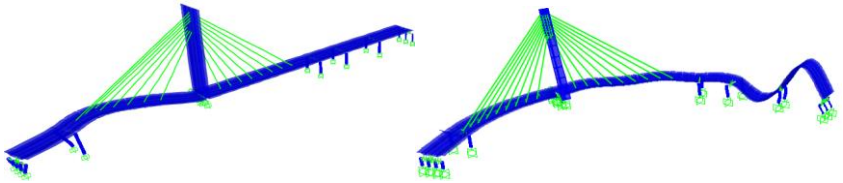

Fig.6. 27 10th mode for staight (L) and single plane curved cable-stayed bridges (R)

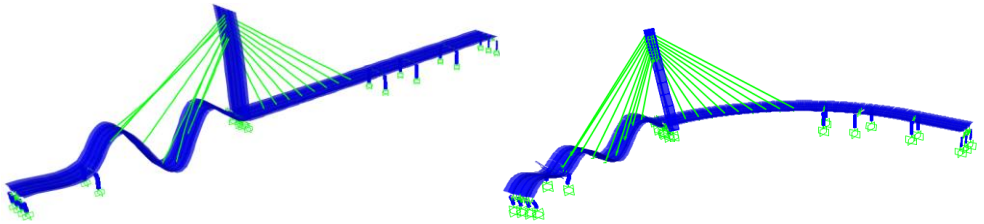

Fig.6. 28 11th mode for staight (L) and single plane curved cable-stayed bridges (R)

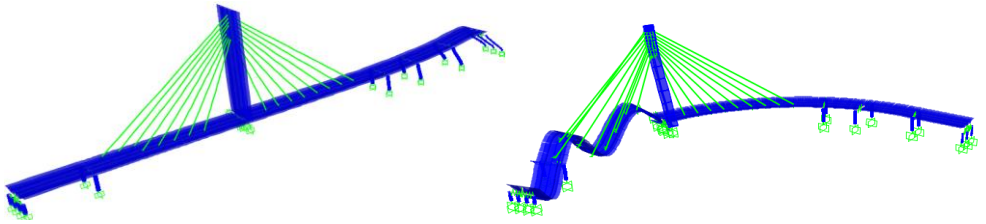

Fig.6. 29 12th mode for staight (L) and single plane curved cable-stayed bridges (R)

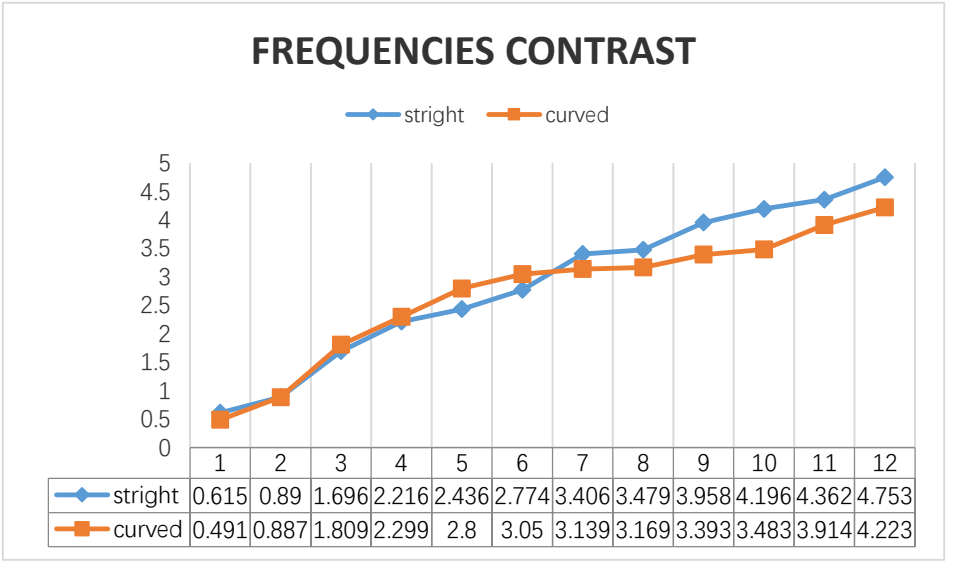

	1	2	3	4	5	6	7	8	9	10	11	12
stright	0.615	0.89	1.696	2.216	2.436	2.774	3.406	3.479	3.958	4.196	4.362	4.753
curved	0.491	0.887	1.809	2.299	2.8	3.05	3.139	3.169	3.393	3.483	3.914	4.223

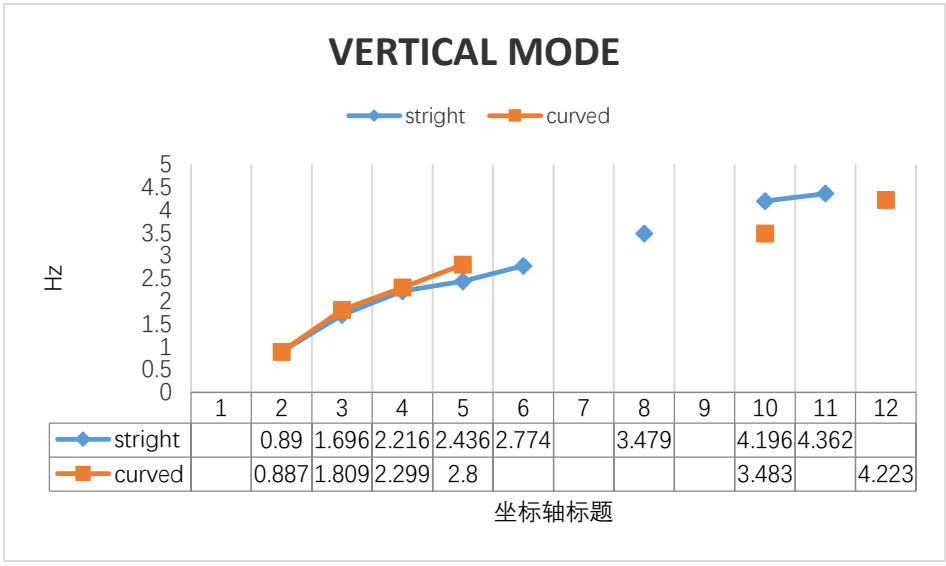

	1	2	3	4	5	6	7	8	9	10	11	12
stright		0.89	1.696	2.216	2.436	2.774		3.479		4.196	4.362	
curved		0.887	1.809	2.299	2.8					3.483		4.223

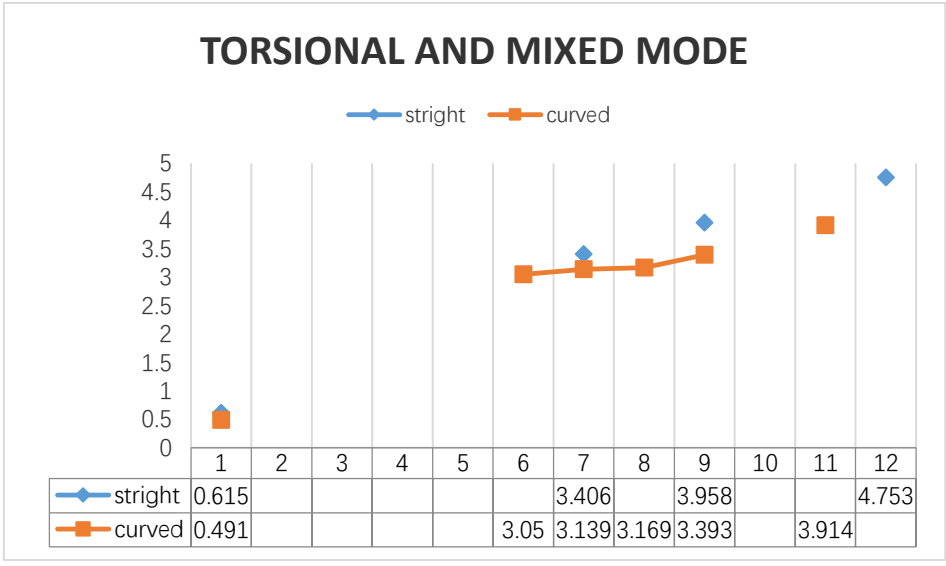

	1	2	3	4	5	6	7	8	9	10	11	12
stright	0.615						3.406		3.958			4.753
curved	0.491					3.05	3.139	3.169	3.393		3.914	

Fig.6. 30 The frequency contrast of stright and curved continuous cable-stayed bridges

Modal analysis of straight and curved continuous girders bridges is carried out to understand frequencies and mode shapes. Figures 6.18-6.29 are representative, showing similar mode shapes obtained from the free vibrational analysis of straight and curved single plane cable-stayed bridge.

For the straight cable-stayed bridge, Figures 6.18 to 6.22 6.24 6.28 show the first to fifth, sixth and seventh vertical bending mode shape, Figure 6.23 shows pylon transverse bending mode and Figure 6.26 and 6.27 shows torsional mode of the

deck of straight cable-stayed bridge. It is observed that in curved cable-stayed bridges almost all modes are mixed with pylon and deck modes. It is also clear that deck torsion is observed almost in all modes, which is obvious due to a shift in the center of gravity away from the mid width of the deck. Therefore, curvature in the deck introduces mixing of torsion in the deck almost in all the modes, which is not desirable for any regular conventional design. So, special care has to be taken for designing against developed forces and detailing of reinforcements of the curved cable-stayed bridges.

Frequencies of the first twelve modes of straight and curved cable-stayed bridges are compared in detail. For better representation and qualitative evaluation, mode numbers and their corresponding frequencies and their shape description are given in Tables 6.2. From the results presented in these tables, it is found that for vertical pylon of the straight cable-stayed bridge, the first five modes are pure deck modes in vertical bending. Because of the high stiffness of vertical pylon of the straight cable-stayed bridge, frequency of first mode is very high. The sixth mode is pylon mode. From the eighth mode torsion modes of decks are observed, but they are mixed with pylon modes.

Looking into the curved cable-stayed bridges, as inclined pylon, it could be observed that pylon mode occurs first and at very low frequency. All mode shapes are not very distinct and there is combination of modes. Due to the smaller stiffness of pylon, pylon and deck modes are mixed. On the other hand, in the inclined pylon, as pylon stiffness is lower than for the straight pylon, the pylon transverse mode is found at much lower frequency (as presented in Figure 6.18). It is observed that vertical bending modes occur first followed by pylon modes; if pylon stiffness is very low then pylon modes occurs at very low frequency.

From the above results it is observed that, with the introduction of curvature in deck of cable-stayed bridge, first frequency decreases obvious, frequency of similar modes decreases with the difference is notable. Torsional modes occur earlier in curved bridges. Even in first vertical bending mode some torsion in deck is observed. From Tab.6.2 it is clear that as curvature is introduced in the deck, the difference of frequencies of the cable-stayed bridge goes on increasing, which in turn introduces torsion in deck.

6.1.3 Dynamic analysis of straight double plane cable-stayed structure and curved double plane cable-stayed structure

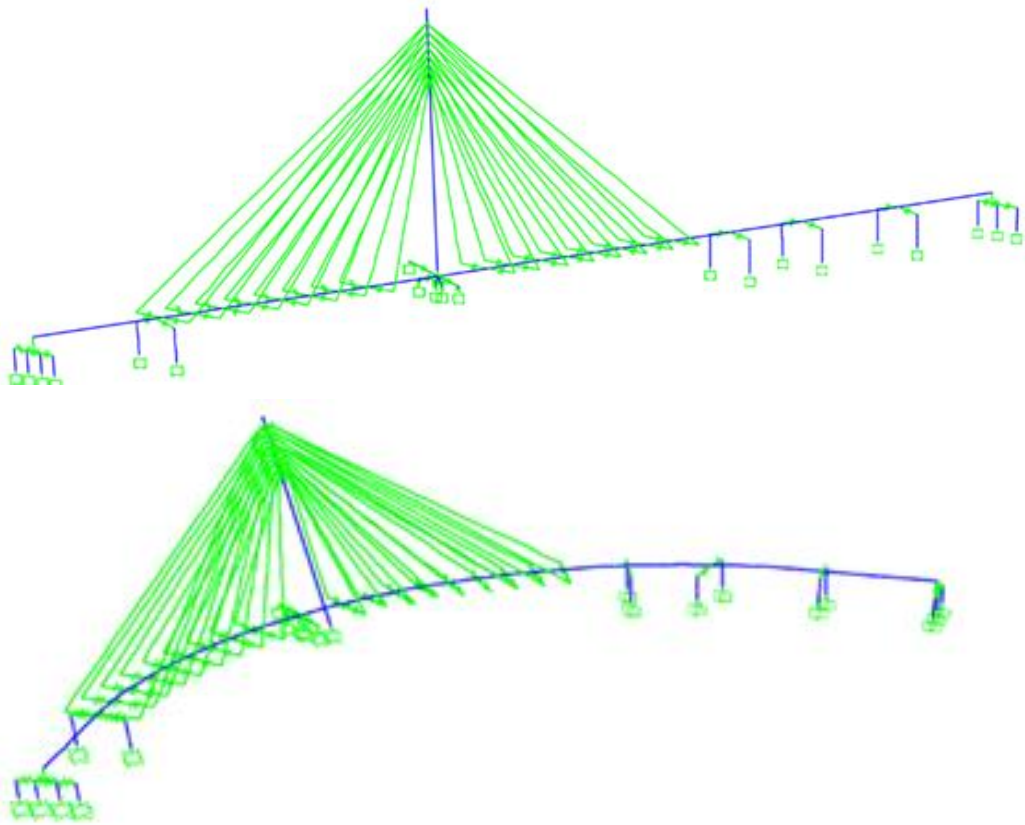

Fig.6. 31 FEM model of straight (top) and curved (below) double planes cable-stayed bridges

Tab.6. 3 Modal characteristics and frequencies (Hz) for straight and curved double planes cabl-stayed bridges

	Stright Structure		Curved Structure	
No.	frequency (Hz)	Mode type	frequency (Hz)	Mode type
1	0.615	TP	0.491	TP
2	0.890	V	0.887	V
3	1.696	V	1.809	V
4	2.216	V	2.299	V
5	2.436	V	2.800	V
6	2.774	V	3.050	M
7	3.406	T	3.139	M
8	3.479	V	3.169	M
9	3.958	T	3.393	M
10	4.196	V	3.483	V
11	4.362	V	3.914	T
12	4.753	T	4.223	V

T: torsional mode V: vertical mode M: the mixed of torsional and vertical modes

TP: transverse bending of pylon

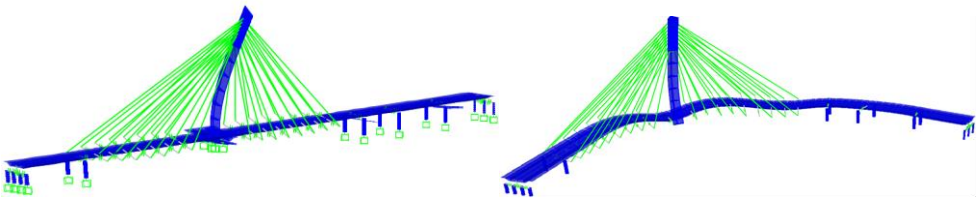

Fig.6. 32 1st mode for staight (L) and double plane curved cable-stayed bridges (R)

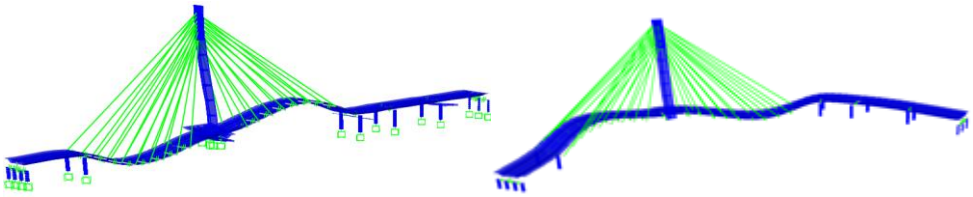

Fig.6. 33 2nd mode for staight (L) and double plane curved cable-stayed bridges (R)

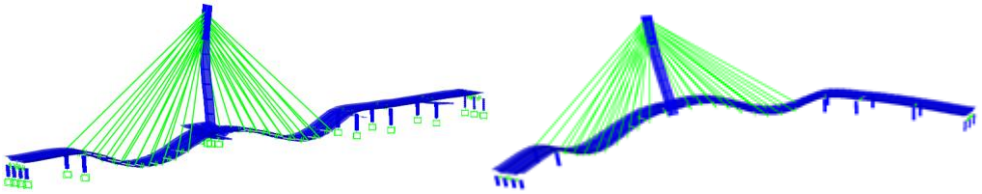

Fig.6. 34 3rd mode for staight (L) and double plane curved cable-stayed bridges (R)

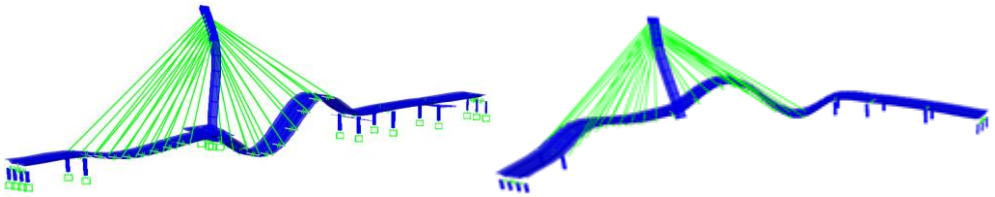

Fig.6. 35 4th mode for staight (L) and double plane curved cable-stayed bridges (R)

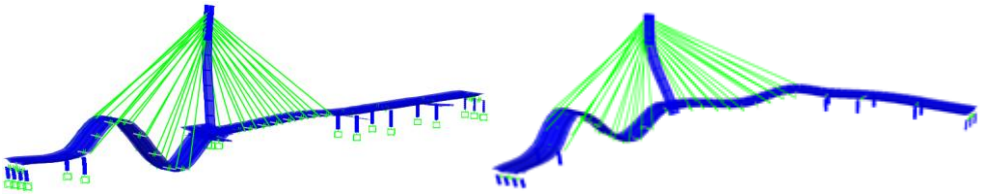

Fig.6. 36 5th mode for staight (L) and double plane curved cable-stayed bridges (R)

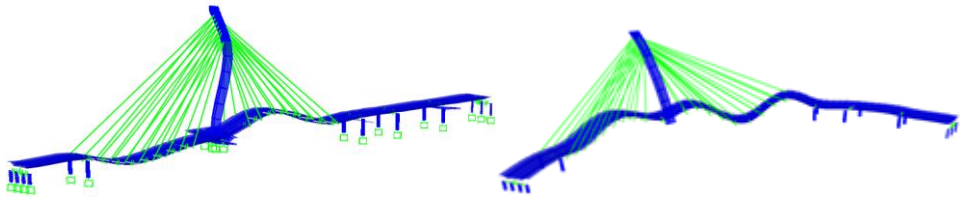

Fig.6. 37 6th mode for staight (L) and double plane curved cable-stayed bridges (R)

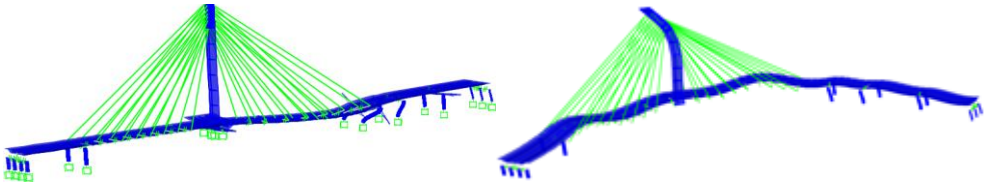

Fig.6. 38 7th mode for staight (L) and double plane curved cable-stayed bridges (R)

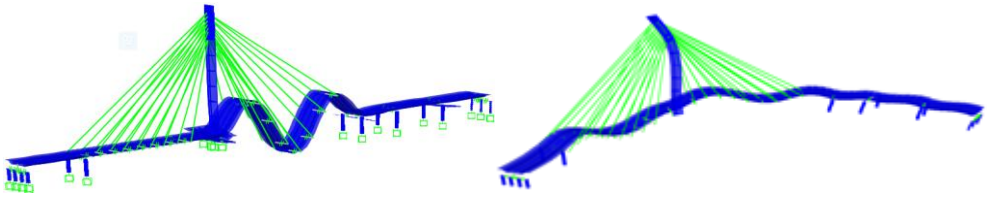

Fig.6. 39 8th mode for staight (L) and double plane curved cable-stayed bridges (R)

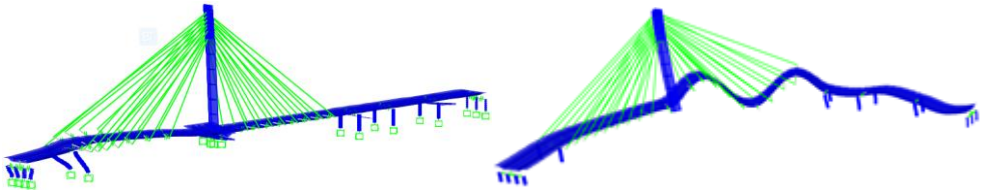

Fig.6. 40 9th mode for staight (L) and double plane curved cable-stayed bridges (R)

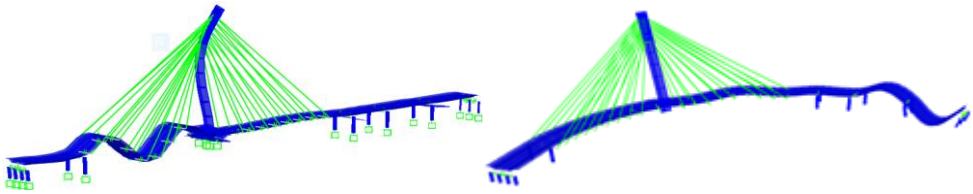

Fig.6. 41 10th mode for staight (L) and double plane curved cable-stayed bridges (R)

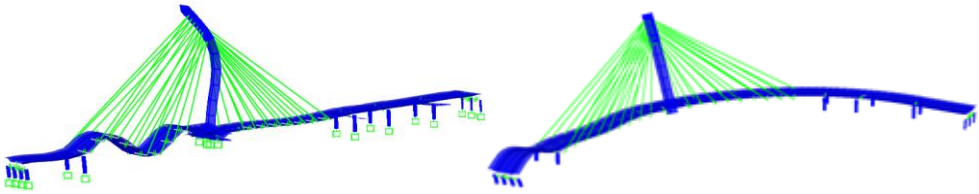

Fig.6. 42 11th mode for staight (L) and double plane curved cable-stayed bridges (R)

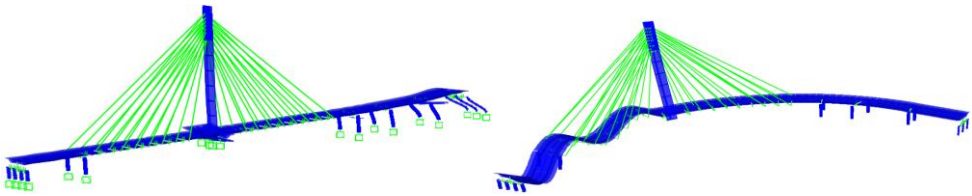

Fig.6. 43 12th mode for staight (L) and double plane curved cable-stayed bridges (R)

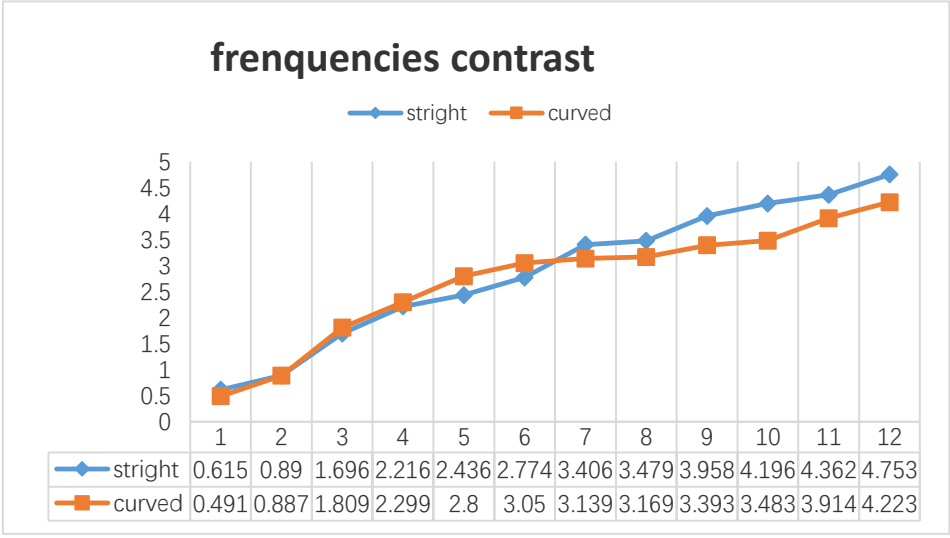

	1	2	3	4	5	6	7	8	9	10	11	12
stright	0.615	0.89	1.696	2.216	2.436	2.774	3.406	3.479	3.958	4.196	4.362	4.753
curved	0.491	0.887	1.809	2.299	2.8	3.05	3.139	3.169	3.393	3.483	3.914	4.223

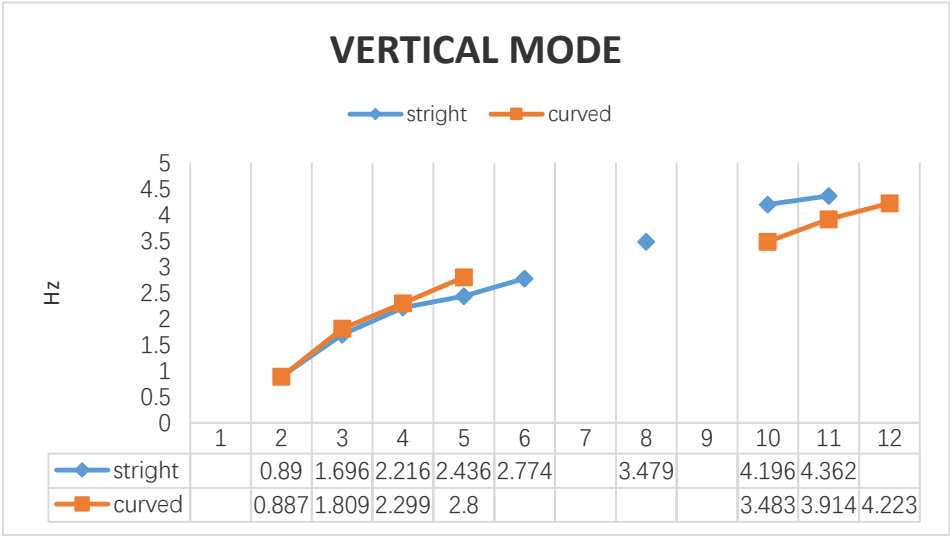

	1	2	3	4	5	6	7	8	9	10	11	12
stright		0.89	1.696	2.216	2.436	2.774		3.479		4.196	4.362	
curved		0.887	1.809	2.299	2.8					3.483	3.914	4.223

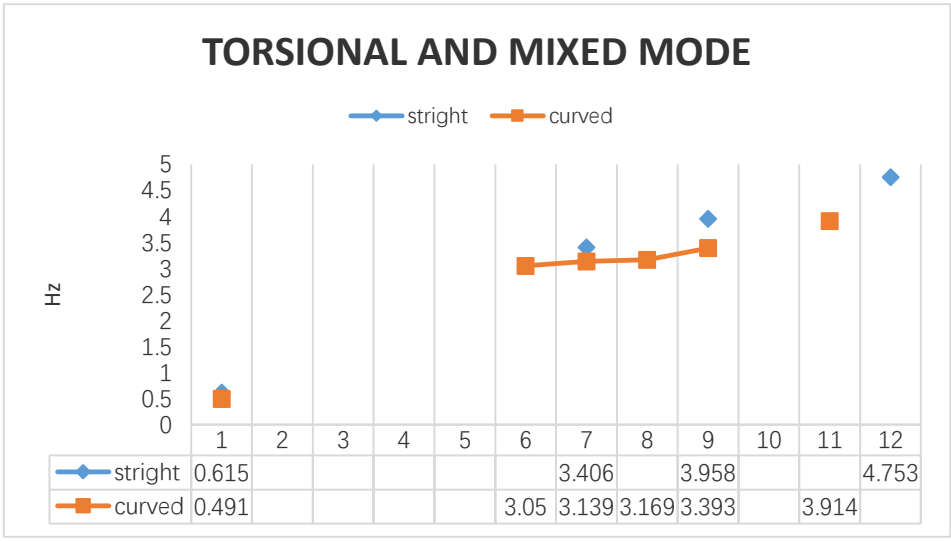

	1	2	3	4	5	6	7	8	9	10	11	12
stright	0.615						3.406		3.958			4.753
curved	0.491					3.05	3.139	3.169	3.393		3.914	

Modal analysis of straight and curved continuous girders bridges is carried out to understand frequencies and mode shapes. Figures 6.32-6.43 are representative, showing similar mode shapes obtained from the free vibrational analysis of straight and curved double plane cable-stayed bridge.

For the straight cable-stayed bridge, Figure 6.32 shows pylon transverse bending mode is the first mode. Figures 6.43 to 6.36, 6.41 and 6.42 show the first to fifth, sixth and seventh vertical bending mode shape, Figure 6.38 6.40 and 6.43 shows torsional mode of the deck of straight cable-stayed bridge.

It is observed that in curved cable-stayed bridges almost all modes are mixed with pylon and deck modes. It is also clear that deck torsion is observed almost in all modes, which is obvious due to a shift in the center of gravity away from the mid width of the deck. Therefore, curvature in the deck introduces mixing of torsion in the deck almost in all the modes, which is not desirable for any regular conventional design. So, special care has to be taken for designing against developed forces and detailing of reinforcements of the curved cable-stayed bridges. As inclined pylon, it could be observed that pylon mode occurs first and at very low frequency. All mode shapes are not very distinct and there is combination of modes. Due to the smaller stiffness of pylon, pylon and deck modes are mixed. On the other hand, in the inclined pylon, as pylon stiffness is lower than for the straight pylon, the pylon transverse mode is found at much lower frequency (as presented in Figure 6.32). It is observed that vertical bending modes occur first followed by pylon modes.

Frequencies of the first twelve modes of straight and curved cable-stayed bridges are compared in detail. For better representation and qualitative evaluation, mode numbers and their corresponding frequencies and their shape description are given in Table 6.3. From the results presented in these tables, it is found that for vertical pylon of the straight cable-stayed bridge and inclined pylon cable-stayed bridge, the first mode is pylon bending mode, from 2rd to 6th modes are mainly deck modes in vertical bending. Because of the high stiffness of vertical pylon of the straight cable-stayed bridge, frequency of first mode is higher than curved cable-stayed bridge. From the eighth mode torsion modes of decks are observed, but they are mixed with pylon modes.

From the above results it is observed that, with the introduction of curvature in deck of cable-stayed bridge, first frequency decreases obvious, frequency of similar modes decreases with the difference is notable. Torsional modes occur earlier in curved bridges. Even in first vertical bending mode some torsion in deck is observed. From Tab.6.3 it is clear that as curvature is introduced in the deck, the difference of frequencies of the cable-stayed bridge goes on increasing, which in turn introduces torsion in deck.

But also It is observed that with the introduction of the double plane cable, the stiffness of the bridge is increased, all the frequencies are increased both straight and curved cable-stayed bridge, but there is an interesting thing, when introduced the double plane cables, the first mode of straight cable-stayed bridge was changed to pylon bending mode.

6.2 Dynamic analysis of curved structure with different curvature

Cable-stayed bridges are investigated using FEM software SAP2000 V16 by developing 3D models. For optimization of time and accuracy of results, the deck and pylon using 3D BEAM element. FEM models of straight and curved continuous girder bridges in SAP2000 are shown in Figure 6.40. The following assumptions are made in the study: (a) material is homogeneous, isotropic and linearly elastic; (b) only geometric nonlinearities are taken into consideration; (c) cables are perfectly flexible and have only tension stiffness; (d) cable–deck, cable–pylon and deck–pylon deck-pier connections are assumed to be fixed. To study the behaviour of cable-stayed bridge with change in its geometry, in-plane curvature is introduced to the deck. The total length of 387 m on six spans (42 m + 105 m + 126 m + 30 m +

42 m + 42 m) which is kept constant. The radius of curvature is 123m,175 m,400m and straight.

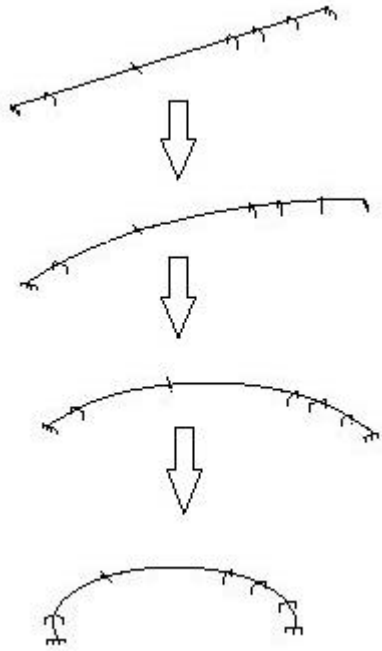

Fig.6. 44 The schematic diagram of continuous girder bridge model by increased curvture

Tab.6. 4 The comparison of multi girder bridge by increased of curvature

	Curved Structure (R=123m)		Curved Structure (R=175m)		Curved Structure (R=400m)		Straight Structure	
No.	frequency (Hz)	Mode type	frequency (Hz)	Mode type	frequency (Hz)	Mode type	frequency (Hz)	Mode type
1	0.500	V	0.511	V	0.518	V	0.611	V
2	0.691	V	0.744	V	0.723	V	0.755	V
3	0.779	V	1.402	V	1.405	V	1.621	V
4	1.378	V	2.005	V	1.969	V	2.018	V
5	1.827	T	2.718	V	2.677	V	3.127	V
6	2.125	V	3.186	T	3.15	T	3.443	T
7	2.423	M	3.357	M	3.232	M	4.009	T
8	2.661	M	3.813	V	3.47	V	4.064	V
9	2.970	M	3.963	M	3.761	M	4.634	T
10	3.057	M	4.088	V	4.018	V	5.264	V
11	3.697	M	4.438	T	4.180	T	5.465	V
12	3.767	T	4.451	T	4.581	M	5.623	T

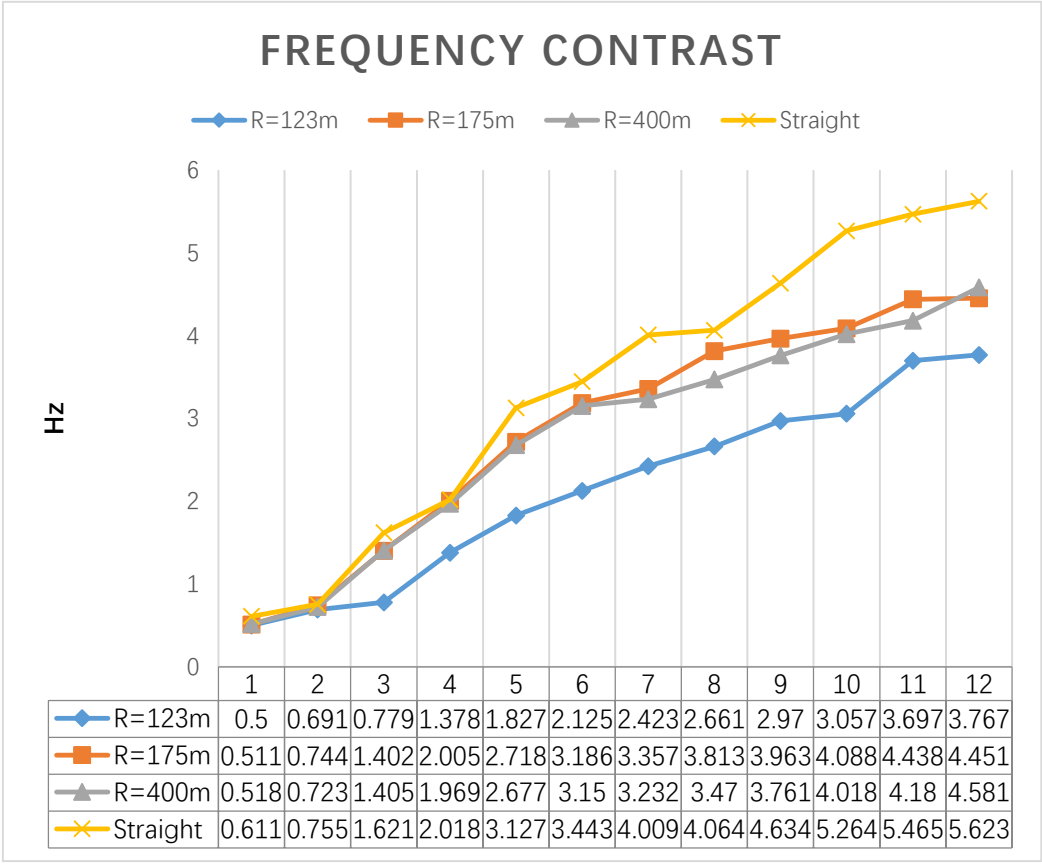

	1	2	3	4	5	6	7	8	9	10	11	12
R=123m	0.5	0.691	0.779	1.378	1.827	2.125	2.423	2.661	2.97	3.057	3.697	3.767
R=175m	0.511	0.744	1.402	2.005	2.718	3.186	3.357	3.813	3.963	4.088	4.438	4.451
R=400m	0.518	0.723	1.405	1.969	2.677	3.15	3.232	3.47	3.761	4.018	4.18	4.581
Straight	0.611	0.755	1.621	2.018	3.127	3.443	4.009	4.064	4.634	5.264	5.465	5.623

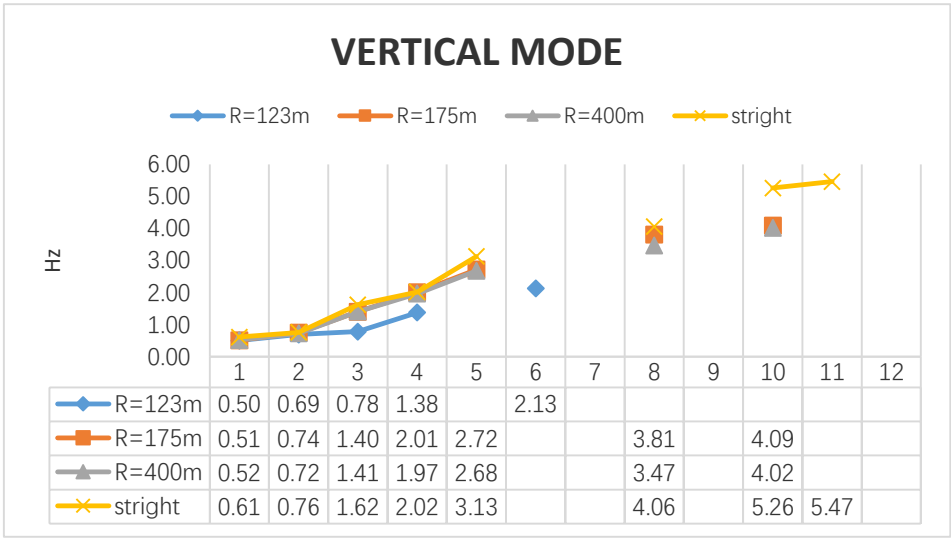

	1	2	3	4	5	6	7	8	9	10	11	12
R=123m	0.50	0.69	0.78	1.38		2.13						
R=175m	0.51	0.74	1.40	2.01	2.72			3.81		4.09		
R=400m	0.52	0.72	1.41	1.97	2.68			3.47		4.02		
stright	0.61	0.76	1.62	2.02	3.13			4.06		5.26	5.47	

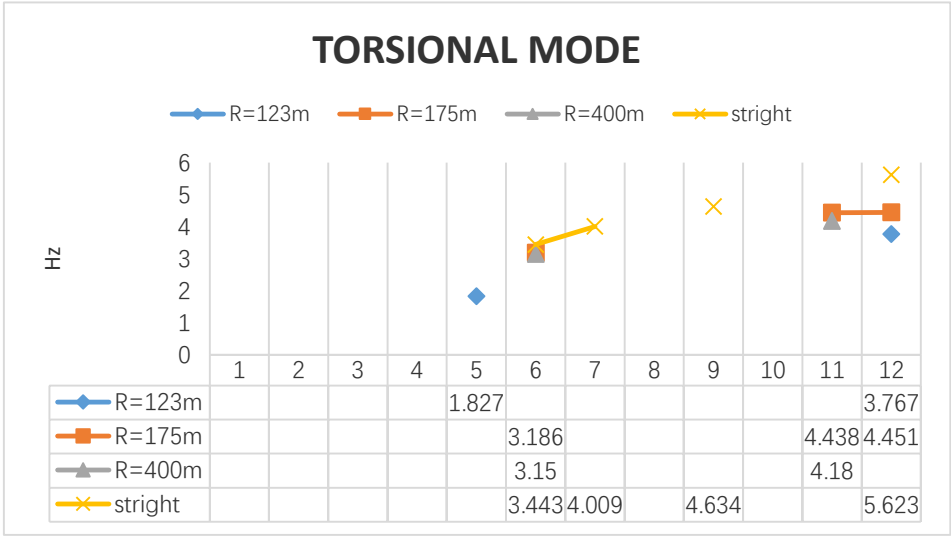

	1	2	3	4	5	6	7	8	9	10	11	12
R=123m					1.827							3.767
R=175m						3.186					4.438	4.451
R=400m						3.15					4.18	
stright						3.443	4.009		4.634			5.623

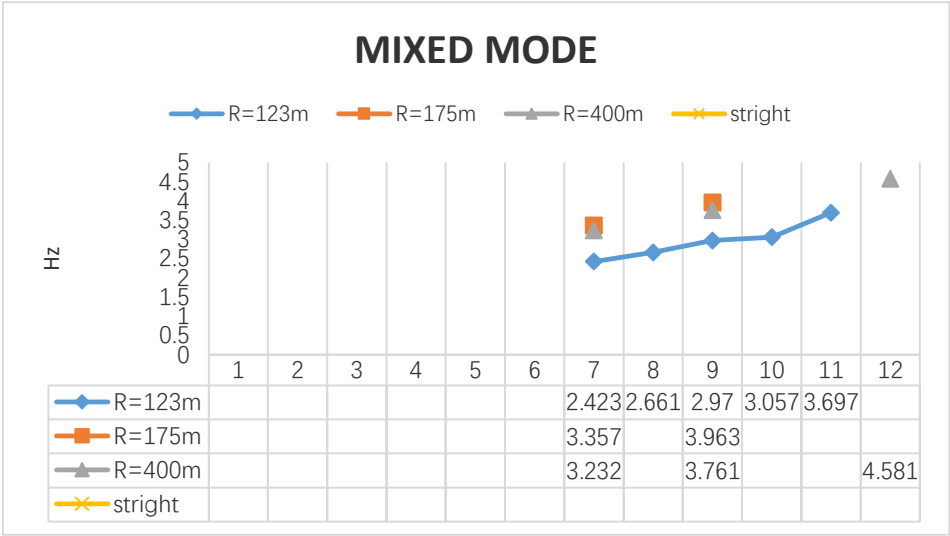

	1	2	3	4	5	6	7	8	9	10	11	12
R=123m							2.423	2.661	2.97	3.057	3.697	
R=175m							3.357		3.963			
R=400m							3.232		3.761			4.581
stright												

Fig.6. 45 The frequency contrast of continuous girder bridge by increased curvature

For the straight and curved continuous girder bridge, Tab 6.4 show the first to fifth, eighth, tenth and eleventh are vertical bending mode shape. It is observed that in curved bridges, from sixth modes almost all modes are mixed with torsional and vertical modes. It is also clear that deck torsion is observed almost in all modes, which is obvious due to a shift in the center of gravity away from the mid width of the deck. Therefore, curvature in the deck introduces mixing of torsion in the deck almost in all the modes, which is not desirable for any regular conventional design. From the above results it is observed that, with the introduction of curvature in deck of continuous girder bridge, first frequency decreases obvious, frequency of similar modes decreases with the difference is notable. Torsional modes occur earlier in curved bridges. Even in first vertical bending mode some torsion in deck is observed. From Tab.6.4 it is clear that as curvature is introduced in the deck, the difference of frequencies of the cable-stayed bridge goes on increasing, which in turn introduces torsion in deck.

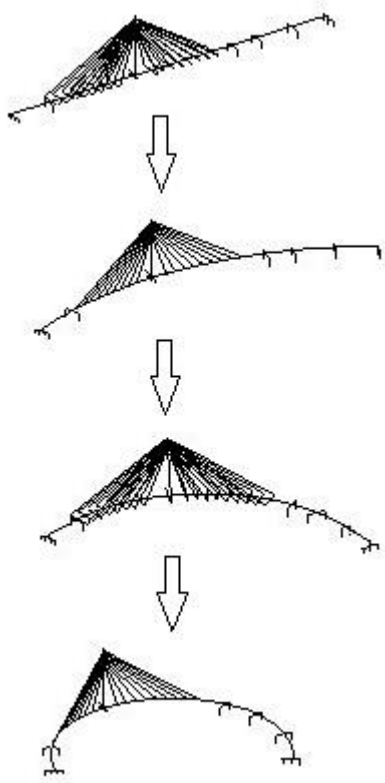

Fig.6. 46 The schematic diagram of cable-stayed bridge model by increased curvture

Tab.6. 5 The comparison of cable-stayed bridge by increased of curvature

	Curved Structure (R=123m)		Curved Structure (R=175m)		Curved Structure (R=400m)		Straight Structure	
No.	frequency (Hz)	Mode type	frequency (Hz)	Mode type	frequency (Hz)	Mode type	frequency (Hz)	Mode type
1	0.600	PV	0.396	TP	0.588	PV	0.686	V
2	0.691	V	0.759	V	0.748	V	1.101	V
3	0.820	VP	1.382	V	1.302	V	1.745	V
4	1.416	V	1.848	V	1.792	V	1.930	V
5	1.738	T	2.327	M	2.116	V	2.238	V
6	1.832	V	2.403	V	2.332	V	2.246	V
7	2.092	M	2.925	M	2.920	V	3.215	P
8	2.413	M	3.177	T	3.146	V	3.416	V
9	2.427	T	3.206	M	3.248	M	3.671	P
10	2.803	T	3.357	V	3.470	V	3.978	T
11	3.017	T	3.926	M	3.604	T	4.121	V

12	3. 060	T	3. 977	V	3. 783	PV	4. 634	T

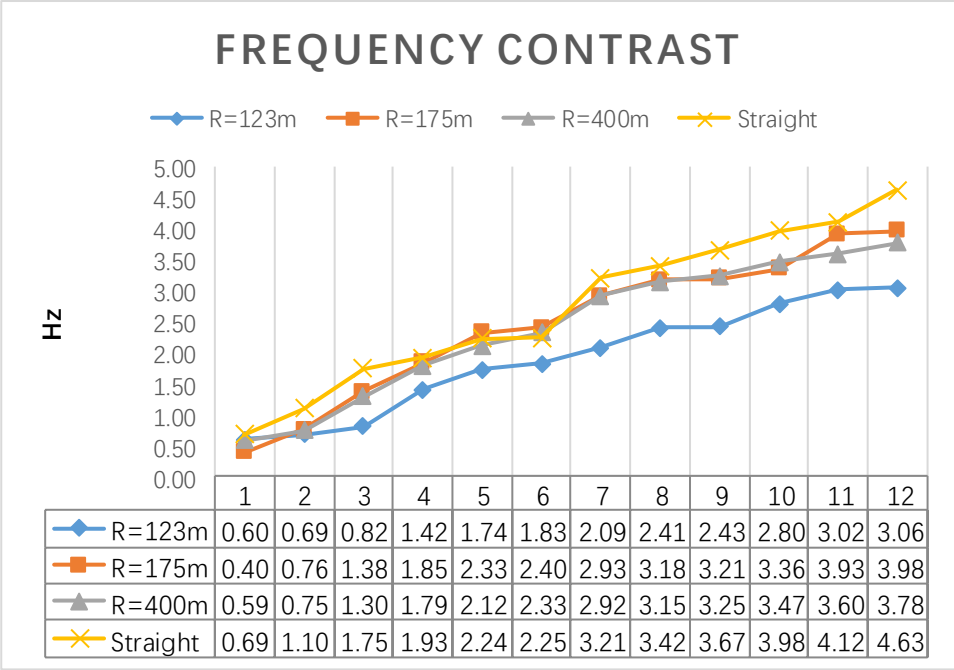

	1	2	3	4	5	6	7	8	9	10	11	12
R=123m	0.60	0.69	0.82	1.42	1.74	1.83	2.09	2.41	2.43	2.80	3.02	3.06
R=175m	0.40	0.76	1.38	1.85	2.33	2.40	2.93	3.18	3.21	3.36	3.93	3.98
R=400m	0.59	0.75	1.30	1.79	2.12	2.33	2.92	3.15	3.25	3.47	3.60	3.78
Straight	0.69	1.10	1.75	1.93	2.24	2.25	3.21	3.42	3.67	3.98	4.12	4.63

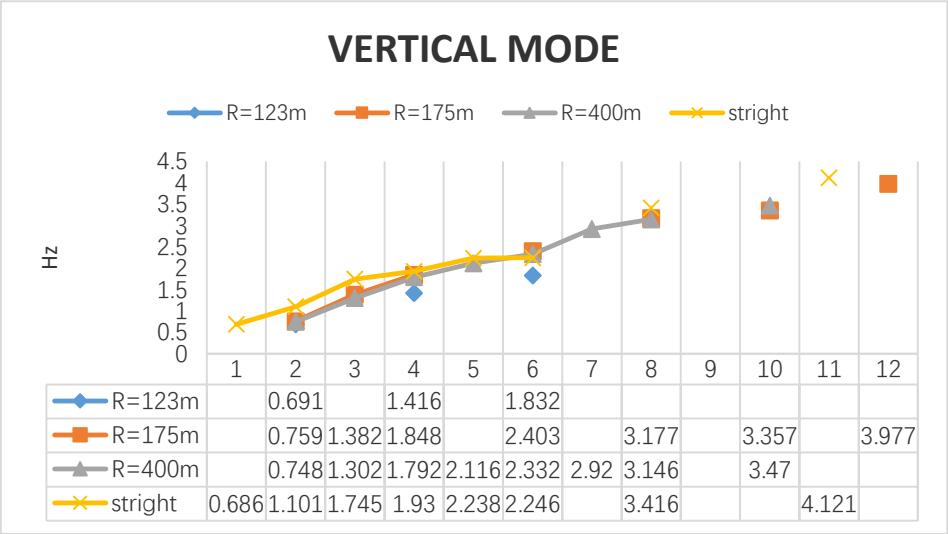

	1	2	3	4	5	6	7	8	9	10	11	12
R=123m		0.691		1.416		1.832						
R=175m		0.759	1.382	1.848		2.403		3.177		3.357		3.977
R=400m		0.748	1.302	1.792	2.116	2.332	2.92	3.146		3.47		
stright	0.686	1.101	1.745	1.93	2.238	2.246		3.416			4.121	

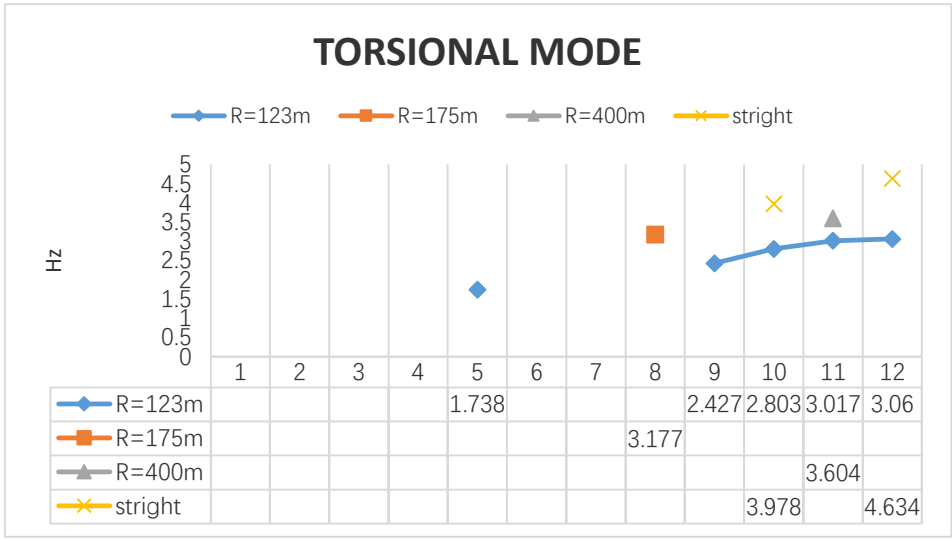

	1	2	3	4	5	6	7	8	9	10	11	12
R=123m					1.738				2.427	2.803	3.017	3.06
R=175m								3.177				
R=400m											3.604	
stright										3.978		4.634

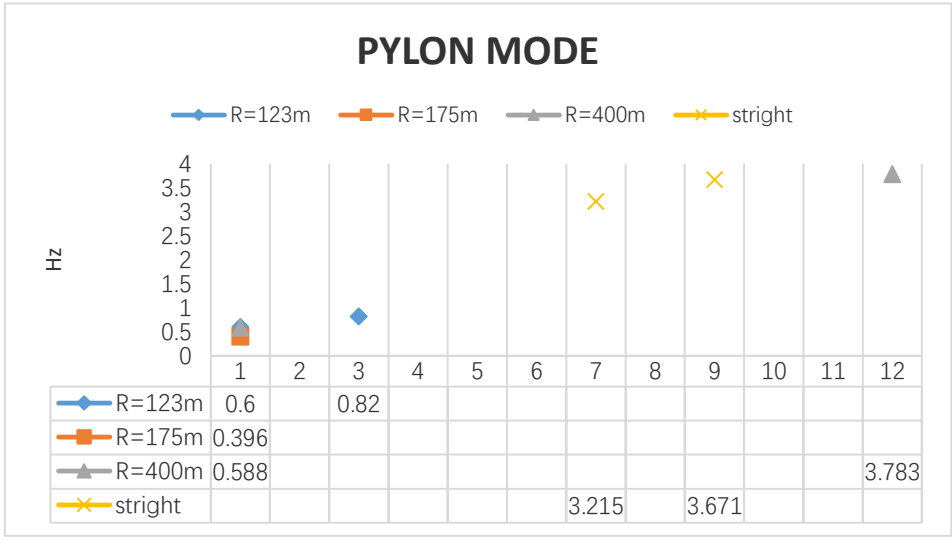

	1	2	3	4	5	6	7	8	9	10	11	12
R=123m	0.6		0.82									
R=175m	0.396											
R=400m	0.588											3.783
stright							3.215		3.671			

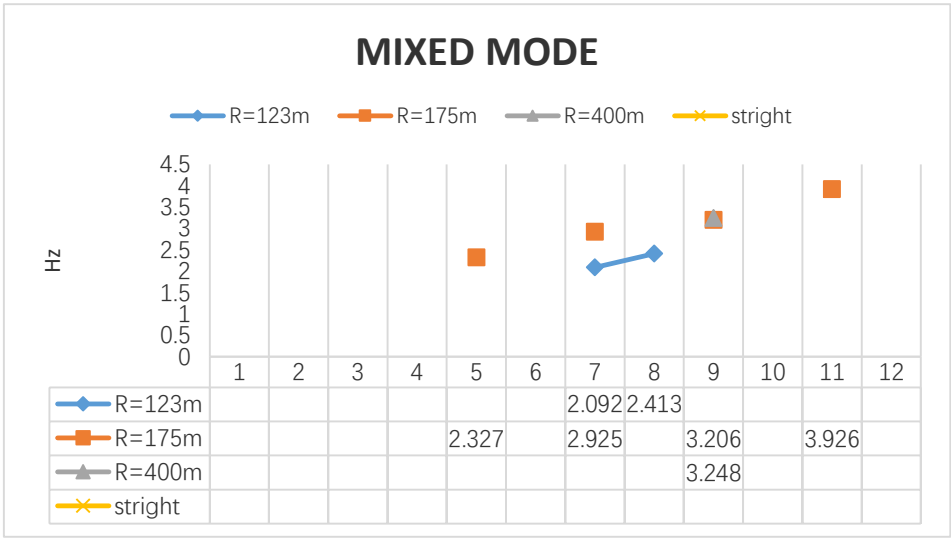

Fig.6. 47 The frequency contrast of cable-stayed bridge by increased curvature

For the straight cable-stayed bridge, Tab 6.5 show the first to sixth and eighth eleventh are vertical bending mode shape, seventh and ninth modes are pylon transverse bending mode and tenth and twelfth modes are torsional mode of straight cable-stayed bridge. It is observed that in curved cable-stayed bridges almost all modes are mixed with pylon and deck modes. It is also clear that deck torsion is observed almost in all modes, which is obvious due to a shift in the center of gravity away from the mid width of the deck. Therefore, curvature in the deck introduces mixing of torsion in the deck almost in all the modes, which is not desirable for any regular conventional design. So, special care has to be taken for designing against developed forces and detailing of reinforcements of the curved cable-stayed bridges. Paying particular attention to the curved bridge, the first mode changed to pylon mode with inclined pylon, it seems that the stiffness is less than vertical pylon.

Frequencies of the first twelve modes of straight and curved cable-stayed bridges are compared in detail. For better representation and qualitative evaluation, mode numbers and their corresponding frequencies and their shape description are given in Fig.6.47. From the results presented, it is found that for vertical pylon of the straight cable-stayed bridge, the first five modes are pure deck modes in vertical bending. Because of the high stiffness of vertical pylon of the straight cable-stayed

bridge, frequency of first mode is very high. The seventh mode is pylon mode. From the tenth mode torsion modes of decks are observed, but they are mixed with pylon modes.

Looking into the curved cable-stayed bridges, as inclined pylon, it could be observed that pylon mode occurs first and at very low frequency. All mode shapes are not very distinct and there is combination of modes. Due to the smaller stiffness of pylon, pylon and deck modes are mixed. On the other hand, in the inclined pylon, as pylon stiffness is lower than for the straight pylon, the pylon transverse mode is found at much lower frequency (as presented in Tab.6.5). It is observed that vertical bending modes occur first followed by pylon modes; if pylon stiffness is very low then pylon modes occurs at very low frequency.

From the above results it is observed that, with the introduction of curvature in deck of cable-stayed bridge, first frequency decreases obvious, frequency of similar modes decreases with the difference is notable. Torsional modes occur earlier in curved bridges. Even in first vertical bending mode some torsion in deck is observed. From Tab.6.5 it is clear that as curvature is introduced in the deck, the difference of frequencies of the cable-stayed bridge goes on increasing, which in turn introduces torsion in deck.

6.3 Dynamic analysis of curved structure with different stiffness of pylon

Due to inclined pylon has small stiffness, compared with ambient vibration testing in 2010 (chapter 5), so three modal analyses were done with increasing 1.25 times, 2 times and 2.75 times inertia of pylon. With increasing inertia of pylon, when the inertia of pylon to 2.75 times, the first frequency seems to close the experimental value. But other frequencies are not match with experimental values. It is observed that, some deck dominated modes (2^{nd},3^{rd} ,4^{th}, 6^{th},7^{th}) are not sensitive to modify inertia of the pylon. Just some pylon mode (1^{st}, 8^{th},9^{th},10^{th},11^{th}) changed frequencies obviously. t is observed that in curved cable-stayed bridges almost all modes are mixed with pylon and deck modes. It is also clear that deck torsion is observed almost in all modes, which is obvious due to a shift in the center of gravity away from the mid width of the deck. Therefore, curvature in the deck introduces mixing of torsion in the deck almost in all the modes, which is not desirable for any regular conventional design. So, special care has to be taken for designing against developed forces and detailing of reinforcements of the curved cable-stayed bridges.

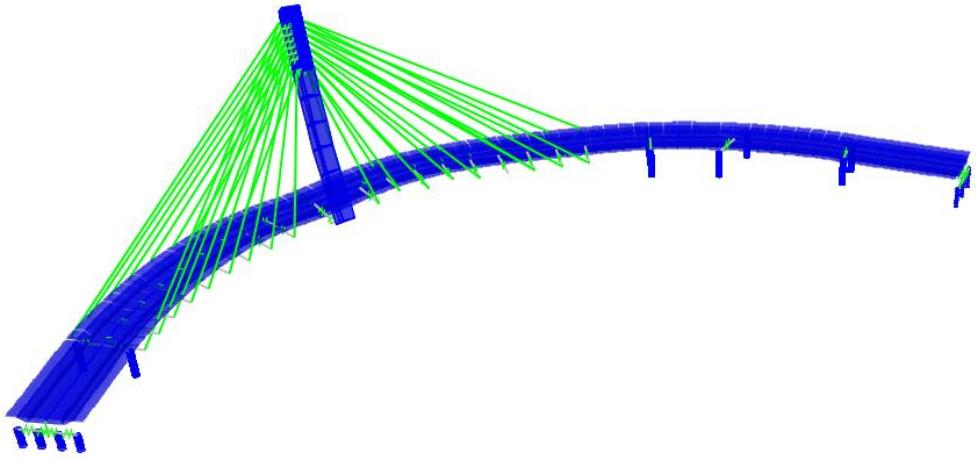

Fig.6. 48 the simplified FEM of Marghera bridge

Looking into the curved cable-stayed bridges, as inclined pylon, it could be observed that pylon mode occurs first and at very low frequency. All mode shapes are not very distinct and there is combination of modes. Due to the smaller stiffness of pylon, pylon and deck modes are mixed. On the other hand, in the inclined pylon, as pylon stiffness is lower than for the straight pylon, the pylon transverse mode is found at much lower frequency (as presented in Tab.6.6). It is observed that vertical bending modes occur first followed by pylon modes; if pylon stiffness is very low then pylon modes occurs at very low frequency. From the results of Fig.6.49 it is observed that, with the increased inertia of pylon, first frequency increased obvious, frequency of similar modes increases with the difference is notable.

Tab.6. 6 The comparison of models Marghera bridge by increased of inertia of pylon

			1.25inertia	2inertia	2.75inertia
No.	Mode type	frequency (Hz)	frequency (Hz)	frequency (Hz)	frequency (Hz)
1	TP	0.491	0.526	0.583	0.636
2	V	0.887	0.961	0.991	1.016
3	V	1.809	1.881	1.888	1.891
4	V	2.299	2.457	2.472	2.479
5	V	2.8	3.025	3.073	3.089
6	M	3.05	3.209	3.262	3.299
7	M	3.139	3.381	3.383	3.383

8	M	3.169	3.499	3.722	3.727
9	M	3.393	3.737	3.819	3.819
10	V	3.483	3.820	4.199	4.200
11	T	3.914	4.198	4.363	4.363
12	V	4.223	4.363	4.396	4.687

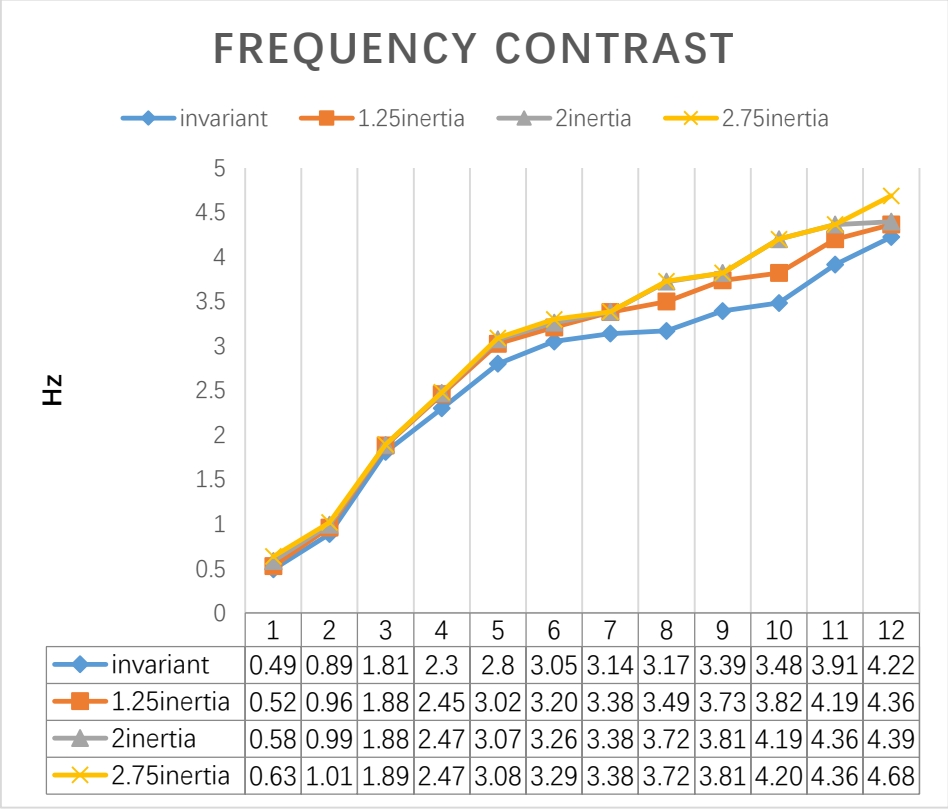

	1	2	3	4	5	6	7	8	9	10	11	12
invariant	0.49	0.89	1.81	2.3	2.8	3.05	3.14	3.17	3.39	3.48	3.91	4.22
1.25inertia	0.52	0.96	1.88	2.45	3.02	3.20	3.38	3.49	3.73	3.82	4.19	4.36
2inertia	0.58	0.99	1.88	2.47	3.07	3.26	3.38	3.72	3.81	4.19	4.36	4.39
2.75inertia	0.63	1.01	1.89	2.47	3.08	3.29	3.38	3.72	3.81	4.20	4.36	4.68

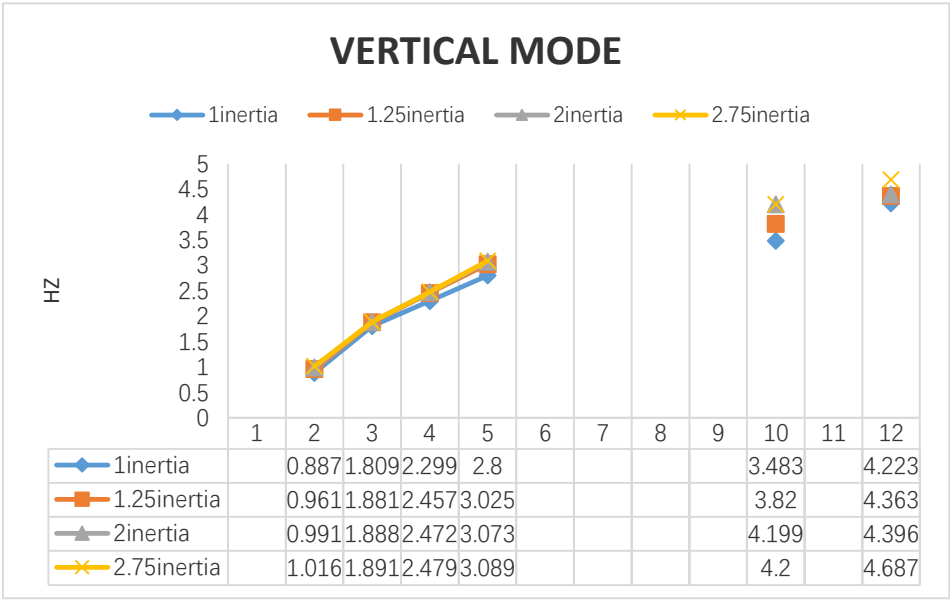

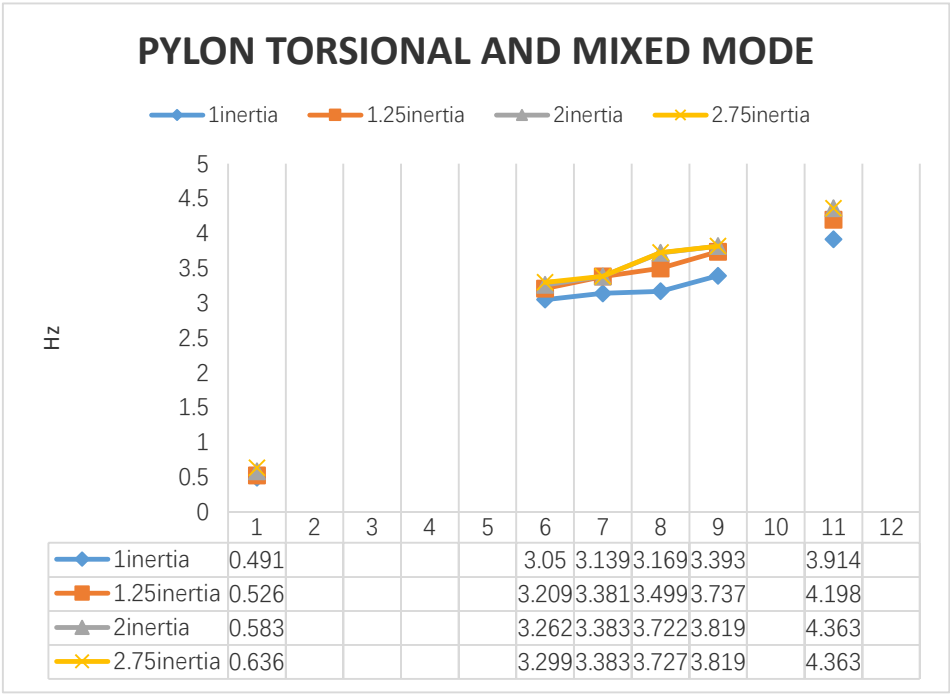

Fig.6. 49 The frequency contrast of cable-stayed bridge by increased inertia of pylon

After model updated of straight continuous girder bridge of Magaz and curved cable-stayed bridge of Marghera. The results of modal analyses (Tab.6.7 and Tab.6.8) keep in good relations with the summery that got before. Because of Magaz bridge has symmetric structure, the first four modes are vertical bending modes, just fifth and sixth modes are torsional modes. As curved structure and inclined pylon, it is observed that in curved cable-stayed bridges almost all modes are mixed with pylon and deck modes. It is also clear that deck torsion is observed almost in all modes, which is obvious due to a shift in the centre of gravity away from the mid width of the deck. Therefore, curvature in the deck introduces mixing of torsion in the deck almost in all the modes, which is not desirable for any regular conventional design. Developing accurate FE models that are representative of the structure is important for several applications such as structural control, evaluating the seismic response of the structure, assessing post-earthquake condition of structures, validating new innovative structural designs, assessing structural health and investigating vehicle–structure interactions, so it makes sense that on this research.

Tab.6. 7 The experimental and Model updating dynamic charisteristic of Magaz bridge

Nr.	f_{2011}*(Hz)*	$f_{FE\text{-}I}$*(Hz)*	$\Delta f_{FE\text{-}I}$ *(%)*	MAC_I	*Mode type*
1	*2.489*	*2.492*	*0.13*	*0.92*	*Vertical bending*
2	*4.833*	*4.813*	*-0.41*	*0.88*	*Vertical bending*
3	*5.417*	*5.633*	*3.99*	*0.94*	*Vertical bending*
4	*7.089*	*6.949*	*-1.97*	*0.91*	*Vertical bending*
5	*8.290*	*7.991*	*-3.60*	*0.84*	*Torsional*
6	*10.130*	*9.774*	*-3.51*	*0.93*	*Torsional*
7	*11.312*	*11.372*	*0.53*	*0.87*	*Vertical bending*

Tab.6. 8 The experimental and Model updating dynamic charisteristic of Marghera bridge

Nr.	f_{2010}*(Hz)*	$f_{FE\text{-}I}$*(Hz)*	$\Delta f_{FE\text{-}I}$ *(%)*	MAC_I	*Mode*
1	*0.635*	*0.64*	*0.78*	*0.96*	*Vertical bending*
2	*0.996*	*0.97*	*-2.98*	*0.95*	*Vertical bending*
3	*1.143*	*1.13*	*-1.24*	*0.98*	*Vertical bending*
4	*1.387*	*1.39*	*0.11*	*0.98*	*Torsional*
5	*1.523*	*1.49*	*-2.22*	*0.97*	*Mixed*
6	*1.602*	*1.54*	*-3.81*	*0.85*	*Torsional*
7	*1.953*	*2.00*	*2.64*	*0.87*	*Vertical bending*
8	*2.637*	*2.63*	*-0.37*	*0.94*	*Torsional*
9	*3.174*	*2.98*	*-6.18*	*0.93*	*Torsional*

10	*4.053*	*4.10*	*1.19*	*0.94*	*Torsional*
11	*4.932*	*4.97*	*0.74*	*0.92*	*Torsional*
12	*5.596*	*5.69*	*1.65*	*0.95*	*Torsional*
13	*6.826*	*6.90*	*1.05*	*0.92*	*Torsional*

6.4 Conclusions

The following are some of the major observations from the study:

- Under modal vibration analysis, mode shapes in straight bridges with cables or without cables are clear and no combinations of modes. Due to the greater stiffness of pylon and symmetric structure, pylon and deck modes are clear and separate.
- Due to less stiffness of the inclined pylon compared to straight pylon, curved cable-stayed bridges with would vibrate in transverse mode at the first low frequency.
- Due to introduction of the double plane cable, the stiffness of the bridge is increased, all the frequencies are increased both straight and curved cable-stayed bridge, but there is an interesting thing, when introduced the double plane cables, the first mode of straight cable-stayed bridge was changed to pylon bending mode.
- With the introduction of curvature in deck of cable-stayed bridge, first frequency decreases obvious, frequency of similar modes decreases with the difference is notable.

CONCLUSIONS

Conclusions

On the basis of the findings of the literature reviews, presented approaches, ambient vibration tests and FEM updating, the conclusions are drawn as following:

- Under dynamic analysis, mode shapes in straight continuous girder bridge are clear and no combinations of modes. Due to the greater stiffness of girder, vertical and torsional modes are clear and separate.
- Due to less stiffness of the inclined pylon compared to the straight pylon, cable-stayed bridges with an inclined pylon would vibrate in transverse mode at a very low frequency.
- From the above results, with the introduction of curvature in deck of cable-stayed bridge, first frequency decreases obvious, frequency of similar modes decreases with the difference is notable. Torsional modes occur earlier in curved bridges. Even in first vertical bending mode some torsion in deck is observed.
- The principle of modal measurement technique is introduced and formulas of calculating modal response by using measured outputs are given. With introduced structure health monitoring to improve the accurate of the FE model.
- Both a direct method and a sensitivity-based iterative method are applied to update a Finite Element model of a curved cable-stayed bridge. The direct method is known as the Douglas-Reid algorithm. The sensitivity-based method is a Trust-Region algorithm. An a-priori Finite Element model is built by using the SAP2000 software. It is firstly manually tuned and then updated through computational procedures implemented in MATLAB. The results of the direct and the iterative methods are compared to each other on the specific case study.
- A Matlab toolbox was developed that a custom MATLAB based Sap2000 program for parameter estimation and FE model updating.

From the entire study it has been observed that the characterization of dynamic response of cable-stayed bridges is tedious but possible. It should be mentioned that a curved suspended is not rare but, most of the time, it is oversimplified in design. The present study shows the very different response with coupling modes obtained from structure with the introduction of curvature. The study presented here would certainly be useful for design engineers for understanding the behaviour of straight and curved suspended under dynamic vibration.

Recommendations for Future Investigations

Recently, curved suspended structure, due to their pleasant aesthetics, and economical and efficient construction techniques, have increased in prevalence all over the world. Although analysis of such a complex structure is very tedious, after development of computer programs and software, idealization of these types of bridges is simplified. With the development of high strength materials and construction technologies, cable-stayed bridges with aesthetically appealing geometries such as curvature in the deck and inclined of pylon cannot be ruled out in the right circumstances.

Although some of the differences and uncertainties can be minimized by developing detailed FE models, it is not possible to obtain a highly accurate match between the analytical and measured dynamic responses before calibrating the FE model. Model calibration processes are usually formulated to minimize an objective function based on the residuals between the measured and analytically computed frequencies and mode shapes. The parameters of the FE model are adjusted to obtain a better match between the analytical and recorded modes and frequencies.

Developing accurate FE models that are representative of the structure is important for several applications such as structural control, evaluating the seismic response of the curved suspended structure, assessing post-earthquake condition of structures, validating new innovative structural designs, assessing structural health and investigating vehicle–structure interactions. Also through the study process, to improve the application of structure health monitoring technique in curved suspended structure.

A MATLAB TOOLBOX WITH SAP2000 FOR MODEL UPDATING IN CIVIL ENGINEERING

USER'S GUIDE

1.Introduction

MUS (Model Updating System) is the abbreviation for a custom MATLAB based Sap2000 program for parameter estimation and FE model updating. The software was developed by Leqia He (2015) with his graduate students at Fuzhou University. Using modal measurements as input data, it could be used for stiffness and mass parameter estimation at the element level. Then it uses to FE model updating for planar and spatial structures. The in-house FEA solver for MUS was also written in MATLAB. Text based finite element modelling, MUS is suitable for full-scale model updating. Figure (1) illustrates the FE model updating process in MUS. The flowchart connectors labelled as API describe the two-way automatic data exchange between MATLAB and SAP2000. This section contains description of the model updating process using MUS.

2.Toolbox Functionality

MUS has the most advantage in the broader range of finite elements available through SAP2000. Its emphasis is on using MATLAB Optimization Toolbox because of its better performance for full-scale FE model updating. Analytical sensitivity based optimization option has also been retained in MUS but only with Trust region method for solving problems.

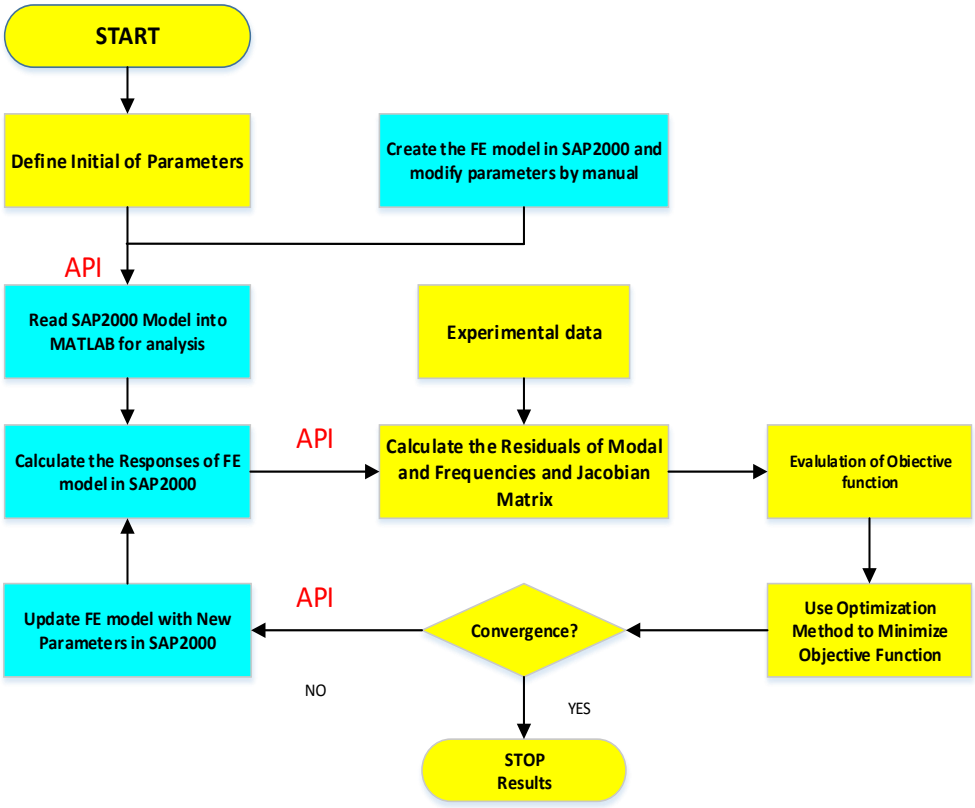

Figure 1 MUS Flowchart

The main features of the function in the MUS toolbox can be divided in 6 categories: In my opinions, the main features should be

a) Initialization of the updating parameters;
b) Calculation of the numerical modal data;
c) Matching of the vibration modes;
d) Formulation of the objective function;
e) Calculation of the Jacobian matrix;
f) Solving the optimization problem.

There may be an additional feature about the API procedure of SAP inside the above Item 2) calculation of the numerical modal data, i.e., how the SAP reads and writes the input and output as the parameters and modal results. Their correspondence to the flowchart and their respective subroutines should be explained in the Description.

Nr	Feature	Description
1	Initialization of the updating parameters	Data input and output, conversion. These functions can read data into MATLAB workspace.
2	Calculation of the numerical modal data	The aim of these functions is to extract calculating data from SAP2000.
3	Matching of the vibration modes	These functions are used to match the mode shapes of numerical with the experimental mode shapes.
4	Formulation of the objective function	The aim of these functions is to form the objective function of mode shapes and frequencies.
5	Calculation of the Jacobian matrix	These functions are used to determine the direction of each iteration.
6	Solving the optimization problem	These functions are used to solve the least square problem of the objective function, it is the core of the all the scripts.

Table 1. The description of respective subroutines

All of these categories are discussed in detail as follow. The purposes are to provide a structured outline of the functions used in the MUS toolbox and some related functions supplied by MATLAB.

2.1 Initialization of the updating parameters

These functions allow to define the updating parameters, for example: modulus of elasticity, selected by sensitivity analysis; the number of the mode shapes to update and weight of frequencies, mode shapes and penalty; If the measurements are performed and the data are stored as MAT format, they can be read into the MATLAB workspace by means of the function load_expe_model and the main function FEM_Updating. The MUS toolbox does not provide functions to read data from other file formats, such as ASCII files. These files have to read using MATLAB functions. Use help file formats and for more information.

In the MUS toolbox, all functions are applicable to multiple channels simultaneously, provided that the data are stored in the MATLAB workspace as a N * R matrix, where N is the number of samples and R is the number of channels. If the function load_expe_model is used, this format is automatically adopted. Otherwise, the user has to enforce this format explicitly.

2.2 Calculation of the numerical modal data

We use sap2000 API programming with Matlab to calculate the numerical modal data, the script is in the APPENDIX. The aim of these functions is to extract calculating data from SAP2000.The numerical data is calculated by SAP2000, so there must be a function to control the SAP2000. The function Call_fem is to control the SAP2000 and give the parameters value which will be different by iterative loop and order the SAP2000 to calculate the simulation results. The results were stored in the Output file by dat format.

2.3 Matching of the vibration modes

Two major problems are encountered in matching the experimental data (frequencies and mode shapes) and the corresponding analytical estimates. First, the natural frequencies and mode shapes in the experimental and numerical data must relate to the same mode, that is they must be paired correctly. Arranging the natural frequencies is not sufficient, especially when two modes are close together in frequency. The function mac_match is used to calculate the MAC value to pair the modes correctly. And the finding the frequencies and mode data of paired mode will be prepare for the objective function.

The second problem with matching the experimental and numerical data is mode shape scaling. Because the mass distribution of the FE model and real structure may be different, the mode shapes may not be scaled coincidently. The measured mode shapes scaled by function mode_scale and numerical data multiples by the modal scale factor MSF will solve the problem that the experimental and numerical mode shapes could be 180˚ out of phase. The function MSF is used to do this.

2.4 Formulation of the objective function

The function residual is to calculate the difference between the experimental and numerical eigenvector. The residual contains two parts: one part is the weighted residuals of the mode shapes, the another part is the weighted residuals of the

frequencies. The square sum of the elements in residual is defined as the objective function Obj_Fun.

2.5 Calculation of the Jacobian matrix

Jacobian matrix is a slope index to understand if the objective function is going in the right direction, in other words, if it close to a minimum. The function Jw is to calculate the Jacobian matrix and give the direction to next iterative step.

2.6 Solving the optimization problem

The function Jw and function residual provided the necessary to solve the least square problem. The function lsqnonlin (@Obj_Fun, p_start, p_low, p_up, optimset ('Jacobian',' on', 'TolX', tol_X)) is used to solve the least square optimization problem. The start point of the iterative is calculate by means of the function p_start. The function p_low and function p_up is provided the limit of the solver. The function Jacobian give the direction to go.

3.Methodology

The general procedure of the FE model updating method is shown in figure 1. Initially, the numerical modal data are calculated using the FE model with initially estimated values for the unknown model parameters. The experimental modal data are obtained from ambient vibration tests on the structure. They are identified with the stochastic subspace identification technique, developed at the Department of Civil Engineering of K.U.Leuven. In an iterative process the unknown model parameters are adjusted until the discrepancies between the numerical and experimental modal data are minimized. In this way the FE model is corrected such that it better represents the real structure and at the same time the unknown parameters are identified.

3.1 Objective function - Least squares problem

Many efforts has been spent in literature for the development of FE model updating methodologies using experimental modal data. The standard work is undoubtfully the book of Friswell and Mottershead, which dates back to 1995.

The authors propose to perform the procedure by solving a least squares problem （Madsen, K. 1975). The least squares approach is very efficient and has become the common way to solve the updating problem, as it is shown in several publications on FE model updating: amongst others the works by Link [1993, 1996,1998,1999], Mottershead et al. (2000). Shi et al. (2000), Zhang et al. (2000), Brownjohn et al. [18] and Modak et al. [104].

The objective function in an ordinary least squares problem is defined as a sum of squared differences:

$$f(\theta) = \frac{1}{2}\sum_{j=1}^{m}\left[z_j(\theta) - \tilde{z}_j \right]^2 = \frac{1}{2}\sum_{j=1}^{m} r_j(\theta)^2 \qquad (1)$$

where each $z_j(\theta)$ represents an analytical modal quantity which is a nonlinear function of the optimization or design variables2 θ ($\in IR_n$).

$\tilde{z}$ refers to the measured value of the quantity z. In order to obtain a unique solution, the number m of residuals $r_j(\theta) = z_j(\theta) - \tilde{z}_j$ should be greater than the number n of unknowns θ.

Equation (1) represents the basic least squares function, but several variants exist and are tried out in literature. In a weighted least squares problem, the residual vector is multiplied with a weighting matrix in order to take the relative importance of the different types of residuals and their accuracy into account. The classical weighted least squares method can be further extended in case it is difficult to obtain a convergent solution due to ill-conditioning problems. In this extended weighted least squares problem the objective function is extended with terms that represent the perturbation in the design variables. This approach corresponds to the regularization techniques developed in linear algebra and explained by 3.8.2.

Besides its efficiency proven by the multiple successful applications, the least squares problem definition can also be justified from a statistical viewpoint. In fact, the discrepancies between model and observations could also be measured by a sum of terms to any power or by a sum of absolute differences or even by some

more complicated function. However, the least squares criterion is solid grounded in statistics, it is shown that under certain statistical assumptions the use of the objective function defined as a sum of squared differences minimizes the statistical errors in the identified parameters, evolving from the measurement errors.

3.2 Residual vector

In FE model updating, the residual vector r of the least squares problem:

$$min\frac{1}{2}\left\|\mathrm{r}\left(\theta\right)\right\|^2$$

contains the discrepancies between the numerical dynamic data and the observations. In general, two approaches exist, based on whether frequency domain or modal data are used for correlation. In both cases several types of residuals exist, each type having its own advantages and drawbacks. In the first approach, one can use the input error (defined by substituting the measured frequency response into the equation of motion), the output error (defined by multiplying the input error with the frequency response matrix of the model) or the error in frequency response data (which differs from the previous type in the way the sensitivity matrix is calculated). An extensive overview of the different residual types and their characteristics is given (M. Link,1999). Since the number of measured degrees of freedom (DOFs) is generally much smaller than the number of analytical DOFs, it is necessary for most residual types to expand the measured vector to full model size or to condense the model order down to the number of measured DOFs. Furthermore, an implicit weighting is performed which depends on the proximity of the chosen frequency points to resonance. Therefore, the weighting is less controllable. On the other hand, an advantage of frequency response updating is the possibility to identify damping parameters.

In civil engineering, however, the second approach using modal data is most often applied since the frequency response functions of heavy civil structures are not available over a wide frequency domain. In this case, the residual vector contains the differences in the identified modal data (and possibly some derived quantities), such as the eigenfrequencies, the mode shapes, the modal curvatures, etc. No expansion or condensation operation is necessary for calculating the residuals or modal sensitivities. On the other hand, additional inaccuracies are included since the modal extraction operation is subject to errors and omission, exacerbated by increased modal density at high frequencies. The relative weighting between the different residual types can be controlled by the definition of the residual functions

and by an additional weighting matrix in order to account for the measurement and identification errors.

Before the numerical and experimental modal data can be compared, they must be paired correctly, i.e. the data must relate to the same modes. Arranging the eigenfrequencies in ascending order is not sufficient, since due to incorrect parameter estimates, the order of the modes in both dynamic models numerical and experimental can differ. Furthermore, some modes of the structure may be measured inaccurately, e.g. because an accelerometer is placed close to a node of a particular mode shape, or may even not be excited. The most common and easy way to pair mode shapes correctly is based on the modal assurance criterion (MAC) [3]:

$$MAC(\phi_i, \tilde{\phi}_j) = \frac{\left|\phi_i^T \tilde{\phi}_j\right|^2}{(\phi_i^T \phi_i)(\tilde{\phi}_j^T \tilde{\phi}_j)}$$

a numerical and experimental mode shape vector, respectively.

MAC values always lie between 0 and 1. A MAC value close to 1 indicates a good correlation, whereas a value close to 0 indicates a bad correlation. For an experimental mode, the corresponding analytical mode is defined as the analytical mode that shows the highest MAC value in combination with that experimental mode. No expansion of the experimental mode shapes is needed. Although highly effective for many structures, the MAC is unreliable in the correlation of local modes that are described by only very few DOFs. Also in case of a very limited number of experimental DOFs, an analytical mode can have comparable MAC values for a number of experimental modes. Next, one has to decide which modal data have to be included in the residual vector and how to formulate the residual functions.

3.3Eigenfrequencies

The first part of the residual vector contains the differences between the numerical and experimental undamped eigenfrequencies. In fact, differences in eigenvalues are used in order to simplify the sensitivity formulations. Each eigenfrequency residual is formulated as:

$r_f(\theta) = \frac{\lambda_j(\theta) - \tilde{\lambda}_j}{\tilde{\lambda}_j}$, for $\lambda_j = \omega_j^2 = (2\pi f_j)^2$ and $j \in \{1,\ 2,\ \ldots,\ n_\lambda\}$ where the upper tilde denotes the experimental values and *f* (or ω) stands for the (angular)

natural frequency. For the mode shape ($z = \varphi$), the residuals $\varepsilon_{\phi,i}(\theta)$ are given by with eigenvalue $\lambda_j = \left(2\pi\nu_j\right)^2$ and eigenfrequency ν_j. λ_j and $\tilde{\lambda}_j$ denote the numerical and corresponding experimental eigenvalue, respectively. mf refers to the number of identified eigenfrequencies that are used in the updating process. Relative differences are taken in r_f in order to obtain a similar weight for each eigenfrequency residual, since the higher the eigenfrequency, the higher the absolute difference between the analytical and experimental quantity will be.

The eigenfrequencies provide global information of the structure and they are very sensitive with respect to its stiffness properties. Furthermore, they can be accurately measured and identified. Hence, the eigenfrequencies are indispensable quantities to be used in the updating process and have a favorable effect on the condition of the optimization problem.

3.4 Mode shapes

A limited set of eigenfrequencies is a too poor basis for the definition of the dynamic behaviour. Although they contain very valuable information, the eigenfrequency residuals must be complemented with spatial information about the dynamic behaviour of the structure, i.e. with information on the degree of freedom level. Therefore, the residual vector is extended with differences in mode shape displacements. Since the civil engineering structures are most often measured in operational conditions, the exciting forces come from ambient sources (wind, traffic, etc.) and thus are unknown. As a result, the identified experimental mode shapes cannot be absolutely scaled. Furthermore, only the translation degrees of freedom of the mode shapes can be measured.
Each mode shape residual is formulated as:

$$\varepsilon_{\phi,i}(\theta) = \frac{\varphi_i(\theta) - \tilde{\varphi}_i}{\left\|\tilde{\varphi}_i\right\|_1} \quad \text{for } i \in \{1, 2, \ldots, n_\phi\}$$

the numerical and corresponding experimental mode shape vector, respectively. φ_i and φ_j denote single components of the vector φ, the former refers to any component that is used in the updating process, the latter to a reference component. m_s denotes the number of identified mode shapes used in the updating process.

Since an absolute scaling factor is missing for the experimental mode shapes, the numerical and experimental mode shapes are normalized to 1 in a reference node, which is a node at which the mode shapes have their largest amplitude or at least a large amplitude and is chosen for each mode separately.

3.6 Jacobian matrix

The nonlinear least squares problem is solved with an iterative sensitivity-based optimization method. Therefore, the Jacobian matrix (or sensitivity matrix) needs to be calculated in each iteration. The matrix contains the first-order derivatives of each residual r_j in the residual vector with respect to each design variable θ_i:

$$J_\theta = \begin{bmatrix} \vdots & \\ \cdots & \frac{\partial r_j}{\partial \theta_i} \quad \cdots \\ \vdots & \end{bmatrix}_{m \times n} \quad with \begin{cases} j = 1,...,m \\ i = 1,...,n \end{cases}$$

3.5 Modal scale factor (MSF)

In literature, one can find other proposals to formulate mode shape residuals. Instead of normalizing the mode shapes in one reference node, Friswell and Mottershead propose to scale the measured mode shape to the analytical one by multiplying it with the modal scale factor (MSF) which is defined by Allemang and Brown (1983) as:

$$MSF(\varphi_i, \tilde{\varphi}_i) = \frac{\varphi_i^* \tilde{\varphi}_i}{\left\| \tilde{\varphi}_i \right\|^2}$$

with matching the experimental and numerical data is mode shape scaling. Because the mass distribution of the FE model and real structure may be different, the mode shapes may not be scaled coincidently. The measured mode shapes scaled by function mode_scale and numerical data multiples by the modal scale factor MSF will solve the problem that the experimental and numerical mode shapes could be 180˚ out of phase.

3.7 Weighting

The least squares problem formulation allows the residuals to be weighted separately corresponding to their importance and amount of noise. The weight factors influence the result only in case of an overdetermined set of equations, i.e. when the number of residuals is higher than the number of design variables. Furthermore, only the relative proportion of the weighting factors is important, not their absolute values. The ability to weight the different data sets gives the method its power and versatility, but at the same time requires engineering insight to provide the correct weights. In a weighted least squares problem the following minimization problem is solved:

$$min\ \frac{1}{2} r(\theta)^T W r(\theta) = \frac{1}{2} \left\| W^{\frac{1}{2}} r(\theta) \right\|^2$$

with *W* the weighting matrix. If the weighting matrix is a diagonal matrix, i.e. *W* = diag (..., w_2...,), the problem can be equivalently written as:

$$min\ \frac{1}{2} \sum_{j=1}^{m} \left[w_j r_j(\theta) \right]^2$$

where w_j is the weighting factor of the residual r_j.

As stated before, the experimental eigenfrequencies are in general the most accurate experimental data that are available and due to their high sensitivity to the physical properties of the structure, they have a favourable effect on the problem condition. Experimental mode shapes on the other hand are much noisier and hamper the stability of the minimization. An appropriate weighting is therefore necessary.

The eigenfrequency residuals are already equally weighted by their definition as relative differences. All the mode shape residuals are of the same order of magnitude, since the mode shape components vary between +1 and −1 due to the normalization in a reference node. It depends on each particular updating problem if an additional weighting is necessary. A balance should be made between the advantages and drawbacks of both residual types. If the mode shapes are measured rather accurately (e.g. in laboratory) and they provide relevant information (e.g. by revealing a significant discrepancy with the analytical mode shapes), a higher weight can be assigned to the mode shape residuals than when the differences between model and measurement are less than the noise level, in

which case their information is irrelevant. The latter can occur for example when non-smooth mode shapes are identified from in situ measurements.

It is difficult if not impossible to state beforehand or in a general way which relative weighting factor should be assigned to the mode shape residuals. Due to the modelling and measurement errors, different results will always be obtained for different weighting factors, hence no unique ideal solution exists. The most likely and realistic result should be selected based on engineering insight. Appropriate weights can be identified in an iterative way, namely, if for the obtained result the eigenfrequencies correspond fully but the mode shapes show a considerable discrepancy, it can be assumed that too much weight is given to the eigenfrequency residuals. On the other hand, if a very non-smooth result is obtained which refers to a too high influence from the mode shape measurement errors that corresponds with eigenfrequencies which deviate much from the experimental eigenfrequencies, the weight for the mode shapes should be decreased.

3.8 Optimization algorithm

The nonlinear least squares problem is generally solved with the iterative sensitivity-based Gauss-Newton method. This means that the Hessian is approximated by using only the first-order term and neglecting the second-order derivatives, which is justified in the FE model updating problem since the residuals are small at the minimum if an adequate model is used. It is equivalent with solving the following linear least squares problem in each iteration k:

$$\min_d \frac{1}{2}\left\| r\left(\theta_k\right) + J_\theta\left(\theta_k\right) d \right\|^2$$

or, for the case of a weighted residual:

$$\min_d \frac{1}{2}\left\| W^{\frac{1}{2}} r\left(\theta_k\right) + \left[W^{\frac{1}{2}} J_\theta\left(\theta_k\right) \right] d \right\|^2$$

followed by a line search: $\theta_{k+1} = \theta_k + \alpha_k d_k$.

As stated by Beck and Arnold [10], the method is effective in seeking minima that are reasonably well-defined, provided that the initial estimates are in the general

region of the minimum. But parameter identification problems, such as in the FE model updating application, are prone to be ill-posed and to diverge. Therefore, the Gauss-Newton method is implemented with a trust region approach in order to stabilize the optimization process, instead of using the line search version that characterizes the pure Gauss-Newton method.

3.8.1 Large Scale Nonlinear Least Squares

An important special case for f(x) is the nonlinear least-squares problem:

$$\min_x \sum_i f_i^2(x) = \min_x \left\| F(x) \right\|_2^2$$

where $F(x)$ is a vector-valued function with component i of $F(x)$ equal to $f_i(x)$. The basic method used to solve this problem is the same as in the general case described in Trust-Region Methods for Nonlinear Minimization. However, the structure of the nonlinear least-squares problem is exploited to enhance efficiency. In particular, an approximate Gauss-Newton direction, i.e., a solution s to

$$min \left\| Js + F \right\|_2^2$$

(where J is the Jacobian of $F(x)$) is used to help define the two-dimensional subspace S. Second derivatives of the component function $f_i(x)$ are not used.
In each iteration the method of preconditioned conjugate gradients is used to approximately solve the normal equations, i.e., $J^T Js = -J^T F$ although the normal equations are not explicitly formed.

3.8.2 Large Scale Linear Least Squares

In this case the function $f(x)$ to be solved is $f(x) = \left\| Cx + d \right\|_2^2$, possibly subject to linear constraints. The algorithm generates strictly feasible iterates converging, in the limit, to a local solution. Each iteration involves the approximate solution of a large linear system (of order n, where n is the length of x). The iteration matrices have the structure of the matrix C. In particular, the method of preconditioned conjugate gradients is used to approximately solve the normal equations, i.e., $C^T Cx = -C^T d$, although the normal equations are not explicitly formed.

The subspace trust-region method is used to determine a search direction. However, instead of restricting the step to (possibly) one reflection step, as in the nonlinear minimization case, a piecewise reflective line search is conducted at each iteration, as in the quadratic case. Ultimately, the linear systems represent a Newton approach capturing the first-order optimality conditions at the solution, resulting in strong local convergence rates.

3.8.3 Levenberg-Marquardt method

The Levenberg-Marquardt method（Marquardt, D，1963） is a standard technique used to solve nonlinear least squares problems. Least squares problems arise when fitting a parameterized function to a set of measured data points by minimizing the sum of the squares of the errors between the data points and the function. Nonlinear least squares problems arise when the function is not linear in the parameters. Nonlinear least squares methods involve an iterative improvement to parameter values in order to reduce the sum of the squares of the errors between the function and the measured data points. The Levenberg-Marquardt curve-fitting method is actually a combination of two minimization methods: the gradient descent method and the Gauss-Newton method. In the gradient descent method, the sum of the squared errors is reduced by updating the parameters in the direction of the greatest reduction of the least squares objective. In the Gauss-Newton method, the sum of the squared errors is reduced by assuming the least squares function is locally quadratic, and finding the minimum of the quadratic. The Levenberg-Marquardt method acts more like a gradient-descent method when the parameters are far from their optimal value, and acts more like the Gauss-Newton method when the parameters are close to their optimal value.

The search direction is calculated by solving:

$$\left(J_k^T J_k\right) p^{GN} = -J_k^T r_k$$

while in the Levenberg-Marquardt method it became:

$$\left(J_k^T J_k + \mu_k I\right) p^{LM} = -J_k^T r_k$$

3.8.4 Large-scale algorithm

This algorithm is a trust region method, hence, unlike the medium scale least square algorithm, bound-constrained problem can be solved. A quadratic model function is built at each iteration that approximates the objective function. Since the Hessian is approximated with the Gauss-Newton formulation, second-order derivatives are not used. The search direction defines a two dimensional subspace, calculated taking the bound constrains into account：

$$min\left\| J_k p + r_k \right\|^2$$

For solving nonlinear least square problem in finite element model updating, the large-scale algorithm is used because it allows to apply a trust-region strategy. The fact is that, since the Jacobian Matrix can be ill-conditioned, the calculated search direction is very sensitive to approximation, therefore the designed variables have to be bounded in order to obtain a solution that is not physically unreasonable.

3.8.5 Modified optimization algorithm (Trust-Region-Reflective Least Squares Algorithm)

Many of the methods used in Optimization Toolbox solvers are based on *trust regions,* a simple yet powerful concept in optimization（Coleman, T.F. and Y. Li,1996）. To understand the trust-region approach to optimization, consider the unconstrained minimization problem, minimize *f*(*x*), where the function takes vector arguments and returns scalars. Suppose you are at a point *x* in *n*-space and you want to improve, i.e., move to a point with a lower function value. The basic idea is to approximate *f* with a simpler function *q*, which reasonably reflects the behavior of function *f* in a neighborhood *N* around the point *x*. This neighborhood is the trust region. A trial step *s* is computed by minimizing (or approximately minimizing) over *N*. This is the trust-region sub-problem,

$$mins\left\{ q(s), s \in N \right\}$$

The current point is updated to be $x+s$ if $f(x+s)<f(x)$; otherwise, the current point remains unchanged and *N*, the region of trust, is shrunk and the trial step computation is repeated. The key questions in defining a specific trust-region approach to minimizing *f*(*x*) are how to choose and compute the approximation *q* (defined at the current point *x*), how to choose and modify the trust region *N*, and how accurately to solve the trust-region sub-problem. This section focuses on the unconstrained problem. Later sections discuss additional complications due to the presence of constraints on the variables.

In the standard trust-region method (Moré, J.J.1983) the quadratic approximation *q* is defined by the first two terms of the Taylor approximation to *F* at *x*; the neighborhood *N* is usually spherical or ellipsoidal in shape. Mathematically the trust-region subproblem is typically stated

where *g* is the gradient of f at the current point *x*, *H* is the Hessian matrix (the symmetric matrix of second derivatives), *D* is a diagonal scaling matrix, Δ is a positive scalar, and $\|\cdot\|$ is the 2-norm. Good algorithms exist for solving; such algorithms typically involve the computation of a full eigensystem and a Newton process applied to the secular equation

$$\frac{1}{\Delta}-\frac{1}{\|s\|}=0.$$

These algorithms provide an accurate solution. However, they require time proportional to several factorizations of *H*. Therefore, for trust-region problems a different approach is needed.

The two-dimensional subspace *S* is determined with the aid of a preconditioned conjugate gradient process described below. The solver defines *S* as the linear space spanned by s_1 and s_2, where s_1 is in the direction of the gradient *g*, and s_2 is either an approximate Newton direction, i.e., a solution to

$$H\cdot s_2=-g,$$

or a direction of negative curvature,

$$s_2^T\cdot H\cdot s_2<0.$$

The philosophy behind this choice of *S* is to force global convergence (via the steepest descent direction or negative curvature direction) and achieve fast local convergence (via the Newton step, when it exists).

A sketch of unconstrained minimization using trust-region ideas is now easy to give:

1. Formulate the two-dimensional trust-region subproblem.
2. to determine the trial step *s*.
3. If $f(x+s)<f(x)$, then $x=x+s.$

4. Adjust Δ.

These four steps are repeated until convergence. The trust-region dimension Δ is adjusted according to standard rules. In particular, it is decreased if the trial step is not accepted, i.e., $f\left(x+s\right) \geq f\left(x\right)$. Optimization Toolbox solvers treat a few important special cases of *f* with specialized functions: nonlinear least-squares, quadratic functions, and linear least-squares. However, the underlying algorithmic ideas are the same as for the general case. These special cases are discussed in later sections.

4.Annex.

4.1 MatLab Routine for Extraction of Modal Parmeters

We use sap2000 API programming with Matlab to calculate the numerical modal data, the script is:

```
function [f,Z,indr_fem] = Call_fem(p);

% Run fem to calculate eigenmodes and eigenfrequencies of the model for the first
n modes
%
% OUTPUT:
% 1.f [p*c*m] eigenfrequenices of the numerical model
% p = number of modes
% c = number of modal analysis cases = number of updating parameters + 1
% m = number of starting points =1

% 2.Z [q*p*c*m] eigenmodes of the numerical model
% q = number of measurment points
% p = number of modes
% c = number of modal analysis cases = number of updating parameters + 1
% m = number of starting points =1
%% Run the SAP2000 input-file
% check the current version of femd
%choice = questdlg('Calla fem', 'Yes', 'No', 'No');
%switch choice
 %   case 'Yes'
```

```
%% Define general path for files
gen = pwd;

for i = 1:7
   gen(end) = [];
end

%% Call SAP2000
% This function must be modified any time according to the specific
% analysis which is performed

in = strcat(gen,'\fem\p_update.dat');
load(in);
p_update

in = strcat(gen,'\Matlab\data.txt');
load(in);

num = size(data,1);

cd ([gen,'\Matlab\parameters']);
load dimension;

in = strcat(gen,'\fem\p_update.dat');
load(in);

%[FileName,PathName] = uigetfile('*.sdb','Select the MATLAB code file');
filename = strcat([PathName, FileName]);
Save = 'temp.sdb';
savename = strcat([PathName, Save]);
iterations = n_cases;              %Number of iteration
mode_shapes = n_extract_modes;             %Number of mode shapes to extract

startpunt = 1;

for j = 1:iterations
  %% pass data to Sap2000 as one-dimensional arrays
    feature('COM_SafeArraySingleDim', 1);
```

```
  %% pass non-scalar arrays to Sap2000 API by reference
    feature('COM_PassSafeArrayByRef', 1);

  %% create Sap2000 object
    SapObject = actxserver('Sap2000v16.SapObject');

  %% start Sap2000 application
    SapObject.ApplicationStart;

  %% hide application
    ret = SapObject.Hide;

  %% create SapModel object
    SapModel = SapObject.SapModel;
    ret = SapObject.SapModel.File.OpenFile(filename);

  %% Section to update the mechanical properties of the materials

%%%%%%%%%%%%%%%%%%%%%%%%%%%%%%%%
CONCRETE  %%%%%%%%%%%%%%%%%%%%%%%%%%%%%%%%
  %% set material weight and mass per unit volume
%         w = 25*p_update(j,1);
%       ret_mas_con = SapModel.PropMaterial.SetWeightAndMass('Concrete',1, w);

  %% set material mechanical properties
    e = 36750000*p_update(j,1);
    u = 0.20;
    a = 1.000E-05;
    ret_mec_con = SapModel.PropMaterial.SetMPIsotropic('Concrete', e, u, a);

%%%%%%%%%%%%%%%%%%%%%%%%%%%%%%%%
CONCRETE_REDUCT  %%%%%%%%%%%%%%%%%%%%%%%%%%%%%%%%
%%
  %% set material weight and mass per unit volume
%       w = 78.5*p_update(j,3);
%       ret_mas_con_red = SapModel.PropMaterial.SetWeightAndMass('Steel',1, w);

  %% set material mechanical properties
```

```
    e = 2.3575E+08*p_update(j,2);
    u = 0.30;
    a = 0;
    ret_mec_con_red = SapModel.PropMaterial.SetMPIsotropic('Steel', e, u, a);

 %%%%%%%%%%%%%%%%%%%%%%%%%%%%%%%%
Slab  %%%%%%%%%%%%%%%%%%%%%%%%%%%%%%%%
  %% set material weight and mass per unit volume
%      w = 25*p_update(j,5);
%      ret_mas_slab = SapModel.PropMaterial.SetWeightAndMass('Slab',1, w);

  %% set material mechanical properties
%      e = 36000000*p_update(j,6);
%      u = 0.20;
%      a = 9.900E-06;
%      ret_mec_slab = SapModel.PropMaterial.SetMPIsotropic('Slab', e, u, a);

%%%%%%%%%%%%%%%%%%%%%%%%%%%%%%%%
SLAB_REDUCT  %%%%%%%%%%%%%%%%%%%%%%%%%%%%%%%%
  %% set material weight and mass per unit volume
%      w = 25*p_update(j,7);
%      ret_masslab_red =
SapModel.PropMaterial.SetWeightAndMass('Slab_reduct',1, w);

  %% set material mechanical properties
%      e = 36000000*0.9*p_update(j,8);
%      u = 0.20;
%      a = 9.900E-06;
%      ret_mec_slab_red = SapModel.PropMaterial.SetMPIsotropic('Slab_reduct', e,
u, a);

  %% set number of modes
    ret = SapModel.LoadCases.ModalEigen.SetNumberModes('MODAL',
mode_shapes, 2);

  %% save model
    ret =  SapObject.SapModel.File.Save(savename);

  %% run model (this will create the analysis model)
```

```
    ret = SapObject.SapModel.Analyze.RunAnalysis();

  %% get Sap2000 Frequencies
      NumberResults = 1;
      ACase = cellstr(' ');
      StepType = cellstr(' ');
      StepNum = zeros(1, 1, 'double');
      Period = zeros(1, 1, 'double');
      Frequency = zeros(1, 1, 'double');
      CircFreq = zeros(1, 1, 'double');
      EigenValue = zeros(1, 1, 'double');
      ret = SapModel.Results.Setup.DeselectAllCasesAndCombosForOutput;
      ret = SapModel.Results.Setup.SetCaseSelectedForOutput('MODAL');
      [ret, NumberResults, ACase, StepType, StepNum, Period, Frequency,
CircFreq, EigenValue] = SapModel.Results.ModalPeriod(NumberResults, ACase,
StepType, StepNum, Period, Frequency, CircFreq, EigenValue);
   for i = 1 : mode_shapes
      Per(i, j) = Period(1, i);
      Fre(i, j) = Frequency(1, i);
      Circ(i, j) = CircFreq(1, i);
      Eigen(i, j) = EigenValue(1, i);
   end

   %% get Sap2000 MODAL displacements
   for i = 1 : mode_shapes
      %% Print mode shapes on txt files
      out = strcat([gen,'\fem\Output\NodeData' int2str(startpunt) '_' int2str(j) '_'
int2str(i) '.dat']);
      fid = fopen(out, 'wt');            % open or create a new file: 'w' it is possible to
write results, 't' text file
      for k = 1 : num
         NumberResults = 0;
         Obj = cellstr(' ');
         Elm = cellstr(' ');
         ACase = cellstr(' ');
         StepType = cellstr(' ');
         StepNum = zeros(1, 1, 'double');
         U1 = zeros(1, 1, 'double');
         U2 = zeros(1, 1, 'double');
```

```
            U3 = zeros(1, 1, 'double');
            R1 = zeros(1, 1, 'double');
            R2 = zeros(1, 1, 'double');
            R3 = zeros(1, 1, 'double');
            GroupElm = 0;
            ret = SapModel.Results.Setup.DeselectAllCasesAndCombosForOutput;
            ret = SapModel.Results.Setup.SetCaseSelectedForOutput('Modal');
            str = num2str(data(k,1));
            [ret, NumberResults, Obj, Elm, ACase, StepType, StepNum, U1, U2, U3,
R1, R2, R3] = SapModel.Results.ModeShape(str, GroupElm, NumberResults, Obj,
Elm, ACase, StepType, StepNum, U1, U2, U3, R1, R2, R3);
            Sap_MODAL_U1 = U1;
            Sap_MODAL_U2 = U2;
            Sap_MODAL_U3 = U3;
            Sap_MODAL_Result_U1(k, i) = Sap_MODAL_U1(1, i);
            Sap_MODAL_Result_U2(k, i) = Sap_MODAL_U2(1, i);
            Sap_MODAL_Result_U3(k, i) = Sap_MODAL_U3(1, i);
            modal = ([Sap_MODAL_Result_U1(:, i), Sap_MODAL_Result_U2(:, i),
Sap_MODAL_Result_U3(:, i)]);
            fprintf(fid,'%12.8f %12.8f %12.8f \r\n',modal(k, :));
        end
        fclose(fid);
    end

    %% Lock model
      %ret = SapModel.SetModelIsLocked(false);

    %% save model
      %ret =  SapObject.SapModel.File.Save(filename);

   %% close Sap2000
      ret = SapObject.ApplicationExit(false());
      SapModel = 0;
      SapObject = 0;

      %% Print frequencies on txt files
      out = strcat([gen,'\fem\Output\Frequencies' int2str(startpunt) '_' int2str(j) '.dat']);
      fid = fopen(out, 'wt');              % open or create a new file: 'w' it is possible to
write results, 't' text file
```

```
    fprintf(fid,'%12.8f \n', Fre(:, j));
    fclose(fid);
end

cd ([gen,'\Matlab\']);

%% Save the calculated modal frequencies and mode shapes
% Load the parameters
cd ([gen,'\Matlab\parameters']);
load ('dimension');
cd ([gen,'\Matlab\']);

f = [];
Z = [];

% extract the calculated modal frequencies and mode shapes Z
aantalfiles = dir([gen,'\fem\Output']); % Check the fem output directory
if size(aantalfiles,1) ~= (n_extract_modes + 1)*n_cases + 2;
  indr_fem = 0;
  f = 0;
  Z = 0;
  beep;
  fprintf('!!!ATTENTION fem RUN FAILED!!!');
else;
   indr_fem = 1
   startpunt = 1
   for casu = 1:n_cases;
      f_temp = [];
      f_temp = load([gen,'\fem\Output\Frequencies'  int2str(startpunt) '_' int2str(casu)
'.dat']);
      for mode = 1:n_extract_modes;
         f(mode,casu,startpunt) = f_temp(mode);
         z = load([gen,'\fem\Output\NodeData' int2str(startpunt) '_' int2str(casu) '_'
int2str(mode) '.dat']);
         Z(:,mode,casu,startpunt) = mode_scale(z(:,3)); % modesacle: scale the
mode shape to maximum unity
      end
   end
end
```

```
    %case 'No'
%end



%% Define optimization paramters

% Main Dimension
prompt = {'Number of measurement nodes: ','Number of modes to update: ','Total
number of modes: ', 'Number of references paramenters: '}
name = 'General parameter';
numlines = 1;
defaultanswer = {'95','13','50','2'};
general = inputdlg(prompt,name,numlines,defaultanswer);
n_meas_nodes = str2num(char(general(1,1)));                %number of
measurements nodes
n_update_modes = str2num(char(general(2,1)));              %number of modes you
want to update
n_extract_modes = str2num(char(general(3,1)));             %number of modes you
want fem to extract
n_parameters = str2num(char(general(4,1)));                %number of parameters
chosen
n_cases = n_parameters + 1;

prompt = {'Turn off re-run after each 5 iterations? (Y\N)','How many optimization
processes will run?',...
        'increase (Relative increment of p for Jacobian cal.','Tolx (Termination
tolerance on x)'};
name = 'Optimization';
numlines = 1;
defaultanswer = {'Y','1','0.001','0.001'};
initiatie = inputdlg(prompt,name,numlines,defaultanswer);
nachtrun = char(initiatie(1,1));
n_runs = str2num(char(initiatie(2,1)));
increase = str2num(char(initiatie(3,1)));
tol_X = str2num(char(initiatie(4,1)));

prompt = {'Weight of freqs','Weight of mode shapes','Weight of penal. terms'};
name = 'Input';
```

```
numlines = 1;
defaultanswer = {'2','4','1'};
gewicht = inputdlg(prompt,name,numlines,defaultanswer);
wf = str2num(char(gewicht(1,1)));
wZ = str2num(char(gewicht(2,1)));
wp = str2num(char(gewicht(3,1)));
```

6.1. Matching of the vibration modes

In order to get more exact match of experiment mode with numerical mode data, the starting point's modal data is chosen as the reference modal, first of all, we calculate MAC value to pair them.

```
%% Reference Volume Data
% Modes Data of the fem's model chosen as Starting Point for the
% Optimization process

ind_num_modes = [2 4 5 7 8 9 12 14 17 27 29 32 36];  %index number of the fem
model you want to update
cd ([gen,'\Matlab\parameters']);
load dimension;
save dimension ind_num_modes -append;
cd ([gen,'\Matlab']);
```

Then we use the numerical modal data to match with iterative modal data of new model, it is easy to get exact modal relation between experiment data to numerical data.

```
%% MATCHING
% Load the eigenfrequencies and the eigenmodes of the fem's Reference
% Model (FEM Starting Point)

ind_num_modes = [2 4 5 7 8 9 12 14 17 27 29 32 36];

cd ([gen,'\Matlab\parameters']);
load dimension;
load modaldata_fem;       %fem modal data
```

```
m = size(Z_meas_ref,2); %number of row
n = size(Z,2);              %number of column

cd ([gen,'\Matlab\']);
% Write the array of MAC values
% MAC matrix is created for each cases and with a number of column equal
% to the modes extract from fem.
% (N.B. due to the oscillation, caused by updating,the eigenfrequencies
% can change in position (e.g. the third modes can become the fourth) so it's
% better to extract from fem a safety number of modes and not just the
% ones that seems to match at first).

%COUPLES
% Couples contain, for each cases, the index of the Mac_matching procedure,
% so it finding the best Couples for each case

%% FIND
% The Couple matrix assing the matching frequencies and modal shape to f1
% and Z1 (that will become the new f and Z in output)
```

4.3 Formulation of the objective function

```
%%%%%%%%%%%%%%%%%%OBJECTIVE-FUNCTION %%%%%%%%%%%%%
 OUTPUT
% 1.Rw: is the weighted residual vector of the objective function. The square
% sum of the Rw's elements represent the objective function.

% 3.JW: is the weighted Jacobian matrix, an index to understand if the
% objective function is going in the right direction, in other words, if we
% are close to a minimum.
% LOADING OF THE WEIGHTS AND PARAMETERS

function [Rw,Jw] = Obj_Fun(p0);

  %% Modal analysis by fem
  % fem will update the reference model following the *_updating.inp file's
instructions
  % and, thanks to the p_update matrix, the chosen will be updated
  % one by one by the increase of 1%
```

```
  % OUTPUT
  % 1.f: is the vector of the eigenfrequencies extracted from the numerical model

  % 2.Z: is the eigenmodes matrix; one column for each modal shape, one row
  % for each measurement nodes, one matrix for each cases

 [f,Z,indr_fem] = Call_fem(p);

 %% Match the modes of the reference fem's model with the updated ones
  %Using the Mac value and the 'find' function, fun_mac_match adjust the
  %dimension of f and Z to make them fit with the number of modes you want to
  %update

  [f, Z] = fun_mac_match(f, Z);

  %% Construction of the Residual Vector RW
  % R the weighted residuals in the objective function for all the modal analysis
cases
  % N.B. the square sum of the elements in Rw rappresent the definition of
Objective Function

  [R] = fun_residuals(f, Z);
```

4.4 Calculation of the Jacobian matrix

```
%% Calculate the Jacobian matrix
  % It's the Slope of the Function Is an index to understand if the
  % objective function is going in the right direction, in other words,
  % if we are close to a minimum.

  Jw = zeros(size(Rw,1),n_parameters);
  ptemp = p0;
  Jw=(R(:,2:n_cases)-repmat(R(:,1),1,n_cases-1))./(-
increase*repmat(ptemp(1,1:n_parameters),size(R,1),1));
```

4.5 Solving the optimization problem

```
%   Optimization
%   OUTPUT
%   p0: the vector of the optimization variables
%   resnorm: the squared 2-norm of the residual at p0, = sum(fun(p0).^2)
%   Rw: the value of the residual fun(p0) at the solution p0
%   exitflag: the exit condition
%   output: information about the optimization
%   lambda: the Lagrange multipliers at the solution p0
%   Jw: the Jacobian of fun at the solution p0
%   INPUT
%   Obj_Fun: the function whose sum of squares is minimized
%   p_start: the optmization starts at the point p_start
%   p_low: Vector of lower bounds
%   p_up: Vector of upper bounds
%   'Jacobian','on': the function fun must return, in a second output argument, the
Jacobian value J, a matrix, at x (p).
%   'TolX',tol_X: Termination tolerance on x (p0), a positive scalar. The default is
1e-6.
%   VarLoc: the updating variables (parameters) location, = [1 2 3 4 5 6 7 8 9 10 11
12 13], to be passed to objfunc1
%   W: weight matrix to be passed to objfunc1, being unity!

%   The kernel of the codes !
   [p0, resnorm, Rw, exitflag, output, lambda, Jw] = lsqnonlin(@Obj_Fun, p_start,
p_low, p_up, optimset('Jaco bian','on','TolX',tol_X));
```

Bibliography

ANSYS Inc. (2007) *Elements reference, ANSYS release 11.0*, January.

Avitabile P. (2001) *Experimental modal analysis. a simple nonmathematical presentation*, University of Massachusetts Lowell, Lowell, Massachusetts.

Brincker R. et al. (1992) *Identification of the dynamical properties from correlation function estimates*, Danish Society for Structural Science and Engineering, 33 p. Bygningsstatiske Meddelelser; No. Vol. 63, No.1.

Brincker R. (2007) *Automated frequency domain decomposition*. Proceeding of the 25th IMAC, Orlando, FL, USA.

Brincker R. et al. (2000) *Modal identification from ambient response using frequency domain decomposition*, proceeding of the 18th IMAC, St. Antonio, Texas, USA.

Caetano E. et al. (2007). *Comparison of stochastic identification method applied to the natural response of Millau viaduct*, EVACES '07, Experimental Vibrations of Civil Engineering Structures, Porto, Portugal.

Chopra A.K. (2007) *Dynamics of structures: Theory and application to earthquake engineering*, Prentice Hall, USA.

Garrett, D. S., Powers, R., Gronenborn, A. M., & Clore, G. M. (2011). *A common sense approach to peak picking in two-, three-, and four-dimensional spectra using automatic computer analysis of contour diagrams*. Journal of Magnetic Resonance, 213(2), 357-363.

Coleman T. F., Zhan Y. (2007) *Optimization Toolbox User's Guide*. The MathWorks, Inc.

Computer & Structures, Inc. (2013) *CSI Analysis reference manual, for SAP2000*, Berkeley, California, USA.

Craig R., et al. (2006) *Fundamentals of structural dynamics*, John Wiley, Hoboken, N.J.

Cunha A. et al. (2006) *From input-output to output-only modal identification of civil engineering structures*. SAMCO final report, f11 selected papers.

Di Biagio E. (2003) *A Case study of Vibrating-Wire Sensors That Have Vibrated Continuously for 27 Years*. 6th International Symposium on Field Measurements in Geomechanics (FMGM)

Engström B. (2006) *Design analysis of deep beams and other discontinuity regions*, Chalmers University of Technology, Göteborg.

Friswell M. I., Mottershead J. E. (1995) *Finite element model updating in structural dynamics*, Kluwer Academic Publishers, Dordrecht; Boston.

Mottershead, J. E., Link, M., & Friswell, M. I. (2011). *The sensitivity method in finite element model updating: a tutorial.* Mechanical systems and signal processing,

Chapra, Steven C., and Raymond P. Canale. *Numerical methods for engineers*. Vol. 2. McGraw-Hill, 1998.25(7).

Ibrahim S.R., Mikulcik E.C. (1977) *A method for the direct identification of vibration parameters from the free response*, Shock and Vibration Bulletin, 47, p. 197.

Jaishi B., et al. (2007) *Finite element model updating of concrete-filled steel tubular arch bridge under operational condition using modal flexibility*". Mechanical Systems and Signal Processing, Vol. 21, No. 6, pp. 2406-2426.

Schlune, H., Plos, M., & Gylltoft, K. (2009). *Improved bridge evaluation through finite element model updating using static and dynamic measurements.* Engineering structures, 31(7), 1477-1485.

Kwon Y. W., Bang H. (2000) *The finite element method using MATLAB*, CRC Press, Boca Raton.

Maia N.M.M., Silva J.M.M. (1997) *Theoretical and experimental modal analysis*, Research Studies Pre; 1st edition, Sussex, England.

Mottershead J. E. et al. (2011) *The sensitivity method in finite element model updating: A tutorial,* Mechanical Systems and Signal Processing Vol. 25, Issue 7, Pages 2275–2296.

Ottosen N., Petterson H. (1992) *Introduction to the Finite Element Method,* Prentice Hall Europe.

Palacios J. G., et al. (2013) *Operational modal analysis of rad, higway and railway bridges: Vibration measurements, system identification and fem modeling"*. Summary report of performance validation of the Fomento wireless sensor network for structural health monitoring.

Peeters B., De Roeck G (2001) *Stochastic system identification for operational modal analysis: A review*, Journal of Dynamic Systems Measurement and Control, 123(4).

Peeters B., De Roeck G. (1999) *Reference-based stochastic subspace identification for output-only modal analysis,* Mechanical Systems and Signal Processing 13(6), 855-878 No. mssp.1999.1249, available online at http://www.idealibrary.com

Reynders E et al. (2011) *MACEC 3.2: A MatLab toolbox for experimental and operational modal analysis.* Report BWM-2011-01, Katholieke Univ. Leuven.

Reynders E. et al. (2006) *"Finite element modeling and analysis of two higway bridges across the M50 ring at Madrid"*, BWM-2006-10.

Ronald A. Cook, et al. (2009) *Stiffness evaluation of neoprene bearing pads under long term loads*, University of Florida, Florida. Department of Transportation. Research Center, University of Florida.

Teughels A. (2003) *Inverse modeling of civil engineering structures based on operational modal data*, PhD thesis, Department of Civil Engineering, KU Leuven, Belgium.

Unger J.F., et al. (2005) *Damage detection of a prestressed concrete beam using modal strains,* Journal of Structural Engineering, Vol 131, Issue 9, 1456-1463.

Van Overschee, P., De Moor P.L. (1996) *Subspace identification for linear systems: Theory, implementation, applications"*, Springer; Softcover reprint of the original 1st ed.

Ventura C.E., Horyna T. (1997) *Structural assesment by modal analysis in western Canada*. Proceeding 15th IMAC, Orlando, FL, USA.

Zhang Q. W., et al. (2001) *Finite-element model updating for the Kap Shui Mun cable-stayed bridge.* Journal of Bridge Engineering, Vol. 6, No. 4, pp. 285.

Zivanovic Set al. (2007) *Finite element modelling and updating of a lively footbridge: The complete process*. Journal of Sound and Vibration, Vol. 301, No. 1-2, pp. 126.

FRISWELL M.I., MOTTERSHEAD J.E., *Finite element model updating in structural dynamics*, SPRINGER-SCIENCE+BUSUNESS MEDIA, B.V. 1996

GENTILE C., SAISI A., Ambient vibration testing of historic masonry towers for structural identification and damage assessment, *Construction and Building Materials, 21(6), 2007,* pp. 1311-1321.

Reynders E., Teughels A., De Roeck G., Finite element model updating and structural damage identification using OMAX data *Mechanical Systems and Signal Processing* Vol.24,2010, pp.1306–1323.

BRISEGHELLA, B., SIVIERO, E., LAN, C., MAZZAROLO, E., ZORDAN, T., (2010) *Safety Monitoring of the Cable Stayed Bridge in the Commercial Harbor of Venice*, Italy, Bridge Maintenance, Safety, Management and Life-Cycle Optimization – Proceedings of the 5th International Conference on Bridge Maintenance, Safety and Management, pp.1935-1942.

GENTILE, C. & SIVIERO, E. 2007. Dynamic characteristics of the new curved cable-stayed bridge in Porto Marghera (Venice, Italy) from ambient vibration measurements; *Proc. 25th Int. Modal Analysis Conference (IMAC), Orlando 2007.*

ZORDAN, T., BRISEGHELLA B., LIU T., Finite element model updating of a tied-arch bridge using Douglas-Reid method and Rosenbrock optimization algorithm, *Journal of Traffic and Transportation Engineering (English Edition)*, 2014,1(4), pp. 280-292.

BRISEGHELLA B., CHEN, A., LI, X., ZORDAN, T., LAN, C., MAZZAROLO, E. (2012) Analysis on applicability of health monitoring techniques on a curved cable stayed bridge; Bridge *Maintenance, Safety, Management, Resilience and Sustainability –Proceedings of the Sixth International Conference on Bridge Maintenance, Safety and Management,* pp. 2617-2624

Briseghella, B., Zordan, T., Lan, C., Mazzarolo, E., Busatta, F.& Gentile, C., 2010. *Safety Monitoring of the Cable Stayed Bridge in the Commercial Harbor of Venice*. IABMAS 2010 Conference, The Fifth International Conference on Bridge Maintenance, Philadelphia, USA.

SVS, ARTeMIS Extractor 2011. <http://www.svibs.com/>, 2012.

SMITH, SUZANNE WEAVER BEATTIE, CHRISTOPHER A *Secant-Method Adjustment for Structural Models*, AIAA journal,1991, pp.119-126.

Allemang R.J. and Brown D.L.: Correlation coefficient for modal vector analysis, *Proc. 1st Int. Modal Analysis Conf. (IMAC)*, 110-116, 1983.

Bendat J.S. and Piersol A.G.: *Engineering applications of correlation and spectral analysis*, Wiley Interscience, 1993.

Brincker R., Zhang L. and Andersen P.: "Modal identification from ambient responses using Frequency Domain Decomposition", *Proc. 18th Int. Modal Analysis Conf. (IMAC)*, San Antonio, 2000.

Brownjohn J.M.W. and Xia P.Q.: *Dynamic assessment of curved cable-stayed bridge by model updating,* J. Structural Engineering, ASCE, 126, 252-260, 2000.

Deger Y., Cantieni R., DeSmet C.A.M. and Felber A.J.: Finite element model optimization of the new Rhine bridge based on ambient vibration testing, *Proc. Eurodyn '96*, 817-822, 1996.

Gentile C. and Martinez y Cabrera F.: *Dynamic investigation of a repaired cable-stayed bridge,* Earthquake Engineering & Structural Dynamics, 26, 1997.

Peeters B. and De Roeck G.: "Reference-based stochastic subspace identification for output-only modal analysis", *Mechanical Systems and Signal Processing*, 6(3), 855-878, 1999.

Van Overschee P. and De Moor B.: "Subspace identification for linear systems: Theory, implementation, applications", Kluwer Academic Publishers, 1996.

Waters T.P.: *Finite element model updating using measured frequency response functions*., Ph.D. Thesis, Department of Aerospace Engg., University of Bristol, 1995.

Welch P.D.: *The use of Fast Fourier Transform for the estimation of Power Spectra: a method based on time averaging over short modified periodograms*, IEEE Transactions, AU-15, 70-73. 1967.

Wilson J.C. and Liu T.: *Ambient vibration measurements on a cable-stayed bridge*, Earthquake Engineering & Structural Dynamics, 20, 723-747,

Gimsing, N. J.: *Cable Supported Bridges, Concept & Design.* John Wiley & Sons. Chichester,1998.

Scott, R.: *In the Wake of Tacoma*. ASCE Press. Resno 2001.

Troyano, L. F.: *Bridge Engineering. A Global Perspective*. Thomas Telford Publishing, London 2003.

Jiri Strasky: *Stress ribbon and cable supported pedestrian bridges.* ISBN: 0 7277 3282 X.Thomas Telford Publishing, London 2005.

Lin, T.Y., - Burns, N. H.: *Design of Prestressed Concrete Structures.* John Wiley & Sons.New York 1981.

GENTILE C., SAISI A., *Ambient vibration testing of historic masonry towers for structural identification and damage assessment,* Construction and Building Materials, 21(6), 2007, pp. 1311-1321.

Douglas B. M., Reid, W. H., 1982*. Dynamic tests and system identification of bridges*. Journal of the Structural Division, 108 (10) :2295-2312.

Rosenbrock, H. H., 1960. An automatic method for finding the greatest or least value of a function. Computer Journal, 3 (3): 175-184.

Inaudi D, Elamari A, Pflug L, et al. *Low-coherence deformation sensors for the monitoring of civil-engineering structures[J].* Sensors and Actuators A: physical, 1994, 44(2): 125-130.

GENTILE C&Gsllino.N. *Monitoraggio dinamico del ponte strallato sul Canale Industriale Ovest del porto commerciale di Marghera ,* 2006

GENTILE C.et al. *Monitoraggio dinamico del ponte strallato sul Canale Industriale Ovest del porto commerciale, commerciale di Marghera 26-28 luglio 2010*, 20 Agosto 2010

GENTILE C.et al. *Monitoraggio dinamico del ponte strallato sul Canale Industriale Ovest del porto commerciale di Marghera 26-28 luglio 2010,* 20 Agosto 2010

BERGAMINI, A., 2001, *Non-destructive testing of stay cables, Proc. of IABSE Conference on Suspended Bridges*, Seoul, Korea, 2001.

BRINCKER R., ZHANG, L.M. and ANDERSEN, P., 2000, *Modal identification from ambientresponses using Frequency Domain Decomposition*, Proc. 18th Int. Modal Analysis Conference(IMAC), San Antonio, 2000.

BROWNJOHN, J. M. W., XIA, P.Q., 2000, *Dynamic assessment of curved cable-stayed bridge by model updating, J. Structural Engineering,* ASCE, 126, 2000: p.252-260.

DEGER, Y., CANTIENI, R., DESMET, C. A., M., AND FELBER, A.,J., 1996, *Finite element model optimization of the new Rhine bridge based on ambient vibration testing*, Proc. Eurodyn '96, 1996:p817-822.

GENTILE, C., MARTINEZ Y CABRERA, F., 2004*, Dynamic performance of twin curved cable-stayed bridges,* Earthquake Engineering & Structural Dynamics, 33, 2004: p.15-34.

GENTILE, C., SIVIERO, E., 2007*, Dynamic characteristics of the new curved cable-stayed bridge in Porto Marghera (Venice, Italy) from ambient vibration measurements*, Proc. 25th Int. Modal AnalysisConference (IMAC), Orlando, 2007.

INAUDI, D. et al., 1994, *Low-coherence Deformation Sensors for the Monitoring of Civil-engineering Structures*, Sensors and Actuators A, Vol. 44, 1994: p. 125-130.

LLORET, S., RASTOGI, P., K., THÉVENAZ, L. and INAUDI D., 2003, *Measurement of dynamic deformation using a path-unbalance Michelson-interferometer-based optical fiber sensing device*, Optical Engineering, Vol. 42, n. 3, 2003, p. 662-669.

MARTINEZ Y CABRERA, F., IMPARATO, V., 1999, *Access bridges for Milan's "Malpensa 2000"air station*, L'Industria Italiana del Cemento, LXX, 1999, p.634-661.

VIRLOGEUX M., 1999, *Recent evolution of cable-stayed bridges*, Engineering Structures, 21, 1999, p. 737-755.

DANIELL W.E.; MACDONALD J.H.G. 2007, *Improve Finite Element Modelling of a Cable-Stayed Bridge through systematic Manual Tuning*, Engineering Structures, Vol. 29(3), pp. 358-371.

PEETERS B. 2000, *System identification and damage detection in civil engineering structures, Ph.D. Thesis*, Heverlee, Belgium, Katholieke Universiteit Leuven.

Gentile, C. 2006. *Modal and structural identification of a R.C. arch bridge,* Structural Engineering and Mechanics, Vol. 22, No. 1, pp. 53-70.

SMITH, SUZANNE WEAVER BEATTIE, CHRISTOPHER *A Secant-Method Adjustment for Structural Models*, AIAA journal,1991, pp.119-126.

Madsen, K. (1975). *An algorithm for minimax solution of overdetermined systems of non-linear equations.* IMA Journal of Applied Mathematics, 16(3), 321-328.

M. Link, R. G. Rohrmann, and S. Pietrzko. (1996) *Experience with automated procedures for adjusting the finite element model of a complex highway bridge to experimental modal data*. In Proceedings of IMAC XIV: 14th International Modal Analysis Conference, Dearborn, Michigan.

M. Link. *Updating of analytical models - Procedures and experience. In Proceedings of Conf. on Modern Practice in Stress and Vibration Analysis,* pages 35–52, Sheffield, UK, April 1993.

M. Link. *Updating analytical models by using local and global parameters and relaxed optimization requirements*. Mechanical systems and signal processing, 12(1):7–22, 1998.

M. Link. *Updating of analytical models - Basic procedures and extensions. In N. M. M. Maia and J. M. M. Silva, editors,* Modal Analysis and Testing. Kluwer Academic Publisher, 1999.

J. E. Mottershead, C. Mares, M. I. Friswell, and e.a. *Selection and updating of parameters for an aluminium space-frame model*. Mechanical systems and signal processing, 14(6):923–944, 2000.

Z. Y. Shi, S. S. Law, and L. M. Zhang. *Structural damage detection from modal strain energy change.* Journal of Engineering Mechanics, 126(12):1216–1223, 2000.

Q. W. Zhang, C. C. Chang, and T. Y. P. Chang. *Finite element model updating for structures with parametric constraints.* Earthquake Engineering and Structural Dynamics, 29:927–944, 2000.

Moré, J.J. and D.C. Sorensen, *Computing a Trust Region Step,* SIAM Journal on Scientific and Statistical Computing, Vol. 3, pp 553–572, 1983.

Marquardt, D*., An Algorithm for Least-Squares Estimation of Nonlinear Parameters*, SIAM J. Appl. Math. Vol. 11, pp 431–441, 1963.

Coleman, T.F. and Y. Li, *An Interior, Trust Region Approach for Nonlinear Minimization Subject to Bounds*, SIAM Journal on Optimization, Vol. 6, pp 418–445, 1996.

Str'ask'y, Jiř'i. *Stress ribbon and cable-supported pedestrian bridges*. Thomas Telford, 2005.

Sasmal S, Ramanjaneyulu K. *Dynamic behaviour of bridge decks curved in plan[J].* International Journal of Applied Mechanics and Engineering, 2007, 12(4): 1117-1134.

APPENDIX

The following papers were written during my Ph.D. research period (chronological order):

Conference papers:

1. Aymerich F, Fenu L, Francesconi L, **Fa Guanzhe**, Evaluation of The Fracture Behaviour of a Fibre Reinforced Earthen Material Using Digital Image Correlation [C]. Proceeding of the 23th Annual International Conference on Composites/Nano Engineering, Chengdu, July, 2015.
2. **Fa Guanzhe**, Leqia He, Luigi Fenu, Briseghella Bruno. *Comparison of Direct and Iterative Method for Model Updatin*g of a Curved Cable-stayed Bridge Using Experimental Modal Data [C]. International Association for Bridge and Structural Engineering, IABSE-2016, June.